

# Feasibility study of a novel load alleviation system on the UH-60A Blackhawk helicopter

M.R. Verhagen

Master of Science Thesis





# Feasibility study of a novel load alleviation system on the UH-60A Blackhawk helicopter

by

**M.R. Verhagen**

In partial fulfillment of the requirements for the degree of

**Master of Science**  
in Aerospace Engineering

at the Delft University of Technology,  
to be defended publicly on Thursday August 6, 2015 at 9:30 AM.

Thesis committee:

Supervisor:	Dr. ir. M. Voskuijl
Chairman:	Prof. dr. ir. L. L. M. Veldhuis
Reader:	Ir. J. A. Melkert
Reader:	Dr. ir. S. Hartjes

Thesis registration number: 034#15#MT#FPP  
Cover page image courtesy of HighDefinitionWallpaper.com



# Preface

In the final year of completing my Masters of Science degree in Aerospace Engineering, I have been able to apply the previously attained skills and knowledge to this M.Sc. Thesis project. Nonetheless, this hallmark achievement would not have been possible without the support of others.

I want to express great gratitude to two people in particular; my supervisor Mark Voskuijl, who always knew what I was doing, and my mother, Soesila Jainandusing, who always knew how I was doing.

Mark Voskuijl always found time to provide valuable feedback, allowing for important insights. His devoted guidance and support throughout my thesis has provided me with the confidence to complete this seemingly daunting task, making this process a pleasant one. I would like to thank my thesis committee members Leo Veldhuis, Sander Hartjes and Joris Melkert for taking the time to assess my work and providing their expert insights.

My word of thanks extends to my parents for their support throughout my studies, and my grandfather, who's assistance has played a key role in making this achievement possible. I am very thankful towards my mother, who's patience, wise words and support has provided me with the perseverance to complete my thesis.

Lastly, I would like to express my appreciation towards the many friends that I have met throughout my studies, having provided me with everlasting, fond memories of Delft. My fraternity friends from JC Babylon, roommates from the Aerospace Engineering thesis room, Formula Student Team Delft, and many others, have made my student experience a memorable, wonderful and unforgeable one.

*M.R. Verhagen  
Delft, August 2015*



# Abstract

Though structural load alleviation (SLA) schemes for helicopters traditionally solely use rotor controls to reduce loads, Voskuijl [54] presents an SLA system for the Sikorsky UH-60A Blackhawk, making combined use of longitudinal cyclic and horizontal tailplane actuation. In high speed flight, when performing maneuvers around the longitudinal axis, utilization of these combined controls reduces pitch link loads and shaft bending moments, due to lower use of longitudinal cyclic. The manoeuvre of choice is the 1.75g doublet at 130kts, mimicking the UTTAS manoeuvre. This particular SLA system is of interest since its application to helicopters currently featuring a variable incidence stabilizer requires minimal hardware changes. The system is also practically implementable since use is made of two feedback signals that are measured aboard most helicopters. While results in the Flightlab simulation environment are promising when testing the system under design conditions, load reduction capabilities in off-design conditions are unknown. It is also unknown if this SLA system is safe if failure occurs. Furthermore, if loads of the regular UH-60A performing the 1.75g doublet are considered as a reference, the degree of component downsizing or gross weight increase is unknown. Within Flightlab, this research aims to assess off-design performance, safety after SLA system failure, as well as determining potential weight savings that the implementation of this system may allow.

Four off-design conditions are considered, consisting of maximum forward or aft cg, and low or high speed flight. Due to adverse attitudes at airspeeds below 60kts, it is decided to phase in the SLA system at airspeeds above 60kts, being fully functional at 80kts. In all off-design conditions, shaft bending moment load reduction exceeds 10%. The third design variable used during SLA development, gross weight (GW), is not considered.

Concerning safety, tailplane deflection limits are chosen based on longitudinal cyclic margin following a maximum tailplane deflection failure case. It is decided to limit the stabilator to incidence angles of -7deg (trailing edge up) and 10deg (trailing edge down). These limits also allow for a safe landing attitude at the maximum landing airspeed of 60kts. A tailplane actuation rate of 45deg/s is imposed, being the required amount for full load alleviation at 80kts forward speed. Tailplane deflection at this actuation rate, for all off-design conditions, yields maximum peak load factors of 1.54g. However, tailplane actuation limits may constrict the helicopter's agility. This is assessed on the basis of five metrics: attitude quickness, agility quickness, flightpath agility quickness, flightpath bandwidth and pitch rate bandwidth. Of these, flightpath bandwidth is a novel approach developed here. These newly developed metrics are proposed as current metrics and norms do not paint a complete picture concerning agility. Agility assessment according to these five metrics indicate equal or superior performance of the SLA system for changes in pitch rate and flightpath trajectory. Three failure cases; -7deg, 10deg fixed tail incidence and 0.1deg/s rate limited tailplane demonstrate sufficient capability to change aircraft pitch attitude or flightpath trajectory. While ADS-33E solely requires the helicopter to remain within the OFE after FCS failure, it is felt that the proposed flightpath bandwidth metric would be a valuable addition to ADS-33E, more adequately ensuring safe operation after failure.

If loads on the baseline UH-60A are considered as a reference for maximum tolerable loads, the design of the SLA equipped UH-60A can be altered, or GW can be increased, before similar shaft normal stresses are experienced during the 1.75g doublet at 130kts flight. It is found that the main rotor radius cannot be downsized based on this parameter. Rotor shaft downsizing results in a shaft weight reduction of 0.31kg, down from 11.11kg. When increasing payload instead of downsizing main rotor components, the mixed control SLA system allows the design gross weight to grow from 15283lbs to 16409lbs; an increase of 7.4%. Finally, the relevance of findings is determined by comparing the transients for variations in inflow and interference models. Differences in load predictions for similar pitch rate transients indicate valid results. Nonetheless, flight tests must be conducted due to the difficulty of proper tailplane interference modeling (Prouty [47]).

Therefore, it can be concluded that the proposed SLA system provides significant load reductions in the considered off-design conditions, potentially allowing for a substantial GW increase. With the chosen tailplane actuator limits, the SLA system is considered safe for all failure scenarios, while allowing for similar or improved agility in terms of pitch attitude and flightpath trajectory.



# Contents

<b>1</b>	<b>Introduction</b>	<b>1</b>
<b>2</b>	<b>Helicopter basics and previously developed SLA schemes</b>	<b>5</b>
2.1	Helicopter basics . . . . .	5
2.2	Various rotorcraft SLA schemes: various approaches and applications . . . . .	6
2.2.1	FCS schemes applied to helicopters for load alleviation or mitigation . . . . .	7
2.2.2	SLA schemes applied to tiltrotors . . . . .	10
<b>3</b>	<b>The mixed control SLA system</b>	<b>13</b>
3.1	Background information and working principle . . . . .	13
3.2	Selection of helicopter . . . . .	17
3.3	Relevance of the mixed control SLA system and selection of maneuver . . . . .	19
<b>4</b>	<b>Flight dynamics, loads and off-design performance</b>	<b>25</b>
4.1	Flightlab simulation model theory . . . . .	26
4.1.1	Equations of motion . . . . .	26
4.1.2	Tail rotor model . . . . .	26
4.1.3	Main rotor inflow models. . . . .	28
4.1.4	Aerodynamic behavior of blades . . . . .	31
4.1.5	Horizontal tailplane modeling . . . . .	34
4.2	Simulation of maneuver loads . . . . .	35
4.2.1	Hub forces and moments . . . . .	37
4.2.2	Conclusions on the sources of loads during the doublet . . . . .	41
4.3	Suboptimal conditions . . . . .	42
4.3.1	Determination of airspeeds for which the SLA scheme will be functional . . . . .	42
4.3.2	Selection of off-design conditions. . . . .	43
4.3.3	Mixed control SLA performance in off-design conditions. . . . .	43
4.3.4	Conclusions concerning off-design performance . . . . .	45
<b>5</b>	<b>Safety analysis and subsequent handling qualities</b>	<b>47</b>
5.1	Background . . . . .	47
5.1.1	Dynamic and static stability . . . . .	47
5.1.2	ADS-33E and MIL-DTL-9490E: two norms pertaining to safety. . . . .	49
5.2	Safety constraints and failure cases . . . . .	53
5.3	Constraints allowing for safety . . . . .	53
5.3.1	Failure cases considered for analysis . . . . .	53
5.3.2	Stabilator actuation limits based on trimmability . . . . .	54
5.3.3	Stabilator limits for sufficient longitudinal cyclic margin. . . . .	58
5.3.4	The constrained SLA system. . . . .	59
5.3.5	Assessment of loadfactor and safe landing for chosen stabilator deflection limits . .	60
5.4	Agility following constraints . . . . .	63
5.4.1	Attitude quickness . . . . .	63
5.4.2	Agility quickness . . . . .	67
5.4.3	Flightpath agility quickness . . . . .	69
5.4.4	Flightpath bandwidth . . . . .	71
5.4.5	Pitch rate bandwidth. . . . .	75

5.5	Model fidelity analysis . . . . .	76
5.6	Conclusions on safety analysis and handling qualities . . . . .	81
5.6.1	Actuator limits that provide safety . . . . .	81
5.6.2	Newly proposed agility metrics . . . . .	81
5.6.3	Agility with imposed actuator constraints. . . . .	82
5.6.4	Validity of inflow and interference modeling . . . . .	83
<b>6</b>	<b>Weight estimation</b>	<b>85</b>
6.1	Various weight estimation schemes . . . . .	85
6.2	Results . . . . .	87
6.2.1	Main rotor shaft downsizing . . . . .	88
6.2.2	Main rotor radius downsizing . . . . .	91
6.2.3	Increase in Design Gross Weight. . . . .	93
6.3	Conclusions on weight alterations . . . . .	96
<b>7</b>	<b>Conclusions</b>	<b>99</b>
7.1	Conclusions on off-design load alleviation performance. . . . .	99
7.2	Conclusions on safety and handling qualities . . . . .	100
7.2.1	Actuator limits that provide safety . . . . .	100
7.2.2	Newly proposed agility metrics . . . . .	100
7.2.3	Agility with imposed actuator constraints. . . . .	101
7.2.4	Validity of inflow and interference modeling . . . . .	102
7.3	Conclusions on weight alterations . . . . .	103
7.4	Concluding remarks . . . . .	104
<b>8</b>	<b>Recommendations</b>	<b>105</b>
	<b>Bibliography</b>	<b>107</b>
<b>A</b>	<b>Prouty's parametric weight estimation</b>	<b>111</b>
<b>B</b>	<b>Aerodynamics as modeled in NDARC</b>	<b>113</b>
<b>C</b>	<b>Agility with corrective control</b>	<b>117</b>
<b>D</b>	<b>Empty weight alteration for main rotor downsizing</b>	<b>123</b>

# 1

## Introduction

The development of rotorcraft in the past has been a long and challenging process of iterations. Structural loads and handling qualities in particular have always been properties that required further attention or fine tuning. The importance of structural loads already became evident in the first autogyro designs where the requirement of flapping and lead-lag hinges soon became evident to avoid high structural loads and an adverse roll moment in forward flight (Prouty [48]). This latter notion was the start of a series of cross coupled rotorcraft motions evidenced in flight; inputs in pitch causing rolling motion, inputs in roll also resulting in pitching moments and so on. Complex flow phenomena also significantly impact handling qualities, such as the highly irregular flow caused by the main rotor downwash on the tail surfaces. This is still not fully understood to date (Padfield [42]). To improve handling qualities, structural alterations can be made, however, due to recent developments in fly-by-wire systems, advanced flight control systems (FCS) can be used to improve handling qualities by actively deflecting control surfaces. An FCS is defined by MIL-DTL-9490E [4] (MIL) as any system used to transmit flight control commands from pilot to appropriate force and moment producers. Due to the geometry of a helicopter, the main rotor shaft can experience severe loads during extreme maneuvers. These stresses must be taken into account when dimensioning the helicopter's main rotor shaft, resulting in higher weight, production costs, and maintenance costs. Because of more demanding agility requirements, military helicopters in particular face penalties in terms of the three aforementioned parameters. FCS can be used for load alleviation purposes as well. FCS systems may inform the pilot of load limit encroachment, known as a tactile cueing system, or may actively reduce loads, known as a structural load alleviation (SLA) system. Tactile cueing systems may allow for carefree handling (CFH), if the pilot can now fly throughout the aircraft's operational flight envelope (OFE) without being preoccupied with monitoring limit exceedances (Loy [38]), reducing pilot workload. SLA systems will actuate control surfaces, such as main rotor controls, to reduce critical loads. Such systems are of particular interest, allowing for more severe maneuvers before load limit encroachment. For a UH-60A Blackhawk helicopter, Datta and Chopra [15] demonstrate the severity of the oscillatory nature of the pitch link loads with blade rotation azimuth angle for the UH-60A; increasing with forward airspeed. Kufeld and Bousman [34] furthermore indicate the strong impact of load factor on the loads measured in the main rotor hub. Yeo et al. [62] states the correlation between shaft bending moments and blade flapping. With increased flapping during attitude and flightpath changes, shaft bending moments will be of larger magnitude. Gotzfried [18] indeed states that pull-up and pushover mission task elements as performed by the Eurocopter TIGER helicopter, cause shaft bending moments near the boundaries of the structural load envelope. For reduction of such loads, either a structural redesign is required, or use can be made of a suitable SLA system. The benefit of the latter approach is that implementation on current helicopter designs is more easily accommodated. Also, if more severe maneuvers are permitted before structural load limit encroachment, the helicopter may prove to be more agile.

A novel SLA system is developed by Voskuijl, aimed at reducing pitch link loads and main rotor shaft bending moments during high speed pitch attitude maneuvers, through the combined use of blade pitch actuation and a variable incidence horizontal stabilizer (Voskuijl [54]). This SLA system will from now on be referred to as the mixed control SLA system. The use of the variable incidence stabilizer for SLA purposes has not been done previously, making it a novel approach. Conventional

helicopters typically make use of longitudinal cyclic for commanded changes in pitch attitude. Though some helicopters currently feature a variable incidence stabilizer, also known as a stabilator, this device is currently not used for load alleviation purposes. In the case of the current UH-60A, this stabilator is used for flightpath stabilization (FPS), maintaining a fixed aircraft pitch attitude in cruise flight. The mixed control SLA helicopter sees a change in downforce at the tailplane, providing a pitching moment, reducing the required amount of cyclic, thus lowering loads at the main rotor. The mixed control SLA system is of particular interest due to the significant load reduction observed in the Flightlab simulation environment, when operating in design conditions. Secondly, accommodating this SLA system requires minimal hardware changes, if applied to a helicopter currently featuring a stabilator. Furthermore, the SLA system is practically implementable in real-life, requiring airspeed and pitch rate as feedback signals. These variables are already currently measured in most helicopters. Due to the novelty of this SLA system, there is a deficiency in knowledge on system safety after failure. Also, the application of this SLA system will require a horizontal tail redesign if the helicopter currently features a fixed horizontal stabilizer, while the main rotor can now be designed with less over-design due to lower structural loads. With these two opposing weight alterations in place, the overall impact on weight is currently unknown. The scope of analysis in this research is limited to SLA application on the UH-60A Blackhawk helicopter. The choice of helicopter is threefold: there is ample data on this helicopter type, literature has shown that the UH-60A faces significant pitch link loads and shaft bending moments during a pull-up manoeuvre, and because the UH-60A already currently features a stabilator. If this SLA system proves to be safe, its implementation is most easily accommodated on a helicopter currently featuring a stabilator, such as this particular helicopter. This master thesis therefore sets out to determine the feasibility of the mixed control SLA system as applied to the UH-60A. Assessment will take place in the Flightlab simulation environment. Feasibility is assessed in terms of off-design performance, safety performance after failure and subsequent agility, while potential empty weight (WE) savings are also investigated due to rotor downsizing. Since the UH-60A already features a stabilator, the addition of this SLA system will not result in a local increase in tailplane weight. If critically loaded components are not downsized, an increase in gross weight (GW) may be accommodated. Therefore, there are four research questions which will be addressed:

1. To which extent does the SLA system reduce loads in off-design conditions?
2. Is this novel SLA approach feasible for implementation on the UH-60A Blackhawk concerning safety after system failure?
3. If controller properties are altered to guarantee a safe helicopter, what is its impact on overall aircraft performance in terms of agility?
4. What is the overall impact on the helicopter's weight with the SLA system in place?

In chapter 2, helicopter basics will be discussed, including the working principle of a variable incidence tail. Subsequently, various SLA designs will be covered, based on their application, feasibility and novelty. The relevance of this particular SLA system will be discussed in chapter 3, followed by an explanation concerning the choice of the UH-60A Blackhawk as testbed for the SLA system. Chapter 4 will discuss the UH-60A model in the Flightlab simulation environment, as well as the SLA's ability to reduce loads in off-design conditions; answering the first research question. Off-design performance is important since this determines the operational realm of the SLA system. This in turn determines the off-design conditions which are used for safety and weight alteration assessment. In response to the second research question, relevant safety criteria and metrics are discussed in chapter 5, according to which the UH-60A is assessed concerning safety. On the basis of two SLA failure scenarios; maximum positive and negative tailplane deflection angles, stabilator actuator limits are chosen. A trimsweep analysis is conducted, from which the allowable tailplane actuation limits are determined, guaranteeing sufficient longitudinal cyclic margin in case of maximum tailplane deflection. Maximum actuator deflection rate is chosen to allow for full load alleviation at the lowest airspeed at which the SLA system is active. Based on these actuator deflection angle and rate limits, resultant landing aircraft attitudes and load factor transients are assessed, determining whether safety criteria are met. In response to the third research question, after potential alterations to guarantee a safe SLA system, section 5.4 compares the helicopter's agility to that of the baseline Blackhawk that does not feature the SLA system;

---

the latter not utilizing its tailplane for load alleviation. Agility assessment also covers the two maximum deflection stabilator angles failure cases, as well as a rate impaired stabilator failure scenario. Next, section 5.5 covers the validity of results of the UH-60A simulation model, comparing transients of various off-design doublets with differing inflow and interference models. Following the evaluation of various weight estimation approaches in chapter 6, allowable main rotor shaft and main rotor radius downsizing is determined, as well as the permitted gross weight (GW) increase, if similar loads are considered acceptable as experienced on the regular UH-60A. From this, the fourth research question will be answered. Lastly, conclusions and recommendations are provided in chapters 7 and 8 respectively. First, however, chapter 2 provides insight in basic helicopter controls, current SLA schemes, and other FCS systems.



# 2

## Helicopter basics and previously developed SLA schemes

In order to reduce loads in differing flight conditions, one may redesign critically loaded components, or use can be made of an SLA system. In this chapter, a selection of previously devised SLA systems will be presented. Their field of application, development and their effectiveness will be discussed. From this, the relevance of a novel SLA system will be presented in chapter 3. Before discussing the various SLA schemes, a brief explanation is provided concerning helicopter controls.

### 2.1. HELICOPTER BASICS

In a helicopter, a pilot has four controls at hand, these being: the lateral cyclic stick, the longitudinal cyclic stick, the collective stick, and the pedals. To increase thrust, the pilot uses the collective stick, changing blade pitch altering lift across the entire disc. In hover, variations in collective will result in vertical translation, while in forward flight, the amount of collective, together with the disc tilt, will determine the forward airspeed of the helicopter. For roll control, the pilot uses lateral cyclic, which causes a difference in blade pitch at the front and rear of the disc. Because of gyroscopic precession, this causes a difference in lift at the left and right side of the disc, resulting in roll motion. For aircraft pitch attitude control, the pilot uses longitudinal cyclic, which works in a similar fashion as lateral cyclic, yet now changing lift at the front and rear of the disc. Lastly, pedals are used to change thrust of the tail rotor, causing yawing motion. The three stick controls change blade pitch through means of a swash plate. The swash plate is attached at the top of the helicopter rotor mast, and can translate in the axis of the shaft or tilt along the two axes perpendicular to the shaft. Blade pitch links are connected to the swash plate at one end, and to the rotor blades at the other end. By following the swash plate, the blade pitch links cause the rotor blade to take on a different incidence angle, changing the angle of attack. A swash plate is shown in figure 2.1, as featured on a hingeless, bearingless rotor. A hingeless rotor allows for blade pitch changes, flapping and feathering through twisting and bending of elastomeric composites at the blade root. The working principle in terms of control input is the same for the articulated rotor, as found on the UH-60A. Through its working principle and geometry, it has been shown that pitch links as well as the main rotor shaft are critical components when it comes to peak structural loads. Insight on the severity of the stresses at these locations will be provided in chapter 4.2.

While conventional helicopters make use of the four aforementioned controls, horizontal tailplane incidence may also be utilized, working in the same plane as longitudinal cyclic. By using a stabilator, the horizontal tailplane will see a change in lift. Being mounted at the end of a tailboom, this change in lift will result in a pitching moment. The current UH-60A Blackhawk makes use of a stabilator for FPS, reducing the amount of download at low speed flight caused by the main rotor, maintaining near-constant pitch attitudes in cruise flight. More on current stabilator usage for the UH-60A can be found in chapter 3. With its longer moment arm from the helicopter's center of gravity compared to the main rotor, the stabilator can significantly reduce the amount of longitudinal cyclic required, hence reducing main rotor loads caused by blade cyclic actuation. In terms of air flow velocity, while

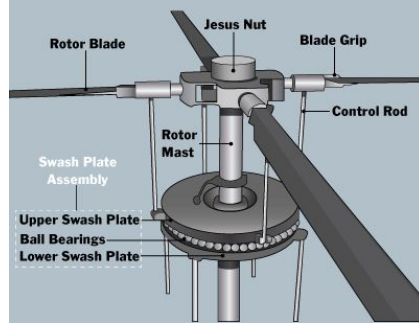


Figure 2.1: The working principle of a helicopter rotor, with blade pitch control by means of a swashplate. A bearingless hingeless rotor is displayed (Brian and Harris [10]).

effectiveness of longitudinal cyclic depends on forward airspeed and main rotor rotational velocity, stabilator effectiveness depends solely on forward airspeed. However, the stabilator may be located in a highly irregular flow pattern caused by the downwash of the main rotor, as is the case for the UH-60A. Stabilator actuation can occur in three ways. Stabilator actuation can occur through common controls as longitudinal cyclic, applying a control actuation ratio. This is done in the mixed control SLA system. Secondly the stabilator may be controlled by the pilot through use of an independent stick control, uncoupling stabilator and longitudinal cyclic usage. Lastly, stabilator deflection can be solely actuated by a flight control system, where the pilot has no direct authority over the stabilator. This latter approach is applied in the current UH-60A.

While the pilot has command over the aforementioned cockpit controls, these input signals will pass through various FCS systems before final output for control actuation is determined. As mentioned earlier, these FCS systems are used for purposes such as load alleviation, load mitigation, handling quality improvements such as FPS, stability, load alleviation, or for other purposes. In the following section, a selection of load alleviation or mitigation FCS schemes is provided to give insight in the current state of technology; their development, their range of applications and their effectiveness. From this, the relevance of the novel SLA system will be discussed.

## 2.2. VARIOUS ROTORCRAFT SLA SCHEMES: VARIOUS APPROACHES AND APPLICATIONS

FCS systems allowing for load reduction or mitigation have been applied to rotorcraft; helicopters as well as tiltrotors. Such FCS systems have been developed from two distinctly different ideologies: systems that actively change aircraft response by causing control deflections, and systems that instead cue the pilot when approaching a boundary condition, but where the control system does not actuate surfaces. The former approach is referred to as an SLA system, while the latter is referred to as a tactile cueing system. An SLA system is designed to reduce critical loads, while tactile cueing systems aim to provide load mitigation capability. While load reduction will lower the probability of load exceedance for a given maneuver, this is not considered to be a form of load mitigation. This is because critical loads may in theory still be exceeded if the performed manoeuvre is severe enough; the pilot is not made aware of structural load envelope encroachment. For helicopters, SLA schemes have been devised to limit pitch link loads, hub moments, blade flapping and main rotor torque values. Tiltrotor SLA schemes were developed to reduce blade flapping, blade bending moments and differential torque on the interconnect shaft. Tactile cueing systems devised for helicopters warn pilots of potential angle of attack (AoA), loadfactor, main rotor torque, main rotor bending moment, and/or blade flapping limit exceedances. These FCS schemes provide insight in the development, applications and effectiveness of current SLA or tactile cueing systems. Previously devised FCS systems furthermore provide valuable insight in effectiveness and HQ metrics, as well as safety analysis techniques which may be applied to assess the novel SLA system in this research.

In table 2.1, an overview is given of the various FCS schemes that are treated in the proceeding subsections.

Table 2.1: A selection of FCS schemes for load reduction or mitigation, applied to rotorcraft simulation models.

Ref.	Aircraft	Load reduction/mitigation	Feedback vars.	Control vars.	Controller	Summary
[57]	UH-60A Helicopter	Pitch link loads, shaft bending moment	Pitch att. and rate	Coll. and long. cyclic	H-infinity	85% load reduction Lower collective; less agile
[55]	Bell 412 Helicopter	Engine torque	Height rate and engine torque	coll.	H-infinity, iterative tuning	Lower overshoot torque peak, also for off-design
[24]	UH-60A Helicopter	MR hub moment	Lat. and long. cyclic	-	Tactile cueing, using fixed linear model	Uses elliptical constraints Off-design: 12% load excursions
[22]	UH-60A Helicopter	AoA, loadfactor, MR torque, blade flapping	Coll., lat. and long. cyclic	-	Tactile cueing; adaptive neural network	Smallest combination of lat./long./coll. that triggers excursion
[56]	ERICA Tiltrotor	Interconnect shaft torque, flap bearing loads	Coning, lat. and long. flapping	Elevator	Lookup table for blade pitch	90% shaft load reduction (210kts roll step) 6% flapping reduction
[41]	V-22 Tiltrotor	Osc. yoke chord bending moment	Pitch rate	Long. cyclic, elevator	Linear Quadratic controller	20% load reduction for pull-up HQ properties maintained
[39]	Eurotilt  Tiltrotor	Osc. yoke chord bending moment and gimbal flapping	Pitch rate, long. flapping	Long. cyclic, elevator	H-infinity; dual-objective, opposite flapping to pitch rate	Bending moment 50 % lower 30% reduction of long. flapping Flightpath quickness 20% lower
[40]	Eurotilt Tiltrotor	Interconnect shaft torque, flap bearing loads	TAS, rates, lat. & long. flapping	Coll.,lat. and long. cyclic	Linear Quadratic controller, opposite flapping to pitch rate	Almost complete bending moment and torque allev. (rudder/ail. pulse at 200kts)

### 2.2.1. FCS SCHEMES APPLIED TO HELICOPTERS FOR LOAD ALLEVIATION OR MITIGATION

The SLA system presented by Voskuijl et al. [57] demonstrates the effectiveness of pitch link load and shaft bending moment reduction when using collective and longitudinal cyclic actuation; with a trade-off in agility. A H-infinity controller is used to minimize the gain from the reference to the error signal, where pitch attitude and rate are the feedback signals. The use of H-infinity allows for combined handling quality objectives and structural load objectives; in this case pitch load reduction, and allows for control of uncertain systems. This latter property is important due to model uncertainties compared to the real UH-60A, including blade elastic properties, inertias, and complex inflow phenomena. For a 2g pull-up maneuver, resembling the UTTAS maneuver, helicopter maneuverability decreases compared to the baseline situation; climb rate is lower with the controller in place, as is evident from fig. 2.2. Furthermore, longitudinal control margin is reduced significantly because the SLA controller requires full actuator authority to meet its objectives of level 1 HQs and load alleviation. Agility is reduced because lower collective is applied by the controller at the start of the maneuver to reduce loads, meaning that the main rotor is providing less power. Pitch link loads show a characteristic cyclic nature as function of azimuth (Datta and Chopra [15]), but now its transient following the 2g maneuver show considerably lower peaks with the SLA system in place, reducing on average by 85%. Hence, there is a trade-off between load reduction versus performance in terms of control authority and available power, with the latter reducing at the maneuver initiation to reduce structural loads.

Voskuijl et al. [55] devises an SLA system for main rotor torque reduction for the Bell 412 around hover, using H-infinity control, as was done by Voskuijl et al. [57] for pitch link load reduction. Again, H-infinity control was applied due to model uncertainties compared to the actual helicopter. Here, the linear model uses engine torque and vertical velocity as state variables, with main rotor collective pitch as control variable. Parameter weights are iteratively tuned to meet ADS-33E and MIL stability requirements concerning closed-loop and open-loop roots, phase margin (PM), gain margin (GM), as well as overshoot ratio requirements for level 1 HQs. Fig. 2.3 shows that there is a lower transient peak overshoot and that there are less oscillations in torque; the result of a smaller imaginary part of the poles. While modeled around one linear model for a single weight and center of gravity configuration, variations in these parameters also demonstrate favorable results in reducing the peak overshoot.

Aside from FCS systems designed for SLA purposes, FCS systems can apply active control for the sole purpose of handling quality improvements. Johnson et al. [29] discusses the development of an FCS system with this purpose for the AH-64D Apache attack helicopter, demonstrating the capabilities of the HACT CONDUIT control system environment. Here, the user can select a range of HQ and stability requirements from ADS-33E and MIL criteria, or can set own criteria for response characteristics such as rise time, overshoot or steady state response. Optimization parameters in this example include rate

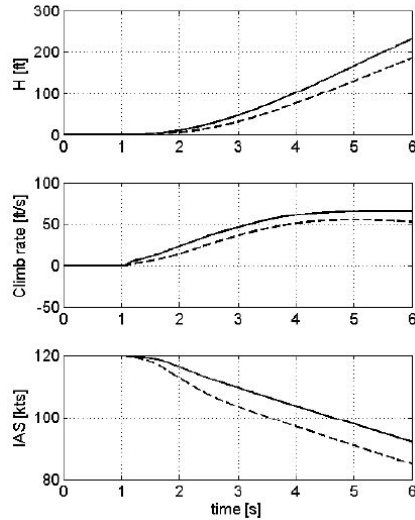


Figure 2.2: Aircraft response for conventional and SLA controllers (Voskuijl et al. [57]).

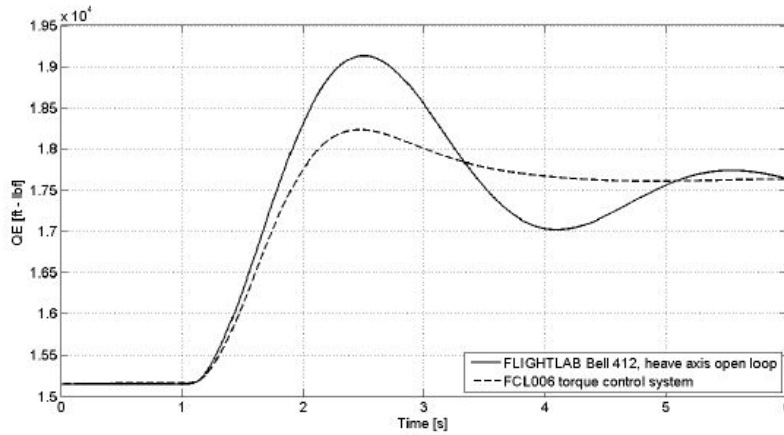


Figure 2.3: Torque response to a collective step input at 10 knots forward flight, for the Bell 412HP with and without torque protection SLA (Voskuijl et al. [55]).

feedback gains, attitude feedback gains, and desired bandwidths for pitch, roll and yaw. Optimized bandwidths and gains are significantly reduced, meaning less over-design. The optimization results in better HQs, better stability properties and reduced actuator saturation. This paper clearly demonstrates the effectiveness of the CONDUIT tool for tuning a controller for optimization, and the ease for the user to select input for controller optimization for desired aircraft HQ and stability requirements.

Aside from SLA systems changing aircraft response, some FCS solutions instead opt for a tactile cueing system. These systems cue the pilot that exceedance of boundary conditions will likely follow if a given input follows. Two such tactile cueing systems are presented by Horn and Sahani [24] and Horn et al. [22]. While effective in avoiding flight envelope boundary excursions, they cannot be used to alter handling qualities. This downside however does provide additional safety and predictability, as the failed FCS system will never deflect the control surfaces opposite to the pilot's desired input. Cueing systems require predictive algorithms since maximum response lags behind a given control input. The algorithm must therefore predict if an additional amount of stick input will cause an overshoot that will exceed a limit, such as a structural one. Horn and Sahani [24] use a cueing system for the UH-60A to avoid maximum transient main rotor hub moments by providing cues to lateral and longitudinal cyclic stick. The algorithm assesses an onboard linear model of the UH-60A for one fixed configuration to predict a boundary excursion. Constraints are combined in a single elliptical constraint, where the hub moment is the vector sum of the moments in both directions. Flight test results show an increased agility in terms of attitude quickness as pilots can now approach flight envelope boundaries with more

confidence. In off-design conditions, hub moments show a maximum 12 % excursion, as shown in figure 2.4. Instead of static exceedance predictions, Horn et al. [22] makes use of an adaptive algorithm. Here, a fixed linear aircraft model is applied to determine potential exceedance, but which also compares its prediction to the actual response. The SLA system provided in Horn et al. [22] uses a neural network that predicts the magnitude following a given input, yet ahead of the actual response. This way, the neural network ‘learns and adapts’ its corrective soft tops to more accurately predict excursions for a differing configuration. This system assesses the steady state transient of angle of attack, load factor, torque, and peak overshoot of blade flapping. Fig. 2.5 shows the effectiveness of predicting exceedance when flying in an off-design condition. Evidently, for a cueing system aimed at enhancing maneuverability by permitting more confident operation near aircraft limits, an adaptive scheme is preferable over a fixed system. This is because the fixed system must cap the helicopter operating envelope further than what is strictly needed to avoid limit exceedance.

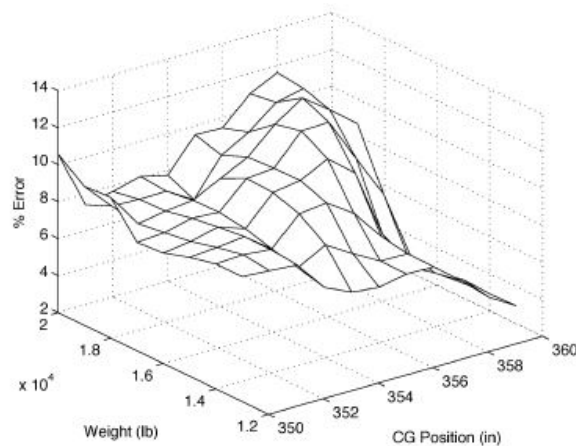


Figure 2.4: Percentage error in predicting load exceedances in off-design configurations for the UH-60A cueing system (Horn and Sahani [24]).

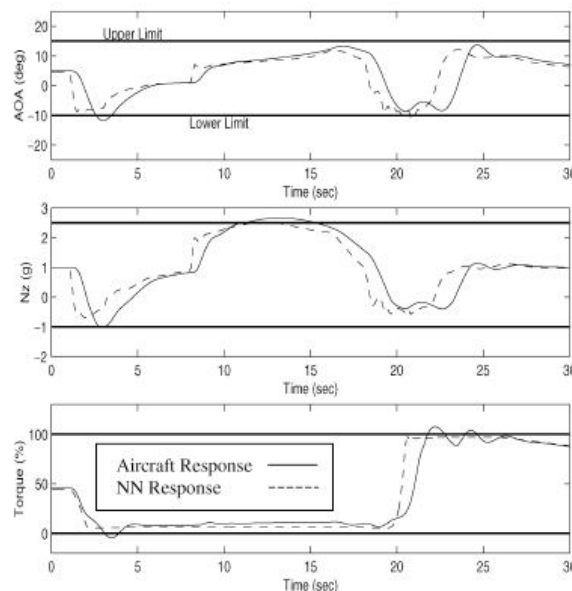


Figure 2.5: Effectiveness of the adaptive neural network in predicting load excursions, for an off-design condition (Horn et al. [22]).

### 2.2.2. SLA SCHEMES APPLIED TO TILTROTORS

Aside from helicopters, SLA systems have also been proposed for tiltrotor applications. In the selected SLA schemes, different approaches are utilized to reduce loads on the interconnect shaft, as well as loads associated with flapping. At first, two approaches on interconnect shaft load reduction will be discussed. Subsequently, SLA approaches reducing flapping related loads will be discussed.

Voskuijl et al. [56] and Manimala et al. [40] note that the critical loads for the tiltrotor occur due to excessive torque on the interconnect shaft, linking the engines to the propellers. Manimala et al. [40] uses a more complex single Linear Quadratic (LQG) controller, with feedback to minimize the linear quadratic performance measurement, incorporating requirements on performance and control authority; prioritized by a weight factor. For a rudder pulse input at 200kts, no more than 1.8deg control authority is required, almost completely alleviating differential torque. For differential torque alleviation of the interconnect shaft, Voskuijl et al. [56] does not apply complex controllers; instead using a lookup table for required blade pitch angle for given combinations of airspeed to yaw or roll rates. Both references indicate that the influence of roll or yaw rate on differential torque is very linear at a given airspeed, as indicated in figure 2.6. Voskuijl et al. [56] suggests that the required pitch to alleviate both motions is simply the addition of both required blade pitches for the two separate motions. This simple and elegant solution allows for almost complete load alleviation on the interconnect shaft and proves to be very effective. For a roll-step mission task element at 210kts, this SLA system demonstrates an ability to reduce differential torque for the tiltrotor by 90%.

For reduction of flapping-related loads in airplane mode, Voskuijl et al. [56], Miller et al. [41], Manimala et al. [39] and Manimala et al. [40] provide various solutions. Miller et al. [41], Manimala et al. [39] and Manimala et al. [40] consider the significance of elevated rotor yoke chord bending moments when performing pull-up maneuvers in airplane mode. Voskuijl et al. [56] aims to reduce elastomeric flapping bearing loads in steady cruise flight.

Voskuijl et al. [56] provides an SLA system which uses elevator deflection to align the rotor with incoming flow to reduce flapping, when in cruise flight. The feedback signal consists of rotor coning as well as lateral and longitudinal flapping. While the elevator changes the aircraft's longitudinal attitude, the controller makes use of rotor coning and lateral flapping, as these too provide a contribution to elastomeric flapping bearing loads. Elevator deflection is chosen to perpendicularly align the rotor discs more with oncoming flow, reducing steady state flapping. This perpendicular alignment furthermore shows a required power reduction of 1-3% in most flight conditions, while reducing flapping by 6 degrees. The system provided by Voskuijl et al. [56] is preferred; it uses a more intuitive look-up scheme, proves to almost completely alleviate all differential torque loads caused by roll and yaw, and has more implementable feedback variables.

Miller et al. [41], Manimala et al. [39] and Manimala et al. [40] consider SLA approaches to reduce oscillatory yoke chord bending moments  $M_z$  during pull-up maneuvers. Miller et al. [41] states that these bending moments are caused by the rotor disc leading the rotor shaft during precession, causing excessive flapping and chord bending moments. Manimala et al. [39] considers the flapping direction, in the same direction as pitch rate, to be the cause of high  $M_z$  loads. Manimala et al. [40] attributes this same-direction behavior to the excitation of the short period mode during a pull-up. This causes a change in vertical velocity, altering blade incidence, causing flapping to occur in the same direction as the change in aircraft pitch.

Miller et al. [41] simulates a V-22 tiltrotor in the Flightlab environment. In a feed forward scheme, comparing actual with desired pitch rate, the SLA system determines the amount of longitudinal cyclic and elevator deflection to reduce rotor yoke chord bending moments. The SLA system's effectiveness, in terms of transient rotor yoke bending moments reduction, is demonstrated for a pull-up using maximum stick longitudinal cyclic. For the SLA system, this transient is reduced by 20% as compared to the regular V-22 tiltrotor. From a bandwidth analysis, assessing rotor yoke chord bending moment for various frequency longitudinal cyclic stick inputs, the SLA system shows load reductions for frequency inputs between 0.2 and 10rad/s. A maximum load reduction of 7dB is achieved at a stick frequency input of 0.5deg/s, as compared to the regular V-22 tiltrotor. Flight tests demonstrate this SLA system's ability to maintain Cooper-Harper level 1 handling qualities (HQs), for various MTEs. Interestingly, this reference determines the amount of control authority based on a worst-case failure situation, causing maximum negative longitudinal cyclic at the rotors, resulting in an adverse pull-up. Control authority is limited to a few degrees, based on the maximum longitudinal cyclic deflection required for load alleviation for a maximum intensity pull-up. Safety analysis used by this reference; looking at transients

following worst-case control deflection, will also be incorporated in the assessment of the novel SLA system.

Manimala et al. [39] demonstrates the ability of H-infinity dual-objective control design on the Eurocopter Eurotilt helicopter. Similar to Miller et al. [41], rotor yoke bending moments are assessed for pull-up maneuvers in airplane mode, yet now incorporating requirements on gimbal flapping angles as well. Through the application of longitudinal cyclic and elevator deflection, the SLA system forces the rotor to flap against the direction of pitch rate. Pitch rate and longitudinal gimbal flapping are feedback signals for the SLA system, determining longitudinal cyclic and elevator command signals that minimize rotor yoke bending moment and longitudinal gimbal flapping. Load reduction of rotor yoke bending moment is quantified in terms of load quickness, considering peak loads during a pull-up singlet. HQs are assessed in terms of flightpath quickness; a metric also applied in this research, and will be covered further in chapter 5.4. Without the criteria of flapping minimization, similar to Miller et al. [41], blade flapping will be larger in magnitude and in opposite direction of pitch rate. This almost completely reduces  $M_z$ , yet still results in large flapping, be it in the direction opposite to the baseline tiltrotor. By incorporating both criteria, an optimum in terms of minimum flapping and  $M_z$  will be achieved. The SLA system is capable of reducing peak rotor bending moment by 50% while reducing gimbal longitudinal flapping by 30%. By causing opposite flapping as compared to pitch rate, flightpath quickness on average reduces by 20%. Similar to Miller et al. [41], load reduction in the frequency domain is assessed. When flying at 160kts, the SLA system reduces rotor bending moments by 5-10dB, while reducing gimbal flapping by 13-15dB. While this SLA system was developed around a linear model of the Bell XV-15 and tuned for the Eurotilt tiltrotor, the SLA system shows promising results in terms of loads and flapping reduction, though with penalties in terms of HQs.

The SLA system provided by Manimala et al. [40] expands on the feedback signals used by Manimala et al. [39]. Aside from longitudinal gimbal flapping and rotor bending moment  $M_z$ , this controller aims to minimize the lateral counterparts of these two variables. Feedback variables include the three velocity components, aircraft rates, lateral and longitudinal flapping. Control variables now include collective and lateral cyclic, on top of the previously utilized longitudinal flapping. For an elevator pulse input at 200kts forward flight,  $M_z$  is reduced by 70%. However, the SLA controller requires 4deg control authority of longitudinal cyclic pitch control, flapping contrary to pitch rate direction, reducing control margin. This SLA system, though effective in  $M_z$  reduction, requires a choice of longitudinal blade pitch authority, being a trade-off between performance and control authority.

It is interesting to note that while Voskuijl et al. [56] considers steady state response to be a main determinant for fatigue life of the flapping hinge, Manimala et al. [40] considers the overshoot of flapping to already have an unacceptable impact on fatigue life.

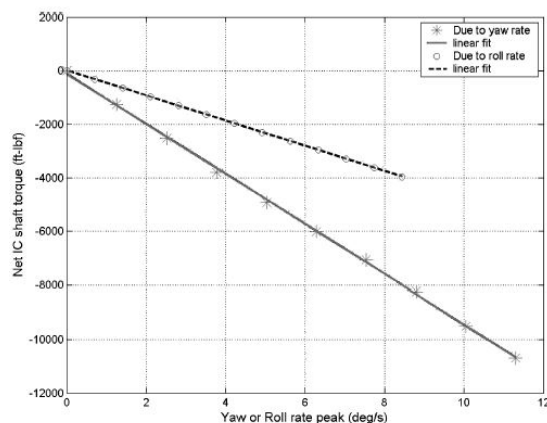


Figure 2.6: Torque split versus peak roll and yaw rate (Manimala et al. [40]).

The FCS schemes discussed above give an indication of the current state of technology; which loads have been considered critical, inspiring the development of these new FCS schemes. Assessment of these FCS schemes indicates that such systems, when designed properly, are indeed capable of significant load reductions, or provide accurate load mitigation prediction. Based on previous research, a novel SLA scheme has been developed by Voskuijl [54] to reduce main rotor loads during high speed pitching

maneuvers. However, properties such as off-design handling, safety assessment and subsequent agility performance after alterations, as well as potential weight savings due to component downsizing, are currently unknown. The previously discussed FCS systems provide insight in possible metrics and approaches to assess some of these aspects, particularly off-design performance, safety, and agility. In chapter 3, the mixed control SLA scheme and its relevance is discussed. The mixed control SLA scheme is subsequently assessed based on the above mentioned parameters.

# 3

## The mixed control SLA system

### 3.1. BACKGROUND INFORMATION AND WORKING PRINCIPLE

The mixed control SLA system developed by Voskuijl [54] aims to reduce main rotor pitch link loads and shaft bending moments when the helicopter is subjected to pitch rate command in high speed flight. This is done by deploying stabilator actuation in addition to longitudinal cyclic at the main rotor, when the pilot provides a longitudinal cyclic stick input. Functioning in the same plane as longitudinal cyclic, the stabilator's incidence change will result in a local change in lift. Being mounted at the end of a tailboom, this will result in a pitching moment. With its longer moment arm from the helicopter's center of gravity compared to the main rotor, the stabilator can significantly reduce the amount of longitudinal cyclic required, hence offloading the main rotor in terms of pitch link loads and shaft bending moments.

As both longitudinal cyclic and stabilator act in the same plane of motion, a weighted pseudo inverse (WPI) method is used to design the controller, determining the ratio of control allocation to both control surfaces. The WPI method minimized the difference between the actual control and the desired control vectors. The control vector contains longitudinal cyclic and tail incidence angle, given in equation 3.1. Vector  $v$  includes pitch rate and loads, such as pitch link loads and shaft bending moments, and is given in equation 3.2.

$$u = \begin{bmatrix} \theta_{1c} \\ i_{tail} \end{bmatrix} \quad (3.1)$$

$$v = \begin{bmatrix} \dot{q} \\ Load \end{bmatrix} = \begin{bmatrix} \dot{q} \\ 0 \end{bmatrix} \quad (3.2)$$

SLA controller design is performed around one design condition, in terms of center of gravity, weight, airspeed, inflow and interference conditions. The SLA system is designed using a linear model of the UH-60A with a 6932kg gross weight, 9.14m center of gravity, flying at 130kts. The three state Pitt-Peters inflow model is considered at the main rotor. Interference effects of main rotor and empennage are included at the stabilator. Aerodynamic effectiveness matrix  $B$  contains results from the numerical perturbation of the fixed linear model; perturbations of vector  $v$  with respect to control vector  $u$ . This is given in equation 3.3.

$$B = \begin{bmatrix} \frac{\partial \dot{q}}{\partial \theta_{1c}} & \frac{\partial (Load)}{\partial \theta_{1c}} \\ \frac{\partial \dot{q}}{\partial i_{tail}} & \frac{\partial (Load)}{\partial i_{tail}} \end{bmatrix} \quad (3.3)$$

Control allocation between longitudinal cyclic and stabilator incidence is determined through WPI formulation. For off-design conditions, the ratio of control allocation will remain unchanged. The explanation given here on the determination of control allocation is rather topical, as this research is mainly concerned with the application of the SLA system; not with its development. For more detailed information on the WPI algorithm or its application in the specific development of this SLA system, please consult Bordignon [9] and Voskuijl [54] respectively.

A schematic of the entire longitudinal control architecture, including the mixed control SLA system, is shown in fig. 3.1, as applied to the nonlinear UH-60A helicopter simulation model used for assessment.

Pilot input is provided in the form of a loadfactor. This is converted into a desired pitch rate, using airspeed. The helicopter's pitch rate response is compared to the desired response, forming a feedback loop. This longitudinal control architecture, with the exception of the mixed control SLA system component, represents a simple (auto)pilot system, providing corrective action for differences in desired and actual pitch rate. Therefore, the longitudinal control architecture excluding the SLA system and helicopter dynamics will be referred to as the 'longitudinal controller' in this research, and forms an outer loop of the control system. This so-called longitudinal controller should not be confused with the entire longitudinal control architecture, which also encompasses the SLA controller. Of main importance is the mixed control SLA system included within the longitudinal control system architecture, translating a required pitch rate via means of control allocation to tailplane incidence deflection and longitudinal cyclic. The SLA system is depicted in figure 3.2, including the control allocation from the WPI analysis. The baseline UH-60A, not featuring the SLA system, is modeled with the same longitudinal control architecture, yet circumventing SLA control allocation, indicated as the 'SLA OFF' control signal; only longitudinal cyclic is actuated for the required pitch rate, while the stabilator remains at a zero incidence angle. The stabilator is limited to  $-8\text{deg}$  (trailing edge up) and  $39\text{deg}$  (trailing edge down) incidence deflections. Throughout this research, the baseline UH-60A will be used as a reference for the conventional UH-60A, in order to determine differences in response and performance.

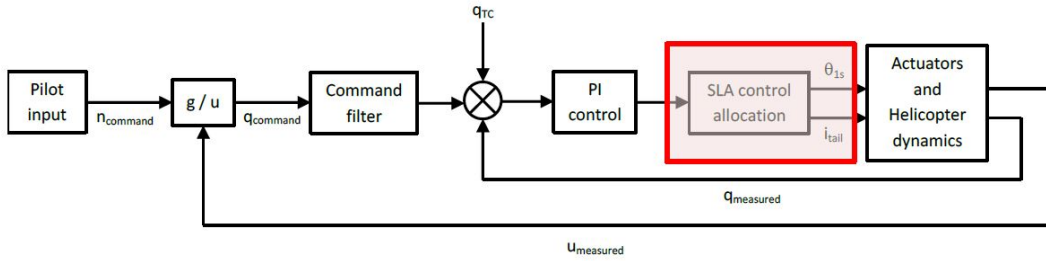


Figure 3.1: Longitudinal control system architecture with SLA functionality (Voskuijl [54]).

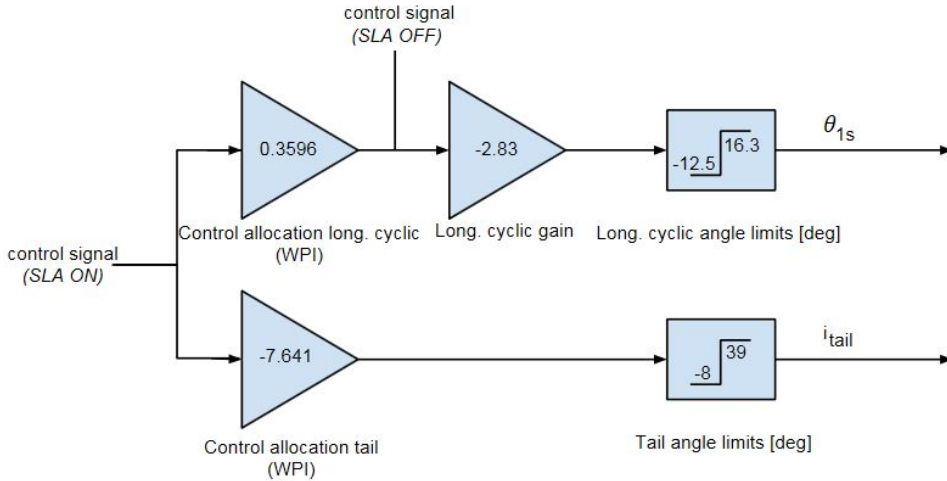


Figure 3.2: The mixed control SLA system architecture, depicting tail incidence and longitudinal cyclic control allocation.

The manoeuvre used for assessment is a doublet, starting from level flight at 130kts, followed by a pull-up and reaching a  $1.75g$  loadfactor after 2 seconds. Subsequently, opposite longitudinal cyclic stick input is provided for 2 seconds resulting in a minimum loadfactor of  $0.5g$ . After this, stick longitudinal cyclic is set to return to level flight. This manoeuvre will be referred to as the  $1.75g$  doublet throughout this research.

For all results provided in this section, the helicopter is operating in the design conditions of the SLA system; airspeed upon manoeuvre entry, helicopter gross weight and center of gravity being the same as for the design condition.

Fig. 3.3 shows the airspeed, height and loadfactor transients as the SLA and baseline UH-60A perform the 1.75g doublet maneuver.

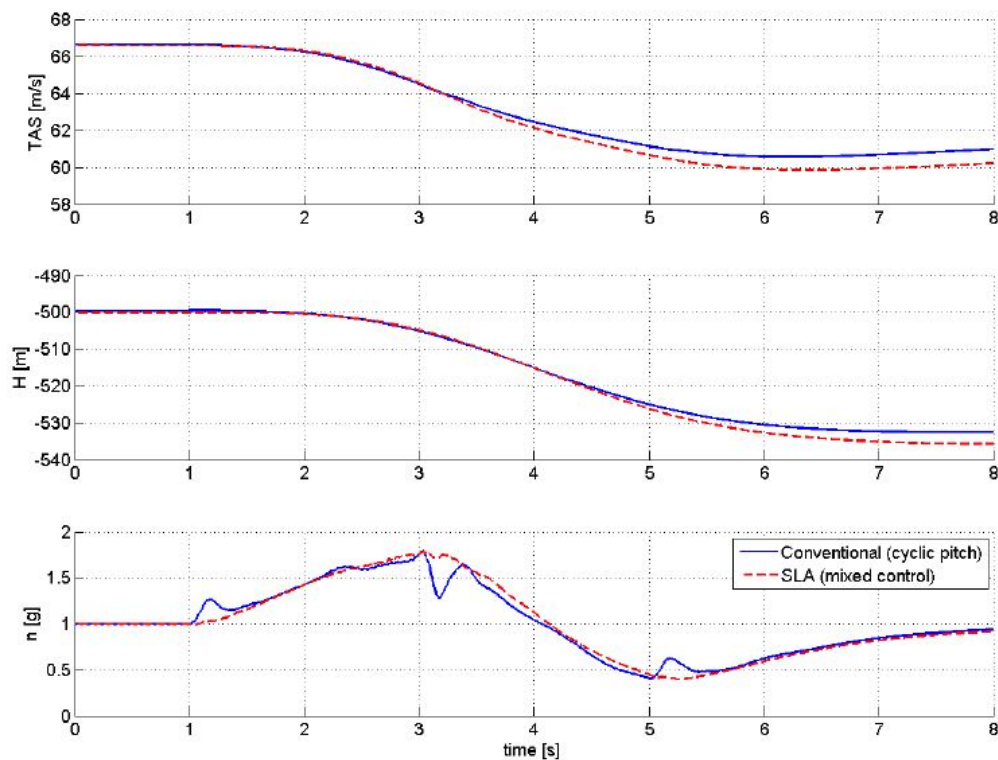


Figure 3.3: Velocity, altitude and load factor for a doublet input at 130kts forward flight (Voskuijl [54]).

Load alleviation capability is expressed in terms of load quickness. This metric is provided in equation 3.4, and divides the peak load by the change in pitch attitude. Therefore, with three hub forces and three hub moments, six load quickness values are found.

$$Q_{li} = \frac{|F_{imax}|}{\Delta\theta}, Q_{li} = \frac{|M_{imax}|}{\Delta\theta} \quad (3.4)$$

Table 3.1 indicates the altered loads, as compared to the baseline UH-60A performing the same maneuver. As can be seen, average load reduction of 25.3% is achieved for all hub forces and moments combined. Fig. 3.3 furthermore shows a very small influence on height and true airspeed (TAS) for the 1.75g doublet.

Table 3.1: Achieved load alleviation in terms of load quickness (Voskuijl [54])

Hub load	Max allev. of load (load quickness)
$F_x$	32.8 %
$F_y$	27.5%
$F_z$	6.3 %
$M_x$	56.9 %
$M_y$	30.2 %
$M_z$	-2.2 %
Avg.	25.3 %

To gain insight in the differences in control actuation that allows for these reductions, fig. 3.4 is provided. As is evident from this figure, the stabilator now reduces incidence angle (trailing edge moves

up), increasing downwash from the main rotor, generating part of the pitch-up moment. This reduces the pitching moment requirement at the main rotor. As such, the amount of longitudinal cyclic needed to generate a given pitch rate is lower, resulting in reduced blade flapping and a lower shaft bending moment  $M_y$ . The significance of shaft bending moments is presented further on in chapter 3.3. A detailed analysis on the cause of all six loads is provided in chapter 4.

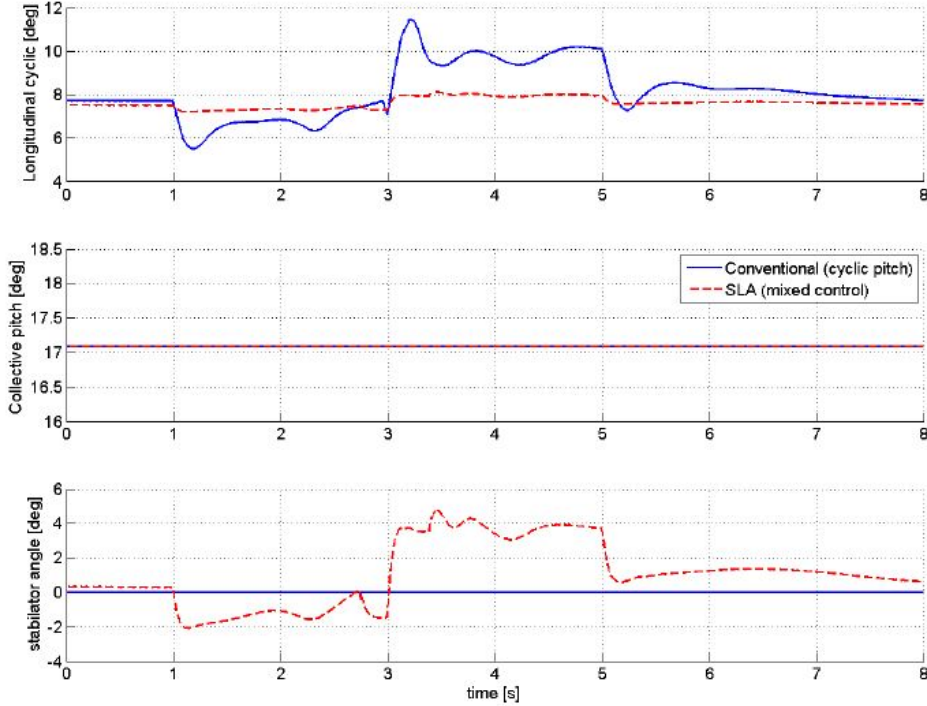


Figure 3.4: Longitudinal control usage for a doublet input at 130kts forward flight (Voskuijl [54]).

Aside from load reduction, it is desirable to either maintain or enhance handling qualities, as compared to the baseline UH-60A. Since response in longitudinal axis is of primary concern, attitude quickness is assessed. This metric gives an indication of how rapidly aircraft attitude can be changed, and is defined as the peak pitch rate for a change in pitch attitude, as given in equation 3.5. For three push-pull longitudinal stick commands of varying intensity starting from 130kts level flight, attitude quickness is equal to or two percent higher than the baseline helicopter.

$$Q_{\theta} = \frac{q_{pk}}{\Delta\theta_{max}} \quad (3.5)$$

The reader is reminded of the SLA system presented by Voskuijl et al. [57], aimed at reducing pitch link loads and shaft bending moments by solely deploying longitudinal cyclic. While direct comparison of results from from both systems may not be fair, since different maneuvers are carried out, the smaller decrease in altitude and airspeed while performing a more aggressive maneuver implies that the performance trade-off is smaller for the mixed control SLA system of Voskuijl [54], to attain similar load envelope protection. This is also because Voskuijl [54] does not apply changes in collective to reduce loads, instead relying on stabilator actuation to change aircraft attitude and flightpath. The amount of control authority of longitudinal pitch used by the mixed control SLA system, shown in figure 3.4, is smaller than that of the conventional SLA system of Voskuijl et al. [57].

Aside from the mixed control SLA system, the UH-60A simulation model also features a lateral-directional control system. This latter system functions completely separately and independently from the SLA system. While the mixed control SLA scheme allocates longitudinal stick inputs to two co-planar control surfaces, the lateral-directional controller aims to remove cross-coupled helicopter response. As such, an input in pitch should not cause adverse rolling or yawing motion. This controller

is shown in figure 3.5.

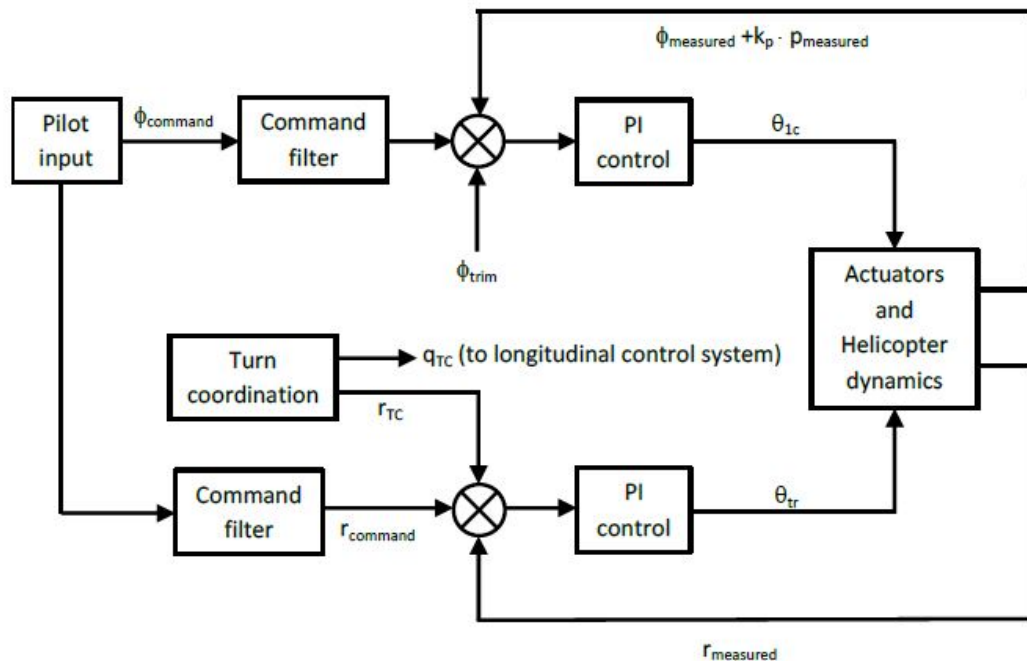


Figure 3.5: The lateral-directional controller (Voskuijl [54]).

While load reduction capability and handling qualities are promising when operating in design conditions, the feasibility of this system will also depend on off-design performance, safety after SLA system failure, potential weight savings caused by component downsizing, or the increase in permitted gross weight. However, before assessing these properties, information will be provided on why this SLA system is of particular relevance for application on the UH-60A helicopter.

### 3.2. SELECTION OF HELICOPTER

The helicopter to be assessed is the Sikorsky UH-60A Blackhawk, depicted in fig. 3.6. The reason for choosing this particular helicopter is fourfold. Firstly, the UH-60A currently features a variable horizontal stabilizer, known as a stabilator. If the mixed control SLA system proves to be safe, its application would be most easily accommodated on a helicopter currently featuring a stabilator, requiring minimal modifications to the tail plane assembly. Secondly, Kufeld and Bousman [34] show that this particular helicopter experiences severe loads during given pull-up maneuvers such as the UTTAS mission task element (MTE). These loads, in the form of pitch link loads and shaft bending moment, are discussed further in section 3.3. Thirdly, there is ample available data for this helicopter type. Lastly, this helicopter type is still in production, while 4,000 Blackhawk helicopters have been built since 1974. Financial feasibility is more likely if the SLA system is applied to one of world's most sold helicopters; implementable as minimal-redesign retrofit or incorporated in the FCS design of new Blackhawk helicopters.

Currently, the stabilator is actuated to maintain an almost constant aircraft attitude for all flight regimes. The current stabilator scheduling scheme is shown in figure 3.7. At flight speeds below 35 knots, the main rotor wake causes a large download on a fixed incidence horizontal tailplane, causing a strong nose-up attitude. This unfavorable nose-up tendency was experienced during initial flight tests with the UH-60A prototype that initially featured such a fixed horizontal stabilizer. To counter this adverse effect, the UH-60A was modified to feature a stabilator (Prouty [47]). At speeds below 35 knots, the stabilator is tilted to its maximum positive pitch angle, aligning the tail surface with the main rotor downwash and reducing the download. As forward velocity increases, the stabilator pitch angle is reduced to maintain similar lift properties to maintain an almost constant nose attitude. Figure 3.8 shows the pitch attitude with variations in airspeed for the UH-60A with stabilator versus

fixed stabilizer. From the fixed incidence stabilizer configuration, it is evident that the main rotor wake has a larger presence at low speed, providing more download, causing a stronger pitch up moment. At higher forward speeds where the horizontal stabilizer experiences less interference effects, the stabilizer is controlled by the stability augmentation (SAS) and flight path augmentation (FPS) control schemes (Cooper [13]). The SAS system has two functions: to increase longitudinal cyclic margin, and to provide short term rate damping in pitch, roll and yaw axes. With increased airspeed, the SAS system will cause the stabilator to gradually decrease its incidence angle. This is done to create another control trim situation; the tail experiences less lift, and longitudinal cyclic is decreased to fly in trim. This in turn increases the longitudinal cyclic static margin to increase maneuverability, where additional longitudinal cyclic is available at the upper end of the actuator range. The importance of longitudinal cyclic static margin at high speed flight is elaborated on in section 5.3, where actuator limits are chosen. The second SAS function is to provide short term rate damping along the three axes. For pitch rate damping, use is solely made of stabilator deflection. Functioning in tandem with the SAS system, the FPS system determines the amount of longitudinal cyclic and stabilator deflection required to maintain a fixed pitch attitude in cruise flight.

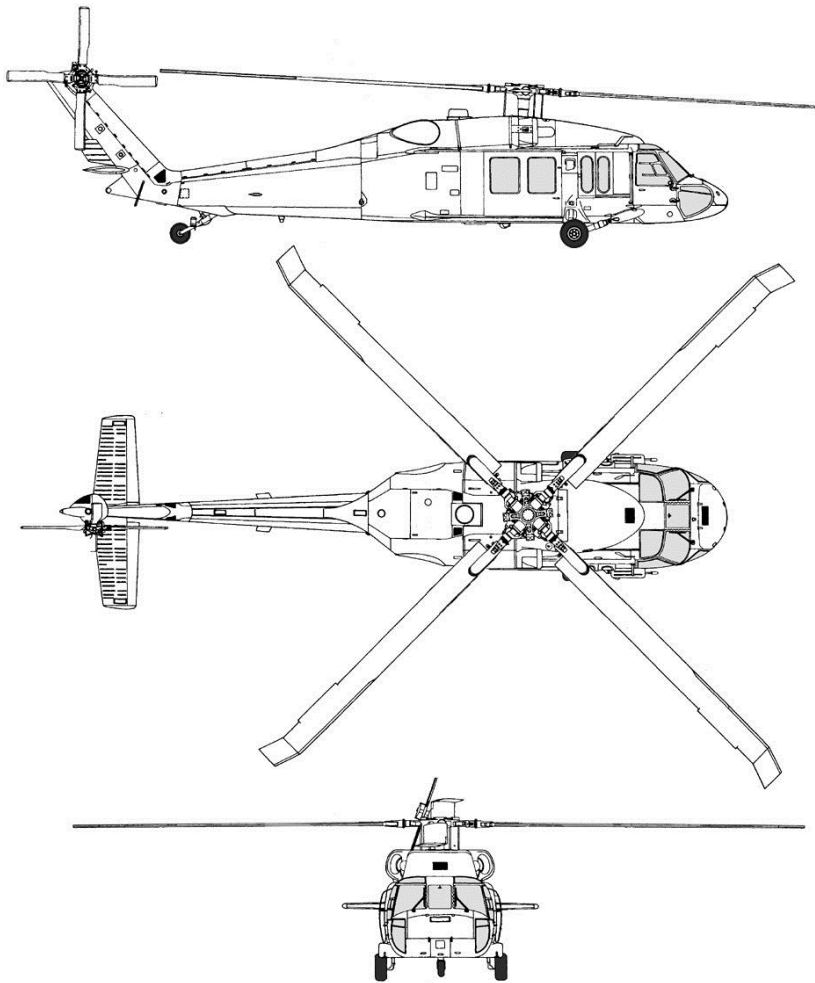


Figure 3.6: The Sikorsky UH-60A Blackhawk helicopter (Ref. nr[1]).

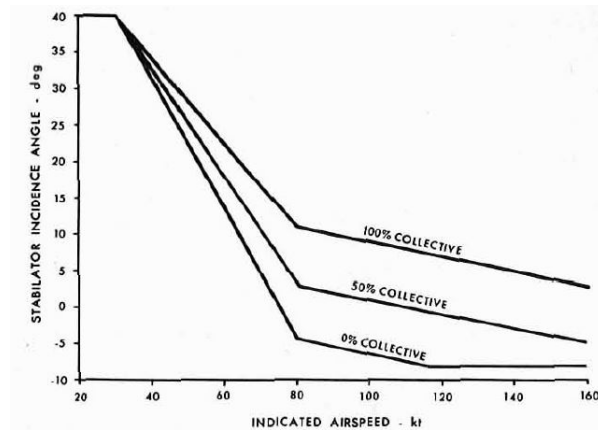


Figure 3.7: The current stabilator schedule of the UH-60A Blackhawk (Cooper [13]).

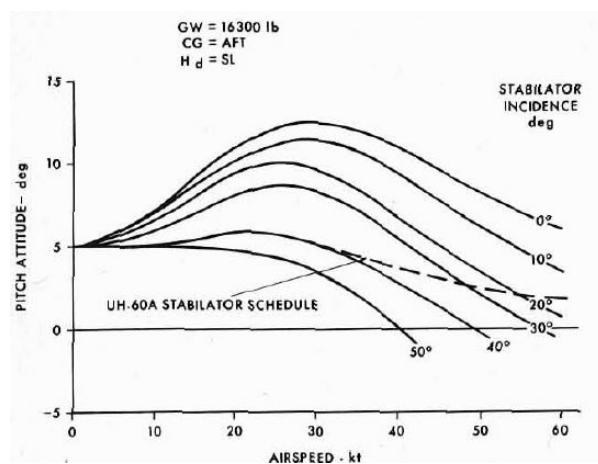


Figure 3.8: Level flight pitch attitude of UH-60A Blackhawk (Cooper [13]).

### 3.3. RELEVANCE OF THE MIXED CONTROL SLA SYSTEM AND SELECTION OF MANEUVER

The mixed control SLA system aims to reduce the pitch link loads and shaft bending moments in the main rotor. These loads are significant and increase in magnitude with airspeed and load factor. To gain insight in the nature and significance of these loads, their cause and their severity, various references are consulted. First, pitch link loads will be discussed, followed by main rotor shaft bending moments.

#### THE SIGNIFICANCE OF PITCH LINK LOADS DURING LONGITUDINAL MANEUVERS

Through means of flight tests, Datta and Chopra [15] show the variation of pitch link loads on a given blade for a complete revolution of 360 degrees. Figure 3.9 is included for clarity. Starting from the rear, the first quadrant shows positive loading, followed by negative loading in the second quadrant, indicating the characteristic positive-negative oscillation with tension at the rear and compression at the front. This is shown in figure 3.10. During each complete revolution, the blade encounters a maximum given load at a certain location. Fig. 3.12 demonstrates that this maximum pitch link load encountered during a revolution increases with forward velocity. Therefore, pitch link loads may pose a severe threat to the operational life of a helicopter, especially in the high speed regime. An SLA system that can reduce loads in these components can significantly lengthen the helicopter's operational life while also reducing maintenance costs.

Kufeld et al. [33] performs a similar analysis, conducting flight tests with the UH-60A. When flying in cruise with constant airspeed, these loads will, as expected, repeat for each following cycle. This is shown in fig. 3.11. The transient pattern of the pitch link loads for a single revolution are furthermore in agreement with those shown in fig. 3.10.

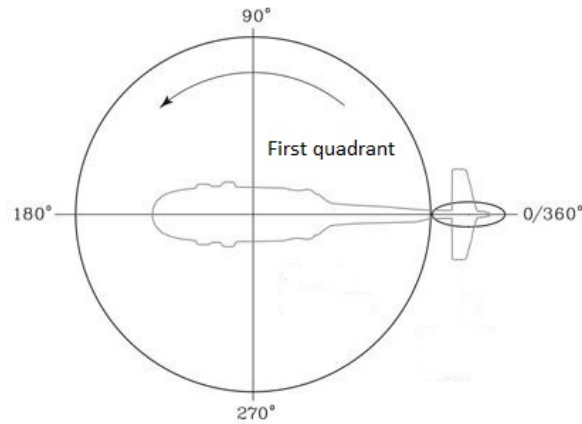


Figure 3.9: A schematic of the four quadrants as the main rotor completes a full revolution.

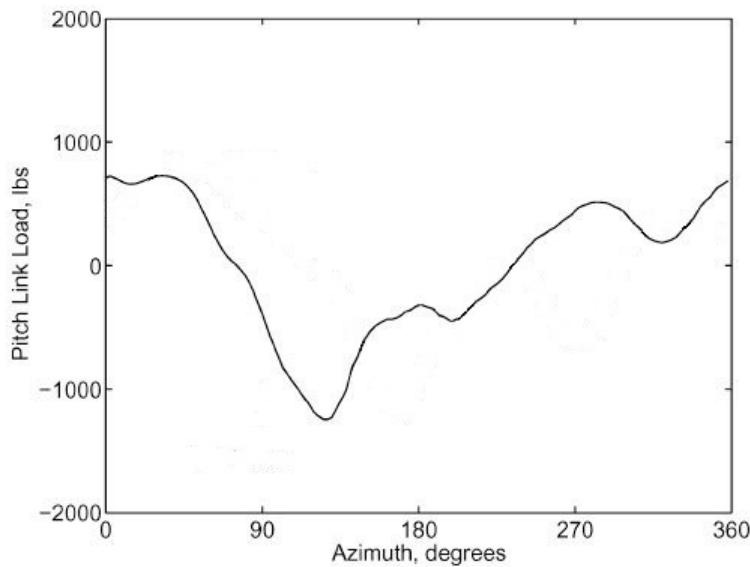


Figure 3.10: Flight test data concerning pitch link loads of the UH-60A as a function of azimuth, for level flight (Datta and Chopra [15]).

Kufeld and Bousman [34] perform flight tests assessing 68 maneuvers set in the UH-60A Airloads Program based on pitch link loads, torsion moment, blade flap bending and blade chord bending moment. Within the UH-60A structural envelope it is found that two maneuvers, the UTTAS maneuver, and the maximum dive speed maneuver, have the largest impact on pitch link loads. The maximum dive speed maneuver is a classic design parameter for helicopters, requiring a pull-up following a dive at maximum dive speed. Contrary to the maximum dive speed manoeuvre, the UTTAS maneuver starts from 130kts level forward flight and includes a pull-up, where a maximum loadfactor of 2.1g must be attained. During this pull-up, the loadfactor must also exceed 1.75g for at least 3 seconds, followed by a push-over, maintaining a loadfactor of 0g for at least 2 seconds. During this maneuver, the helicopter may not lose more than 30kts of its initial airspeed (Kufeld and Bousman [34] and Yamakawa et al. [60]). The UTTAS maneuver was set in the Utility Tactical Transport Aerial System (UTTAS) program which resulted in the development of the UH-60A. The reason for this new maneuver was the requirement by the US military that the new helicopter would be able to maneuver over objects suddenly encountered during high speed, low altitude flight with sufficient agility, such as buildings or trees. The strict conditions set in the UTTAS maneuver however proved unfeasible; the UH-60A Blackhawk could perform a 2.1g pull-up, but could not maintain a loadfactor exceeding 1.75g for 3 seconds (Kufeld and Bousman [34]).

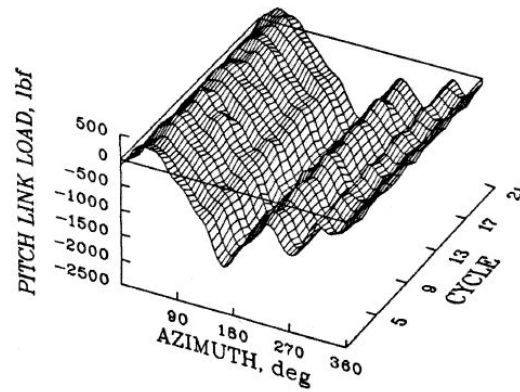


Figure 3.11: Pitch link loads as a function of blade azimuth and cycle for the UH-60A in forward flight (Kufeld et al. [33]).

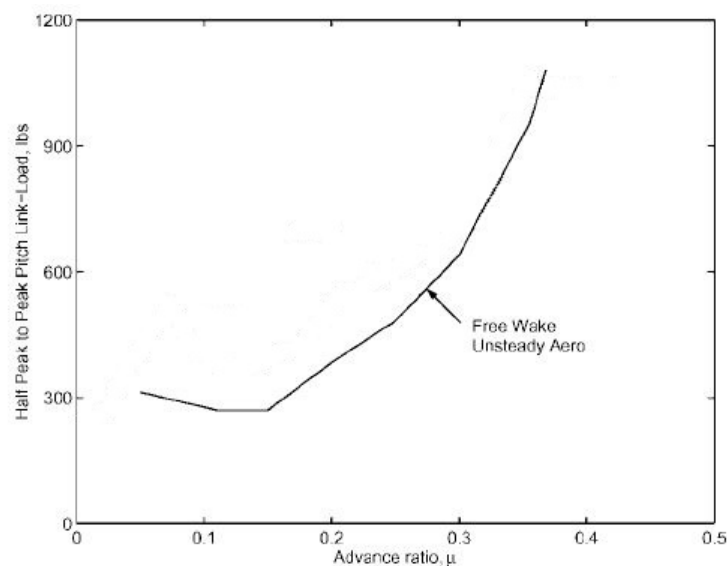


Figure 3.12: Pitch link load variations with advance ratio for the UH-60A (Datta and Chopra [15]).

While the pitch link loads have a cyclic nature, the maximum amplitude not only increases with higher forward velocity, but also increases significantly during a pull-up manoeuvre. This is shown in fig. 3.13. Here, the maximum pitch link load is plotted for three different pull-up manoeuvres, where the UTTAS manoeuvre proves to pose the greatest threat to the pitch link fatigue life. The cause of the high alternating pitch link loads can be found in fig. 3.14. As the number of revolutions progress, three areas with large negative blade pitch moment coefficients can be identified. This indicates that blade stall occurs at these azimuth angles, causing large compressive loads on the pitch links. While Kufeld and Bousman [34] do not provide an explanation for this 3 per rev stall pattern, to the best knowledge of the author, the two stall regions near the rear of the disc occur due to interference flow from the helicopter body. The stall occurring on the right hand side of the rotor disc, as the blade moves forward, is most likely caused by flow separation, resulting from the large angle of attack of the blade at this location. This local large angle of attack is required to force the rotor disc to move maximally up at the front.

From fig. 3.13 it is evident that the UTTAS manoeuvre has the most pronounced effect on pitch link loads for the UH-60A, making it the manoeuvre of choice to assess the impact on pitch link loads with or without the SLA mixed control system in place.

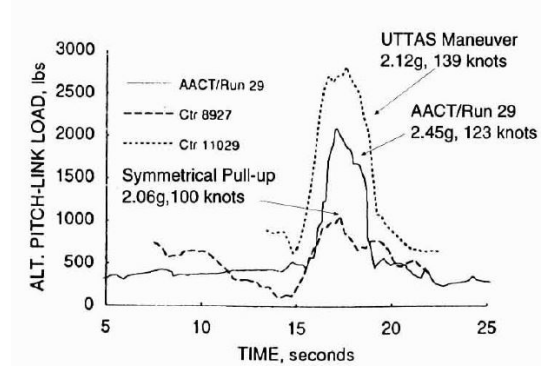


Figure 3.13: Pitch link loads as a function of blade revolution and azimuth during a UTTAS pull-up maneuver (Kufeld and Bousman [34]).

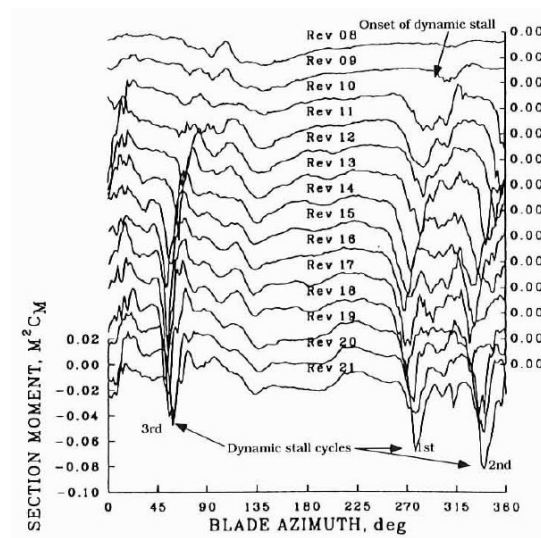


Figure 3.14: Offset plot for pitch link loads per revolution during a UTTAS pull-up maneuver (Kufeld and Bousman [34]).

### THE SIGNIFICANCE OF SHAFT BENDING MOMENT DURING LONGITUDINAL MANEUVERS

Unlike pitch link loads, the shaft bending moment is related to blade flapping. As given in equation 3.6, Yeo et al. [62] relates the main rotor hub moment  $M_H$  to the main rotor shaft moment  $M_{Hs}$  and to flapping  $\beta$ . Therefore, main rotor shaft bending moment is related to flapping. In this equation,  $F_c$  is the centrifugal force,  $e_\beta$  is the bearing offset, and  $\beta_1$  is the first harmonic flap angle. This equation is applicable for both bending moments  $M_y$  and  $M_x$ , using longitudinal or lateral flapping respectively.

$$\begin{aligned} M_H &\cong M_{Hs} \\ M_H &\cong M_{H\beta} \cong 2e_\beta F_c \sin \beta_1 \end{aligned} \quad (3.6)$$

The notion that main rotor shaft bending moment is related to first harmonic bending is further reaffirmed by Yeo and Johnson [61]. This states that “the hub moment derived from flap angle measurement shows a good agreement with the measured shaft bending moment, which means the shaft bending moment and 1/rev flap angle measurement are consistent.” Similarly, Kufeld et al. [33] calculates shaft bending moments on the basis of 1/rev blade flapping. This is compared to measured shaft bending moments as experienced during flight tests. Results are provided in fig. 3.15. Here, it can be seen that calculated shaft bending moments for the first and third blade (flap 1 and 3) is in close accordance with the measured shaft bending moments, lying on or in close proximity to the identity line. From this, one can deduce that shaft bending moments are closely related to blade flapping, as the latter can be used to predict the former with high accuracy. Because of the strong correlation between blade flapping and shaft bending moment, Howitt [25] develops a tactile cueing system using blade flapping instead of a neural network to predict shaft bending moment excursions. This system is referred to as the non-linear

inversion (NLI) system. Equation 3.7 indicates the amount of demanded longitudinal flapping based on the difference in desired and actual pitch rate, and the longitudinal shaft bending moment. Subscript  $d$  indicates demanded quantities, while  $s$  indicates a measured sensor value. In similar fashion, the demanded lateral flapping is determined, considering demanded and sensed roll rate, and lateral bending moment. While this system is developed for a bearingless rotor, being more prone to bending moment stresses than articulated rotors (Howitt [25]), equation 3.7 may still be applied for an articulated rotor, substituting eq. 3.6 for bending moment caused by longitudinal cyclic. Howitt et al. [26] develops a similar system, requiring rotor state feedback, limiting flapping angles to avoid shaft bending moment exceedance. This source confirms the causal relationship between flapping and bending moments; roll and pitch hub moments being the result of out-of-plane flapping.

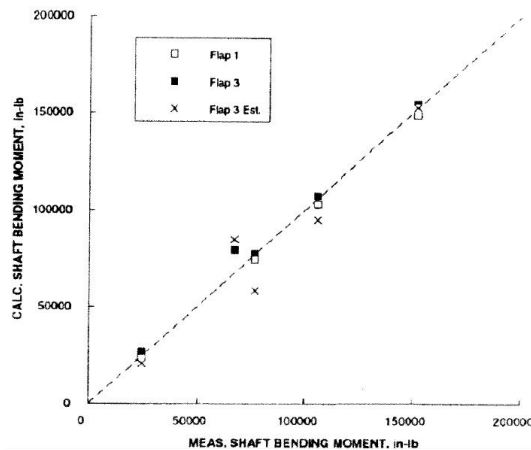


Figure 3.15: Calculated versus measured shaft bending moment for the UH-60A, based on blade flapping (Kufeld et al. [33]).

$$\beta_{1cd} = (\dot{q}_d - \dot{q}) \frac{I_{yy}}{M_{H\beta_{1c}}} + \beta_{1cs} \quad (3.7)$$

Having determined the relation between blade flapping and shaft bending moments, it becomes evident that this load reaches critical levels during any pitching or rolling motion. With a commanded change in blade longitudinal cyclic, the blades change incidence angle at either side of the rotor, causing maximum flapping to occur at the front and rear of the rotor disc, with resultant rotor shaft bending moments around the longitudinal axis of the rotor shaft. Similarly, changes in blade lateral cyclic will cause maximum flapping at the front and rear of the rotor disc, with a shaft bending moment around the rotor's lateral axis. For this reason, Howitt [25] assesses the effectiveness of the NLI scheme based on a pitch step input, stating that such maneuvers currently cause large transient peak hub moments. Findings by Gotzfried [18] support this reasoning, subjecting the Eurocopter TIGER helicopter to various mission task elements during flight tests. Within the structural load envelope of shaft bending moment, it can be seen that a pull-up and push-over indeed yield some of the highest experienced shaft bending loads. This is shown in fig. 3.16. While shaft bending moment intensity will differ for the UH-60A helicopter, the notion remains the same; that commanded changes in attitude cause increased flapping and a higher shaft bending moment. From fig. 3.16, it can also be seen that a push-over causes shaft bending loads of opposite sign as compared to a pull-up. An opposite moment around the rotor's longitudinal axis is required, forcing the blades to flap and the rotor disc to tilt in opposite direction. That these loads are approximately of similar magnitude for the same intensity stick command demonstrates that the rotor's center of gravity is in close proximity of the helicopter's center of gravity, along the lateral axis. As such, the required moment around the longitudinal axis is similar for a nose-up or nose-down command of similar intensity. Therefore, blade flapping will be of similar magnitude yet in opposite direction.

From the aforementioned, it can be concluded that the UH-60A is subjected to elevated pitch link loads and rotor shaft bending moments during manoeuvres involving pitch attitude changes; the UTTAS manoeuvre in particular. Because the mixed control SLA system makes use of stabilator actuation to

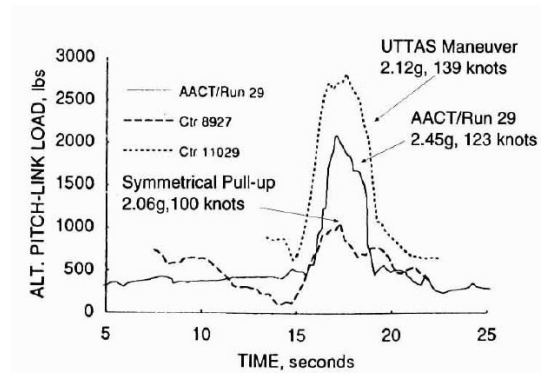


Figure 3.16: Pitch link loads as a function of blade revolution and azimuth during a UTTAS pull-up manoeuvre (Gotzfried [18]).

change download resulting in a pitching moment, the amount of required rotor longitudinal cyclic is reduced. This reduces pitch link loads resulting from a smaller stall region at the advancing blade, as well as longitudinal shaft bending moments, because of less longitudinal flapping. With this system, by altering control allocation between stabilator and rotor longitudinal cyclic, one could hypothetically even create opposite blade flapping to a pitch rate command. This would require increased stabilator deflection and negative control allocation to longitudinal rotor cyclic, now providing a local countering pitch moment component to the desired pitch rate. The working principle is similar to the SLA systems proposed for tiltrotors by Manimala et al. [39] and Manimala et al. [40], utilizing elevator and opposite rotor longitudinal cyclic during a pitching manoeuvre. However, such SLA systems require greater control authority. As such, the mixed control SLA system with the previously determined control allocation will be assessed, applying reduced rotor longitudinal cyclic in the same direction as desired pitch rate, as compared to the baseline helicopter. In design conditions, it has already been shown that this system adequately reduces loads while maintaining handling qualities. However, for this SLA system to be feasible in real-life, off-design performance must also be assessed; the helicopter will not always fly at 130kts, with a fixed gross weight and center of gravity. In the proceeding chapter, the helicopter's off-design performance will be assessed after discussing the simulation model; its scope and limitations.

# 4

## Flight dynamics, loads and off-design performance

While the SLA system has proven capable of load reductions when operating in design conditions, its off-design performance is also a determinant in determining system feasibility. Further assessment of the proposed SLA system must be done by means of flight tests, wind tunnel tests, or by means of a high fidelity simulation model. Of these approaches, a simulation model is the method of choice. With recent developments in simulation model fidelity, the more complex dynamic and aerodynamic behavior of helicopters can be captured with more accuracy, while costs are lower than flight or wind tunnel tests. In the past, simulation models were very basic and were mainly tailored to fixed-wing applications. Higher fidelity for helicopter simulations required significant computational power. More recently, Advanced Rotor Technology Inc. (ART) has developed the Flightlab simulation tool, allowing for the rapid development and assessment of high fidelity helicopter simulation models. A simulation model for assessment of this SLA system should incorporate the following properties:

- Allow for analysis of a non-linear dynamic model
- Allow for incorporation of control systems and pilot inputs
- Assess transient properties such as helicopter height, airspeed, pitch attitudes, rates, inflow properties and loads at local components, as well as control deflections
- Incorporate interference effects of main rotor and empennage at the stabilator
- Allow for selectable fidelity through use of alternatives in component modeling
- Allow for viscous and stall effects on section lift and drag coefficients at the main rotor
- Allow for large angle of attack effects on section lift and drag coefficients at the stabilator

The analysis of a non-linear dynamic model is of importance in this assessment since the helicopter will perform maneuvers with large variations in state variables, such as pitch attitude. A linear model, incorporating parameter sensitivities around a slightly perturbed trim state, will therefore not suffice. As the Flightlab simulation environment allows for the above properties, it is chosen to use this tool. To allow for the final two requirements, a lookup table is used, based on wind tunnel data, incorporating viscous effects and stall. However, one of the most significant downfalls of helicopter simulation tools to date has been the inability to properly model the effects of the main rotor at the horizontal tail. In practice, the wake flow at the horizontal tail has proven to be highly irregular and has not been properly predicted (Prouty [47]). Simulation results must therefore be validated based on flight test data.

In the following section, the Flightlab simulation model will be covered in more detail; model assumptions and resulting limitations. The helicopter's off-design conditions will be determined in section 4.3, from which off-design performance will be assessed in section 4.3.3.

## 4.1. FLIGHTLAB SIMULATION MODEL THEORY

The model used for analysis is a UH-60A Blackhawk helicopter featuring the SLA system in the Flightlab environment. The model is composed of numerous subcomponents, each designed under certain assumptions. The helicopter is an assembly consisting of multiple rigid bodies with 6 degrees of freedom (DOF). The tail rotor is modeled as a Bailey rotor, inflow at the main rotor is modeled using the Pitt-Peters dynamic inflow model, while the main rotor blades are aerodynamically modeled under the quasi-steady assumptions. The main rotor is modeled as an articulated rotor, similar to the actual UH-60A. The stabilator's aerodynamic properties are found through a lookup table. In this section, the above mentioned modeling approaches will be evaluated as compared to alternatives. Limitations and the impact of these approaches on results will furthermore be discussed.

### 4.1.1. EQUATIONS OF MOTION

In the Flightlab simulation environment, the equations of motion are modeled by means of multi-body dynamics. The helicopter model consists of multiple rigid bodies that are connected through various joints. The subcomponents include the empennage, the main rotor, tail rotor, vertical tail, stabilator, engine shafts and landing gear. The main and tail rotor are assemblies containing hinges and blades. The rotor blades are modeled as being rigid; neglecting aeroelastic effects such as blade bending and torsion. By means of hinges, the blades will change incidence and will subsequently flap and feather. The assumption of rigid blades is acceptable due to the importance of first harmonic behavior of flapping and inflow model, as elaborated on in section 3.3. The non-elastic assumption of blades primarily effects predictions of higher harmonic phenomena related to vibratory behavior (Padfield [42]). Some components will see structural and/or aerodynamic loads. Through the multi-body formulation, these forces and moments are transmitted to adjacent components, resulting in a non-linear dynamic model for the helicopter as a whole. The dynamic model used for assessment is left in non-linear form, since the model is subjected to a range of differing conditions, with large variations in airspeed, center of gravity and aircraft attitude. Since analysis does not occur for small perturbations around a trim state, a linear model should not be used. In the most generic form, when contributions of all individual components are grouped together, the equations of motion can be expressed as given in eqs. 4.1 through 4.4, according to the reasoning of Boiffier [8]. In these equations consider the helicopter to solely consist of rigid bodies; omitting elastic properties. Here,  $F_{aero,fuse}$  and  $M_{aero,fuse}$  indicate aerodynamic forces and moments experienced by the fuselage, in the body reference frame.  $I_{fuse}$  and  $m_{fuse}$  are the helicopter's inertia and mass. In this basic representation, fuselage mass, inertia and experienced loads are grouped together in a single term. In the multi-body dynamic model, these will be a sum of all individual components, translated and rotated with respect to one another. Six equations of motion are included; three translations and three rotations around the three primary axes.

$$\begin{pmatrix} \dot{x}_N \\ \dot{x}_E \\ \dot{x}_Z \end{pmatrix} = \begin{pmatrix} V_N \\ V_E \\ V_Z \end{pmatrix} \quad (4.1)$$

$$\begin{pmatrix} \dot{u} \\ \dot{v} \\ \dot{w} \end{pmatrix} = - \begin{pmatrix} qw - rv \\ ru - pw \\ pv - qu \end{pmatrix} + g \begin{pmatrix} -\sin\theta \\ \cos\theta \sin\phi \\ \cos\theta \cos\phi \end{pmatrix} + \frac{F_{aero,fuse}}{m_{fuse}} \quad (4.2)$$

$$\begin{pmatrix} \dot{p} \\ \dot{q} \\ \dot{r} \end{pmatrix} = I_{fuse} \left[ M_{aero,fuse} - \begin{pmatrix} p \\ q \\ r \end{pmatrix} \times \left[ I_{fuse} \begin{pmatrix} p \\ q \\ r \end{pmatrix} \right] \right] \quad (4.3)$$

$$\begin{pmatrix} \dot{\phi} \\ \dot{\theta} \\ \dot{\psi} \end{pmatrix} = \begin{pmatrix} 1 & \frac{\sin\theta \sin\phi}{\cos\theta} & \frac{\sin\theta \cos\phi}{\cos\theta} \\ 0 & \cos\phi & -\sin\phi \\ 0 & \frac{\sin\phi}{\cos\theta} & \frac{\cos\phi}{\cos\theta} \end{pmatrix} \begin{pmatrix} p \\ q \\ r \end{pmatrix} \quad (4.4)$$

### 4.1.2. TAIL ROTOR MODEL

The Bailey rotor model (Bailey [6]) is used to approximate the tail rotor. This approach makes significant simplifications in modeling a rotor, for a small trade-off in accuracy. Here, thrust coefficient, flapping coefficient, torque coefficient and profile power are reduced to simple functions of inflow velocity

and collective blade pitch angles. Being a tail rotor, lateral and longitudinal cyclic are not considered as control variables. The Bailey rotor assesses an articulated rotor with no hinge offset. Effects of blade solidity and the blade mass constant are neglected. A generic blade mass constant of 15 is taken, lying between the normal range of 0 to 25. This model also states that a rotor with non-linear twist can be accurately predicted by modeling a blade that has linear twist, when the  $\frac{3}{4}$  span blade pitch of the non-linearly twisted blade is used. As such, blade twist is considered linear, while blade chord is also assumed to be uniform. Blade section lift coefficient is taken to be linear while section drag is given by a second order drag polar. These coefficients are given in equation 4.5.

$$\begin{aligned} c_l &= c_{l\alpha}\alpha \\ c_d &= \delta_0 + \delta_1\alpha + \delta_2\alpha^2 \end{aligned} \quad (4.5)$$

The Bailey rotor model ignores stall, compressibility and radial flow effects and assumes uniform inflow. With all simplifications in place, section lift and drag coefficients over the entire rotor disc deviate by around 5% for variations in mass constant. Of the thrust coefficient, flapping coefficient, torque coefficient and profile power, thrust coefficient is the parameter least accurately predicted, deviating by 9% from the exact formulation. For models not requiring extremely high fidelity of tail rotor behavior, errors of this magnitude are acceptable, reducing the complexity of aerodynamic equations significantly.

While the above section indicates accuracy of the Bailey rotor, it is also of importance to know in which conditions this modeling technique is permitted. Figure 4.1 displays the section profile drag increment estimated by this approach, versus the actual value. According to Bailey [6] this approach is valid until a normalized difference of section lift coefficient and optimal section lift coefficient of 0.8. It is also evident that when the lift coefficient is equivalent to the optimal lift coefficient, the theory (dotted line) will over predict the section drag coefficient change. This is however not a large drawback as the helicopter will rarely operate in this optimal region. In the graph normalized values above 0.8 show increasingly inaccurate results in terms of drag prediction, amongst other aerodynamic coefficients. To determine the angle of attack where the normalized difference in lift coefficients is equal to 0.8, eq. 4.6 is applied. This therefore provides the maximum allowable angle of attack for which the Bailey rotor simplifications are still valid. These high angles of attack will always occur at some part of the rotor on the retreating side when the helicopter has a forward speed, but its effects on accuracy are negligible if this region is very small. Combinations of blade pitch and tip speed ratio determine this maximum angle of attack. Also, at the advancing blade, compressibility shock is not predicted by this approximation method. Therefore there is a maximum advance ratio for which this approach is acceptable. Hence, the two limiting conditions for the Bailey Rotor model are: maximum velocity and angle of attack, being the result of blade pitch and tip speed ratio, avoiding shock at the tip.

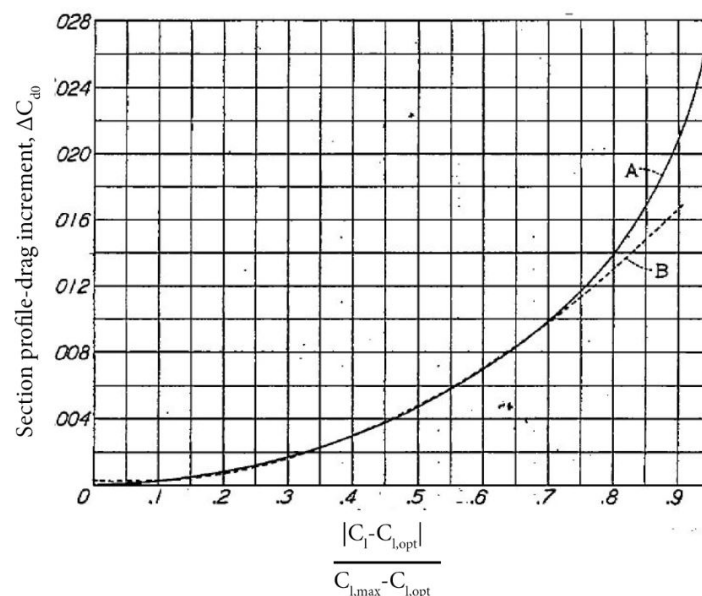


Figure 4.1: Section profile drag coefficient versus normalized difference in section lift coefficient, used to determine validity of Bailey Rotor (Bailey [6]).

$$\alpha_{\tau_{lim}} = \frac{0.8c_{l_{max}} + 0.2c_{l_{opt}}}{c_{l\alpha}} \quad (4.6)$$

Concerning the application of the Bailey rotor to this specific research, the angle of attack is considered to be sufficiently small at high speed flight. The decrease of angle of attack with increased forward airspeed is depicted in figure 4.2. Also, in actual flight conditions, the tail rotor may not see uniform inflow, being affected by the main rotor wake, resulting in torque, power and thrust prediction inaccuracies. Nonetheless, as this research is aimed at assessing the performance of the SLA system, the aerodynamic behavior of the stabilator and main rotor is of primary concern. Since the Bailey rotor model does not predict an induced flow field, it is assumed that there is no interference effect of the tail rotor on the stabilator. Therefore, the Bailey rotor does not directly affect the performance of the SLA system in the simulation environment. In actual flight, at high speed conditions, the stabilator will most likely see no interference from the tail rotor either. Being a so-called push configuration, the tail rotor expels air at a downward angle towards the vertical tail. The 20deg cant angle was introduced in the UH-60A design to generate additional vertical lift. Judging from the tailplane geometry provided in figure 4.3, the condition where interference will most likely occur is the (near)hover condition. Being canted, the tail rotor may cause some interference on the right side of the stabilator at the intersection with the vertical tail. However, judging from the geometry, this interference will most likely have been diminished at low forward airspeeds. Furthermore, the powerful main rotor wake traveling over the stabilator will also deflect the tail rotor wake. Since this SLA system will be activated at high speed flight, potential interference between tail rotor and stabilator at low speed is not of importance. Thus, the application of the Bailey rotor assumption is considered acceptable. Bailey rotor model inaccuracies solely affect the tail rotor performance; tail rotor torque, power and thrust predictions, with no effect on the stabilator. These local tail rotor parameters are not of primary interest in the assessment of the stabilator and the SLA system as a whole.

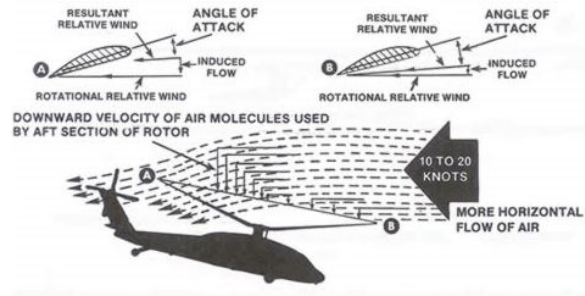


Figure 4.2: A side view of the UH-60A, showing a reduced angle of attack with increased airspeed (ref.nr4 [3]).

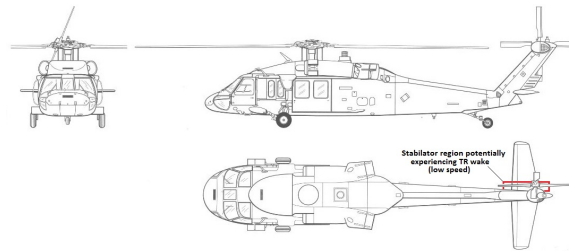


Figure 4.3: A top view of the UH-60A, showing tail rotor downwash on the stabilator for variations in forward airspeed.

#### 4.1.3. MAIN ROTOR INFLOW MODELS

Inflow models can be categorized into three main groups: static, dynamic and free wake models. In this section, static inflow models are discarded, based on their inability to predict rotor loads properly. Two dynamic inflow models are considered; the Pitt-Peters and the Peters-He inflow models, while one free wake model is considered; the Scully inflow model. It is decided to apply the Pitt-Peters inflow model, due to its rapid ability to predict dynamic behavior of the main rotor with sufficient accuracy.

For low bandwidth maneuvers, dynamic interactions between the airflow with the rotor and airframe may be considered negligible at low speed forward flight. This is because there is no significant change in how the airflow passes through the rotor over time, hence not significantly changing blade motion. In such situations, momentum theory will properly provide inflow conditions. Static inflow models assume an instantaneous change in induced velocity caused by changes in rotor inflow, predicting instantaneous load alterations. However, for large changes in aircraft motion over a short time interval, dynamic interactions between the airflow with the rotor and airframe need to be taken into account, altering airflow through the rotor significantly, changing the rotor loads. In forward flight, rotor dynamics will change; blades will flap and may show vibratory response. Since these phenomena do not occur instantaneously after inflow changes, a static model cannot accurately predict these phenomena and the resulting blade loads in forward flight. For such situations, a dynamic inflow model must be applied. As the airflow must be accelerated to reach a new inflow state, dynamic inflow models use a time constant to account for the lag in the development of inflow components. In this section, two such dynamic inflow models will be covered; the Pitt-Peters and the Peters-He inflow models presented by Pitt and Peters [45] and Peters and He [44] respectively. A downfall in dynamic inflow models is vortex and wake predictions. Free wake inflow models determine the rotor induced velocity field as caused by contributions of trailing, shed and bound vortices at a given point in the inflow field. In forward flight, a rotor will shed a wake that affects the induced velocity field of preceding blades. One such free wake inflow model is considered here, known as the Scully inflow model.

In an attempt to model unsteady airloads, Pitt and Peters [45] have developed a linear model that relate the thrust, roll moment and pitch moment rotor loads to the transient response of the induced flow field. Here, the disturbed induced inflow and pressure distributions are given by equation set 4.7.

$$\begin{aligned} \lambda &= \lambda_0 + r\lambda_s \sin(\psi) + r\lambda_c \cos(\psi) \\ P &= \sum_{m=0}^1 \sum_{n=m+1}^{m+3} P_n^m(v) Q_n^m(i\eta) [C_n^m \cos(m\psi) + D_n^m \sin(m\psi)] \end{aligned} \quad (4.7)$$

The total inflow of the rotor consists of three components.  $\lambda_0$  signifies uniform inflow, while  $\lambda_s$  and  $\lambda_c$  correspond to the side-to-side and the fore-aft inflow gradients respectively.

$$[M] \begin{Bmatrix} \lambda_0 \\ \lambda_s \\ \lambda_c \end{Bmatrix}^+ + [L]^{-1} \begin{Bmatrix} \lambda_0 \\ \lambda_s \\ \lambda_c \end{Bmatrix} = \begin{Bmatrix} C_T \\ -C_L \\ -C_M \end{Bmatrix} \quad (4.8)$$

Equation 4.8 follows from the dynamic and static pressure superposition, where M and L represent the apparent mass and dynamic inflow gain matrices respectively. It is this equation which relates the inflow to the resulting thrust, pitching and rolling coefficients as experienced by the rotor. Intuitively, it makes sense that the thrust coefficient depends on the uniform inflow component, while the pitching and rolling coefficients depend on the side-to-side and fore-aft inflow components respectively, due to gyroscopic motion. However, the Pitt-Peters model is a lower order approximation only considering three states. The model only takes into account the zeroth and first harmonics as well as one radial shape per harmonic.

In a follow-up, Peters and He [44] have developed a model where the pressure distribution includes higher harmonic terms. Each harmonic term is defined by an arbitrary number of radial functions. Inflow is now radially described by a polynomial function, and by a Fourier series azimuthally. As such, the Peters-He model can describe inflow based on any witnessed main rotor inflow; unlike the Peters-Pitt model, which prescribes inflow based on lift, thrust and moment coefficients. In theory, the Peters-He inflow model can be expanded to include any number of inflow states; not being bound to three states as the Pitt-Peters model. Increasing the number of states will increase model fidelity, yet reduce real-time ability of rotor dynamics and response (Horn et al. [23]). Since the control systems of the simulated UH-60A require helicopter dynamic response feedback to alter controls, this real-time capability is of importance; helicopter dynamics should be determined rapidly, not lagging in feedback response. For this reason, Flightlab includes a relatively low, six-state Peters-He inflow model.

The new pressure distribution as given by the Peters-He inflow model is provided in eq. 4.9.

$$P = -\frac{1}{2} \sum_{m=0}^{\infty} \sum_{n=m+1, m+3, \dots}^{\infty} P_n^m(v) Q_n^m(i\eta) [\tau_n^{mc} \cos(m\psi) + \tau_n^{ms} \sin(m\psi)] \quad (4.9)$$

In a different analytical framework, free wake models differ from the dynamic inflow models, relating the rotor induced velocity to individual contributions caused by trailing, shed and bound vortices at a given location in the inflow field. Therefore, inflow is not prescribed by controls, or by prescribing the inflow pressure distribution directly, as done in the Pitt-Peters and Peters-He inflow models. Including the influence of vortices in the inflow field should allow for higher accuracy of rotor load predictions. The Scully inflow model (Scully and Sullivan [50] and Kaufmann [32]) has been developed along the lines of the free wake inflow approach, and is based on preceding work by Rankine.

The Rankine [49] inflow model uses a simple algebraic formula to determine swirl velocity of a vortex, as provided in equation 4.10. Here,  $r$  is the radial location,  $r_c$  is the viscous core radius, being the distance from the core till maximum swirl velocity, and  $\Gamma$  is the circulation.

$$v_\theta(r) = \begin{cases} \left(\frac{\Gamma}{2\pi r_c}\right) \frac{r}{r_c} & 0 \leq \frac{r}{r_c} \leq 1; \\ \left(\frac{\Gamma}{2\pi r_c}\right) \frac{r_c}{r} & \frac{r}{r_c} > 1. \end{cases} \quad (4.10)$$

However, at the viscous core radius, there is a discontinuity. To alleviate this discontinuity, the Scully inflow model has been devised. The swirl velocity is given by equation 4.11.

$$v_\theta(r) = \frac{\Gamma}{2\pi r_c} \left( \frac{r}{r_c^2 + r^2} \right) \quad (4.11)$$

Vatistas and Mih [53] have expanded this theory to include multiple swirl velocity components by including integer  $n$ , as shown by equation 4.12.

$$v_\theta(r) = \frac{\Gamma}{2\pi} \left\{ \frac{r}{(r_c^{2n} + r^{2n})^{\frac{1}{n}}} \right\} \quad (4.12)$$

Note that when  $n = 1$ , we have the Scully inflow swirl velocity. Figure 4.4 shows the various swirl velocity predictions for different free wake inflow models. Also included is the Lamb-Oseen vortex model, which is not elaborated on for sake of brevity. The discontinuity of the Rankine model is also shown in this figure.

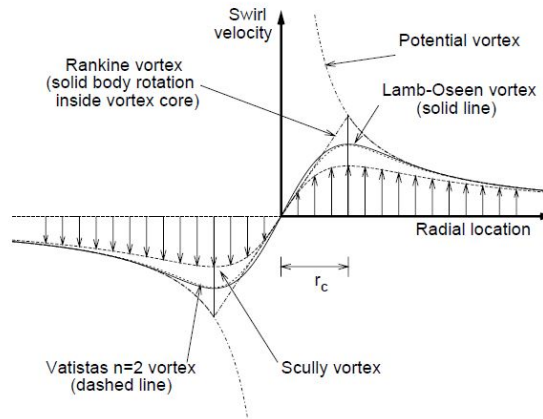


Figure 4.4: Distribution of induced swirl velocity inside a viscous vortex core on the basis of several models (Bahgwat and Leishman [5]).

Of the various free wake models, the Scully inflow model is included in Flightlab. More complex free wake models are not included as these require such significant computation time, that real-time analysis is not possible. Since the control systems require feedback of the helicopter's dynamic states during the maneuver, real-time dynamic response is essential for analysis.

Of the three inflow models presented, the Pitt-Peters dynamic inflow model is used instead of the other two models of higher complexity. First, the load prediction performance of the Pitt-Peters versus the Peters-He dynamic inflow models is discussed. Subsequently, the Pitt-Peters inflow model is compared to the Scully free wake inflow model.

Hamers and Basset [20] state that in dynamic flight conditions, the Peters-He inflow model performs similarly as compared to the Pitt-Peters model, except in the analysis of vibrations and aeroelasticity. Considering the manoeuvre for assessment and the rigid blade modeling, the Pitt-Peters inflow model is deemed sufficient. Secondly, of primary concern in this research is the prediction of 1/rev flapping which forms the main contribution to shaft bending moments, as made evident in section 3.3. As such, the zeroth and first harmonics of inflow are considered sufficient, as provided by the Pitt-Peters inflow model.

A free wake model will in theory provide higher accuracy in terms of induced velocity and loads prediction, when flying in conditions where blade-vortex interactions are significant. Chen [11] assesses load prediction of the Pitt-Peters inflow model as compared to free wake models for various maneuvers, gaining insight for which conditions the simpler Pitt-Peters inflow model is acceptable. Chen [11] concludes that the Pitt-Peters inflow model works well overall in hover, low speed and high speed conditions. In conditions where in-ground effect (IGE) is present, the free wake approach should be applied. Horn et al. [23] states the importance of free wake models in the analysis of vortex ring states. However, as the mixed control SLA scheme will be applied at high speed out-of-ground (OGE) flight, the contribution of vortices in the rotor inflow field may be ignored; the Pitt-Peters inflow model allows for quicker dynamic response analysis with an acceptable trade-off in accuracy.

For this reason, the main rotor of the UH-60A is modeled with the Pitt-Peters inflow model in Flightlab. In chapter 5.5, results of the Pitt-Peters inflow model will be compared to those of the Peters-He and Scully inflow models, to determine the extent of deviations in results.

#### 4.1.4. AERODYNAMIC BEHAVIOR OF BLADES

Aerodynamic loads such as forces and moments can be modeled as being steady, quasi-steady or unsteady. Steady aerodynamics assume that the airflow around an airfoil remains constant, hence, no changes in angle of attack or circulation, meaning that forces and moments will not change over time. Based on momentum theory for an actuator disc, Glauert [17] prescribes the lift experienced by the rotor in forward flight by eq. 4.13. Here  $v_i$  is the induced velocity.  $V'$  is the effective forward velocity, being the airflow's speed as witnessed by the disc. The actuator disc theory treats the main rotor, composed of the individual blades, as a uniform actuator disc. Therefore, the lift does not account for rotational velocity; the velocity increase at the advancing side of the rotor disc is equal to the decrease in velocity at the retreating side. Hence, lift is also considered to be uniform over the disc. This approach, while simple, neglects any dynamic flow phenomena which occur during normal helicopter operation. The local angle of attack of a blade element changes according to collective and cyclic inputs, and is furthermore influenced by the blade twist angle, elastic torsion, blade flapping velocity and elastic bending. Aside from local angle of attack effects, induced downwash caused by the wake system, and local velocity perturbations caused by tip vortices significantly impact airloads across a rotor disc (Wright and Cooper [59]).

$$\begin{aligned} L &= 2\pi R^2 \rho V' v_i \\ V' &= \sqrt{(v_i - V \sin\alpha)^2 + (V \cos\alpha)^2} \end{aligned} \quad (4.13)$$

In a first attempt to model changes in loads due to alterations in airflow, quasi-steady aerodynamics relate an airfoil's velocity perturbation due to heaving and pitching motions to an effective change in circulation, as shown in fig. 4.5. By assessing the airfoil as if it were moving with constant pitching or heaving motion equal to an instantaneous value, the changes in loads for this new effective angle of attack can be determined by simply looking up corresponding loads for that effective angle of attack. Quasi-steady aerodynamics is based on thin-airfoil theory, evident through  $c_{l\alpha}$  equaling  $2\pi$ , and assuming flows to be inviscid and incompressible. From thin airfoil theory, the lift coefficient, accounting for heave and pitch, is given in eq. 4.14. Variable  $b$  denotes the semi-chord,  $\frac{c}{2}$ . Being based on thin airfoil theory, these equations will not properly account for blade stall, in assuming a constant  $c_{l\alpha}$ . In this specific Flightlab model, this inaccuracy is compensated by using a lookup table to find  $c_l$  corresponding to that specific angle of attack and Mach number, instead of assuming the always constant lift curve slope of  $2\pi$ . Values in this table are based on wind tunnel data, therefore including viscous effects and stall. The mathematical approach is rather straightforward, taking instantaneous positions and determining loads assuming constant pitch rate or heave velocity of the blade. However, in this treatment, the potential effects of accelerations in pitch or heave motion are neglected (Wright and Cooper [59]). Other frequency

or time related phenomena are neglected such as flutter or flow separation, where hysteresis causes flow reattachment at a lower angle of attack than where separation occurred. Assuming constant pitching velocities at this instance, forces and moments on the blade would be predicted incorrectly.

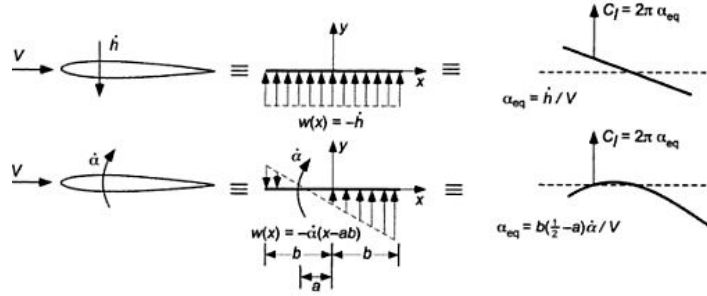


Figure 4.5: Velocity profile around a heaving or pitching airfoil, and effective resulting angle of attack and downwash (Leishman [35]).

$$C_l = 2\pi \left[ \alpha + \frac{\dot{h}}{V} + b \left( \frac{1}{2} - a \right) \frac{\dot{\alpha}}{V} \right] \quad (4.14)$$

Unsteady aerodynamics determines airfoil loads not only based on circulation changes caused by physical displacement and attitude, but also looks at time dependence. Two different approaches are utilized in the unsteady aerodynamics approach: namely in the time or in the frequency domain. In the time domain, Wagner's function takes into consideration the transient change in loads following a step change in angle of attack (Wagner [58]). According to quasi-steady theory, a step change in angle of attack would also result in an immediate step change in lift, as shown in figure 4.6. The non-instantaneous change in loads is caused by the fact that it takes time for the circulation to change around the entire airfoil. In this approach, time required for the lift to change to its final value therefore depends on the airfoil's chord length. For this reason, lift is expressed as a function of non-dimensional time, given in eq. 4.15, and indicates the time required to cover half the chord of the airfoil. Using the convolution integral, the lift is now given by eq. 4.16. The first term denotes the lift due to an initial downwash  $w_0$ , while the second term denotes the change in lift at time  $\tau$  caused by a step change at initial time  $\tau_0$ . By integrating from initial time  $\tau_0$  till the time of interest  $\tau$ , the lift is found (Leishman [35]).

$$\tau = 2 \frac{Vt}{c} \quad (4.15)$$

$$L(\tau) = \frac{1}{2} \rho V c a \left[ w_0 + \int_{\tau_0}^{\tau} \Phi(\tau - \tau_0) \frac{dw}{d\tau_0} d\tau_0 \right] \quad (4.16)$$

In the frequency domain, Theodorsen's function is used, where lift depends on frequency parameter  $k$  (Theodorsen [51]). In this approach, a bound vorticity and wake vorticity distribution, caused by harmonic excitation of the airfoil, cause a resulting downwash. The mathematical model is depicted in figure 4.7. Derivation of the lift and moment coefficients is lengthy and is not considered paramount for current intents and purposes. Therefore, the final lift equation is given in eq. 4.17 (Bisplinghoff et al. [7]). Here, the lift curve slope  $a$  is assumed to equal  $2\pi$ , as this theory is also based on thin airfoil theory. From a multi-body perspective, the first term contains accelerations in the form of linear acceleration, angular velocity, being the product of a distance times an angular rate, and an angular acceleration. The second term contains velocity terms, in the form of linear velocity, velocity under an angle, and angular velocity, this time the product of a distance times angular rate. It is evident that this lift equation takes into account the contributions of both heave and pitching motion to lift, since heave, linear velocity and acceleration are of impact. Linear displacement evidently is not. Pitching moment, pitch angle, pitch rate and pitch acceleration evidently impact airfoil lift. In this equation, variable  $b$  is equal to the semi-chord,  $\frac{c}{2}$ . As expected, compared to the quasi-steady approximation, the lift following harmonic excitation is of lower magnitude, and experiences phase lag. This is shown in fig. 4.8.

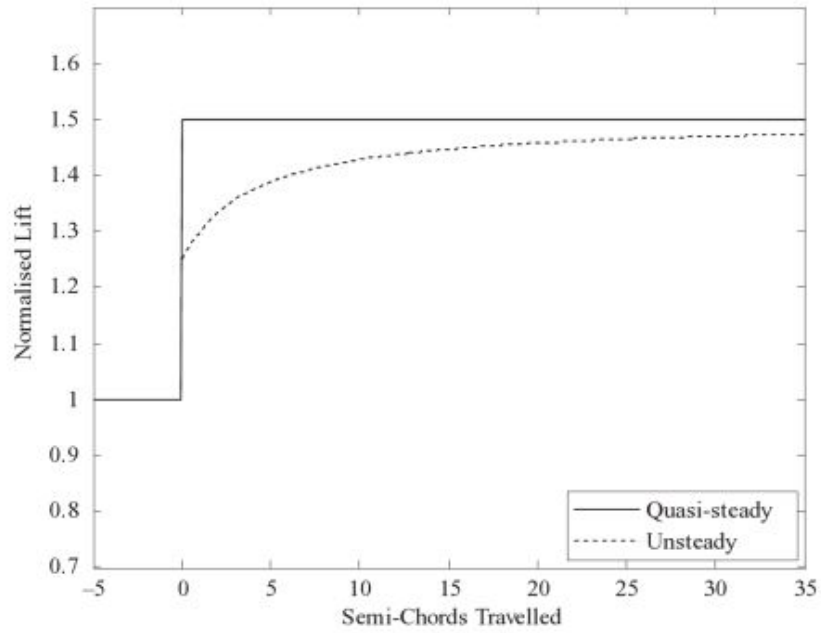


Figure 4.6: Effect on airfoil lift of an instantaneous incidence angle change, as predicted by Wagner’s function (Wright and Cooper [59]).

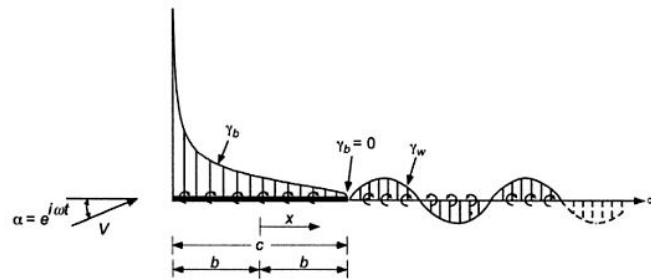


Figure 4.7: Bound vorticity and wake vorticity following a harmonic oscillatory input as modeled by Theodorsen (Leishman [35]).

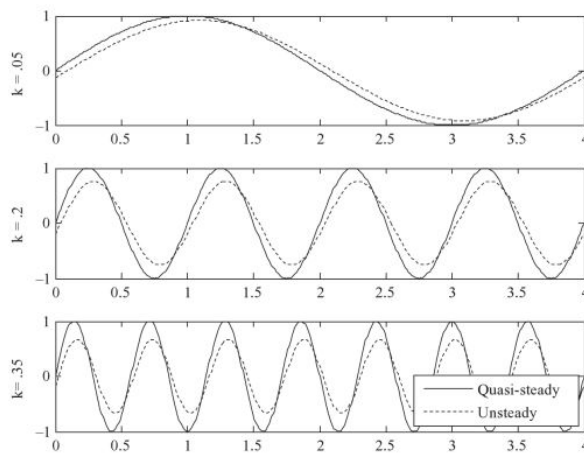


Figure 4.8: Lift over time for an oscillating airfoil at various frequencies, as predicted by Theodorsen compared to quasi-steady theory (Wright and Cooper [59]).

$$L = \pi\rho b^2 [\dot{z} + V\dot{\theta} - ba\ddot{\theta}] + 2\pi\rho VbC(k) \left[ \dot{z} + V\theta + b\left(\frac{1}{2} - a\right)\dot{\theta} \right] \quad (4.17)$$

In the Flightlab model featuring the UH-60A Blackhawk, use is made of the quasi-steady model for airflow around the main rotor blades. The reason for this, is the ease of application of this approach, modified by means of a lookup table to include stall and compressibility effects. This reduces the largest drawback associated with the quasi-steady model, namely the thin airfoil theory assumption of linear section lift. However, as the lift coefficient merely depends on an angle of attack, lift will be overestimated post-stall, as hysteresis is not considered, since the lower angle at which flow reattaches is not accounted for. Frequency-related influences which must be considered for gust or vibration analyses are furthermore neglected, as the proposed research does not look into these phenomena.

To determine the validity of results of the Flightlab model concerning research on the stabilator, it must be determined how aerodynamic properties are modeled for the horizontal tail. Furthermore, it must be determined how interference of the rotor and fuselage are accounted for at the horizontal tail. One of the most significant downfalls of helicopter simulation tools to date has been the inability to properly model the effects of the main rotor at the horizontal tail. In practice, the wake flow at the horizontal tail has proven to be highly irregular and has not been properly predicted. Evidence of this is the fact that production helicopters almost always feature a different horizontal tail, than initially designed during simulation tests (Prouty [47]).

#### 4.1.5. HORIZONTAL TAILPLANE MODELING

The horizontal tailplane is modeled as a wing featuring a NACA0012 airfoil, in accordance with the real UH-60A helicopter. Figure 4.9 shows the shape and planform of the UH-60A stabilator, and its wing-like appearance.

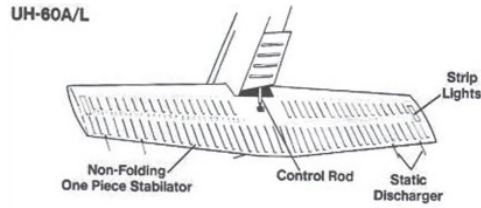


Figure 4.9: A rear view of the UH-60A stabilator (Leoni [36]).

The aerodynamic properties at the tail are determined by means of a look-up table. Fig. 4.10 depicts the section lift, drag, and moment coefficients as read in by Flightlab. These variables are a function of angle of attack and Mach number, though Mach dependency is omitted. This assumption is made because the airflow velocity at the stabilator, affected by the helicopter's airspeed and main rotor induced velocity, is still well below values for which Mach effects become significant. As the NACA0012 airfoil has no camber, the section moment coefficient will always remain zero for all angles of attack. These coefficients are considered uniform over the stabilator span. Together with sweep angle, taper ratio, stabilator span, and tip effects, these coefficients determine the stabilator's lift and drag properties. The local angle of attack at the stabilator is determined by the attitude of the helicopter, the incidence of the stabilator with respect to the helicopter fuselage, the forward airspeed and the interference components caused by the fuselage and downwash from the main rotor. As is evident from fig. 4.10, the look-up table does not consider section lift coefficient to be linear, showing stall properties at larger angles of attack. This is the main reason why a lookup table has been included in this model. Flightlab will normally assume a constant  $c_{l\alpha}$ , though this should not be assumed due to large stabilator deflection angles.

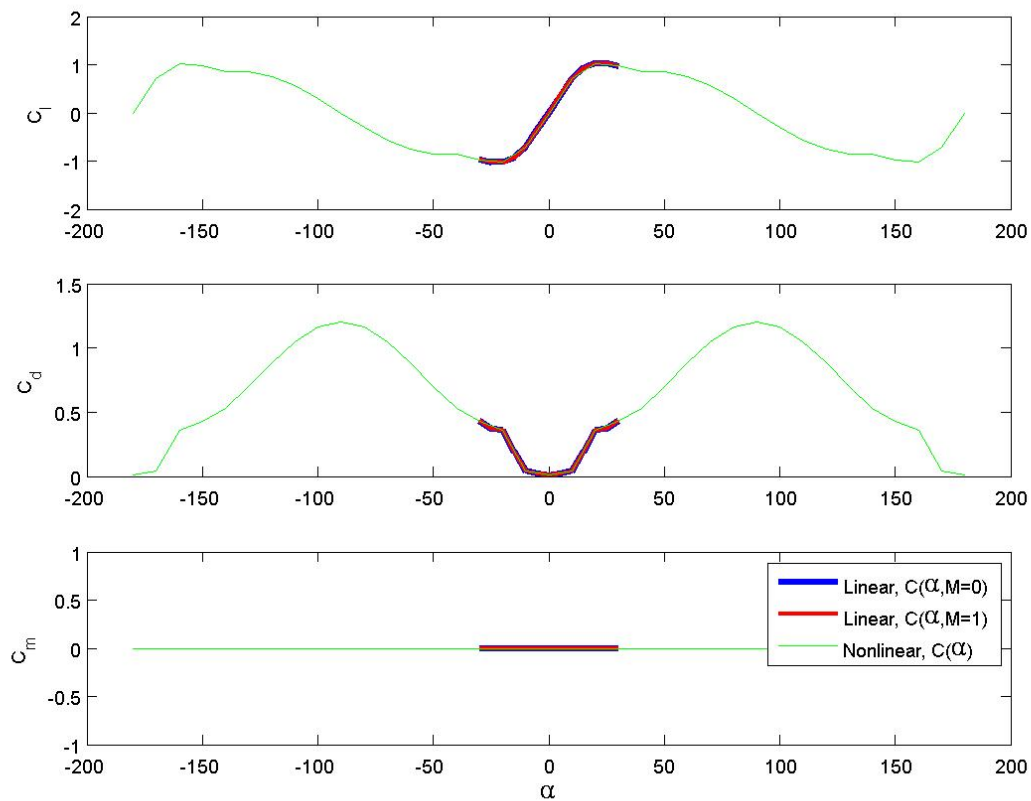


Figure 4.10: Section lift, drag and moment coefficient for the NACA0012 airfoil, read in by Flightlab.

## 4.2. SIMULATION OF MANEUVER LOADS

The UH-60A Blackhawk with mixed control SLA system has been simulated in the Flightlab environment, consisting of the aforementioned modeling components and simplifications. However, before addressing the first research question, namely SLA system's performance in off-design conditions, an explanation will be provided in the various main rotor hub loads. The severity and the causes of these loads must be understood, in order to properly assess the load reduction capability of the mixed control SLA system. The rotor hub sees loads in terms of forces and moments in or along the three principal axes. The local hub body x-axis is aligned with the helicopter's lateral axis; forward is positive. The y-axis is the longitudinal axis; right as seen from above is positive. The z-axis is the directional axis, down being positive. The hub experiences forces in x,y, and z directions, shaft bending moments around the x and y-axes, and torque along the z-axis.

Below, the transients of these six loads are displayed when the SLA helicopter performs the doublet. While the doublet causes a maximum loadfactor of 1.75g when performing this maneuver at 130kts, it should be noted that pitch rate, not load factor, is kept constant when flying the doublet at other airspeeds. Results are shown for flight with the normal center of gravity position, operating at the two airspeeds between which the SLA system may be deployed; 60kts and 160kts. In section 4.3.1, the exact airspeeds will be determined for which the SLA system should be functional. Transients for different airspeeds are shown to gain insight in the airspeed dependency of loads.

The helicopter's response in terms of angular rate transients, as well as the amount of longitudinal and stabilator control required for the doublet are shown in figures 4.11 and 4.12. Figure 4.13 includes trajectory information in terms of flightpath angle, airspeed, altitude and load factor, as the UH-60A performs the doublet. Reference will be made to these figures when discussing the various forces and loads.

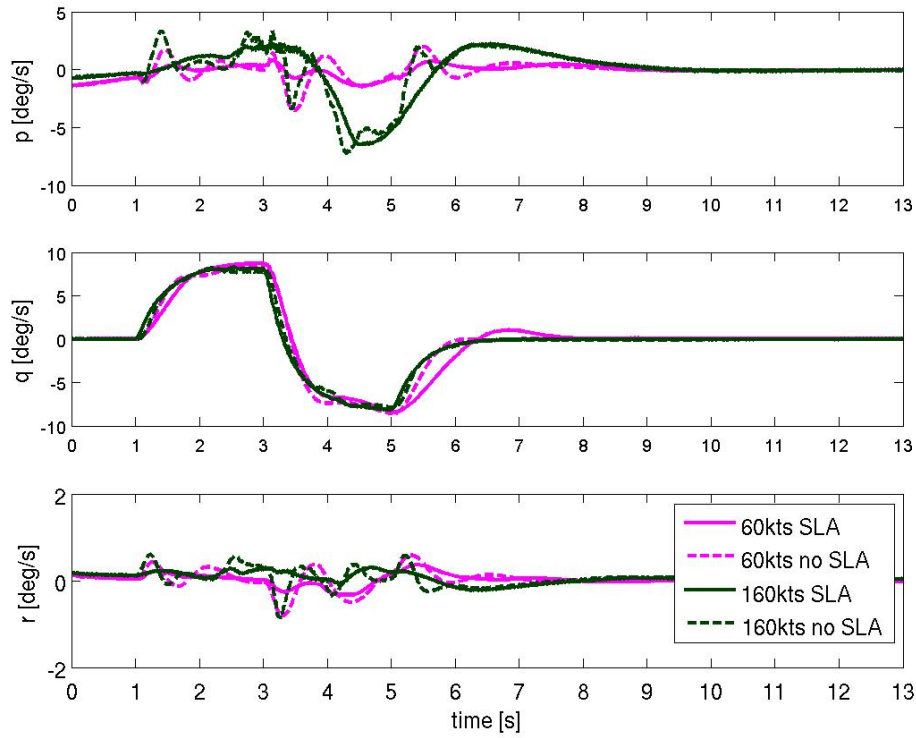


Figure 4.11: Transient of helicopter angular rates for doublet at 60kts and 160kts.

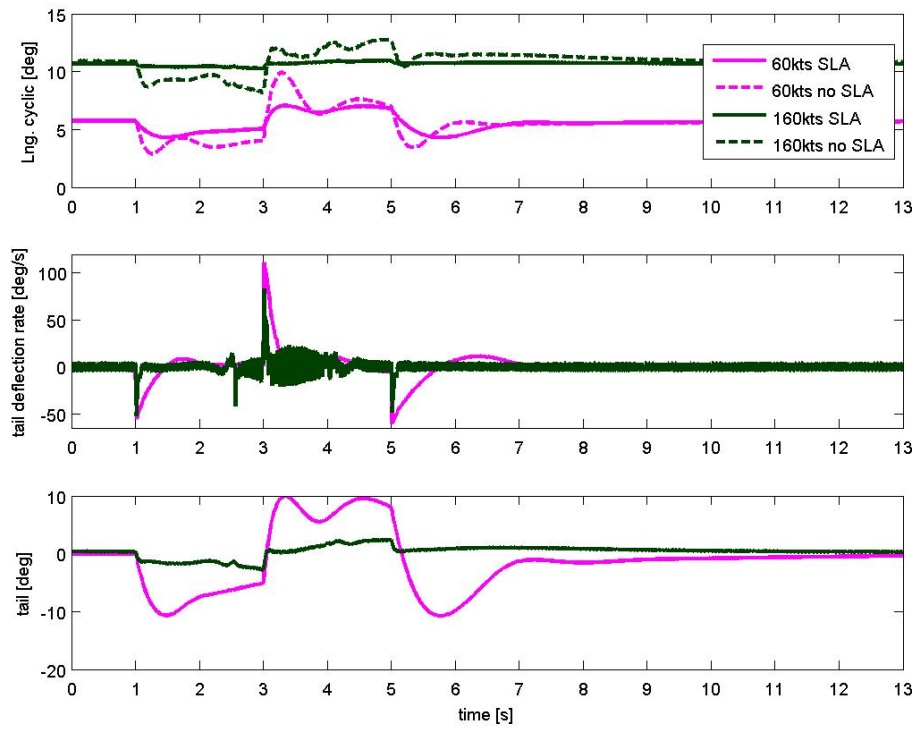


Figure 4.12: Transient of longitudinal cyclic and tail actuation for doublet at 60kts and 160kts.

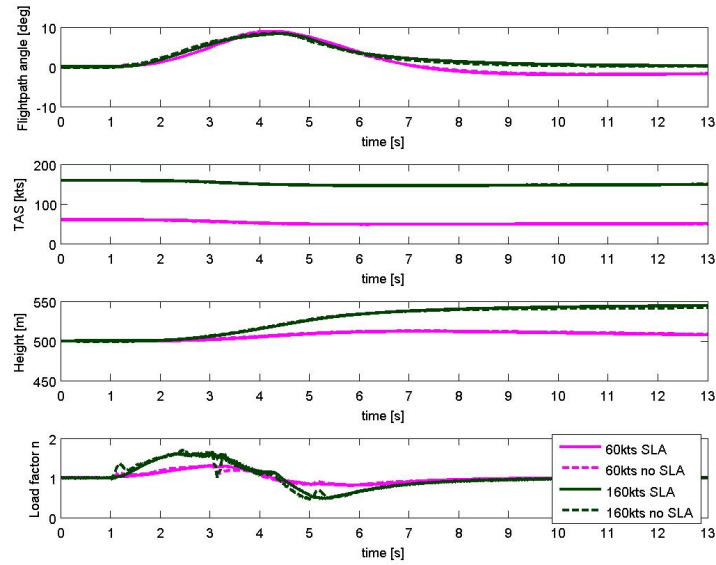


Figure 4.13: Flightpath angle, airspeed, height and loadfactor for the doublet at 60kts and 160kts.

#### 4.2.1. HUB FORCES AND MOMENTS

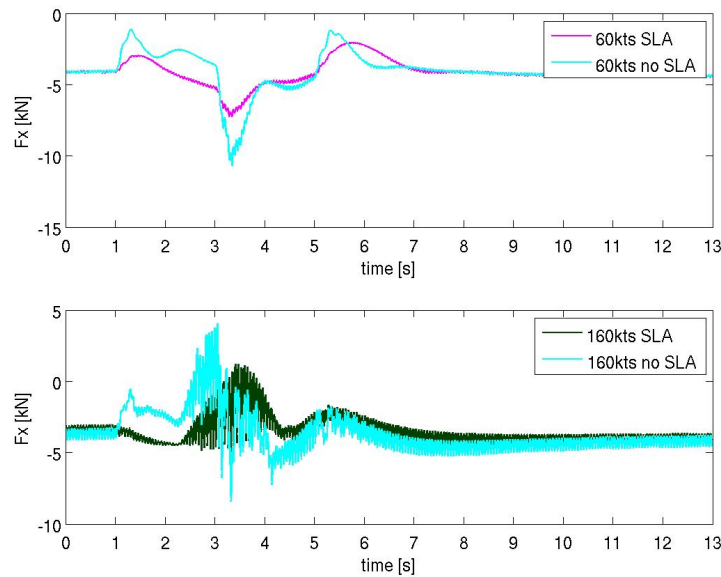


Figure 4.14:  $F_x$  with normal cg flying at 60kts and 160kts.

The force in x-direction at the main rotor shaft, shown in fig. 4.14, is mainly caused by the components of the lift- and drag forces of the rotor blades that are aligned with the shaft's x-axis. During this maneuver, this is mainly the result of longitudinal cyclic actuation at the right and left side of the rotor, rotating lift and drag forces differently in the x-z plane. A change in collective will also rotate lift and drag forces, though the control is kept the same throughout the maneuver. Aside from force rotation, lift and drag force will increase and decrease linearly as the rotor disc changes attitude with respect to the oncoming flow. Fig. 4.12 demonstrates that the SLA system uses a smaller amount of longitudinal cyclic to initiate the pull-up at high speed flight than in low-speed flight. As such, the change in blade pitch angle is smaller, meaning that the lift and drag vectors of the blade rotate less with respect to the rotor shaft axes. The baseline system solely uses longitudinal cyclic instead of

stabilator deflection to perform the doublet. As more longitudinal cyclic is used compared to the SLA system, the blade lift and drag vectors rotate more in the rotor shaft  $x$ - $z$  plane, where the lift vector aligns itself more with the shaft  $x$ -axis, and drag aligns itself more with the shaft  $z$ -axis. Therefore, there are two main aerodynamic contributions to  $F_x$ ; the use of longitudinal cyclic, rotating the lift and drag vectors, and the helicopter pitch attitude, changing the magnitude of these vectors. Assuming almost constant forward airspeed, the blade lift and drag transients will roughly be the transients of helicopter attitude and longitudinal cyclic, as the graphs demonstrate. Since aircraft pitch attitude is fairly similar for SLA and baseline helicopters, as seen in 4.11, the difference in  $F_x$  is mainly attributed to the difference in longitudinal cyclic.

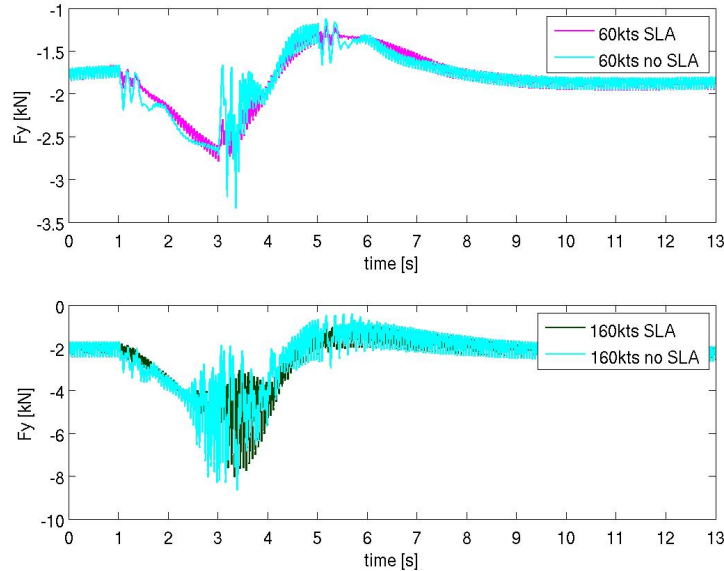


Figure 4.15:  $F_y$  with normal cg flying at 60kts and 160kts.

Hub force  $F_y$ , depicted in fig. 4.15, is directed to the right side of the helicopter. The transient of this force can mainly be attributed to a structural force, caused by blade leading and lagging, being a maximum at the left and right sides of the rotor disc. This behavior takes place in the  $x$ - $y$  plane. A higher angle of attack will result in more resistance to rotate with the shaft, resulting in lagging behavior. As the pushover is initiated, leading and lagging behavior is reversed on either side of the rotor. This is seen in the transient of  $F_y$ . As expected, the leading and lagging contribution to  $F_y$  appears to follow the helicopter's pitch attitude transient. However, the  $F_y$  shows some sudden peaky maxima and minima which are not caused by the smooth lead-lag behavior. These can be attributed to an aerodynamic component. Similar to  $F_x$ , this aerodynamic component relates to the alignment of the lift and drag forces, this time in the  $y$ - $z$  plane, at the front and rear of the rotor disc. With some roll response, lateral cyclic corrections are performed by the lateral-directional controller at the front and rear of the rotor disc, tilting the lift and drag vectors of the blades in the  $y$ - $z$  plane. Therefore, force  $F_y$  sees two main contributions during the doublet; a structural contribution caused by lead-lag at either side of the rotor disc, and an aerodynamic contribution caused by lateral cyclic at the front and rear of the rotor disc.

$F_z$ , shown in fig. 4.16, shows great similarity to the loadfactor transient. Since loadfactor is the helicopter's acceleration along the body  $z$ -axis,  $F_z$  in part consists of these inertial forces.  $F_z$  also contains an aerodynamic contribution, caused by the components of the lift- and drag forces of the rotor blades, this time aligned with the shaft's  $z$ -axis. This is caused by lateral cyclic at the front and rear of the rotor disc and longitudinal cyclic at either side of the rotor disc. At higher forward airspeed, more use is made of collective, though this does not alter during the maneuver. This raises or lowers the average level of  $F_z$ , as seen in the level flight segments. The phenomena explaining the differences between the baseline and SLA transients for  $F_z$  are therefore similar to those of  $F_x$ ; the SLA system causes  $F_z$  to show less strong peaks at high speed due to lower use of longitudinal cyclic. At higher

airspeeds, lift and drag vectors increase in magnitude, therefore, increasing their contribution to  $F_z$ .

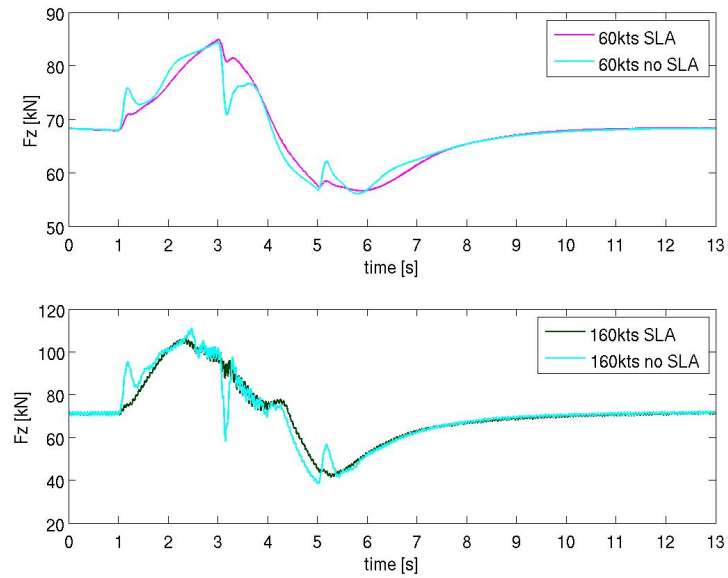


Figure 4.16:  $F_z$  with normal cg flying at 60kts and 160kts.

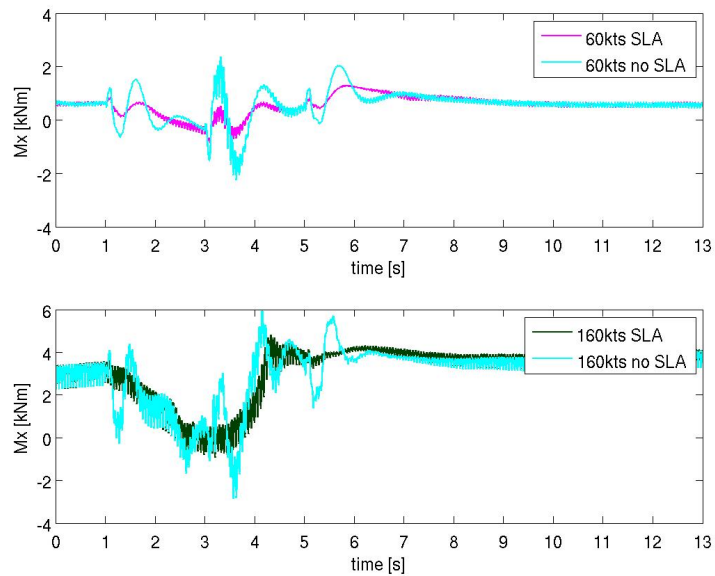


Figure 4.17:  $M_x$  with normal cg flying at 60kts and 160kts.

Shaft bending moment  $M_x$ , shown in fig. 4.17, is related to the rolling motion of the helicopter. Through coupled modes, longitudinal cyclic will cause the helicopter to show a roll response. Stabilator actuation will, however, result in a purely longitudinal response. Because of no stabilator actuation and higher use of longitudinal cyclic by the baseline system, fig. 4.11 shows that the lateral-directional controller can less adequately remove this coupled motion, as compared to the SLA system. Since the SLA helicopter uses less longitudinal cyclic, adverse roll response is lower. As such, shaft bending moment  $M_x$  shows less pronounced peaks for the SLA system.

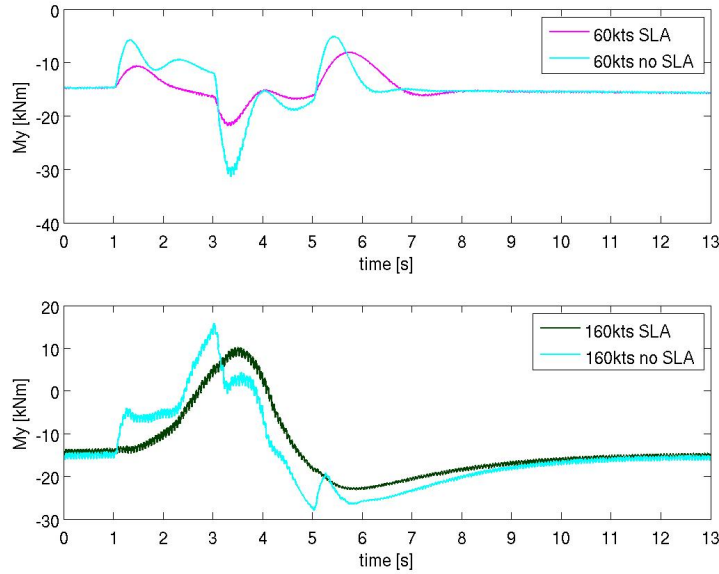


Figure 4.18:  $M_y$  with normal cg flying at 60kts and 160kts.

A pitching moment must be generated to initiate the pull-up portion of the doublet. This can be done at the rotor by applying more negative longitudinal cyclic, or by increasing downforce at the tail. As longitudinal cyclic is applied forcing the pitch-up moment, the main rotor is made to tilt up at the front and down at the rear. The use of longitudinal cyclic causes increased blade flapping and a subsequent increase in the shaft bending moment around the y-axis, hence a rise in  $M_y$ . This shaft bending moment is shown in fig. 4.18. In the case of the SLA system, a smaller amount of rotor longitudinal cyclic is used to cause the same change in attitude; the pitch-up moment is now largely created by a decrease in tail incidence (trailing edge moves up), increasing main rotor download at the tail. The baseline system solely uses longitudinal cyclic to generate a pitch-up moment, requiring more cyclic, causing more significant blade flapping and shaft bending moments.

It is of interest to elaborate on the marked difference in transients for low and high speed flight as observed for  $M_y$ . For all airspeeds below 160kts, similar transients are observed as for 60kts, however with the characteristic peak and trough lying further away from the average  $M_y$  value for level flight. When performing the pull-up at 160kts airspeed, bending moment continues to rise after pull-up initiation till the helicopter is at its maximum aircraft attitude, and decreases following pushover initiation. Reason for this transient behavior is the occurrence of retreating blade stall (RBS) once the doublet is initiated. While an airplane sees such wing stall at low speed flight at high angles of attack, helicopters experience such forms of stall at high speed flight. With an increased forward airspeed and a constant rotor RPM, the retreating blade sees a reduced relative airflow velocity. Also, at higher airspeeds, the increased amount of cyclic required to tilt the rotor disc forward results in high angles of attack at the retreating blade. LeRoy [37] states that RBS will roughly occur at angles of attack between 12deg and 14deg, for any rotor disc. Therefore, the combination of low relative airspeed and large angles of attack at the retreating blade will result in RBS. This form of stall may occur in high speed level flight, but can also be triggered by a high speed pull-up maneuver, as LeRoy [37], Prouty [46], and the U.S. Department of Transportation [52] indicate. In a pull-up, rotor inflow occurs more from below, further increasing the angle of attack. If the rotor is operating near RBS stall conditions in level flight, such a maneuver can thus trigger stall to occur. Another indicator that RBS is indeed occurring, is the observed oscillatory nature shown in the  $M_y$  transient, as each successive blade will experience a stalled region for part of its revolution. The oscillatory nature of  $M_y$ , noted as an RBS indicator by Prouty [46], is followed by a large transient rise in  $M_y$  during a high speed pull-up (LeRoy [37]). The  $M_y$  transient will be similar to that of aircraft pitch attitude; increased angle of attack causing an increasing RBS stall region. Superimposed on the aircraft pitch attitude influence will be the longitudinal cyclic deflection, increasing angle of attack further; clearly evident for the baseline helicopter. That RBS occurs during a 160kts pull-up may be expected; helicopter rotors are often designed to operate

near stall conditions at their maximum operating speed condition (Prouty [46]). As the UH-60A is designed with a maximum operating speed of 160kts, an increased angle of attack caused by a pull-up could therefore trigger RBS. While this research is not concerned with RBS, this issue can be resolved by lower rotor loading, requiring less lift from blade, or by increasing rotor RPM, raising the effective airflow speed at the retreating blade. While causing a pitch up tendency, Prouty [46] states that RBS is relatively harmless during a pull-up, as an inboard region near the front of the rotor disc will be stalled. This region sees the highest angle of attack due to the inflow change, while experiencing the lowest airflow velocity, caused by the inboard radial location. Occurring inboard, this stall therefore covers a small area of the rotor disc. The harmless nature is reaffirmed in this simulation by fig. 4.11, where the longitudinal architecture, including an (auto)pilot, still has the capability to perform the desired manoeuvre with sufficient pitch rate accuracy. For this reason, RBS is not considered further.

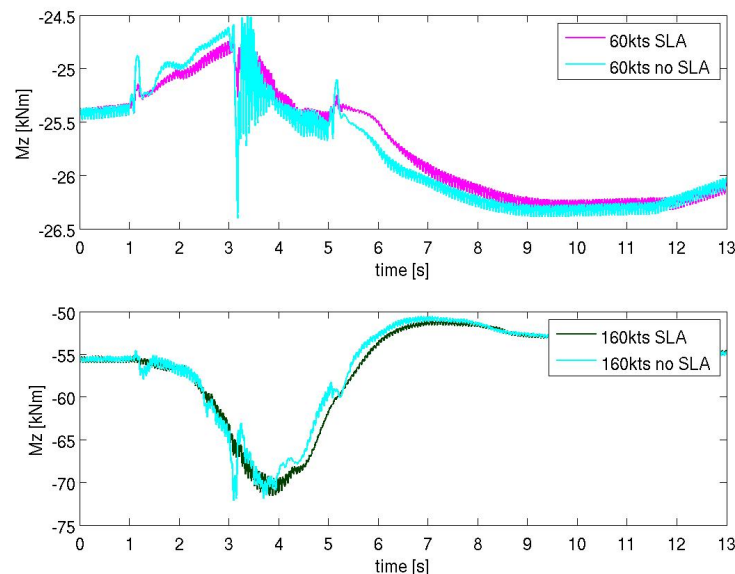


Figure 4.19:  $M_z$  with normal cg flying at 60kts and 160kts.

The moment around the z-axis,  $M_z$ , is shown in fig. 4.19, and is a torsion moment; evident through its alignment with the rotor shaft. As such, shaft torsion is mainly a function of main rotor collective. Thus, the SLA and baseline systems show similar behavior; differences in collective mainly being associated with forward flight speed. On top of the transient caused by collective, torque is also induced by opposing forces in the x-y plane of the rotor shaft. As such, pitching and rolling rates also superimpose variations in  $M_z$ .

#### 4.2.2. CONCLUSIONS ON THE SOURCES OF LOADS DURING THE DOUBLET

During the simulated doublet, shaft forces  $F_x$  and  $F_z$  have an aerodynamic contribution, depending on the lift and drag components of the main rotor blades; differing for the SLA and baseline systems, as different amounts of longitudinal cyclic are used.  $F_z$  furthermore is affected by the inertial forces during the manoeuvre, showing resemblance to the loadfactor transient.  $F_y$  mainly sees a structural force contribution caused by blade lead-lag behavior while there is also a minor aerodynamic influence caused by lateral cyclic required to reduce cross coupled response. Due to stronger cross-coupling for the baseline helicopter, this aerodynamic contribution is more visible in its  $F_y$  transient. Shaft bending moments  $M_y$  and  $M_x$  depend on pitching and rolling moment induced at the main rotor, hence differing for SLA and baseline systems. When the doublet is performed near maximum airspeed, transients of shaft bending moments will differ greatly due to RBS onset. This stall is, however, considered harmless and can be recovered. Shaft torsional moment  $M_z$  depends on the amount of collective, and therefore is a function of forward speed; not differing significantly between SLA and baseline systems.

The significance of bending moment loads, particularly during maneuvers involving changes in attitude, was discussed in chapter 3.3. As such, assessment of shaft bending moment  $M_y$  is of primary interest in various off-design conditions.

### 4.3. SUBOPTIMAL CONDITIONS

The mixed control SLA scheme has shown its ability to reduce shaft bending moments when performing the 1.75g doublet under design conditions; flying at an airspeed of 130kts, with a gross weight of 6932kg, and a center of gravity position of 9.14m. For the mixed control SLA scheme to be relevant for real-life application, it must be able to reduce loads in a range of suboptimal conditions as well. Before assessing the SLA scheme's load alleviation capability in off-design conditions, it must first be determined for which airspeeds the mixed control SLA scheme should be functional. Next, the off-design conditions are determined. From this, performance in these off-design conditions can be assessed.

#### 4.3.1. DETERMINATION OF AIRSPEEDS FOR WHICH THE SLA SCHEME WILL BE FUNCTIONAL

To determine the range of airspeeds for which the mixed control SLA scheme should be active, the same doublet was performed at various airspeeds, keeping gross weight and center of gravity constant. Since the main function of the SLA system is to reduce peak shaft bending moment  $M_y$ , figure 4.20 shows this load for the SLA and baseline schemes, for variations in airspeed. Shaft bending moment  $M_x$  and shaft torque  $M_z$  were also included, giving the reader an indication of their transients over variations in airspeed. Loads are sampled at 20kts airspeed intervals, starting at 60kts.

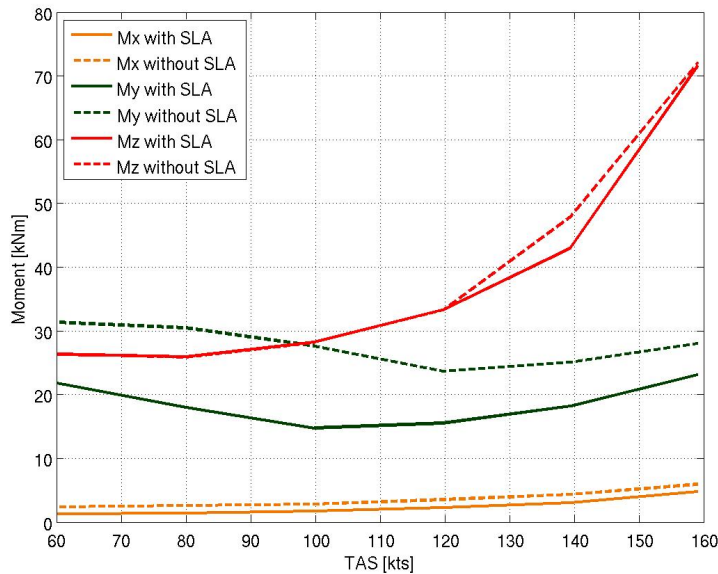


Figure 4.20: Peak shaft bending moments  $M_y$  and  $M_x$ , and shaft torque  $M_z$  for the doublet, as a function of airspeed.

From the data presented in fig. 4.20, it is chosen to gradually phase in the mixed control SLA system beyond 60kts, being fully functional at 80kts. This is because the percentage reduction in shaft bending moment increases till an airspeed of 100kts. At an airspeed of 60kts, shaft bending moment is reduced by 33%, increasing to a maximum load reduction of 46.4% at 100kts. Note that these figures give an indication on the maximum attainable load reductions, as this manoeuvre is one of the most severe in terms of shaft bending moment. While load reduction is already significant at 60kts, the current flight path augmentation (FPS) system should be maintained. Fig. 3.8 shows that main rotor download on the stabilator, at a zero incidence angle, causes a pitch-up attitude at airspeeds below 60kts. In level flight, at any airspeed, the SLA system will place the stabilator at an almost zero incidence angle. Hence, below 60kts, the current FPS system of the UH-60A should be maintained; ensuring favorable attitudes at low airspeeds. Above 60kts, the mixed control SLA system should be phased in gradually, being

fully functional at airspeeds above 80kts. This can be done in linear fashion; stabilator and longitudinal cyclic usage as commanded by the unaltered SLA system are multiplied by a so-called phase-in factor, as given in equation 4.18. Phase in factor  $f$  indicates to which extent the SLA system is active, ranging from zero to one between airspeeds of 60kts and 80kts, as provided in eq. 4.19. Gradual phasing is important; it is undesired to see large differences in helicopter response for a given pilot input following a certain airspeed threshold, beyond which the SLA system is instantly fully active.

$$\begin{aligned} \dot{i}_{tail,phase-in,SLA} &= f \cdot \dot{i}_{tail,SLA} \\ \theta_{1c,phase-in,SLA} &= f \cdot \theta_{1c,SLA} \end{aligned} \quad (4.18)$$

$$f(TAS) = \begin{cases} 0 & \text{if } TAS < 60kts; \\ \frac{TAS}{20} - 3 & \text{if } 60kts \leq TAS \leq 80kts; \\ 1 & \text{if } TAS > 80kts. \end{cases} \quad (4.19)$$

Being the lowest airspeed for which the SLA system is fully active, 80kts will be used as the low speed condition to determine mixed control SLA performance and handling. An upper limit of airspeed of 160kts is used, since this is the maximum cruise flight speed of the UH-60A.

### 4.3.2. SELECTION OF OFF-DESIGN CONDITIONS

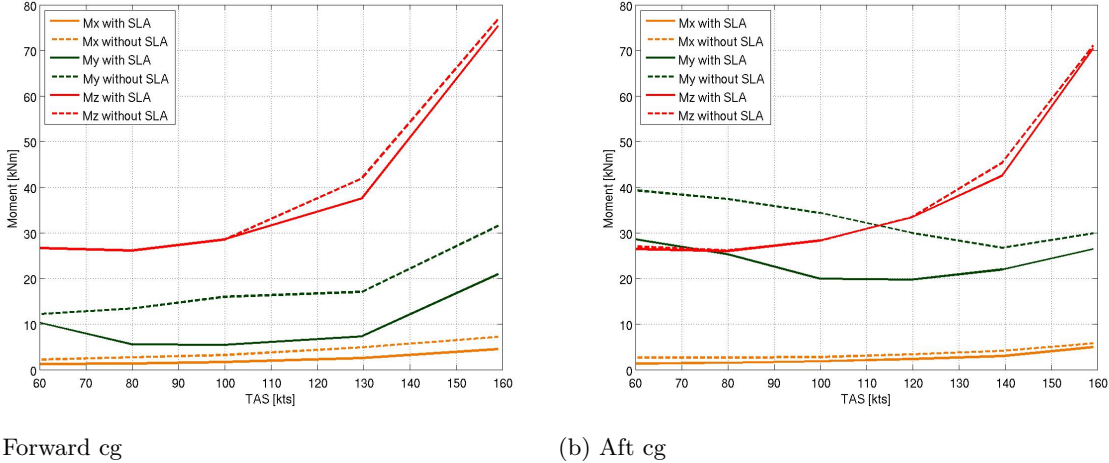
While there are three design variables around with the mixed control SLA scheme was devised, it is chosen to determine off-design performance with variations of two of these variables; airspeed and center of gravity. The third parameter, helicopter gross weight (GW), is kept constant at 6932kg. Center of gravity of the UH-60A may range from 8.53m in the most-forward situation, to 9.30m in the most-aft situation (Howlett [27]). These two center of gravity positions will be tested as the most extreme situations, and will be referred to as the ‘forward cg’ and ‘aft cg’ situations respectively. The design condition center of gravity location of 9.14m will be referred to as the ‘normal cg’ situation. The main rotor center of gravity is located at 8.84m. Therefore, the forward cg condition considers main rotor and stabilator to be located behind the aircraft center of gravity, while the normal and aft cg conditions assume the rotor to be located ahead of the helicopter center of gravity. Also, multiple speeds will be tested, these being 80kts and 160kts. The latter is the maximum operating speed of the UH-60A, while the former is chosen on the basis of the reasoning given in section 4.3.1. As such, four off-design conditions are devised, these being the:

- Forward cg and 80kts airspeed condition
- Forward cg and 160kts airspeed condition
- Aft cg and 80kts airspeed condition
- Aft cg and 160kts airspeed condition

The above off-design conditions will be utilized throughout this research, for various purposes. These conditions encompass the entire realm of the SLA’s operational environment in terms of center of gravity and airspeeds in which the SLA system is fully functional. Note that variations in helicopter gross weight are not considered in this research.

### 4.3.3. MIXED CONTROL SLA PERFORMANCE IN OFF-DESIGN CONDITIONS

To determine the relevance of the mixed control SLA scheme, its performance in off-design conditions is essential. Performance is assessed based on the ability to reduce shaft bending moment  $M_y$ , when performing a similar maneuver, in terms of pitch rate. For this reason, the same doublet maneuver is performed for the four off-design conditions, comparing the mixed control SLA system’s ability to reduce loads while the longitudinal controller, mimicking an (auto)pilot attempts to follow similar transient aircraft attitudes and angular rates as the baseline helicopter. Fig. 4.21 shows the moments for the fore and aft cg configuration, over a range of airspeeds for the SLA and baseline systems.



(a) Forward cg

(b) Aft cg

Figure 4.21: Peak shaft moments and torque for off-design center of gravity positions.

From these off-design conditions, it is evident that alterations in center of gravity have the most pronounced effect on shaft bending moment  $M_y$ . As expected, that a shift of the center of gravity along the body x-axis will primarily result in a different aircraft pitch attitude trim state; shown in Fig. 4.22. As expected, with an aft center of gravity, the helicopter will have a larger pitch up attitude throughout the doublet maneuver. This greater pitch-up attitude results in increased flapping at the front and rear of the disc, caused by a larger difference in effective angle of attack. Thus, shaft bending moment  $M_y$  will differ greatly with change in center of gravity, being highest for an aft cg. With small corrective control differences required for off-axis response and no change in main rotor collective,  $M_x$  and  $M_z$  show lower sensitivity to changes in center of gravity along the helicopter's lateral axis.

As expected, one can observe that the shaft bending moment transients for a normal center of gravity, as presented in fig. 4.20, appear to fit in between the shaft moment bending transients for a forward and aft center of gravity. All three center of gravity positions show highest shaft bending moment load reduction at an airspeed of 100kts. Table 4.1 gives percentage load reductions for all three center of gravity conditions, for the entire airspeed range of the mixed control SLA system.

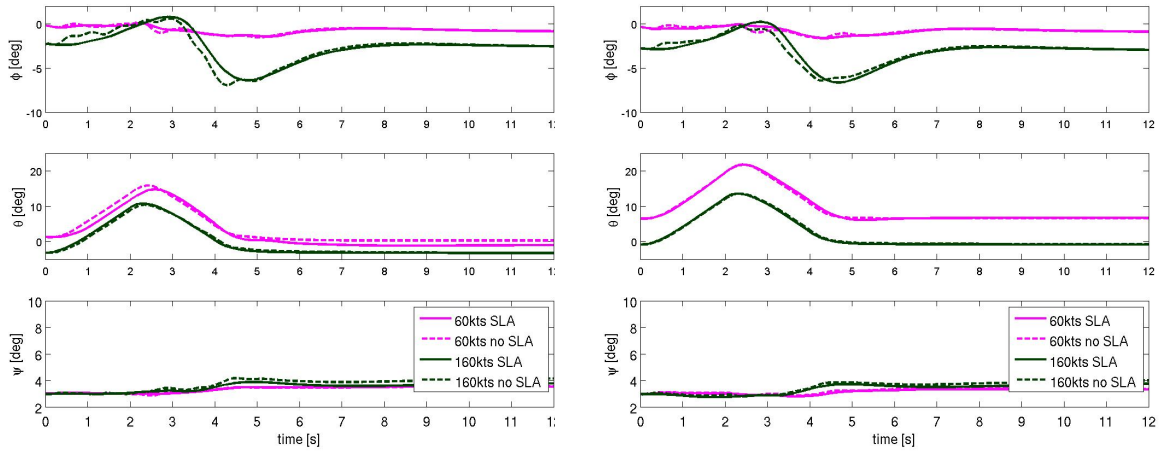
Table 4.1: Relative shaft bending moment reduction for the 1.75g doublet, at various off-design conditions

Airspeed [kts]	Shaft bending moment load reduction [%]		
	cg fore	cg normal	cg aft
60	16	33	25.6
100	70.6	46.4	41.2
160	34.4	17.8	13.3

Table 4.1 shows that relative load reduction is highest at low speed for the normal center of gravity. At higher airspeeds, the forward center of gravity shows largest relative shaft bending moment load reductions. With relative load reductions above 10% for both design and off-design conditions, this SLA scheme is considered relevant in terms of load reduction capability for off-design conditions.

Since loads also depend on the transient aircraft attitudes during the manoeuvre, it is important that SLA and baseline helicopters follow similar pitch attitude transients. Fig. 4.22 provides these transients for the four off-design conditions. What is of interest is the differences between the SLA and the baseline transient for a given airspeed; hence, the difference in dotted and normal line for a given color. In similar fashion, fig. 4.23 shows the angular rates for the off-design conditions.

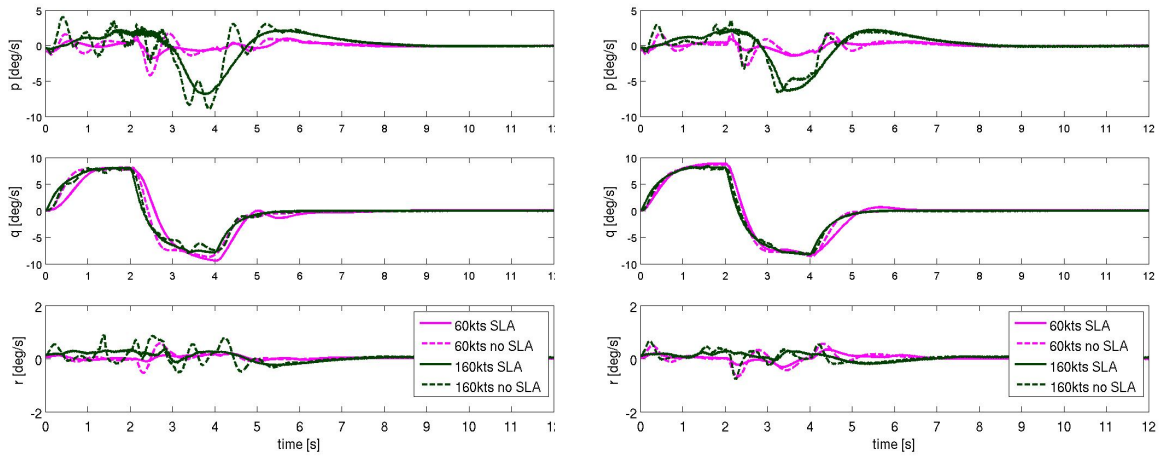
When viewing the aircraft attitude and angular rate transients of fig. 4.22 and 4.23, the similarity of these aircraft state variables can be observed for the SLA and baseline helicopters, for a given off-design condition. This similarity allows for the aforementioned conclusions on  $M_y$  reduction pertaining to a



(a) Forward cg

(b) Aft cg

Figure 4.22: Attitudes for off-design conditions.



(a) Forward cg

(b) Aft cg

Figure 4.23: Rates for off-design conditions.

given maneuver. It can also be concluded that an (auto)pilot has sufficient ability to follow a desired pitch rate transient. A thorough assessment of SLA system agility as compared to the baseline system will be conducted in chapter 5, omitting corrective (auto)pilot action.

While it was initially considered to use different control allocations between stabilator and longitudinal cyclic when flying at different airspeeds, the single cg-airspeed SLA design allows for sufficient load alleviation capability in off-design conditions. For this reason, it is decided to maintain the single control allocation ratio between longitudinal cyclic and tail, irrespective of the airspeed.

#### 4.3.4. CONCLUSIONS CONCERNING OFF-DESIGN PERFORMANCE

For all variations in center of gravity and airspeed, the mixed control SLA system must still allow for load reduction in terms of shaft bending moment  $M_y$ , when performing a similar maneuver. Four off-design conditions are chosen, with maximum forward (28.5ft) and aft (30.5ft) center of gravity, as permitted for the UH-60A, and with airspeeds of 80kts to 160kts. The former is the lowest airspeed at which the SLA system will be fully functional, while the latter is the maximum airspeed of the UH-60A. The combination of these parameters define the corners of the entire operating realm of the SLA system. Thus, analysis at these conditions will show maximum unfavorable deviations. The third variable with

which the SLA system was designed, the helicopter's gross weight, is not altered during the off-design analysis. Since the stabilator is used for pitch attitude control at low airspeeds, it is decided to phase in the mixed control SLA system at airspeeds above 60kts, being fully functional at 80kts flight or higher.

Figures 4.22 and 4.23 demonstrate that the performed manoeuvre is sufficiently similar for SLA and baseline helicopters. This similarity allows conclusions to be drawn in terms of load reduction capability. In these off-design flight conditions, load reduction is assessed in terms of shaft bending moment  $M_y$ . From figure 4.21, load alleviation capability is considered sufficient in off-design conditions. Also, due to the similarity of observed aircraft angular rate transients, it can be concluded that an (auto)pilot, represented here by the longitudinal and lateral-directional controllers, can still properly follow desired angular rate transients in off-design conditions.

While variations in control allocation was considered for various airspeed regimes, the SLA scheme's performance in terms of shaft bending load reduction for a given longitudinal maneuver, have resulted in the choice to maintain a single control allocation, designed around the 130kts, normal cg condition.

# 5

## Safety analysis and subsequent handling qualities

While findings concerning off-design performance of the SLA system are promising, the system's viability in terms of safety is still unknown. Evidently, in case of failure, a pilot must still be able to recover from unfavorable transient behavior, allowing for a safe landing. However, what determines the safety of a helicopter? Section 5.1 will provide insight in metrics and properties related to safety. From this, stabilator incidence angles and actuation rates are chosen to ensure safety after system failure. These limits allow for sufficient longitudinal cyclic margin, acceptable load factor transients after failure, and a safe landing to be carried out. However, alterations to the stabilator will also affect the SLA system's agility. Section 5.4 assesses the agility of the SLA system on the basis of five metrics, pertaining to attitude and flightpath trajectory changes. Flightpath bandwidth, a novel performance metric proposed in this research, demonstrates the potential to significantly enhance safety assessment if incorporated in the guiding ADS-33E norms. Lastly, a fidelity analysis, assessing various inflow and interference models, aims at determining the validity of previously drawn conclusions.

### 5.1. BACKGROUND

In this section safety will be quantified, determining what makes a safe helicopter. First, a classical approach will be discussed that considers stability criteria. Next, two norms pertaining to helicopter safety will be covered, elaborating on their requirements as pertaining to FCS failure.

#### 5.1.1. DYNAMIC AND STATIC STABILITY

Of key importance to quantifying the safety of a helicopter, is the assessment of stability properties. As for a fixed wing aircraft, this can be done in a classical approach by simplifying the helicopter's equations of motion, and deriving these equations with respect to a given independent variable. This methodology is applied by Prouty [48]. These static derivatives are subsequently placed in a matrix following numerous assumptions and simplifications, as is shown in figure 5.1. Assuming uncoupled longitudinal and lateral-directional modes, a simplified 3x3 matrix can be solved, where the eigenvalues of the characteristic equation yield information on the transient behavior of the modes. By mapping the roots on a root-locus plot for various scaling parameters, it can be seen whether a mode will be oscillatory or non-oscillatory, convergent or divergent. Such a root-locus is shown in figure 5.2 for the longitudinal motion of a sample helicopter. As numerous static derivatives together determine the stability of a given mode through the corresponding characteristic equation, stability maps can be created in order to select a combination of static derivatives to obtain desired handling characteristics. For illustrative purposes, such a stability map is shown in figure 5.3.

X	Z	Θ	Y	Φ	Ψ	$\theta_{SM}$	$\theta_{ST}$	$A_1$	$B_1$	
LONGITUDINAL										
$\frac{G.W.}{g} \dot{x}^2 + \frac{\partial X}{\partial \dot{x}}$	$\frac{\partial X}{\partial \dot{z}}$	$\left( \frac{\partial X}{\partial \dot{\theta}} - \frac{G.W.}{g} \dot{\theta} \right)^2 - G.W.$	$\frac{\partial X}{\partial \dot{y}}$	$\frac{\partial X}{\partial \dot{\phi}}$	$\frac{\partial X}{\partial \dot{\psi}}$	$x(t)$	$-\frac{\partial X}{\partial \theta_{SM}}$	$-\frac{\partial X}{\partial \theta_{ST}}$	$-\frac{\partial X}{\partial A_1}$	$-\frac{\partial X}{\partial B_1}$
$\frac{\partial Z}{\partial \dot{x}}$	$\left( \frac{\partial Z}{\partial \dot{z}} - \frac{G.W.}{g} \right)^2 + \frac{\partial Z}{\partial \dot{z}}$	$\left( \frac{\partial Z}{\partial \dot{\theta}} + \frac{G.W.}{g} \dot{\theta} \right)^2$	$\frac{\partial Z}{\partial \dot{y}}$	$\frac{\partial Z}{\partial \dot{\phi}}$	$\frac{\partial Z}{\partial \dot{\psi}}$	$z(t)$	$-\frac{\partial Z}{\partial \theta_{SM}}$	$-\frac{\partial Z}{\partial \theta_{ST}}$	$-\frac{\partial Z}{\partial A_1}$	$-\frac{\partial Z}{\partial B_1}$
$\frac{\partial M}{\partial \dot{x}}$	$\frac{\partial M}{\partial \dot{z}} + \frac{\partial M}{\partial \dot{z}}$	$-I_{yy} \dot{\theta}^2 + \frac{\partial M}{\partial \dot{\theta}}$	$\frac{\partial M}{\partial \dot{y}}$	$\frac{\partial M}{\partial \dot{\phi}}$	$\frac{\partial M}{\partial \dot{\psi}}$	$\Theta(t)$	$-\frac{\partial M}{\partial \theta_{SM}}$	$-\frac{\partial M}{\partial \theta_{ST}}$	$-\frac{\partial M}{\partial A_1}$	$-\frac{\partial M}{\partial B_1}$
LATERAL-DIRECTIONAL										
$\frac{\partial Y}{\partial \dot{x}}$	$\frac{\partial Y}{\partial \dot{z}}$	$\frac{\partial Y}{\partial \dot{\theta}}$	$-\frac{G.W.}{g} \dot{x}^2 + \frac{\partial Y}{\partial \dot{y}}$	$\left( \frac{\partial Y}{\partial \dot{\phi}} + \frac{G.W.}{g} \dot{\phi} \right)^2 + G.W.$	$\left( \frac{\partial Y}{\partial \dot{\psi}} - \frac{G.W.}{g} \dot{\psi} \right)^2$	$y(t)$	$-\frac{\partial Y}{\partial \theta_{SM}}$	$-\frac{\partial Y}{\partial \theta_{ST}}$	$-\frac{\partial Y}{\partial A_1}$	$-\frac{\partial Y}{\partial B_1}$
$\frac{\partial R}{\partial \dot{x}}$	$\frac{\partial R}{\partial \dot{z}}$	$\frac{\partial R}{\partial \dot{\theta}}$	$\frac{\partial R}{\partial \dot{y}}$	$-I_{xx} \dot{\phi}^2 + \frac{\partial R}{\partial \dot{\phi}}$	$\frac{\partial R}{\partial \dot{\psi}}$	$\Phi(t)$	$-\frac{\partial R}{\partial \theta_{SM}}$	$-\frac{\partial R}{\partial \theta_{ST}}$	$-\frac{\partial R}{\partial A_1}$	$-\frac{\partial R}{\partial B_1}$
$\frac{\partial N}{\partial \dot{x}}$	$\frac{\partial N}{\partial \dot{z}}$	$\frac{\partial N}{\partial \dot{\theta}}$	$\frac{\partial N}{\partial \dot{y}}$	$\frac{\partial N}{\partial \dot{\phi}}$	$-I_{zz} \dot{\psi}^2 + \frac{\partial N}{\partial \dot{\psi}}$	$\Psi(t)$	$-\frac{\partial N}{\partial \theta_{SM}}$	$-\frac{\partial N}{\partial \theta_{ST}}$	$-\frac{\partial N}{\partial A_1}$	$-\frac{\partial N}{\partial B_1}$

Figure 5.1: Equations of motion (Prouty [48]).

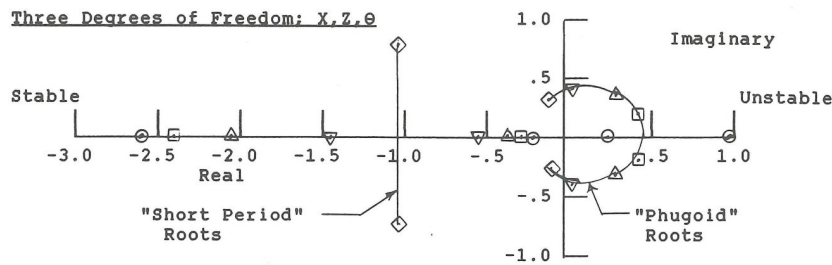


Figure 5.2: Root-locus plot for changes in horizontal stabilizer area (Prouty [48]).

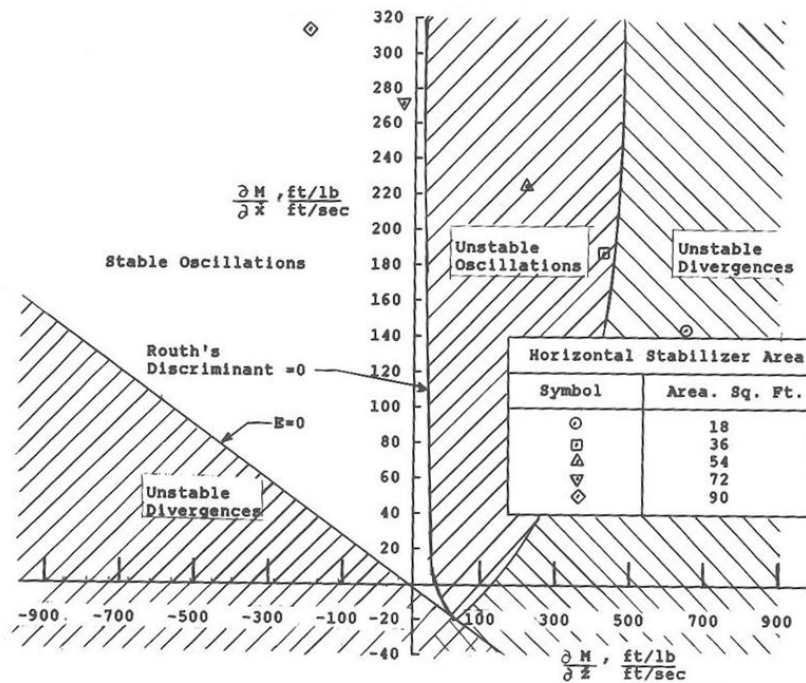


Figure 5.3: Longitudinal stability map for sample helicopter at 115 Knots (Prouty [48]).

While this analytical approach is rather elegant and manages to reduce the vast complexity of the

helicopter to an understandable level, it is rather challenging to set up the equations of motions for an existing helicopter. Furthermore, using the equations requires fundamental assumptions, where certain parameters are neglected, coupling between various modes is ignored, and highly irregular flow phenomena are assumed uniform and steady. In Prouty's approach, induced velocity by the main rotor is assumed to be uniform and cylindrical; having the same influence on any fuselage component downstream. Evidently, the streamtube of the main rotor is not uniform in nature, contracting and expanding in the direction of the flow, having different induced velocities in radial direction, and having a swirl component, amongst other non-uniform properties. It is rather challenging to model an existing helicopter with equations of motions to a high fidelity level. For this reason, such a model must always be compared to a numerical representation of a helicopter, which is perturbed with respect to all independent variables, yielding numeric values for the static derivatives. Note that a new matrix, encompassing all degrees of freedom, must be made for each geometric or aerodynamic change, such as flight speed or aircraft attitude, as this changes the helicopter's modes.

One specific stability characteristic which will be investigated is speed stability. This stability is mainly affected by two components: the main rotor and the stabilator. Longitudinal flapping is always stable with increased airspeed, causing larger flapping at the front and less flapping at the rear, resulting in a tendency to pitch up and reduce airspeed. For the stabilator, two effects cause contradicting effects. Assuming no attitude change with increased airspeed, the larger rotor downwash will cause a stronger download at the stabilator, causing a similar restoring pitch up tendency. The destabilizing factor at the stabilator is the reduced angle of attack, as the helicopter pitches downward with increased airspeed. This will result in a smaller download, causing the helicopter to pitch down further. This destabilizing factor increases in magnitude if the downwash from the main rotor changes with attitude. Figure 5.4 shows various speed stability conditions caused by main rotor and horizontal tailplane properties. Prouty [48] states that a slight positive speed stability is desired during instrument flight. Evidently, stability should not be too large, limiting the forward airspeed.

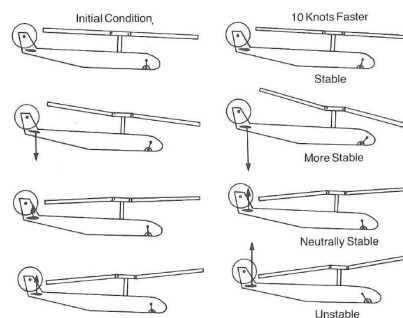


Figure 5.4: Illustration of possible speed stability results (Prouty [48]).

The importance of stability in determining the safety of a helicopter is evident through its inclusion in the important norms related to safety. In the subsequent section, the two dominant norms pertaining to HQs will be discussed. Firstly, an explanation is given on how subjective pilot-experienced HQ levels can be quantified in objective HQ levels. Lastly, the aforementioned SLA systems are benchmarked in light of these safety norms.

### 5.1.2. ADS-33E AND MIL-DTL-9490E: TWO NORMS PERTAINING TO SAFETY

Concerning safety after system failure, the two dominant norms will be assessed; their specific requirements on HQs after failure, as well as requirements during normal flight which also affect safety after FCS failure.

The first norm is the Aeronautical Design Standard (ADS-33E) for rotorcraft performance, and the second is MIL-DTL-9490E (MIL) for flight control system design of military rotorcraft and fixed-wing aircraft. Both norms set criteria for HQs during normal operation, however, HQs and response requirements after an FCS failure are of main interest. Before going into detail on these two norms, their classification shall be discussed. MIL defines operational states (OS) on a scale of 1 to 5, depending on the severity of the limitation on the capabilities of performing its required task. An OS of 1 indicates most favorable handling qualities. The significance of each OS level is elaborated provided below, as

related to FCS failure.

- OS 1: normal operation; operation within the operational flight envelope (OFE)
- OS 2: restricted operation; partial degradation or failure of FCS, still allowing completion of mission, potentially increasing crew workload
- OS 3: minimum safe operation; degraded safety or performance, allowing for safe termination of mission, cruise, descent and landing
- OS 4: controllable to an immediate emergency landing; continued safe flight not possible, though sufficient control for safe descent and landing
- OS 5: controllable to an evaluable flight condition; degraded FCS capability allows for a certain flight condition that allows crew evacuation

The ADS-33E classification of level 1, 2 or 3 HQs is based on the Cooper-Harper scale (Harper and Cooper [21]). This scale quantifies HQs as experienced by pilots of fixed-wing and rotorcraft aircraft alike, and is the industry accepted scale for rating HQs. HQ rating is done through dichotomy with a decision tree shown in fig. 5.5. Cooper and Harper [14] state how these decisions can be made as succinctly as possible, since judgment of certain yes/no questions can be problematic at times. The conversion from Cooper-Harper rating to ADS-33E HQ level classification is also shown in fig. 5.5. ADS-33E divides flying qualities into level 1, 2 and 3 categorization, where level 1 indicates preferred HQs, level 2 indicates sufficient HQs and level 3 indicates that improvement of HQs should be pursued (Johnson et al. [29]). Note that the worst Cooper-Harper ratings of 9 or 10, indicating uncontrollability during a mission task element, are never acceptable according to ADS-33E classification, as this exceeds level 3 HQs. MIL states that an OS of 3 should at least be attained after FCS failure, meaning that safe termination of a maneuvering task is possible, allowing for safe cruise, descent and landing. The following paragraphs cover requirements set in both norms concerning: probability of failure, transients after failure, safe landings, and finally gain and phase margins.

### Probability of failure

Both ADS-33E and MIL require an analysis of the probability of failure and the severity of the outcome. This probabilistic analysis lies outside of the scope of this research, and will not be discussed further.

### Transients after failure in terms of load factor, structural loads and controllability

Concerning transients after failure, ADS-33E states “transients following failure of the flight control system shall be recoverable to a safe steady flight condition without exceptional pilot skill (ADS-33E [2]).” Hard criteria concerning this requirement are listed in table 5.1.

Table III. Transients following failures

LEVEL	FLIGHT CONDITION		
	HOVER AND LOW SPEED	FORWARD FLIGHT	
		NEAR-EARTH	UP-AND-AWAY
1	3° roll, pitch, yaw 0.05g $n_x$ , $n_y$ , $n_z$ No recovery action for 3.0 sec	Both Hover and Low Speed and Forward Flight Up-and-Away requirements apply	Stay within OFE. No recovery action for 10 sec
2	10° attitude change or 0.2g acceleration. No recovery action for 3.0 sec	Both Hover and Low Speed and Forward Flight Up-and-Away requirements apply	Stay within OFE. No recovery action for 5.0 sec
3	24° attitude change or 0.4g acceleration. No recovery action for 3.0 sec	Both Hover and Low Speed and Forward Flight Up-and-Away requirements apply	Stay within OFE. No recovery action for 3.0 sec

Table 5.1: ADS-33E requirements for transients after FCS failure, listed per HQ level (ADS-33E [2]).

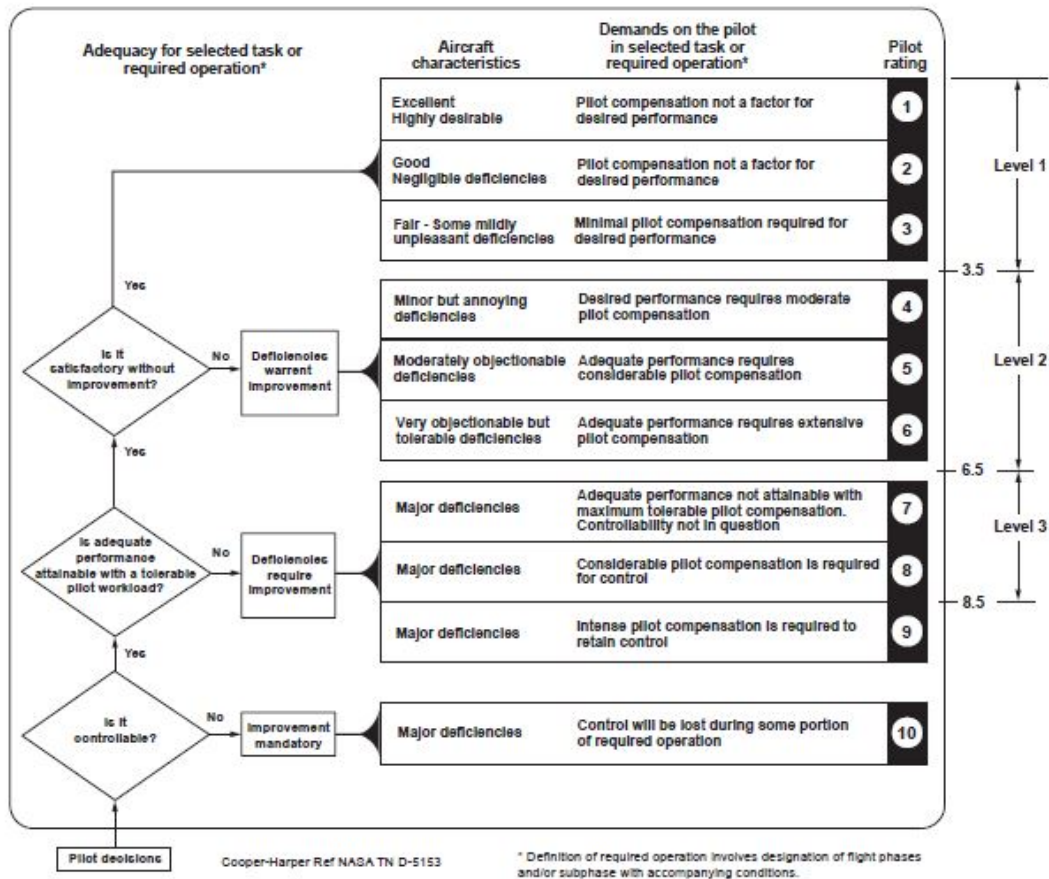


Figure 5.5: Determination of the ADS-33E HQ levels, based on the Harper-Cooper HQ grading scale (ADS-33E [2]).

HQs worse than level 3 are unacceptable; at larger attitude transients, pilots risk losing spatial awareness and the ability to properly control the helicopter (Padfield [42]). The different response times between low and high speed flight are the result of reduced visual cues at high speed and high altitude flight, where a pilot requires more time to notice the malfunction and to respond accordingly. Concerning transients, MIL states that failure may not cause uncontrollable aircraft motions and that limit airframe loads should not be exceeded. Failure of the FCS should not cause worse control than that required for minimum safe (OS 3) HQs, meaning that transients shall not exceed 75% of the limit load factor, or 1.5g, whichever occurs first. Since the UH-60A has a limit load factor of 3.5g, the 1.5g maximum load factor condition is enforced. Therefore, the following criteria concerning transients will be considered during safety analysis:

- No uncontrollable aircraft motions after failure (MIL)
- Transients shall not exceed 1.5g load factor after failure (MIL)

The parametrization of these criteria will be covered in chapter 5.3.

While not specifically related to a failed SLA system, MIL-norms dictate that in-flight engagement and disengagement of electrical controls should not cause large trim shifts that cannot easily be controlled by the pilot, and that the new trim condition should be attainable within 2 seconds. One may argue that such ease of trim would also be desirable after failure of the flight control system. However, with the previous criteria on controllability and load factors, it is felt that this condition is not essential and may be too constricting. It is, however, a desirable property.

It is noticeable that while hard criteria are set by both norms concerning load factors, and in the case of ADS-33E, to changes in attitude, there are no hard criteria for controller authority.

### Redundancy of systems

ADS-33E furthermore requires that pilots will also be given an override capability in case of failed control, and that multiple redundancy is built into the system. Such a system is already in place in the UH-60A, where the pilot can only override the stabilator incidence position after failure of the fly-by-wire control system (Cooper [13]). This redundancy is also present in the mixed control SLA system. As such, this criteria has already been met.

### Safe landing

MIL also sets criteria for a safe landing, though this remains open to interpretation. To gain insight to more tangible criteria for a safe landing, the UH-60A manual [16] is consulted. This sets a maximum safe sink rate of 180 feet per second, a maximum forward speed of 60 knots for a landing on flat terrain, and maximum ground inclination angles for landing of 6 degrees nose-down and 15 degrees nose-up. The latter two inclination constraints are irrespective of configuration such as weight or center of gravity position. Assuming that these maximum inclination angles are determined to provide sufficient stability and clearance during landing, these values can be used as assumptions for UH-60A attitude constraints for landing on flat terrain. Another approach to determine maximum nose-up and nose-down attitude is derived from Prouty's rule of thumb, used for deriving maximum flare angle (Prouty [48]). Prouty states that the maximum flare angle following engine failure is usually the angle made by the helicopter when leaning on its rear landing gear and its tail boom. This is considered to be the maximum safe angle if the aircraft would touch down when still in its nose-up flare attitude. Therefore, using this measure to determine the maximum safe pitch-up attitude for landing seems reasonable. The same can be extended for maximum nose-down attitude, using the angle between the nose and the forward landing gear. As angle limits by this approach are less stringent than the limits set in the UH-60A user manual, the limits of the manual are used. This will therefore also ensure safe flaring. Concerning a safe landing, the following will be considered during the safety analysis:

- At the maximum forward airspeed permitted for landing, helicopter attitude with respect to the ground will not exceed 6 degrees nose-down or 15 degrees nose-up (MIL and UH-60A manual)

### Gain and phase margins

MIL also sets guidelines for minimum required gain (GM) and phase margins (PM) in normal flight, for desired response and stability. Evidently, if these conditions are not met in normal flight, HQs after failure will be even more detrimental, as response and stability qualities are only reduced further. PM and GM requirements are categorized per mode frequency, setting boundaries around the aircraft elastic modes, categorized by airspeed. These requirements can be found in table 5.2. Feedback gains have been manually tuned to meet GM, PM and bandwidth criteria in the design of the mixed control SLA scheme (Voskuijl [54]). Therefore, this criteria will not be discussed further. Also, these requirements concern the entire longitudinal controller architecture, and is not specifically related to the design of the SLA system.

Air speed Mode Frequency Hz	Below $V_{oMIN}$	$V_{oMIN}$ to $V_{oMAX}$	At Limit Airspeed ( $V_L$ )	At 1.15 $V_L$
$f_M < 0.06$	GM= 6 dB (No Phase Requirement Below $V_{oMIN}$ )	GM = $\pm 4.5$ PM = $\pm 30$	GM = $\pm 3.0$ PM = $\pm 20$	GM=0 PM=0 (Stable at Nominal Phase and Gain)
$0.06 \leq f_M < \text{First Aero-elastic Mode}$		GM = $\pm 6.0$ PM = $\pm 45$	GM = $\pm 4.5$ PM = $\pm 30$	
$f_M > \text{First Aero-Elastic Mode}$		GM = $\pm 8.0$ PM = $\pm 60$	GM = $\pm 6.0$ PM = $\pm 45$	

Table 5.2: MIL-DTL-9490E requirements for Gain and Phase Margins (MIL [4]).

### Static derivatives and gust sensitivity

Neither norm states hard criteria for static derivatives, which indicates the sensitivity of the helicopter

to a given disturbance such as a vertical gust. ADS-33E does, however, state maximum peak yaw rate response following vertical gusts of different magnitudes. For hover and low speed, the norm also dictates that pitch and roll sensitivities to disturbances should be small. This could be of importance after failure of FCS systems, where the pilot has limited control of the crippled aircraft. However, such a sensitivity depends on the complete control architecture, and is not conducted within the scope of this research.

## 5.2. SAFETY CONSTRAINTS AND FAILURE CASES

Summarizing the above criteria, the list below indicates which controller properties will be assessed to evaluate its safety after failure.

- No uncontrollable aircraft motions after failure (MIL)
- Transients shall not exceed 1.5g load factor after failure (MIL)
- At the maximum forward airspeed permitted for landing, helicopter attitude with respect to the ground will not exceed 6 degrees nose-down or 15 degrees nose-up (MIL and UH-60A manual)

The first item must be quantified further. A prerequisite for controllability is that the helicopter must be trimmable after failure. Secondly, when failure occurs, the pilot must possess sufficient longitudinal cyclic margin to increase the helicopter's pitch attitude to reduce forward airspeed. It is desirable that the helicopter possesses positive speed stability. This is, however, not set as a criteria. In case of failure, slight negative speed stability is considered acceptable, if there is sufficient longitudinal cyclic margin. Speed stability should, however, be assessed at the chosen stabilator actuator bounds. As such, the criteria are grouped as: controllability, load factor transients, and attitudes during landing, as given in table 5.3.

Table 5.3: Safety criteria after SLA failure.

Crit. nr.	Category	Criteria
1	Controllability; in flight	Helicopter can be trimmed after SLA failure
2	Controllability; reducing airspeed	Sufficient longitudinal cyclic margin for pull-up to reduce airspeed*
3	Load factor	Maximum load factor of 1.5g after failure
4	Airframe loads	No exceedance of airframe loads
5	Controllability; safe landing	No attitude beyond -6 deg. (down) or 15 deg. (up) when flying at 60kts

\*Speed stability should be positive. This is, however, not a hard criterion; slight negative speed stability is acceptable after failure, if there is sufficient longitudinal cyclic margin.

## 5.3. CONSTRAINTS ALLOWING FOR SAFETY

In this section, stabilator actuation limits are chosen on the basis of the first two criteria listed in table 5.3. The other two criteria are assessed after selection of actuation limits, to guarantee satisfactory safety performance.

### 5.3.1. FAILURE CASES CONSIDERED FOR ANALYSIS

To determine the allowable tail actuation angles and rates, worst-case situations must be assessed. Two failure cases specific to the mixed control SLA system may occur. Firstly, the stabilator may deflect to a given position and remain stuck, or the stabilizer actuation rate may be impaired. In the worse-case situation, the stabilator will remain deflected at the maximum deflection angles, or its deflection rate will be impaired to very small values.

Therefore, three failure cases are considered:

- Maximum positive stabilator deflection
- Maximum negative stabilator deflection
- Rate limited stabilator

As such, the permitted stabilator deflection angles for the functioning SLA system must be chosen such that, in case of failure, the helicopter is still trimmable when the stabilator is deflected at these maximum deflection angles. The helicopter must not only be trimmable; the pilot must also possess enough control margin to sufficiently maneuver the crippled helicopter, for example to allow for a safe landing. Trimmability is determined based on the ability to come to a zero pitch rate and constant airspeed.

### 5.3.2. STABILATOR ACTUATION LIMITS BASED ON TRIMMABILITY

To determine if the helicopter is trimmable, a trimsweep is generated for the situation where the helicopter is flying at the center of gravity and airspeed around which the SLA system was devised. From level flight, the tail deflects to a given angle. The longitudinal controller will attempt to correct this malfunction by applying corrective longitudinal cyclic input. While control allocation between tailplane and longitudinal cyclic remains unchanged in the control architecture during the malfunction, the tailplane incidence angle will remain fixed. Hence, only longitudinal cyclic will vary. For a given tail deflection angle, the amount of longitudinal cyclic required to fly level is determined after the helicopter is successfully trimmed. Results are given in figure 5.6.

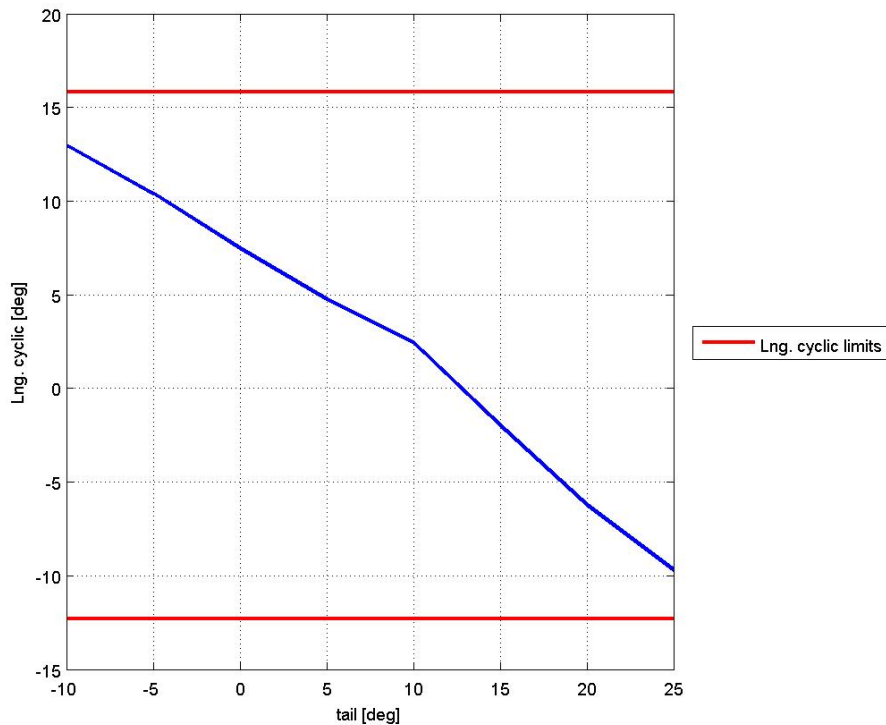


Figure 5.6: Longitudinal cyclic trimsweep for various tail deflection angles, at 130kts with normal cg.

The required longitudinal cyclic for a given tail deflection angle appears to be negatively proportional, as expected. As stabilator incidence angle increases, there is a local reduction of downforce by the main rotor, causing a nose-down pitching moment. More negative longitudinal cyclic must be applied to counter this nose-down moment in order to maintain level flight. While the relationship

between longitudinal cyclic and tail deflection seems linear, there are two visible kinks. Beyond a tail incidence angle of 10 degrees, the amount of additional negative longitudinal cyclic increases. Beyond a 20 degrees incidence angle, the slope becomes less negative again. Fig. 4.10 provides more insight concerning the nature of these kinks. Here, the lift, drag and moment coefficients are provided for the NACA0012 airfoil, representing the UH-60A's tailplane. While moment coefficient remains zero and lift coefficient changes smoothly, the drag coefficient sees the characteristic drag bucket between -10 and 10 degrees angle of attack. Beyond this, drag increases more significantly with angle of attack. Beyond +/- 20 degrees angle of attack, the drag increment is again of smaller magnitude. The drag rise beyond +/-10 degrees will result in a more significant nose-down moment, as the UH-60A's center of gravity in z-direction is located below the tail surface. This requires a larger change in longitudinal cyclic. Beyond 20 degrees angle of attack, drag dependency on angle of attack decreases again, requiring smaller amounts of negative longitudinal cyclic to compensate for the nose-down moment. Evidently, the location of the kinks in the trimsweep will not always match the exact location of changes in  $dC_d/d\alpha$ ; aside from stabilator incidence angle, angle of attack also depends on helicopter attitude and inflow caused by the main rotor downwash. However, in this specific configuration, flying at 130kts with normal cg, stabilator angle of attack is roughly equal to its incidence angle.

While one may limit stabilator deflection based on this trimsweep for sufficient longitudinal cyclic margin, this still may not provide a trimmable helicopter when flying at other airspeeds. Since the stabilator is only deployed once a maneuver is initiated, only the amount of longitudinal cyclic required for trim will vary per flight speed. Thus, with a stuck stabilator, the amount of longitudinal cyclic margin for trim flight at 130kts may prove to be insufficient at some other airspeed. A trimsweep must be conducted at the airspeed where the lowest amount of longitudinal cyclic margin is available. It will be at this given airspeed, that trimmability will be most critical if the stabilator deflects to some incidence angle. To determine this airspeed, the UH-60A with mixed control SLA is flown at various airspeeds with functioning stabilator. The amount of longitudinal cyclic required for trim at each airspeed is shown in figure 5.7. The helicopter is assessed at 20kts intervals, starting from 60kts till maximum airspeed.

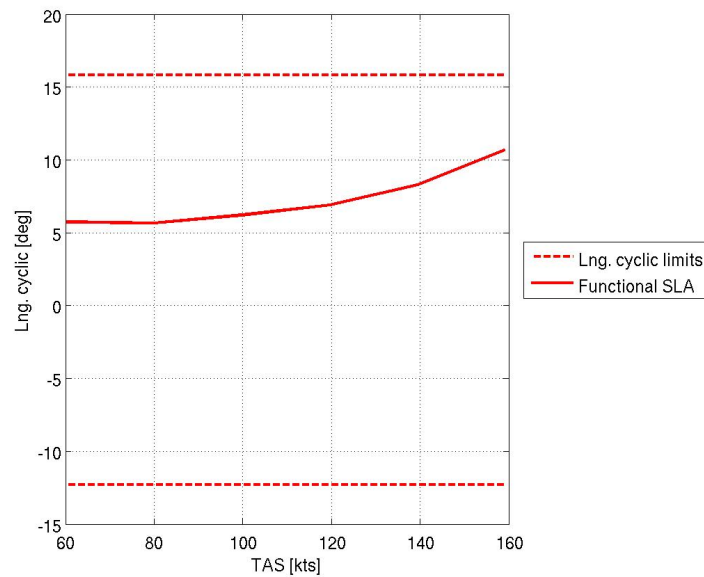


Figure 5.7: Longitudinal cyclic usage versus airspeed, with normal cg.

From figure 5.7, it is clear that the amount of required longitudinal cyclic increases with forward airspeed. This is because a helicopter must fly with a larger nose-down attitude to attain a higher forward airspeed, aligning a larger rotor thrust component with the horizontal. Since the tailplane is only deployed once a maneuver is initiated, positive longitudinal cyclic is required to tilt the main rotor forward, putting the helicopter in a more nose-down attitude. The shape of required longitudinal cyclic shows a quadratic increase at higher airspeeds, caused by a quadratically increasing dynamic pressure

and lift at the tailplane. From this figure, it is evident that flight at 160kts is the most critical flight condition, allowing for the lowest longitudinal cyclic margin at its upper limit.

For this reason, a second trim sweep is conducted at 160kts for various stabilator deflection angles. This plot is given in figure 5.8. As can be seen, the stabilizer incidence angles where  $dC_d/d\alpha$  change are now different from the 130kts situation. This is the result of a different angle of attack for the same stabilator incidence angle.

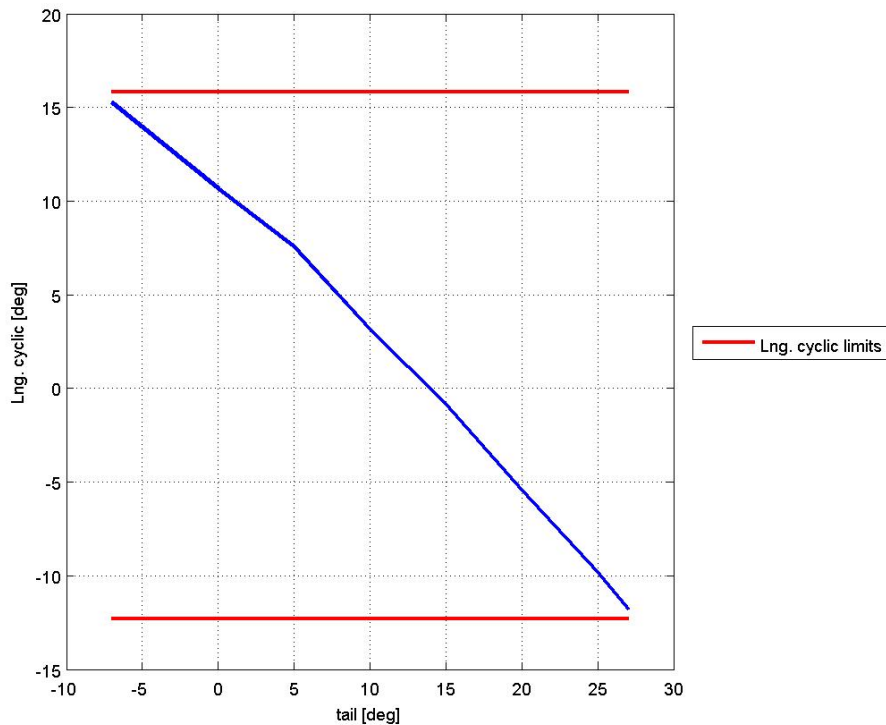


Figure 5.8: Longitudinal cyclic trimsweep for various tail deflection angles, at 160kts with normal cg.

From this plot, being the most critical airspeed condition concerning longitudinal cyclic margin, the maximum tail deflection angles may be chosen to guarantee trimmability of the helicopter flying at any airspeed. As can be seen, the stabilator should not exceed incidence angles of -7deg and 27deg. Figure 5.9 indicates the amount of longitudinal cyclic required to trim the helicopter at various speeds, if the stabilator were to be deflected at these angles. The amount of longitudinal cyclic required at 130kts and 160kts, for these two tail deflection angles, is in accordance with the required longitudinal cyclic as given by trimsweeps at 130kts and 160kts for the same tail deflection angles, shown earlier in figs. 5.6 and 5.8. In fig. 5.9, for a given airspeed, it can be seen that a positive deflection angle will require lower longitudinal cyclic, while a negative tail deflection will require higher longitudinal cyclic for trim.

With the stabilizer stuck at a negative incidence angle, the tail is experiencing an increased downforce than if the stabilator had a zero incidence angle. This requires more longitudinal cyclic to increase nose-down attitude to achieve a higher airspeed. The converse is true for the situation where the stabilator is deflected with a positive incidence angle. This explains why, at each airspeed instance, the amount of longitudinal cyclic will be higher for negative stabilator incidence angles, and lower for most positive deflection angles.

In the situation where the stabilator deflects to a negative or slight positive angle, the pilot will run out of longitudinal cyclic margin at its upper limit. Here, the pilot will not be able to put the helicopter in a further nose-down attitude. While the inability to put the aircraft in a nose-down attitude would be dangerous for a fixed wing aircraft, potentially resulting in stall, the implication in helicopter flight would be that the helicopter cannot further increase its airspeed. By reducing longitudinal cyclic, the helicopter will pitch up, reduce airspeed and recover to a new trim condition.

What might be considered less evident, however, is that the amount of longitudinal cyclic actually decreases with forward airspeed, when the stabilator is stuck at a 27deg incidence angle. The reason for a decrease in longitudinal cyclic with airspeed can be accredited to the fact that the stabilizer has essentially become too effective in reducing download.

With increasing forward speed, the large lift and drag coefficients, combined with the low center of gravity in z-direction and long moment arm in x-axis direction, cause a severe nose-down angle. While an increased nose-down attitude is normally required to increase airspeed, the nose-down attitude change with forward airspeed increase is so severe, that longitudinal cyclic must now be reduced. Hence, the main rotor must compensate this by generating a countering nose-up moment, so that the helicopter pitches down less significantly. Because of this, at high speed, if the stabilator is deflected at 27deg, the helicopter will run out of longitudinal cyclic margin at its lower bound.

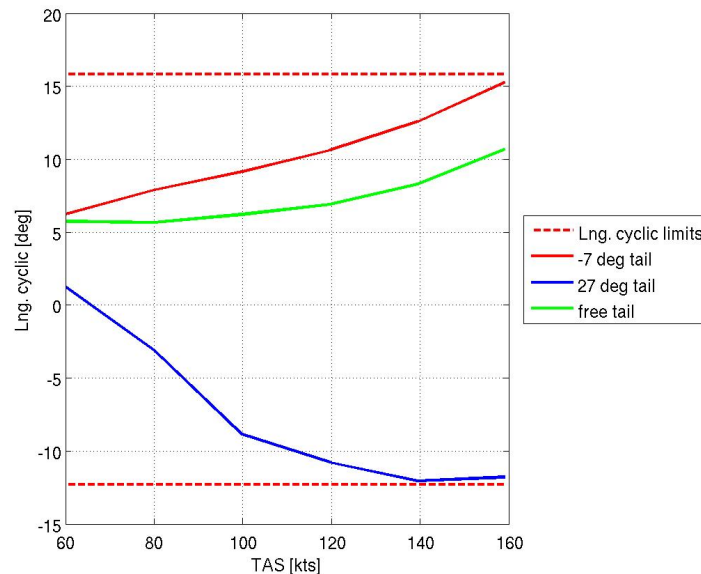


Figure 5.9: Longitudinal cyclic usage versus airspeed, for the -7deg and 27deg stabilator deflection failure cases with normal cg.

The realization that the amount of longitudinal cyclic may decrease with forward speed is of key importance, giving the helicopter unstable speed stability characteristics. The pilot will initially increase longitudinal cyclic to put the helicopter at larger nose-down attitude, to accelerate, and will then reduce longitudinal cyclic to trim the helicopter at constant pitch attitude and airspeed. The reduction of longitudinal cyclic stick position is larger in magnitude than the initial increase required to accelerate.

Concerning the lower bound of longitudinal cyclic, if the stabilator deflects to 27deg when flying 140kts, the pilot may still trim the helicopter in terms of pitch rate with a constant downward flightpath, but will not have any margin to reduce nose-down attitude. This poses great danger as the pilot will not be able to reduce airspeed or fly level. Tail deflections beyond 27 degrees would imply that the pilot would not even be able to trim the aircraft at some airspeed; continuing to pitch down further, increases airspeed, pitching down further, and so on. At this point, the helicopter is not only unstable but also uncontrollable, where the negative pitch attitude-speed stability of the helicopter cannot be overcome by pilot action (Prouty [48]). In summary, table 5.4 indicates key features as found from fig 5.9, and what they entail.

While the helicopter can be trimmed at a 27 degrees stabilator incidence angle, this angle proves dangerous too, flying with a large downward flightpath. There is no longitudinal cyclic margin left to pull the nose up, to change flightpath and to reduce airspeed. Therefore, a trimmable helicopter does not guarantee safety; it demonstrates the ability to remove attitude rates, not the ability to recover to level flight with constant airspeed. As such, trimmability is a prerequisite for safety, but still sets too loose bounds, not taking into account additional control margin required to perform a pull-up following an undesired transient.

Table 5.4: Significant features from the longitudinal cyclic-air-speed trimsweep, and their implications on handling and stability performance.

Attribute	Implication
Upper bound lng. cyclic	Limits maximum airspeed for helicopter in trim.
Lower bound lng. cyclic	No further lng. cyclic margin to pitch up the helicopter and reduce airspeed. Helicopter continues with constant airspeed and downward flightpath. Beyond limit, helicopter is untrimmable; increasing nose-down attitude and airspeed.
Increase lng. cyclic with airspeed	Positive speed stability; increase lng. cyclic to pitch down to achieve higher trim speed. Reduce lng. cyclic for airspeed reduction.
Reduce lng. cyclic with airspeed	Negative speed stability; small increase lng. cyclic to increase speed, subsequently larger decrease in lng. cyclic to maintain larger nose-down attitude and airspeed.

### 5.3.3. STABILATOR LIMITS FOR SUFFICIENT LONGITUDINAL CYCLIC MARGIN

To determine the amount of allowable stabilator deflection, the doublet is performed at off-design conditions, with the two extreme center of gravity locations and at various speeds. Actuation limits are chosen on the basis of the doublet, determining the maximum control authority needed for load reduction during this extreme maneuver. For any other manoeuvre in longitudinal axis, required stabilator actuation will therefore be of smaller magnitude.

Table 5.5 shows the control surface actuation as required by the SLA system to fully reduce loads when performing the doublet. This table shows stabilator actuation for the four considered off-design conditions.

Table 5.5: Stabilator deflection angles as required by the mixed control SLA scheme to maximally reduce loads.

Stab. defl.	C.G. fore, 80kts	C.G. fore, 160kts	C.G. aft, 80kts	C.G. aft, 160kts
positive	8.0	2.6	<b>10.0</b>	2.4
negative	<b>-7.0</b>	-4.9	-4.5	-2.2

From this, it is decided to limit stabilator deflection to incidence angles of -7deg (trailing edge up) and 10deg (trailing edge up). Actuation rate is limited to 45deg/s, allowing for full load alleviation for the off-design conditions. This actuation rate is required for full load alleviation at 80kts, being the lowest airspeed at which the SLA system is fully functional. Here, again, it is evident that the SLA system will command larger stabilator deflection angles at lower airspeeds because of lower control effectiveness. The current UH-60A features a stabilator that is limited to -8deg and 39deg incidence angles, with an actuation rate limit of 7deg/s. The General Dynamics F-16 fighter jet, however, has a maximum elevator actuator rate limit of 60deg/s, an aileron rate of 80deg/s and rudder actuation rate of 120deg/s (Huo [28]). Due to advances in technology, it is felt that one should not be limited to the current UH-60A stabilator actuator. Actuators with minimum rates of 45deg/s should be a viable and affordable option for the UH-60A in the current scope of available technology.

In figure 5.10, the required amount of longitudinal cyclic is given for various stabilator deflection angles, including for the chosen limits of -7deg and 10deg. For the 10deg stabilator angle, it is evident that there is slight speed instability on the 60kts to 100kts interval. Instability is largest on the 60kts to 80kts interval, with  $\frac{\partial \theta_{1s}}{\partial V}$  being  $0.1 \frac{deg}{kts}$ . While Prouty [48] states the desirability of slight positive speed stability, the magnitude of speed instability is considered sufficiently small in this particular failure mode. Secondly, the pilot still possesses enough negative longitudinal cyclic margin when flying at 100kts to perform a pull-up and reduce airspeed. Beyond 100kts, the amount of additional longitudinal cyclic to increase airspeed is positive, as desired, increasing the available longitudinal cyclic margin to allow for a pull-up. Encroaching the upper longitudinal cyclic margin is safe; this only reduces the pilot's ability to tilt the nose forward further, limiting maximum airspeed. Nonetheless, the -7deg tail incidence still allows for flight at 160kts.

In conclusion, from a trimsweep at the most critical airspeed with a normal cg, the UH-60A is trimmable for maximum stabilator angles of -7deg and 27deg. The helicopter possesses a speed instability at positive stabilator deflection angles. At angles below -7deg, the helicopter cannot increase its

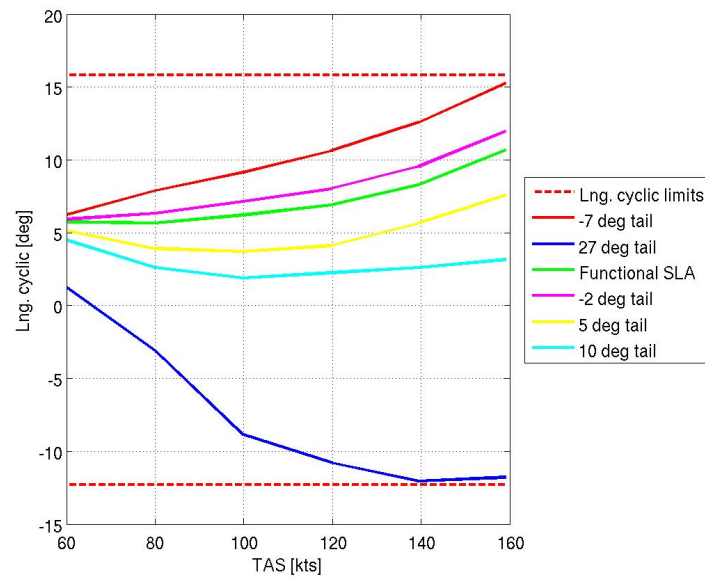


Figure 5.10: Longitudinal cyclic usage versus airspeed, including failure at chosen stabilator deflection limits of -7deg and 10deg, with normal cg.

airspeed beyond 160kts. Stabilator deflection angles are chosen by determining the required deflections for full load reductions, for the most forward and aft center of gravity, and over the airspeed range of 80kts to 160kts. As such, it is determined to limit the stabilator to actuation limits of -7deg and 10deg. At a stabilator deflection of 10deg, the helicopter possesses slight speed instability, being no larger than  $0.1 \frac{\text{deg}}{\text{kts}} \frac{\partial \theta_s}{\partial V}$ . In terms of hardware alterations, the UH-60A would require a different stabilator actuator, capable of reaching 45deg/s actuation rates.

While one may argue that trimsweeps should have also been conducted for the most forward and most aft configurations when flying at 160kts, this is deemed unnecessary. If the longitudinal cyclic upper limit is reached before the -7deg stabilator deflection, this will simply limit the maximum airspeed, posing no danger. With the imposed stabilator upper deflection limit of 10deg, well beyond 27deg deemed necessary for the normal center of gravity, it is felt that sufficient longitudinal cyclic margin is in place for any center of gravity condition.

#### 5.3.4. THE CONSTRAINED SLA SYSTEM

As derived in the aforementioned section, it is decided to limit the stabilator to deflection incidence angles of -7deg and 10deg, as well as imposing a rate limit of 45deg/s. With these constraints in place, the altered SLA system is depicted in fig. 5.11. This system will be used in further assessment. Therefore, the three previously mentioned failure cases to be considered become:

- Maximum positive stabilator deflection of 10deg
- Maximum negative stabilator deflection of -7deg
- Rate limited stabilator; arbitrarily chosen at 0.1deg/s

So far, assessment has taken place with the full longitudinal control architecture in place, as shown in figure 5.12. Here, the outer control loop is also considered which consists of the PI-controller and pitch rate feedback system. These control components are grouped together and are referred to as the longitudinal controller, because of their corrective nature. Together with the lateral-directional controller, the inclusion of this outer loop provides insight in (auto)pilot behavior when flying with the SLA system. Evidently, to attain trim flight with a stuck stabilator, corrective action is permitted. For the agility assessment further on however, the longitudinal and lateral-directional controllers will be excluded. Reason for this is because it is of interest to determine the impact of the SLA system on agility, as compared to the baseline helicopter. An (auto)pilot system providing corrective action will

alter this agility, and will therefore not provide a pure indication of the SLA system agility performance. In real-life, however, an (auto)pilot will respond with corrective action. In appendix C, the SLA system's agility with longitudinal and lateral-directional controllers is provided, giving an indication of behavior following potential (auto)pilot input. In this research, however, these controllers are omitted, to determine the pure impact of the SLA system on agility. In case of no longitudinal controller, a longitudinal cyclic stick command is fed directly to the SLA or baseline system. This subsequently results in control deflection at the main rotor and stabilator, depending on the control scheme or failure case. For the same percentage longitudinal cyclic stick deflection, the amount of longitudinal cyclic and stabilator deflection will vary according to the control scheme and failure state. In the failure states, some of this commanded stabilator deflection will therefore be 'lost'.

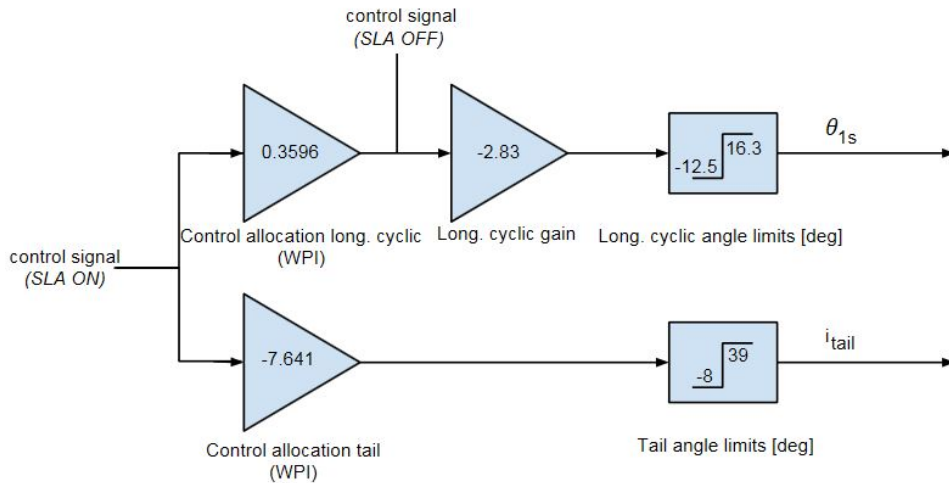


Figure 5.11: The mixed control SLA system architecture, including stabilator actuation deflection and rate limits.

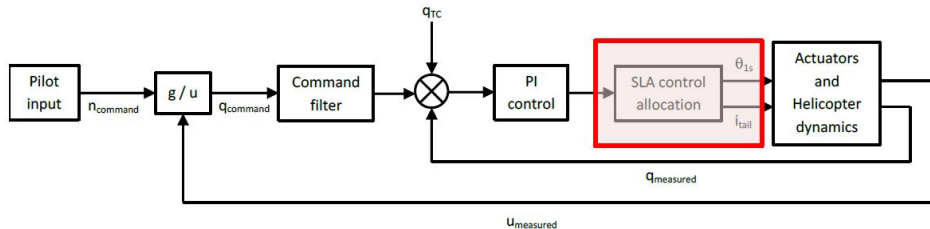


Figure 5.12: Longitudinal control system architecture with SLA functionality (Voskuijl [54]).

For the assessment of loadfactor transients following stabilator deflection, the helicopter will be assessed with and without corrective action, while for the safe landing conditions, corrective action is also considered. For the subsequent agility analysis, the SLA, baseline and failed SLA states are assessed without longitudinal and lateral-directional controllers in place, for the aforementioned reasons.

### 5.3.5. ASSESSMENT OF LOADFACTOR AND SAFE LANDING FOR CHOSEN STABILATOR DEFLECTION LIMITS

The chosen stabilator deflection angles will provide a trimmable helicopter with sufficient longitudinal cyclic margin to perform a pull-up for all off-design conditions. However, the final two criteria set out in table 5.3 must also be addressed.

#### Load factor transient after failure

For the four off-design conditions initially starting from level flight, table 5.6 shows the transient of load factor following maximum positive or negative stabilator deflection angle. Results are included for active longitudinal and lateral-directional controllers, as well as for the bare SLA system without

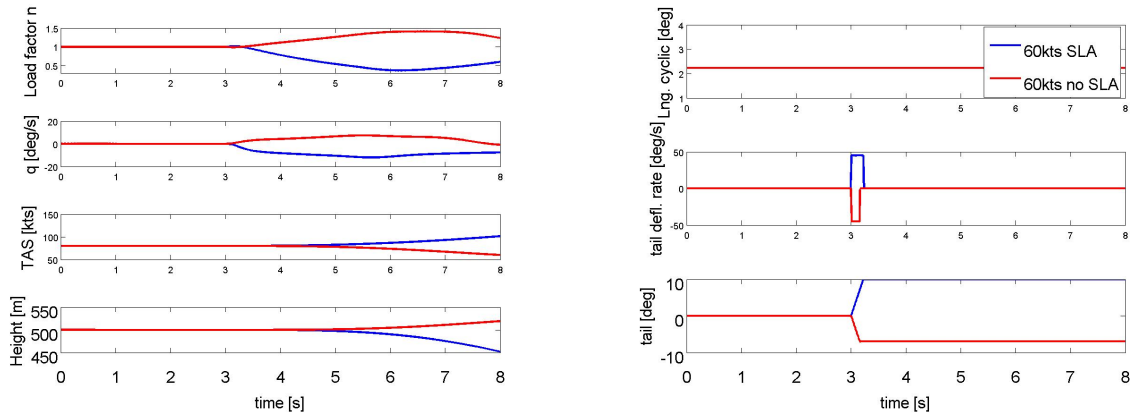
these controllers. This indicates the difference in peak loadfactor for corrected and uncorrected response following stabilator deflection.

Table 5.6: Load factor transients following stabilator deflection, for various flight conditions.

C.G. position	Airspeed [kts]	Stab. defl. [deg.]	Loadfactor n [g]	Loadfactor n [g]
			SLA	SLA + Lng. controller
fore	80	-7	1.41	0.96
fore	80	10	0.37	1.07
fore	160	-7	1.77	0.58
fore	160	10	-1.0	1.54
aft	80	-7	2.0	0.92
aft	80	10	-0.15	1.09
aft	160	-7	2.3	0.56
aft	160	10	-1.8	1.54

From table 5.6, it can be seen that a hardover in level flight, causing maximum positive or negative stabilator deflection will show potentially dangerous peak load factors when left uncorrected, sometimes even exceeding structural load factors of the UH-60A. The stabilator is deflected at its maximum rate of 45 deg/s, being the worst-case situation. The excessive load factors occur due to lack of corrective action, normally supplied by the longitudinal control system. However, MIL does not state that there may not be pilot corrective action. When the same stabilator deflection occurs with the longitudinal controller engaged, aimed at maintaining a zero pitch rate, positive stabilator deflection now causes load factors larger than unity, while negative stabilator deflection causes load factors smaller than unity. To understand this opposite behavior, the load factor, pitch rate and control transients are shown in figures 5.13 and 5.14 for one specific off-design condition, with and without longitudinal controller. Note that these figures are not to scale; aimed at showing transient patterns. Without longitudinal controller active, reduction of stabilator incidence causes a larger pitch rate resulting in a loadfactor increase. However, as figure 5.15 shows for the same system, load factor first decreases briefly, before seeing the rise caused by change in pitch attitude. This observation is of key importance, and is the result of the working principle of the SLA system. The decrease in stabilator incidence causes a larger downforce by the main rotor on the stabilator. This briefly results in a reduction of overall net lift of the helicopter, in body z-axis. This results in a brief downward motion, and, since loadfactor depends on body acceleration  $a_z$ , loadfactor will decrease. However, this decrease in loadfactor for negative stabilator incidence is of short duration. While experiencing a sink rate because of increased stabilator downforce, the helicopter also pitches up, increasing  $F_z$  and loadfactor again. This latter effect of pitch motion has a more pronounced effect on loadfactor in the long run than the initial sinking behavior. With longitudinal controller active, the helicopter sees the initial loadfactor tendency caused by the temporary sink rate; the countering use of longitudinal cyclic to maintain a zero pitch attitude will not increase the overall lift of the helicopter. The longer term tendency of higher load factor with decreased incidence angle is, however, reduced, since the adverse pitch rate is largely compensated by the controller. Therefore, the maximum loadfactor with and without longitudinal controller will be at opposite sides of unity.

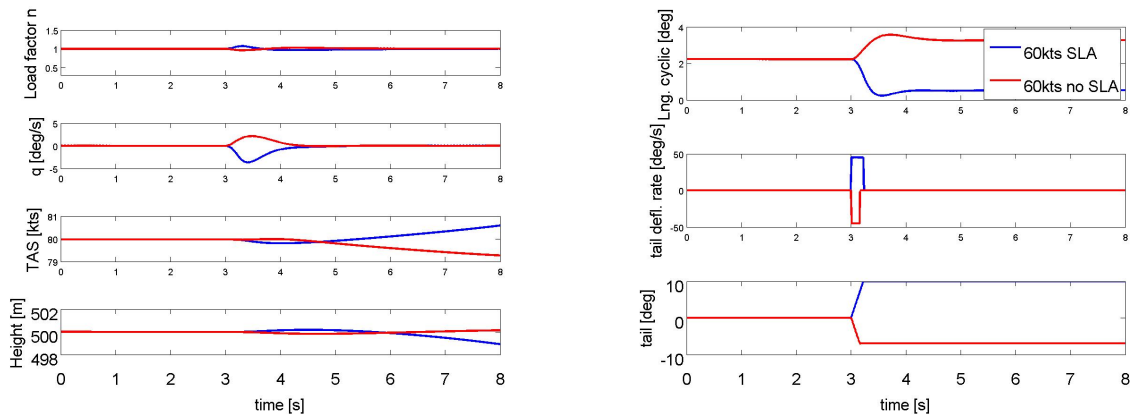
The longitudinal controller demonstrates the ability to avoid excessive loadfactor transients, when applying corrective longitudinal cyclic. Though loadfactor transients now show slight exceedance of 1.5g, an auto(pilot) may compensate the change in net overall helicopter lift by altering collective controls. Nonetheless, as maximum loadfactor is only slightly higher than the arbitrary limit of 1.5g, this SLA system is considered safe.



(a) Velocity, load factor and pitch rate transients

(b) Longitudinal control transients

Figure 5.13: Transients following stabilator deflection, 80kts and fore cg, without longitudinal controller.



(a) Velocity, load factor and pitch rate transients

(b) Longitudinal control transients

Figure 5.14: Transients following stabilator deflection, 80kts and fore cg, with longitudinal controller.

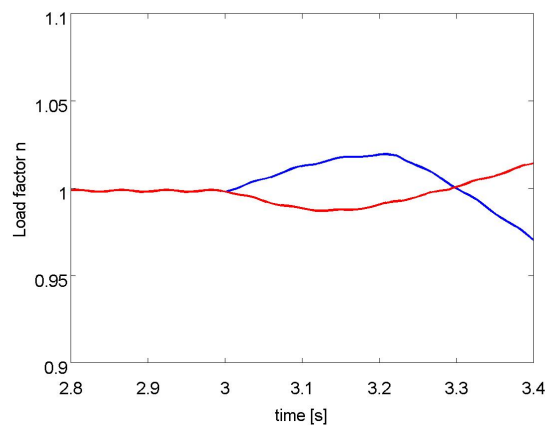


Figure 5.15: Short term response of loadfactor after tail deflection, no longitudinal controller.

### Helicopter attitudes allowing for a safe landing

With a maximum landing speed of 60kts, the stabilator is deflected maximally up and down for the two extreme cg positions. This is done to simulate a landing after SLA system failure. Table 5.7 indicates the helicopter's attitude when trimmed to level flight at 60kts, with positive or negative aileron deflection. From this, it is evident that attitude remains well within the bounds of -6deg and 15deg, allowing for a safe landing. For any center of gravity condition, the helicopter attitude will never exceed -1.5deg or 7deg.

Table 5.7: Helicopter attitudes at 60kts flight, with stabilator deflection.

C.G. position	Stabilator deflection [deg.]	Pitch attitude $\theta$ [deg]	Safe?
fore	-7	-0.9	✓
fore	10	-1.5	✓
aft	-7	6.8	✓
aft	10	5.8	✓

While reducing actuator deflection limits increases longitudinal cyclic margin, there will be an adverse effect on agility. This latter property is of importance, quantifying the response of the helicopter following stick input. Aside from safety, the SLA system must not cause an unacceptably slow or small-magnitude response. To determine the constrained SLA system's handling qualities, its agility will be compared to that of the baseline helicopter. This will be assessed when the SLA system is fully functional. Secondly, three SLA failure cases will be assessed, to determine to which degree agility changes. The failure cases for assessment, as given in section 5.3.4, include maximum stabilator incidence angles of -7deg and 10deg, as well as a 0.1deg/s rate limited stabilator. After failure, there are reduced requirements in terms of agility, as long as pilot input yields some response in the longitudinal axis. In the following section, various metrics quantifying agility are discussed.

## 5.4. AGILITY FOLLOWING CONSTRAINTS

It has been determined previously that limiting the stabilator actuator to deflection angles of -7deg and 10deg, and an actuation rate of 45deg/s provides sufficient off-design performance and safety characteristics. These limits allow for full load reduction above 80kts, performing a maneuver not exceeding the 1.75g doublet. However, constraining the stabilator will impact the agility of the helicopter with the SLA system in place. For this reason, agility of the constrained mixed control SLA system will be compared to that of the baseline system. Secondly, agility is assessed for the three failure cases as well. These may show lower agility, as long as the pilot still has the capability to perform a pull-up.

Since it is of primary concern is to determine the ability to perform a pull-up to reduce airspeed, responsiveness in the longitudinal axis is of importance. Therefore, the maneuver used for assessment is a step pull-up. Agility metrics should therefore solely assess the behavior in longitudinal direction. Three metrics assess agility for this maneuver; attitude quickness, agility quickness, and flightpath agility quickness. However, for inputs supplied at various frequencies, flightpath bandwidth and pitch rate bandwidth assess agility. Of these various metrics, flightpath bandwidth is a novel metric, presented in this research. It is felt that this metric, considering the ability to change flightpath trajectory, would set more adequate safety requirements if included in ADS-33E.

### 5.4.1. ATTITUDE QUICKNESS

The most commonly accepted metric, given by ADS-33E, is attitude quickness. After pilot input, the maximum rate is divided by the attitude change around the same axis. Of specific interest is pitch attitude quickness, being the peak pitch rate, divided by the change in attitude, as given by equation 5.1.

$$Q_{\theta} = \frac{q_{pk}}{\Delta\theta} \quad (5.1)$$

This gives an indication of how quickly an attitude change is attainable; how rapidly the pitch rate

can rise. If pitch rate changes more rapidly, the peak pitch rate will be higher over a shorter attitude change. In fig. 5.16, the various handling quality levels are defined in terms of attitude quickness and change in aircraft attitude, when performing a low speed manoeuvre from level flight. Fig. 5.17 provides a definition for change in attitude.

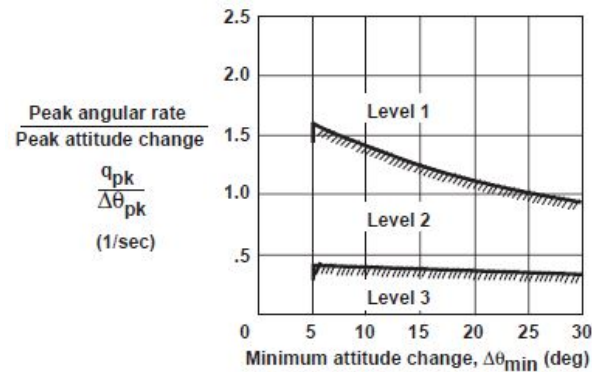


Figure 5.16: HQ ratings in terms of attitude quickness as defined by ADS-33E, applicable for airspeeds of up to 45kts forward flight (ADS-33E [2]).

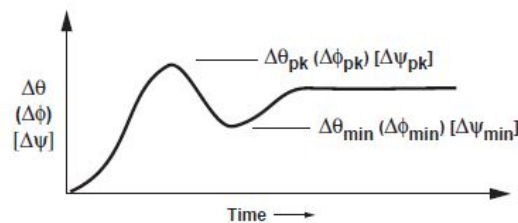


Figure 5.17: The definition of attitude changes as required for pitch attitude analysis (ADS-33E [2]).

Before presenting results for attitude quickness, the pitch rate response to a step longitudinal input is shown in fig. 5.18, for the five control scenarios. This is shown to give an indication of the magnitude of response for an identical control step input of equal intensity and duration. Figure 5.19 shows the pitch rate response when flying at the four off-design conditions. Such transient response is used in the analysis of attitude quickness, agility quickness, and flightpath quickness metrics.

The attitude quickness of the SLA and baseline helicopters is shown in figure 5.20, when flying in the SLA's design conditions of 130kts airspeed and normal cg. For each control case, the attitude quickness was found by providing a step input pull-up command of equal intensity, yet of different durations. For each control situation, four pull-ups of differing duration are considered; 0.5s, 1s, 1.5s and 2s. For a given longitudinal stick input, the helicopter will first see a rapid change in attitude, gradually flattening out. Thus, the longer the step input, the larger the attitude change, and the lower the agility quickness, ie. following a line from top left to bottom right through the plot. Transients start at the left for the 0.5s input and end on the right for the 2s input. From this plot, it can be seen that the SLA system is more agile as compared to the baseline UH-60A, for all stick input durations. For a given change in aircraft pitch attitude, peak pitch rate is considerably higher. When comparing both responses for stick inputs of equal duration, it can be seen that the SLA helicopter will show a larger change in attitude. This is also evident from fig. 5.18.

Concerning the three failure cases, this plot demonstrates that the pilot can still command a pull-up. As expected, the rate limited SLA system has an agility in between that of the SLA and baseline system. The -7deg failure case performs marginally worse than the baseline helicopter, while the 10deg failure case shows smaller variations in attitude quickness for longitudinal stick inputs of varying intensity.

Since the helicopter will also operate in other conditions than those used to design the SLA system, off-design attitude quickness is also considered, as given in fig. 5.21.

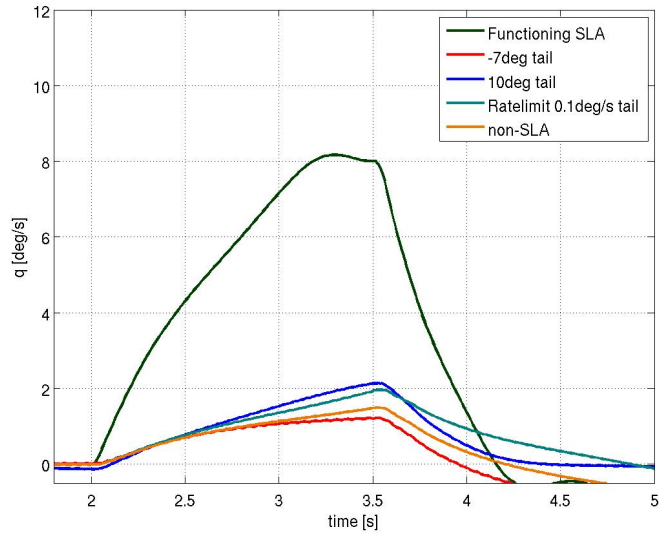
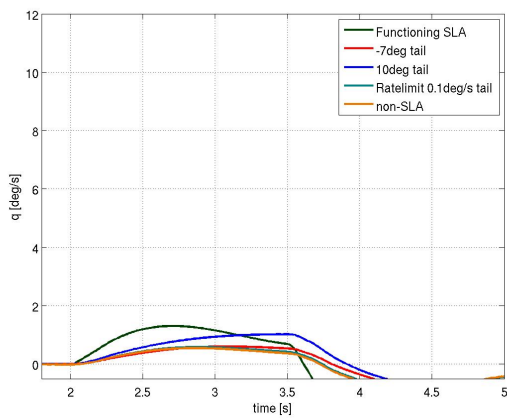
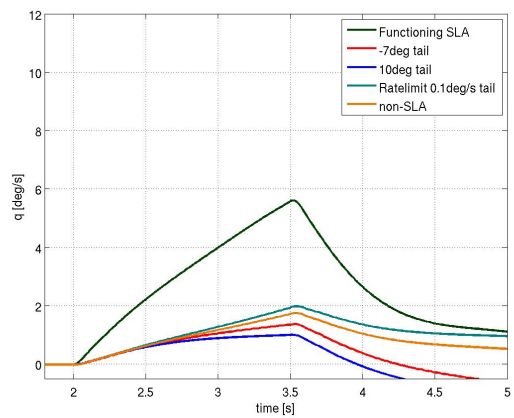


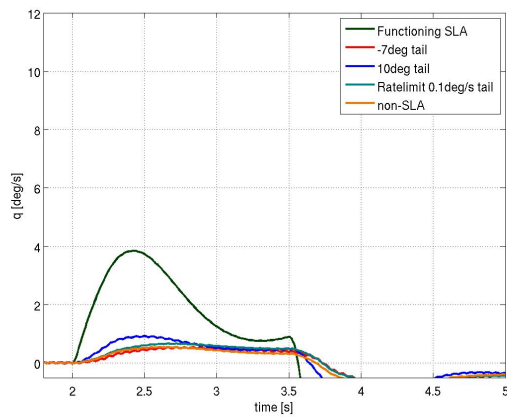
Figure 5.18: Pitch rate response for a step longitudinal cyclic stick input when operating in design conditions, for various control situations.



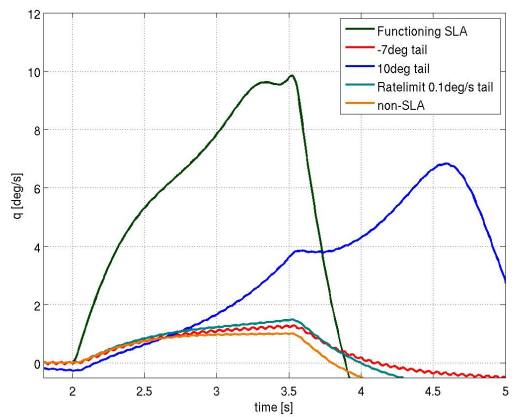
(a) 80kts flight and forward center of gravity



(b) 80kts flight and aft center of gravity



(c) 160kts flight and forward center of gravity



(d) 160kts flight and aft center of gravity

Figure 5.19: Off-design pitch rate response for a step longitudinal cyclic stick input, for various control situations.

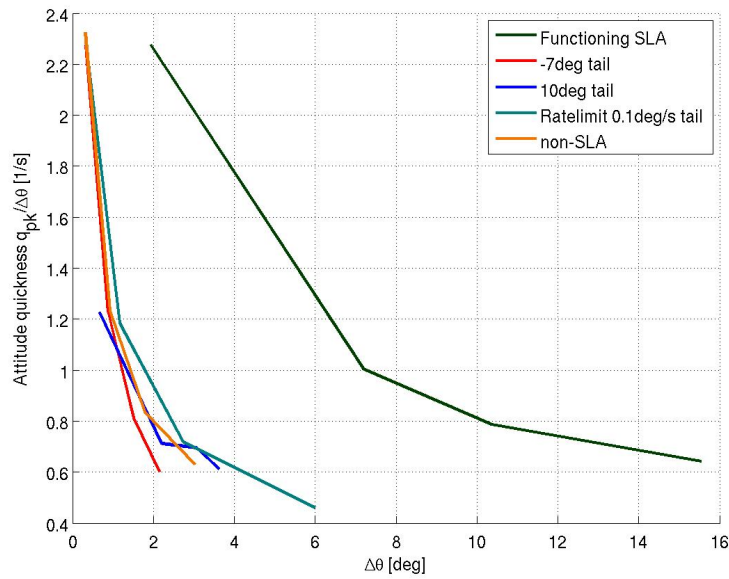
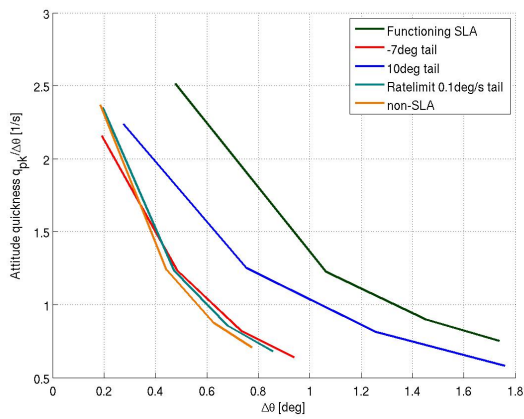
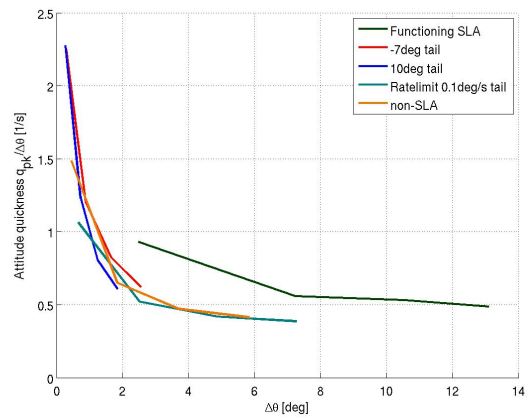


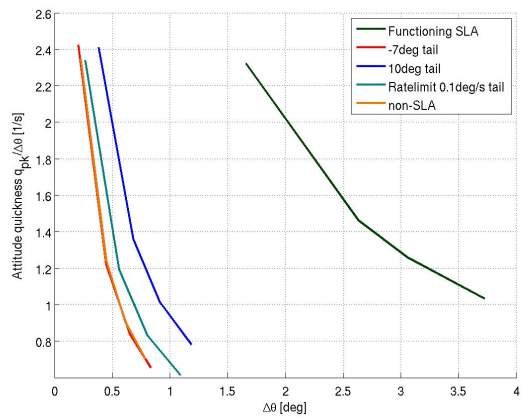
Figure 5.20: Attitude quickness when operating under design conditions; 130kts and normal center of gravity.



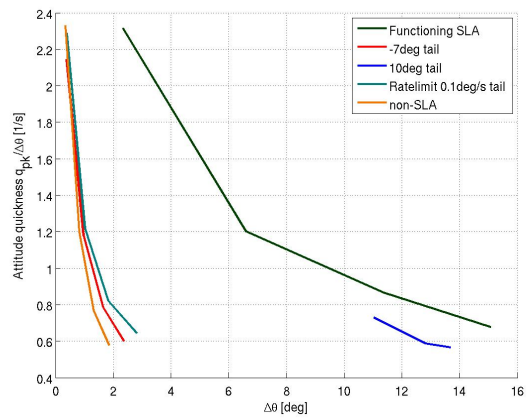
(a) 80kts flight and forward center of gravity



(b) 80kts flight and aft center of gravity



(c) 160kts flight and forward center of gravity



(d) 160kts flight and aft center of gravity

Figure 5.21: Attitude quickness for off-design conditions.

From figure 5.21, it can be seen that the SLA system has a higher attitude quickness than the baseline system. For a 0.5s longitudinal stick input, the 80kts fore cg condition shows the lowest attitude quickness, being farthest from the design condition of the SLA system. Nonetheless, when looking at attitude quickness for a given change in pitch attitude, the SLA system is more agile, though requiring a longer stick input. The three failure cases perform very similar or marginally better than the baseline helicopter.

However, this metric has some major downfalls, as discussed by Pavel and Padfield [43]. Most importantly, attitude quickness handling quality requirements shown in fig 5.16, are only applicable for low speed flight, with airspeeds not exceeding 45kts. At the speeds that are of interest for this SLA application, ADS-33E does not define any pitch attitude requirements. For this reason, the boundaries between handling quality levels, as set in fig 5.16 are not applicable, and one can only make qualitative judgments based on figures 5.20 and 5.21. For the considered flight condition, ADS-33E only requires the helicopter to remain within the operational flight envelope (OFE). Secondly, while this metric considers aircraft attitude agility to be guiding, the pilot is mainly concerned with flightpath trajectory changes.

#### 5.4.2. AGILITY QUICKNESS

Because of the aforementioned downfalls, Pavel and Padfield [43] propose a new quickness metric that is applicable at high speed flight as well. Known as agility quickness, this metric is defined as the maximum load factor experienced over a change in flightpath, given by equation 5.2.

$$Q_n = \frac{n_{pk}}{\Delta\gamma} \quad (5.2)$$

As load factor closely correlates to the flightpath trajectory of a helicopter, this metric shows strong similarities to attitude quickness, though now considering trajectory changes instead of aircraft orientation changes. Figure 5.22 shows the agility quickness for the SLA and baseline UH-60A when flying at 130kts and with a normal center of gravity. The three failure cases are furthermore included. From the short interval in flightpath angle change for which SLA and baseline systems overlap, one can conclude that agility quickness for the SLA system is higher than for the baseline helicopter. It is expected that agility quickness will be higher for the SLA system, especially towards larger changes in flight path angle. As compared to attitude quickness, the helicopter appears to be less agile in changing trajectory. This is caused by the short term adverse change in overall helicopter lift caused by stabilator deflection, as mentioned in section 5.3.5. However, the more rapid change in pitch attitude will result in larger changes in loadfactor for inputs of longer duration, largely offsetting the initial short-term reduction of net lift. Therefore, while allowing for much larger agility differences in terms of pitch attitude, the difference in agility for trajectory changes are of smaller magnitude, as compared to the baseline helicopter. To achieve the same flightpath angle change, longitudinal stick cyclic input must be provided for longer duration, as is seen in figure 5.22. The 7deg and 0.1deg/s failure cases perform similarly to the baseline helicopter, while the 10deg failure case sees higher agility.

Figure 5.23 shows the agility quickness for the off-design conditions, again showing similar agility for the various control situations in terms of flight path trajectory changes. In general, agility quickness appears to be similar for all systems. Though SLA and baseline systems rarely overlap for change in flight path angle, performance for both systems is, in general, similar, though, as stated earlier, the SLA system required a longer stick input for the same change in flightpath angle.

While this metric provides insight in the ability to change flightpath trajectory, it does not allow proper comparison to attitude quickness. This is because units differ, as this metric considers a load-factor instead of a rate change in flightpath angle. For this reason, a third quickness metric is proposed, allowing better comparison to attitude quickness.

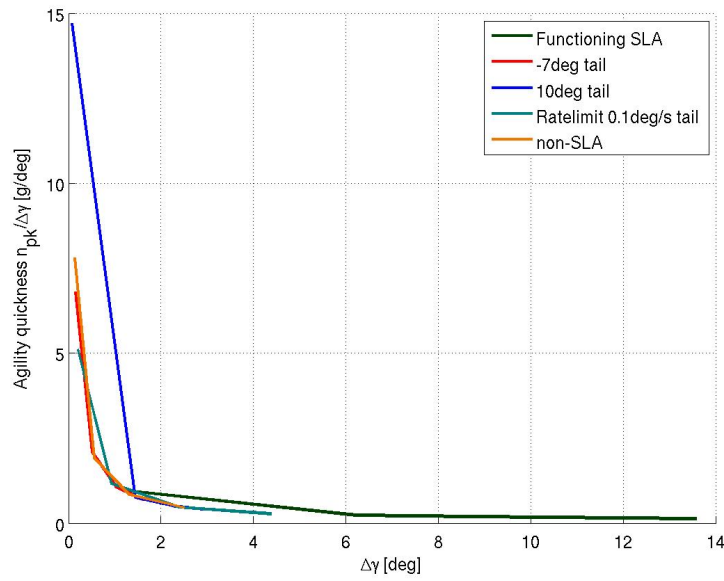
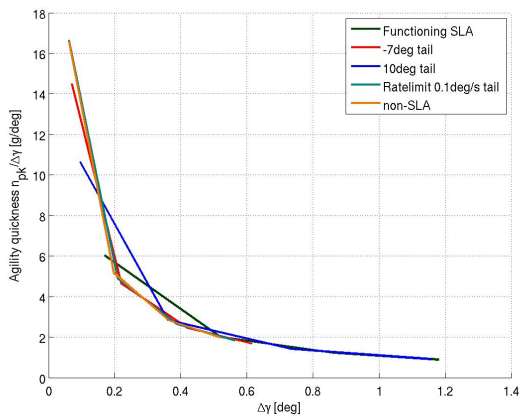
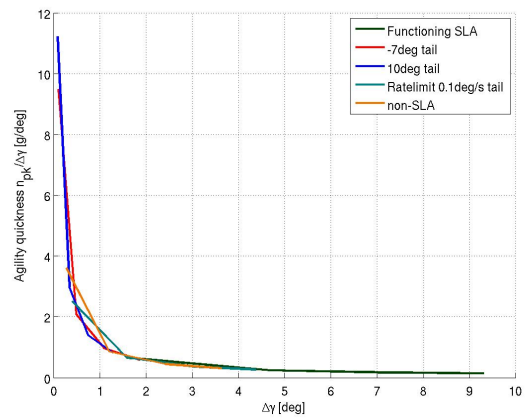


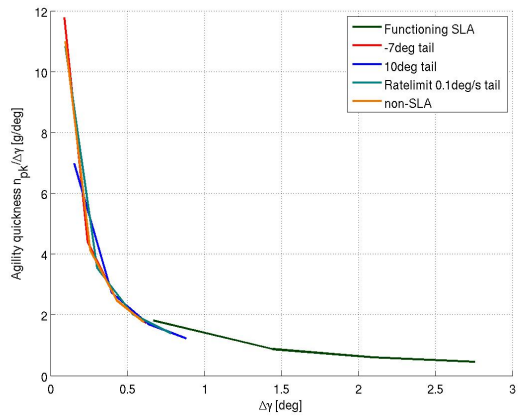
Figure 5.22: Agility quickness when operating under design conditions; 130kts and normal center of gravity.



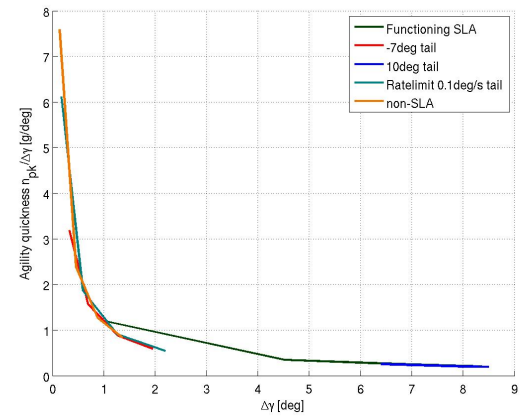
(a) 80kts flight and forward center of gravity



(b) 80kts flight and aft center of gravity



(c) 160kts flight and forward center of gravity



(d) 160kts flight and aft center of gravity

Figure 5.23: Agility quickness for off-design conditions.

### 5.4.3. FLIGHTPATH AGILITY QUICKNESS

A third metric is developed in this research, based on the two preceding metrics. Named longitudinal agility quickness, this metric is defined as the maximum rate of change of flightpath angle divided by the change in flightpath angle, as given by equation 5.3.

$$Q_{\gamma} = \frac{\dot{\gamma}_{pk}}{\Delta\gamma} \quad (5.3)$$

By using maximum rate of change of flightpath angle, this metric allows for better comparison to attitude quickness results; containing similar units, though assessing trajectory changes instead of attitude changes.

Figure 5.24 shows the flightpath agility quickness for the five control situations when flying with normal center of gravity at 130kts. Flightpath agility quickness is larger for the SLA system as compared to the baseline helicopter, and increases with larger changes in flightpath angle. This follows the same reasoning as provided for agility quickness, where there is an initial adverse change in lift caused by stabilator deflection. The three failure cases show the continued ability to change flight path angle after failure.

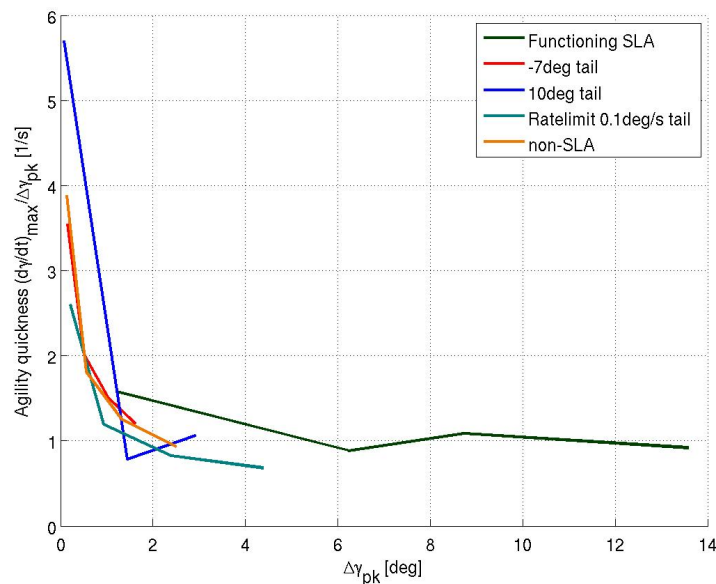


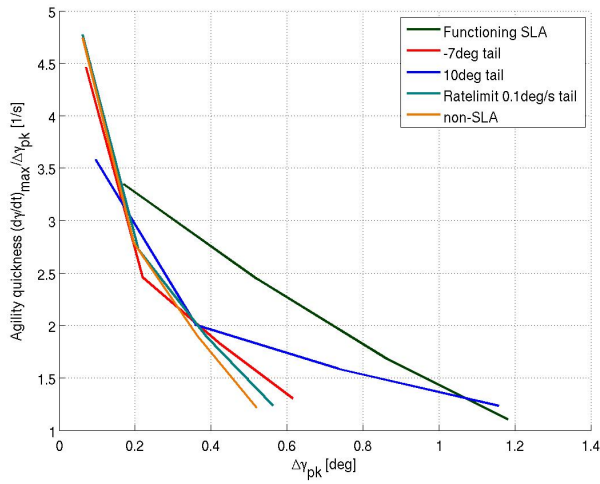
Figure 5.24: Flightpath agility quickness when operating under design conditions; 130kts and normal center of gravity.

In off-design conditions, figure 5.25 shows that, in general, the SLA system will possess greater flightpath agility quickness than the baseline helicopter. The three failure cases still allow for a change in flightpath.

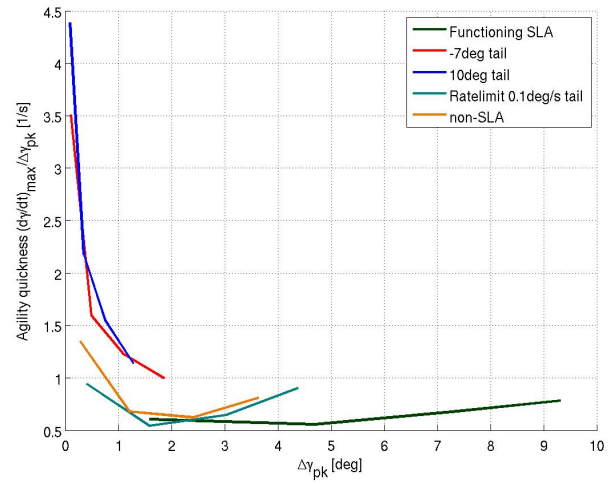
From these plots, it is seen that, in general, the SLA system will perform with less agility than the baseline system and the SLA failure modes. The rate limited SLA failure mode sees performance in between the fixed tail and the functioning SLA system situation, experiencing less initial adverse overall helicopter lift reduction.

As compared to attitude quickness, the SLA and baseline systems show more similar agility when measured in terms of flightpath agility quickness. While allowing for more rapid pitch change due to increased stabilator downforce, the initial adverse effect of reduced net helicopter lift counters the desired trajectory change, as seen in the agility quickness and flightpath agility quickness figures.

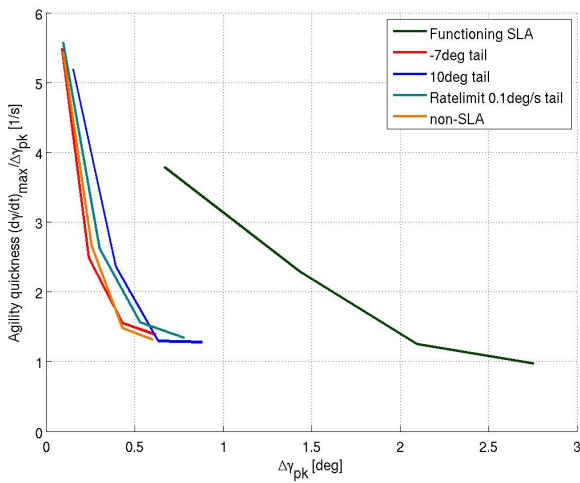
While quickness metrics provide a qualitative means to assess the ability to rapidly change a given response parameter, these metrics have their limitations. By assessing the peak rate change over change in that parameter, there is a qualitative frequency measurement once response starts to occur. However, time dependence of response should also be considered.



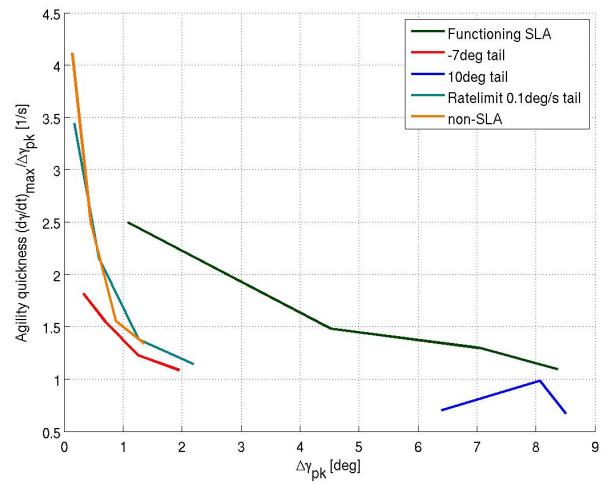
(a) 80kts flight and forward center of gravity



(b) 80kts flight and aft center of gravity



(c) 160kts flight and forward center of gravity



(d) 160kts flight and aft center of gravity

Figure 5.25: Flightpath agility quickness for off-design conditions.

## 5.4.4. FLIGHTPATH BANDWIDTH

A proper agility metric should also consider the time dependence of response for a given control input. Following a control input, a rapid change after considerable time may yield a favorable quickness value, but does not make for an agile helicopter. Figure 5.26 attempts to provide a qualitative measure for this criterion, presenting the pitch rates shown earlier in figure 5.19. A tangent line can be drawn from the moment the stick input is applied, to the transient response. The slope of this tangent line indicates the maximum average change in pitch rate over time, from the time that input was supplied. Note that these graphs are not to scale and should not be compared. Different scale factors have been used to qualitatively show the differing time durations required for the highest average pitch rate response to occur; where the tangent line touches the pitch rate response.

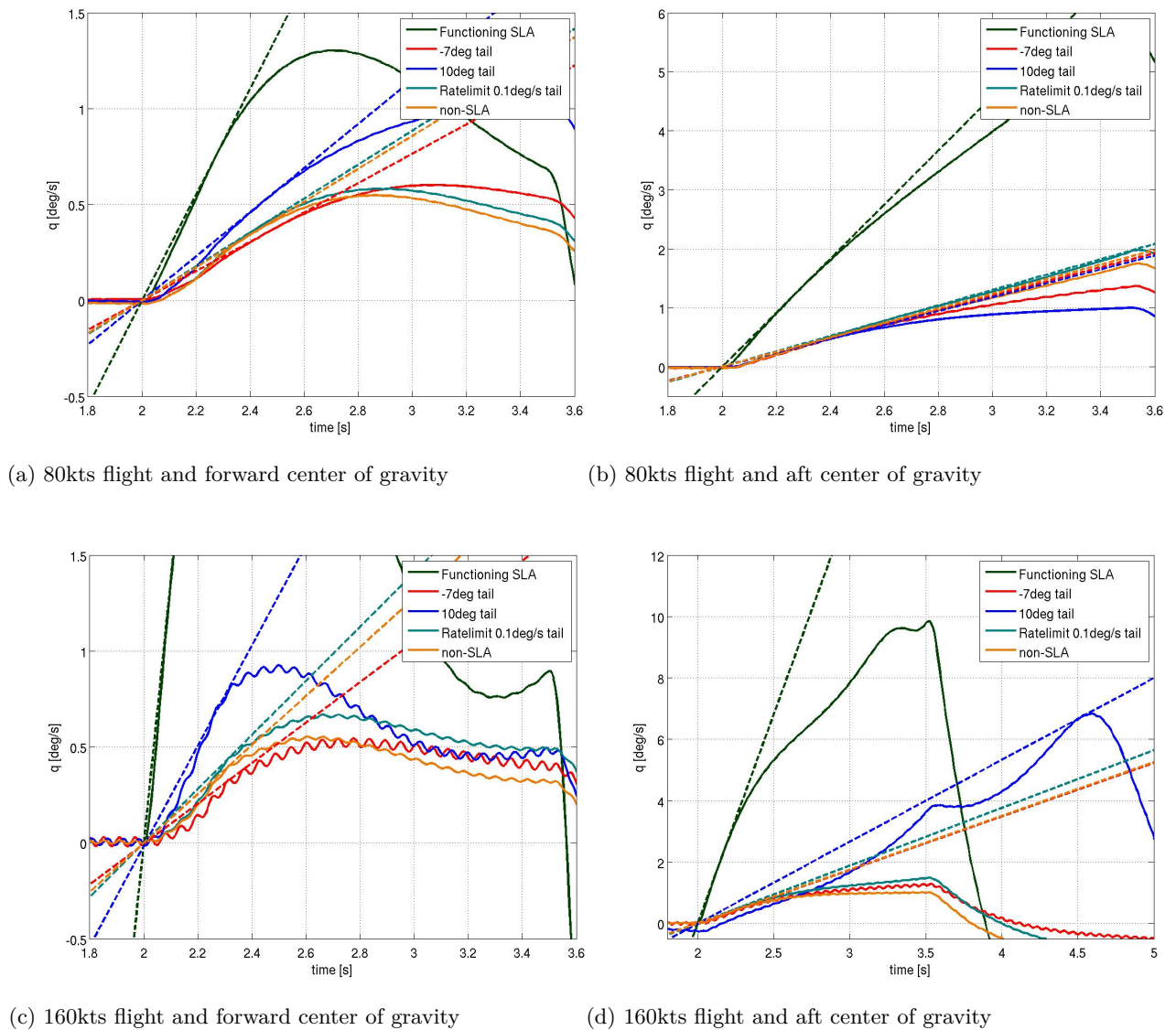


Figure 5.26: Transient pitch rate response and peak change in pitch rate after doublet input, for various control situations.

It was demonstrated earlier that the SLA system has a higher agility quickness than the baseline and failed SLA systems, providing largest pitch rate changes for a given attitude change, once response starts to occur. From their slopes, the tangent lines in figure 5.26 indicate that the functioning SLA system also shows the shortest response time after control input. The need for such a metric is made more evident when considering a control system with feedback response. When operating with the

longitudinal controller, a delay in response may result in sharp overcompensation in pitch rate. This results in a larger pitch rate over a smaller attitude change, resulting in a higher attitude quickness. However, the present analysis only considers the SLA system, omitting any external longitudinal control system. Results when considering the longitudinal control system are provided in appendix C, yet will not be considered further in the present discussion.

From the observation that time dependence following control input is also important, a quantitative measure is developed, known as flightpath bandwidth. The helicopter is seen as a linear system, with longitudinal cyclic stick controls as input signal, and helicopter flightpath as output signal. Instead of a single pull-up step, input to longitudinal stick cyclic is provided in various frequencies. The helicopter model is linearized around a center of gravity and airspeed condition, and is represented in the state-space form given by eq. 5.4.

$$\dot{x}(t) = Ax(t) + Bu(t) \quad y(t) = Cx(t) + Du(t) \quad (5.4)$$

Here, vectors  $u$  and  $y$  contain the input and output vectors. Vector  $x$  is the state vector. The input vector contains all pilot controls; main rotor collective, longitudinal and lateral collective, and tail rotor collective. The output vector contains any parameter of interest, in this case containing flightpath angle. State vector  $x$  contains state parameters such as the three velocity components, as well as angular rates and attitudes. Through linear perturbation of the helicopter model, vectors  $A$  through  $D$  are obtained, indicating the sensitivity to state and control variables.

Through use of a Bode plot, response magnitude is the ratio of various frequency longitudinal cyclic stick inputs to subsequent flightpath angle outputs. Output response will be similar to input, yet with a change in magnitude and phase. At some input frequency, the ratio of output to input magnitude will start to decrease significantly; the helicopter cannot respond quickly enough to the input, causing a decay in magnitude. This is related to the notions of crossover frequency and bandwidth. By convention, the crossover frequency is when the decibel magnitude ratio is zero, meaning that input and output magnitude are equal. Bandwidth is often chosen to be the frequency at which an output/input magnitude ratio is below -3dB. This is because the output signal's amplitude remains below the RMS value of the input, which is arbitrarily chosen as the boundary between sufficient and insufficient response. This definition of bandwidth is arbitrary and will not be applied here. Instead, the gain margin transient shapes are compared to those of the baseline helicopter. When flying at a normal cg and at 130kts, flightpath bandwidth is given in figure 5.27.

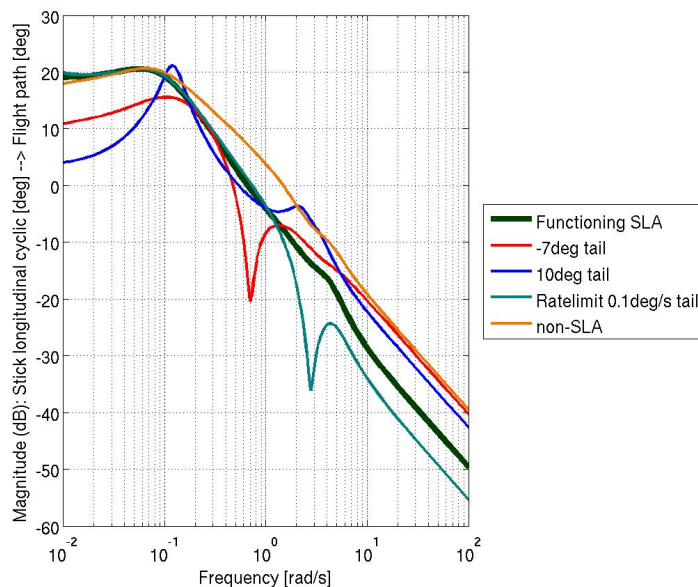
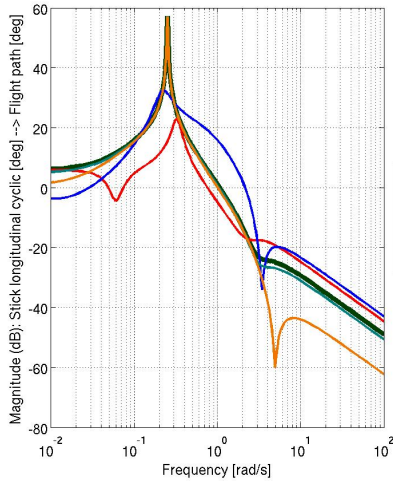


Figure 5.27: Flightpath bandwidth; normal cg configuration.

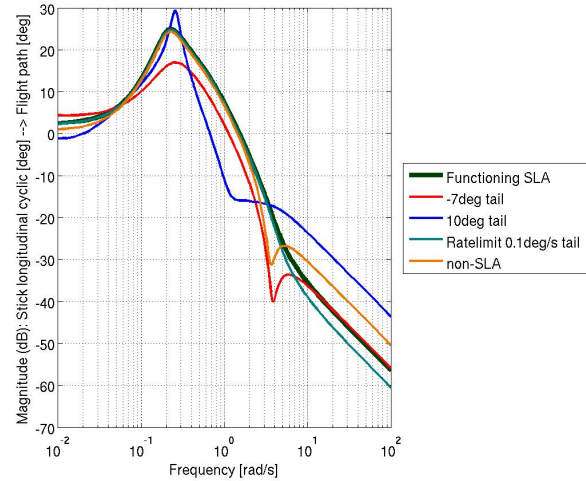
When comparing the SLA and baseline systems in figure 5.27, the SLA system sees a similar gain

as the baseline system at low frequencies. Both systems resemble a first order system, while at higher frequencies, both systems see a fairly linear roll-off rate. The output magnitude of the baseline system is larger. The linear roll-off is desirable, enhancing the predictability of response magnitude for a given pilot input. The difference in gain at higher frequencies is likely caused by the different working principle of the SLA system, with the initial adverse effect of net helicopter lift reduction on flightpath. Therefore, when initiating the pitch attitude, flightpath response is initially lower, yet after more rapid rotor disc tilting, flightpath response will be larger over time. For a step input, therefore, flightpath agility quickness is higher for the SLA helicopter, as shown in figure 5.24. Yet as frequency increases, the delayed benefits of more rapid rotor disc tilt will diminish, and the short term effects of adverse net helicopter lift reduction become more dominant, as the stabilator and longitudinal cyclic are oscillated at higher frequencies.

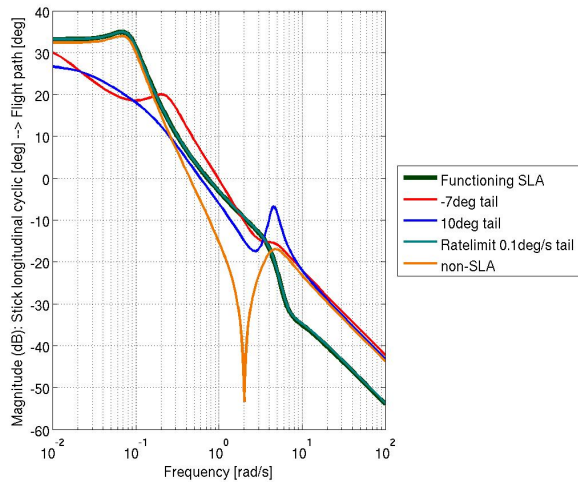
The three failure cases show a difference in response transients. The 10deg failure case shows excitation of two highly damped helicopter modes. The -7deg and 0.1deg/s failure cases see local zeros with lower damping, where output magnitude temporarily decreases. For similar reasons to the SLA system, the 0.1deg/s failure case sees reduced gains at higher frequency oscillations. At lower frequencies, the reduced control authority limits the gains of the -7deg and 10deg failure cases. At higher frequencies, the -7deg and 10deg failure cases do not see the adverse effect of opposite net helicopter lift to flightpath changes, using solely longitudinal cyclic command. The -7deg failure case sees higher gains than the 10deg failure case, caused by a less strong nose-down attitude. The baseline helicopter performs better than the -7deg and 10deg failure cases, possessing larger longitudinal cyclic control authority.



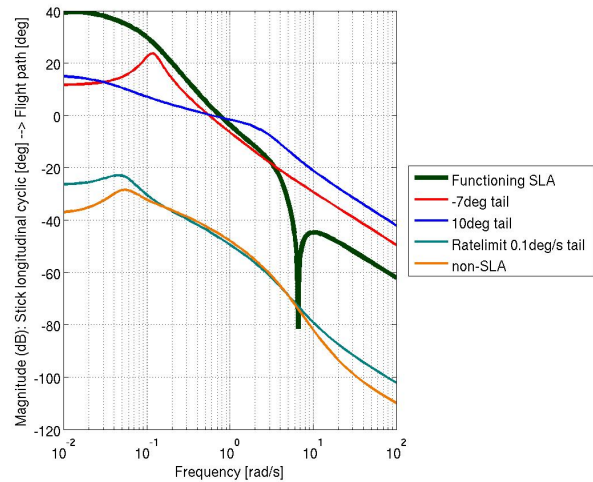
(a) 80kts flight and forward center of gravity



(b) 80kts flight and aft center of gravity



(c) 160kts flight and forward center of gravity



(d) 160kts flight and aft center of gravity

Figure 5.28: Flightpath bandwidth for off-design conditions.

The aforementioned response occurs when flying at the flight conditions around which the mixed control SLA system was devised. To gain insight in the frequency response in off-design conditions, results are provided in fig. 5.28. Ignoring the presence of poles and zeros, this figure shows similar response for the SLA and baseline systems. All systems show increased gain when operating at higher speed flight, caused by increased effectiveness of main rotor longitudinal cyclic. One clear exception is the baseline helicopter, seeing significantly lower gain. As was discussed in chapter 4, the baseline helicopter with aft cg sees the onset of retreating blade stall (RBS) at high speed flight, when changing aircraft pitch attitude. With higher control allocation of main rotor cyclic, this system sees the most significant reduction in gain. The -7deg and 10deg failure cases put the helicopter at pitch attitudes of 4deg and -8deg, yet commanded blade pitch is not significant enough to result in RBS. Here, the SLA system shows its strength, allowing for higher gains as compared to the baseline helicopter, not being limited by RBS. All failure cases show sufficient ability to change flightpath in case of SLA failure.

Therefore, one may conclude that the functional SLA system will provide sufficient response in terms of flightpath changes, for all considered off-design conditions; showing very similar frequency response as the baseline system at lower frequencies. Failure cases show sufficient ability to change flightpath angle.

### 5.4.5. PITCH RATE BANDWIDTH

A frequency analysis is also performed in terms of pitch rate, allowing comparison for flightpath bandwidth agility. Again, longitudinal cyclic stick input is provided at various input frequencies to the linearized system representing the helicopter. This time, pitch rate is the observed output variable. The pitch rate response when operating in SLA design conditions, is shown in figure 5.29.

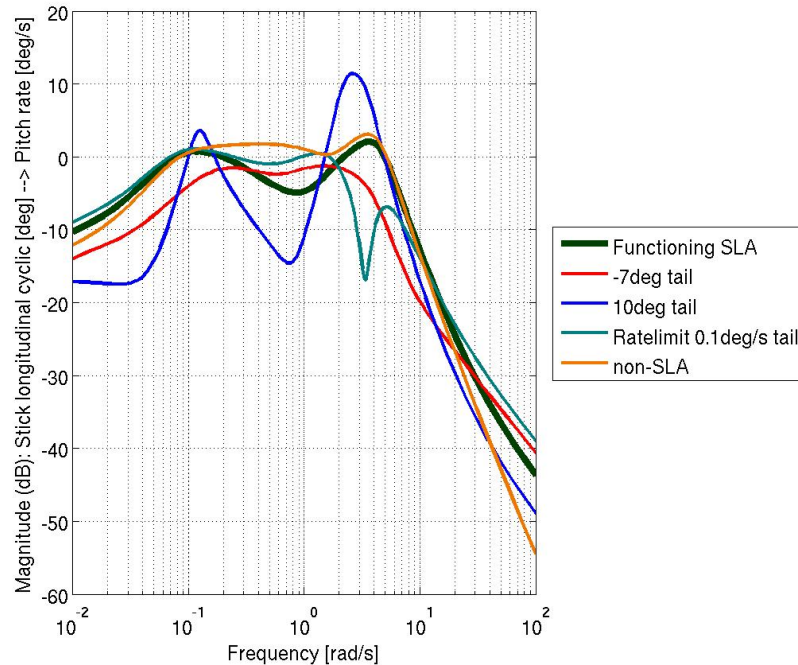
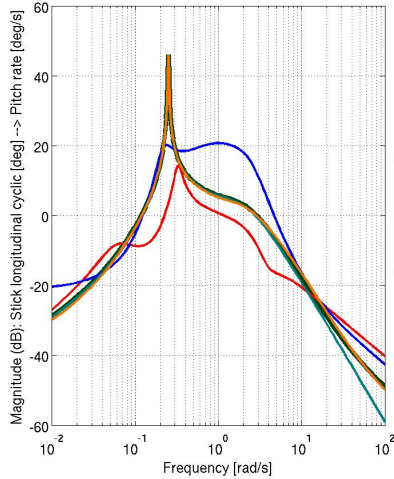


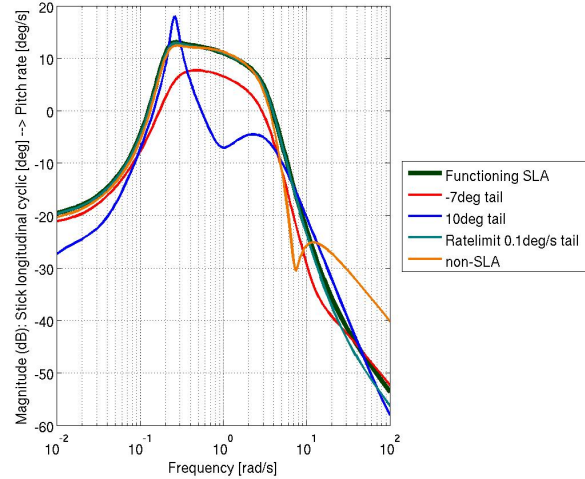
Figure 5.29: Pitch rate bandwidth; normal cg configuration.

Figure 5.29 demonstrates the similar gains for SLA and baseline systems. This is an interesting observation, as attitude quickness suggested far superior agility of the SLA system. This demonstrates the importance of time dependency of response. When considering a given aircraft attitude change, agility is higher for the SLA system. If, however, the time is considered to achieve the given response, this metric demonstrates similar agility. Failure cases show more deviation in their response, implying less predictable response. Nonetheless, gains indicate sufficient responsiveness for a wide range of input frequencies.

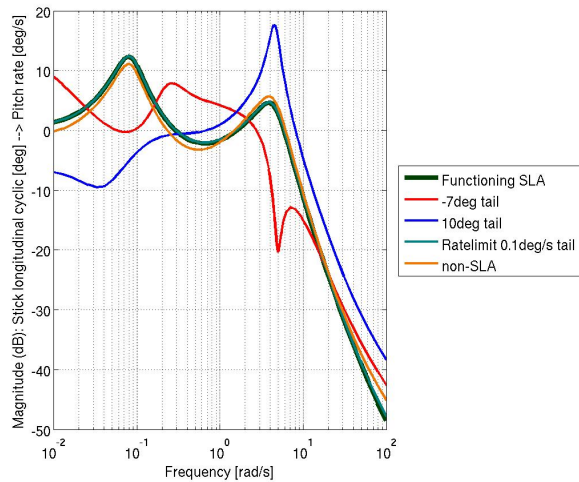
Figure 5.30 shows pitch rate response for off-design conditions. For these conditions, it is evident that SLA and baseline systems respond very similar in terms of magnitude. As expected, for pitch rate bandwidth, the adverse effect of net lift reduction does not alter gains at higher frequencies. Similar to flightpath bandwidth, the baseline helicopter sees significant response impairment in the aft cg 160kts flight condition, caused by RBS. For off-design conditions, gain response is considered sufficient.



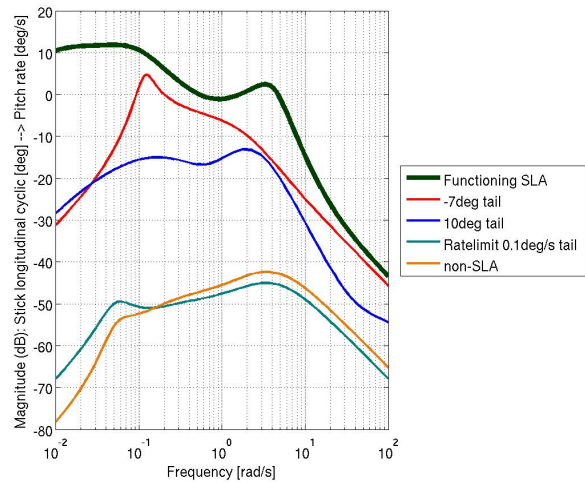
(a) 80kts flight and forward center of gravity



(b) 80kts flight and aft center of gravity



(c) 160kts flight and forward center of gravity



(d) 160kts flight and aft center of gravity

Figure 5.30: Pitch rate bandwidth for off-design conditions.

## 5.5. MODEL FIDELITY ANALYSIS

While the preceding figures show favorable performance results in terms of off-design performance, safety, and agility for the SLA-equipped UH-60A helicopter, the validity of these findings depends on the validity of the helicopter model used for analysis. The simulation model used for analysis features a Pitt-Peters three-state inflow model at the main rotor. Interference is considered at the tailplane, caused by the helicopter fuselage and main rotor. In this section, the same pull-up is performed for all off-design conditions, yet with variations in inflow and interference models. These simulations feature the longitudinal and lateral-directional controllers. Reason for this is the strong dependence of loads on aircraft transient states. By using the aforementioned controllers, the trajectory is corrected to greater degree. Of particular importance is the difference in shaft bending moment  $M_y$ . However, as the longitudinal, lateral-directional and SLA systems were developed within the Pitt-Peters inflow environment, differences in transient predictions of aircraft states or loads may not fully be attributed to the inflow model. Nonetheless, assessment in various inflow environments provides some insight in validity of results.

For the regular Pitt-Peters inflow model with interference, table 5.8 shows the peak values of atti-

tudes, rates, forces and moments, experienced during the 1.75g doublet for the off-design conditions. The amount of longitudinal cyclic and stabilator incidence angles are also given for trim.

Table 5.8: Quantities for the UH-60A with mixed control SLA system for the doublet manoeuvre, modelled with the Pitt-Peters inflow model, including interference effects.

Parameter	Pitt-Peters (3-state inflow)			
	80kts fore cg	160kts fore cg	80kts aft cg	160kts aft cg
$\phi_{pk}$ [deg]	-1.9	-6.4	-2.0	-6.6
$\theta_{pk}$ [deg]	14.9	10.8	20.5	13.5
$\psi_{pk}$ [deg]	3.2	3.9	3.1	3.7
$p_{pk}$ [deg/s]	-1.9	-6.8	-1.4	-6.5
$q_{pk}$ [deg/s]	8.5	8.1	9.0	8.4
$r_{pk}$ [deg/s]	-0.4	0.4	-0.3	0.3
$F_{xpk}$ [kN]	2.3	6.4	-9.9	-6.2
$F_{ypk}$ [kN]	-2.8	-9.1	-3.0	-7.7
$F_{zpk}$ [kN]	96.1	106.5	92.3	105.7
$M_{xpk}$ [kNm]	1.4	4.5	1.5	5.0
$M_{ypk}$ [kNm]	5.6	20.9	-26.7	-26.4
$M_{zpk}$ [kNm]	-26.1	-75.3	-26.0	-70.4
$Lng.cyclic_{trim}$ [deg]	2.3	8.7	7.0	11.4
$Tail_{trim}$ [deg]	0.6	0.1	-0.6	0.3

#### Pitt-Peters inflow model, with versus without interference

Table 5.9 shows the percentage increase of the selected parameters, when performing the same manoeuvre yet discarding interference at the stabilator. The same Pitt-Peters inflow model is utilized. The final column and bottom row indicate the absolute value of the average percentage difference of the preceding parameter or speed-center of gravity condition respectively.

Considering pitch angle, the non-interference model shows a significantly larger nose-down peak attitude during the pull-up manoeuvre. Longitudinal cyclic in trim is also lower, accordingly. Transients of helicopter pitch attitude and longitudinal cyclic (not shown here) show that both interference and non-interference helicopter simulation models follow an almost identical pitch rate response, however with an almost fixed difference in attitude. The stronger pitch-down attitude of the non-interference simulation is the result of no downwash from the main rotor, causing less downforce at the stabilator. The almost constant difference between both pitch attitude transients indicates that the downwash contribution by the main rotor is almost constant for the different attitudes experienced throughout the doublet manoeuvre. As such,  $F_x$  and shaft bending moment  $M_y$  vary significantly. Differences in roll and yaw motion are of smaller magnitude, as well as the resulting differences in moments around these axes. Note that differences between the interference and non-interference simulation models may also partially be attributed to the controllers, which have been designed around the interference situation, with differing airspeed and center of gravity condition. However, most importantly, the interference versus non-interference conditions show the largest differences in parameters related to the helicopters pitch axes; pitch attitude and shaft bending moment around the y-axis.

Table 5.9: Percentage increase in quantities for doublet manoeuvre with Pitt-Peters inflow when discarding interference effects.

Parameter	Pitt-Peters without interference vs. with interference				% Avg. dev. per parameter
	80kts fore cg	160kts fore cg	80kts aft cg	160kts aft cg	
$\% \Delta \phi_{pk}$ [deg]	-6.5	-3.7	-9.5	-3.0	5.7
$\% \Delta \theta_{pk}$ [-]	-25.6	-24.0	-15.3	-13.8	19.7
$\% \Delta \psi_{pk}$ [-]	1.2	5.5	-1.8	3.1	2.9
$\% \Delta p_{pk}$ [-]	-29.1	3.7	-8.5	2.2	10.9
$\% \Delta q_{pk}$ [-]	-5.9	-0.8	-5.7	-3.0	3.9
$\% \Delta r_{pk}$ [-]	-45.1	76.0	8.6	115.9	61.4
$\% \Delta F_{xpk}$ [-]	231.7	73.3	-51.3	-37.9	98.5
$\% \Delta F_{ypk}$ [-]	-8.4	6.8	-19.8	4.8	10.0
$\% \Delta F_{zpk}$ [-]	-2.3	0.1	-1.0	-0.0	0.9
$\% \Delta M_{xpk}$ [-]	22.7	10.9	12.1	13.1	14.7
$\% \Delta M_{ypk}$ [-]	212.1	44.6	-47.3	-26.2	82.5
$\% \Delta M_{zpk}$ [-]	-0.1	3.7	-2.3	1.0	1.8
$\% \Delta Lng.cyclic_{trm}$ [-]	-62.5	-24.0	-36.4	-14.1	34.2
$\% \Delta Tail_{trm}$ [-]	64.1	484.3	-73.4	-83.8	176.4
% Avg. dev. [-]	51.2	54.4	20.9	23.0	-

**Pitt-Peters 3-state versus Peters-He 6-state inflow model**

Table 5.10 depicts percentage differences between the Peters-He and Pitt-Peters inflow models, both with interference. A positive percentage indicates a higher value for the Peters-He inflow model, as compared to the Pitt-Peters model. Note that peak differences are indicated for any time instance, showing worst-case deviations. Not shown is that the transients of both inflow models is near identical, aside from local upsets.

In principle, the Peters-He 6-state interference model should yield more accurate results than the Pitt-Peters 3-state interference inflow model, for reasons presented in section 4.1.3. However, again, the longitudinal, lateral-direction and SLA control systems have been devised around the 3-state inflow model. As such, differences between the two inflow models cannot solely be attributed to the 6-state inflow model's higher accuracy. Concerning responses around the longitudinal axis, differences are no larger than 5.5% in pitch attitude, rate, and longitudinal cyclic trim. Differences in shaft bending moment are of larger magnitude, varying between 3% and 14%. While percentage differences in off-axis yaw rate are above 10%, keep in mind that the absolute value of yaw rate remains below 1deg/s. The parameter seeing the largest percentage differences is the stabilator, where the 6-state inflow model shows a deflection that is almost 5.5 times larger than in the 3-state inflow model. These large percentage differences are caused by the fact that the stabilator, in level forward flight, has an almost zero incidence angle, remaining between 0.1deg and 0.6deg, while longitudinal cyclic is the only surface actuation used to maintain a new airspeed. Remaining around zero in trim, any absolute differences in tailplane deflection will show up as large percentage differences. The 536% deviation implies that the stabilator changes from a 0.6deg trim situation to 3.2deg. The large average percentage differences in the bottom row for the first two off-design conditions are mainly attributed to the large percentage differences for stabilator trim.

Table 5.10: Percentage increase in quantities for doublet manoeuvre with Peters-He inflow model including interference, compared to base situation.

Parameter	Peters-He (6-state) vs. Pitt-Peters (3-state) inflow				% Avg. dev. per parameter
	80kts fore cg	160kts fore cg	80kts aft cg	160kts aft cg	
$\% \Delta \phi_{pk}$ [-]	-11.2	11.4	-10.0	10.5	10.8
$\% \Delta \theta_{pk}$ [-]	-2.8	5.5	-1.8	2.4	3.1
$\% \Delta \psi_{pk}$ [-]	0.3	4.1	-1.7	3.8	2.5
$\% \Delta p_{pk}$ [-]	9.4	18.8	-11.9	26.1	16.5
$\% \Delta q_{pk}$ [-]	2.8	2.7	-3.5	0.6	2.4
$\% \Delta r_{pk}$ [-]	22.2	53.0	23.3	56.5	38.7
$\% \Delta F_{xpk}$ [-]	53.1	-3.3	-4.7	6.5	16.9
$\% \Delta F_{ypk}$ [-]	-13.2	3.4	-9.0	4.7	7.6
$\% \Delta F_{zpk}$ [-]	1.3	-4.2	0.3	-5.6	2.9
$\% \Delta M_{xpk}$ [-]	1.9	19.2	11.1	21.1	13.3
$\% \Delta M_{ypk}$ [-]	13.4	9.7	-3.7	4.3	7.8
$\% \Delta M_{zpk}$ [-]	-1.5	7.7	-1.2	10.7	5.3
$\% \Delta Lng.cyclic_{trim}$ [-]	0.5	6.9	1.6	3.3	3.1
$\% \Delta Tail_{trim}$ [-]	82.4	536.1	45.5	2.9	166.7
% Avg. dev. [-]	15.4	49.0	9.2	11.4	-

### Pitt-Peters 3-state versus Scully inflow model

Table 5.11 shows the transient differences with respect to the Scully inflow model, both including interference effects. Of the three inflow models presented, the Scully inflow model should in theory provide the most accurate results. This model considers the influence of vortices in the main rotor inflow field, and their effects on main rotor loads. The severity of these vortices will determine the extent to which results from the Pitt-Peters inflow model are valid, where Chen [11] and Horn et al. [23] state that free vortex methods such as the Scully inflow model should mainly be considered in cases of vortex-ring states or where in ground effect (IGE) is large. However, again, as the mixed control SLA controller was designed in the 3-state inflow environment, percentage differences given in the above table do not give a one-on-one indication of the degree of accuracy of the 3-state results as compared to the Scully inflow model. Nonetheless, peak differences in pitch attitude and pitch rate remain below 9%. However, differences in longitudinal cyclic are larger, differing by 80% in the least favorable off-design condition. As such, differences in shaft bending moments are generally larger. These lie between 2% and 10% for the two aft cg conditions. For the 80kts and forward center of gravity condition, the bending moment differs most per inflow model, namely by 21%. The large percentage differences in stabilator incidence for level trimmed flight are attributed to the same reason as mentioned earlier.

Table 5.11: Percentage increase in quantities for doublet manoeuvre with Scully wake inflow model including interference, compared to base situation.

Parameter	Scully (wake) vs. Pitt-Peters (3-state) inflow				% Avg. dev. per parameter
	80kts fore cg	160kts fore cg	80kts aft cg	160kts aft cg	
$\% \Delta \phi_{pk}$ [-]	15.3	16.8	15.3	19.0	16.6
$\% \Delta \theta_{pk}$ [-]	8.7	6.0	5.7	6.7	6.8
$\% \Delta \psi_{pk}$ [-]	-6.1	3.0	-7.4	1.1	4.4
$\% \Delta p_{pk}$ [-]	-16.6	-5.4	-6.0	7.4	8.9
$\% \Delta q_{pk}$ [-]	-2.0	2.7	-5.7	-0.2	2.7
$\% \Delta r_{pk}$ [-]	-16.9	186.6	27.3	216.9	111.9
$\% \Delta F_{xpk}$ [-]	19.0	4.3	20.0	18.5	15.4
$\% \Delta F_{ypk}$ [-]	-13.1	-1.2	-4.0	-4.1	5.6
$\% \Delta F_{zpk}$ [-]	4.6	-4.7	5.2	-5.7	5.1
$\% \Delta M_{xpk}$ [-]	67.9	26.7	34.1	22.3	37.7
$\% \Delta M_{ypk}$ [-]	20.7	17.8	9.6	2.5	12.7
$\% \Delta M_{zpk}$ [-]	11.7	18.7	14.6	19.9	16.2
$\% \Delta Lng.cyclic_{trm}$ [-]	79.8	13.2	25.7	10.7	32.4
$\% \Delta Tail_{trm}$ [-]	506.8	611.1	215.0	5.4	334.6
% Avg. dev. [-]	56.4	65.6	28.3	24.3	-

Nonetheless, transient behavior of helicopter states and loads in the Peters-He and Scully inflow models show very similar shapes to the Pitt-Peters model. Having based conclusions on transients in the Pitt-Peters environment, the observed trends remain unchanged. As stated by Prouty [47], simulation models have difficulty in capturing the real-life chaotic flow around the tailplane, as caused by the main rotor downwash. For this reason, the differences in peak values between the various inflow models are deemed acceptable; inaccuracies in tailplane interference of these simulation models as compared to flight tests will most likely be of larger magnitude. For this reason, conclusions within the Pitt-Peters domain are deemed acceptable within the scope of simulation model choice. Evidently, before real-life implementation, wind tunnel and flight tests must be carried out to fine tune the system for actual application.

## 5.6. CONCLUSIONS ON SAFETY ANALYSIS AND HANDLING QUALITIES

Actuator limits have been chosen to guarantee safety after maximum stabilator deflection. With actuation deflection and rate limits in place, the SLA system's agility is assessed as compared to the baseline UH-60A. Lastly, validity of results are determined, by assessing differences in response for various inflow and interference conditions.

### 5.6.1. ACTUATOR LIMITS THAT PROVIDE SAFETY

For the mixed control SLA system, the criteria listed in table 5.12 are considered guiding in determining safety after system failure. In the final column, conclusions on each criterion are displayed.

Table 5.12: Safety criteria after SLA failure.

Crit. nr.	Criteria	Outcome
1	Helicopter can be trimmed after SLA failure	Max. stabilator angles: -7deg and 27deg
2	Sufficient longitudinal cyclic margin to reduce airspeed	Max. stabilator angles: -7deg and 10deg
3	Maximum load factor of 1.5g after failure	Slight exceedance of loadfactor by 0.04g
4	No attitude beyond -6deg (down) or 15deg (up) when flying at 60kts	Never exceeds -1.5deg and 6.8deg

Based on the first and second criteria, trimsweeps are conducted with respect to airspeed, determining the most critical airspeeds with lowest longitudinal cyclic margin. The 140kts and 160kts airspeed situations appear to be most critical. To allow for trim in terms of pitch rate, it is determined that the stabilator should not deflect beyond a -7deg or 27deg position. At the upper longitudinal cyclic bound, the helicopter's forward airspeed will be restricted, while the lower bound will result in the helicopter not being able to pitch up and slow down. At positive stabilator incidence angles, the UH-60A shows speed instability, where the amount of longitudinal cyclic in trim is less at a higher airspeed. This is an undesirable quality. Based on the 80kts airspeed condition, being the lowest airspeed at which the SLA system will be fully functional, maximum stabilator angles are chosen; -7deg and 10deg. The mixed control SLA system will gradually phase in, starting at airspeeds of 60kts. As such, maximum stabilator deflection may occur at this airspeed. In case of 10deg stabilator deflection, the helicopter will possess slight speed instability between airspeeds of 60kts and 100kts, in the order of  $0.1 \frac{\text{deg}}{\text{kts}} \frac{\partial \theta_1 s}{\partial V}$ . This is considered acceptable, due to the sufficient longitudinal cyclic margin available to reduce airspeed. It is furthermore chosen to allow for 45deg/s stabilator deflection angles, based on required actuation rates for full load reduction at 80kts. This will require minimal hardware modifications for the current UH-60A. With these actuator deflection angle and rate constraints, the final two criteria are assessed. Without corrective action provided by the longitudinal and lateral-directional controllers, faulty stabilator deflections result in serious loadfactor exceedances. However, after such failure, a pilot will respond by providing corrective action. With the two aforementioned controllers in place, maximum loadfactor transients remain below 1.5g for most combinations of tailplane deflection, cg location and airspeed. Only when flying at airspeeds of 160kts with a stabilator deflection rate of 45deg/s, resulting in a final stabilator incidence of 10deg/s, will loadfactor be slightly higher, at 1.54g. Concerning a safe landing at 60kts, when trimmed by pilot action, the mixed control SLA system will never cause attitude excursions beyond 1.5deg nose-down or 6.8deg nose-up attitudes, for any center of gravity. As such, the helicopter can safely perform an emergency landing if necessary; aircraft attitudes do not exceed maximum permissible attitudes for landing.

### 5.6.2. NEWLY PROPOSED AGILITY METRICS

Aside from findings on helicopter dynamic behavior of the SLA system, this research has resulted in the development of two novel handling quality metrics; flightpath attitude quickness and flightpath bandwidth. This is because it is considered that current metrics, provided by ADS-33E and MIL, do not provide a complete picture concerning handling qualities. Flightpath quickness is a metric derived from attitude quickness, yet now determining rate of change of flightpath trajectory instead of aircraft attitude. By dividing peak flightpath by change in flightpath, there is a qualitative measure for response time. With same units as attitude quickness, a direct comparison of agility, in terms of flightpath and

attitude changes, can be made.

Flightpath bandwidth is analogous to pitch rate bandwidth, now assessing the flightpath angle response to various stick input frequencies. By comparing flightpath bandwidth to pitch rate bandwidth, differences in agility, in terms of flightpath and pitch rates, can be compared. While ADS-33E sets load factor requirements for aircraft handling at low airspeed failure conditions, high speed constraints are minimal, requiring the helicopter to remain within its operational flight envelope (OFE). Evidently, remaining within the OFE in these conditions should not be considered sufficient; the pilot must still be able to change the flightpath trajectory. Therefore, in style with current ADS-33E metrics, it is felt that this proposed metric can be of value if included within the ADS-33E norms, allowing for better agility and safety assessment of a failed FCS system.

### 5.6.3. AGILITY WITH IMPOSED ACTUATOR CONSTRAINTS

To determine the helicopter's agility after the actuator constraints are imposed, five agility metrics are assessed. These are: attitude quickness, agility quickness, flightpath agility quickness, flightpath bandwidth and pitch rate bandwidth. The first three metrics measure the helicopter's response following a step input in terms of longitudinal cyclic stick. The last two metrics assesses the flightpath and pitch rate response following longitudinal cyclic stick input provided over a range of frequencies. These multiple metrics are required as none of the individual metrics provides a complete picture concerning agility. Attitude quickness determines the helicopter's ability to change pitch attitude. However, ADS-33E does not set HQ boundaries in terms of attitude quickness for high speed flight. Agility quickness measures the ability to change flightpath trajectory, in terms of attainable load factor. Since this metric considers load factor and flightpath angle, units differ from attitude quickness. Results can therefore not be compared on a one-to-one basis to those of attitude quickness. Flightpath agility quickness is proposed in this research, being similar to agility quickness, now assessing flightpath changes instead of load factor, allowing for better comparison with attitude quickness. However, time dependence of response is considered important, and is not considered by the quickness metrics. As such, flightpath bandwidth is proposed. Here, longitudinal stick input is provided at various frequencies, for which flightpath response is assessed. Pitch rate bandwidth analysis is performed in similar fashion, determining the ability to induce a pitch rate at various stick input frequencies. This allows for comparison of frequency response differences in terms of flightpath and pitch rate. Below, results per metric are presented.

- Attitude quickness: ability to change attitude
  - Design condition: SLA system possesses higher agility than baseline system
  - All failure cases show ability to change pitch attitude, also in off-design conditions
- Agility quickness: ability to change flightpath trajectory (quantified by load factor)
  - Design and off-design conditions: All systems perform similarly
  - For a fixed duration input, SLA system required long response time
- Flightpath agility quickness: ability to change flightpath trajectory (quantified by flightpath)
  - Design condition: SLA system performs similarly to baseline system
  - Off-design conditions: SLA system performs better in high speed flight
  - For a fixed duration input, SLA system required long response time
  - All failure cases show ability to change flightpath, also in off-design conditions

- Flightpath bandwidth response: ability to change flightpath for inputs over different frequencies
  - Design and off-design conditions: SLA system performs very similar as compared to baseline system, especially at low frequencies
  - Off-design condition: (160kts flight and aft cg) SLA system performs better than baseline helicopter, avoiding RBS
  - Failure cases show larger differences in gain per frequency, yet gains are similar to the baseline system; considered sufficient
- Pitch rate bandwidth response: ability to change pitch rate for inputs over different frequencies
  - Design condition: SLA system sees similar gain magnitudes for all frequencies as baseline system
  - Off-design conditions: Near identical response for SLA and baseline systems
  - Off-design condition: (160kts flight and aft cg) SLA system performs better than baseline helicopter, avoiding RBS
  - Failure cases show gains of similar magnitude as baseline system; considered sufficient

From the above results, agility quickness conclusions are combined with those of flightpath agility quickness, due to their similarity. This research aims at assessing response in longitudinal axis, as this is what determines the pilot's ability to slow down. Therefore, based on two quickness and two bandwidth analyses, conclusions on agility in terms of attitude and flightpath can be drawn.

- The SLA system shows an increased ability to change pitch attitude as compared to the baseline system in all (design and off-design) flight conditions for step input.
- For a similar step input, the SLA system shows an equal or higher ability to change flightpath as compared to the baseline system in all flight conditions. Differences in agility are smaller than for attitude quickness due to initial adverse change in net helicopter lift by the stabilator.
- For input over low frequencies, the SLA system shows an almost identical flightpath bandwidth response compared to the baseline system, for most flight conditions.
- For input over high frequencies, the SLA system in general shows lower response magnitude compared to the baseline system, caused by the short term adverse change in net helicopter lift after stabilator deflection.
- For input over different frequencies, the SLA system shows a similar frequency response in terms of pitch rate bandwidth as the baseline system, also in off-design conditions.
- For flightpath bandwidth and pitch rate bandwidth, all failure cases show gains which are similar in magnitude to the SLA and baseline systems, irrespective of flight condition.
- In terms of flightpath and pitch rate bandwidths, agility of the SLA helicopter is not limited by RBS, at 160kts flight with an aft cg.

Therefore, the SLA system provides equal or superior agility compared to the baseline system, both in terms of pitch attitude changes as well as flightpath changes.

#### 5.6.4. VALIDITY OF INFLOW AND INTERFERENCE MODELING

Conclusions drawn in preceding sections are only as good as the simulation model that they are based on. Below, conclusions pertaining to validity are presented.

One cannot attribute differences between various inflow models solely to the degree of model fidelity, since the longitudinal, lateral-directional and SLA systems were designed in the 3-state inflow environment. Nonetheless, when comparing pitch attitude for the 3-state inflow model with the higher fidelity 6-state and Scully inflow models, peak differences remain within 10% in any off-design condition. The longitudinal controller manages to maintain pitch within a 3% to 6% margin. This demonstrates the SLA system's consistent pitch rate response, irrespective of inflow model. In the worst off-design condition, the difference in inflow models resulted in a 20% underestimation of shaft bending moments  $M_y$

by the 3-state inflow model, caused by the larger difference in pitch attitude. Differences in lateral and directional axes is generally larger than in longitudinal axes, though the degree to which this depends on the model fidelity, instead of controller design, is unknown.

Nonetheless, transient behavior of helicopter states and loads in the Peters-He and Scully inflow models show very similar shapes to the Pitt-Peters model. Having based conclusions on transients in the Pitt-Peters environment, the observed trends remain unchanged. As stated by Prouty [47], simulation models have difficulty in capturing the real-life chaotic flow around the tailplane, as caused by the main rotor downwash. For this reason, the differences in peak values between the various inflow models are deemed acceptable; inaccuracies in tailplane interference of these simulation models as compared to flight tests will most likely be of larger magnitude. For this reason, conclusions in the Pitt-Peters domain are deemed acceptable within the scope of simulation model choice. Evidently, before real-life implementation, wind tunnel and flight tests must be carried out to fine tune the system for actual application.

# 6

## Weight estimation

For the doublet manoeuvre, use of stabilator deflection requires lower longitudinal cyclic usage, reducing shaft bending moment  $M_y$ . Instead of load reduction, if the helicopter design is adjusted to allow for similar loads, certain helicopter components may be downsized, or the helicopter's gross weight (GW) may be increased. In this section, various optimizations will be performed separately, minimizing main rotor shaft diameter, main rotor radius, and maximizing GW. Implications on other design parameters will also be elaborated on. First, various weight estimation schemes will be considered, which form the basis for further analysis.

### 6.1. VARIOUS WEIGHT ESTIMATION SCHEMES

To determine the implications of the proposed mixed control SLA system on a new helicopter design, the impact on the overall weight of the helicopter must also be assessed. Prouty [48] presents simple weight estimation equations that may be used for preliminary design. These equations, for all major helicopter components, have been developed through use of multiple linear regression techniques, determining the sensitivity of parameters that intuitively affect the weight of a component. Weight estimation equations are provided for all helicopter subcomponents, and are mainly based on geometric parameters relevant for that particular component. The weight of external objects depends on aspect ratios and rotor parameters such as rotational velocities and rotor radius; drive systems are scaled with engine power rating; general furnishings are simply added as an additional percentage of gross weight. Scaling factors must also be applied due to advances in technology since 1986, when these estimates were first derived. While these equations are very straightforward once all sizing and performance parameters are known, the weight estimation technique is too crude; the weight estimation for the tail assembly does not take into account moving stabilizers, nor do controls, electrics or hydraulic systems take into account actuated surfaces, only being dimensioned with main rotor parameters. Therefore, these estimations cannot be applied to determine the difference in weight for a helicopter with stabilator versus a helicopter with a fixed horizontal tail. As an indication, Prouty's equation used to derive horizontal stabilizer weight is provided in eq. 6.1. The full list of equations used to determine all component weights is provided in appendix A.

$$W_H = 0.72A_H^{1.2}A.R.H^{0.32} \quad (6.1)$$

Gunduz et al. [19] uses a radically different approach for weight estimation. Instead of a parametric analysis of previous designs, weight is the sum of all sub-component weights modeled in a CAD system. The accuracy of this weight prediction method therefore solely depends on the accuracy of the CAD model and its level of detail. After each design alteration, the CAD model can immediately provide a new design weight instead of needing to iterate. One parametric input value is however required: that of the material density per component. From this, knowing the component volume, the weight is determined. Gunduz et al. [19] demonstrates this weight estimation capability through the design of a main rotor of the Sikorsky CH-53E. This tool estimated a main rotor weight of 993kg, the equations of Prouty predicted a weight of 1027kg, while the actual main rotor weight is 962kg. In this specific example, the CAD tool allows more precise predictions. Table 6.1 compares main rotor weight estimations

from this CAD tool versus compared to predictions by Prouty [48]. Unfortunately, the actual main rotor masses are not listed, making it impossible to conclusively determine which approach yields more accurate results. However, as the CAD tool considers specific component volumes instead of performance parameters, it will be assumed that this more accurately predicts main rotor weight. In this table, very significant weight prediction differences between the two approaches are listed, such as an estimation that is three times larger for the Robinson R22, using the CAD approach. External fittings, hinges and actuators can be fitted in a CAD model for a helicopter with a stabilator, however, this approach will not easily predict the weight of interior systems such as additional wiring, the sizing of actuators or weight of onboard systems. The accuracy of the weight prediction depends on the accuracy of the 3D CAD model. Furthermore, this approach is not an iterative one; the stabilator still needs to be designed, requiring iterative cycles between geometric sizing, structural weight and performance.

Make and Model	CATIA blade volume (ft <sup>3</sup> )	Weight / Volume ( $d_{app}$ )	Estimated density ( $d_{est}$ )	Estimated Blade Weights (lbs)	Prouty's Blade Weights (lbs)
Aerospatiale/ Eurocopter AS 350B	4.028	43.700	61.10669	243.2404	176.0252457
Eurocopter BO 105LS	3.678	71.778	26.206512	97.49366	176.9745477
MBB/ Kawasaki BK 117	5.769	41.787	25.39844	155.8142	241.0732115
McDonnell Douglas MD 500E	1.162	52.323	33.79633	45.32606	95.32845078
Schweizer/ Hughes 300C	1.039	66.021	214.0503	220.2993	68.59666497
Agusta A109	9.722	26.043	32.57084	348.3768	253.1979527
Robinson R22	0.805	66.287	157.819	160.6157	53.36181113
Sikorsky UH-60A	20.176	33.050	17.38828	333.7174	666.825784
Sikorsky CH-53E	101.666	20.852	20.2695	2189.057	2264.261225
Sikorsky S-76A	9.85	37.176	36.8463	248.1934	366.1893129
Bell JetRanger 206	2.571	74.120	70.1363	209.0921	134.9539122

Table 6.1: Comparison of weight estimates obtained from CAD compared to Prouty's parametric equations (Gunduz et al. [19]).

Johnson [30] provides insight in the capabilities of the NASA Design and Analysis of Rotorcraft (NDARC) tool, used by the Department of Defense for designing and sizing rotorcraft. Input can be parameters such as design gross weight, engine power, or rotor size. It can be chosen to fix these parameters, or to let NDARC iteratively solve two of the three parameters. The user provides a required list of flight segments making up a mission task element (MTE) or a single point design condition. From this, primary sizing is done to meet maximum required power for the most extreme segment, defined within the MTEs. Inputs are provided in list form, where all geometric factors and spatial locations relative to other components can be specified accordingly. A step-by-step approach on how to supply input is given by Johnson [31]. Various combinations of parameters can be given as input, while dependent design parameters following out of the iteration cycles automatically determine all sizing and performance dependencies. An iteration is performed between rotor radius, required power, and GW, so that the free parameters are determined. Rotor radius determines the rotor disc solidity. This, together with flapping angles, determining the six rotor loads. The tool is applicable for standard helicopter configurations such as single-rotor or tandem rotor configuration. However, structural components such as force components, wings, or tails can be added, allowing for analysis of novel and advanced design concepts. All subsystems, including FCS components, can be implemented and sized accordingly. The model is one of low fidelity, which is typical for preliminary design purposes. For weight scaling, use is made of parametric equations based on component weights in current helicopters and tilt rotors. This is done through a SAWE RP8A Group Weight Statement. This parametric weight estimation is more detailed than the approach by Prouty [48] concerning all control subcomponents. Per item, a technology factor due to advances in technology can be set. Since advances in lightweight fly-by-wire control systems have already taken place when NDARC was released in 2009, this tool is most up-to-date and will most adequately give proper weight estimations. Table 6.2 and fig. 6.1 indicate the percentage error in estimating correct weight, as compared to existing designs. Since the helicopter will be developed from the start with this new SLA control system, relative estimation errors for all components are of interest. Error of the control systems is around 10%. The high 22% error of horizontal

tail weight estimation is most likely caused by large variations in actual horizontal tail design. After conceptual design, numerous design iterations usually follow on a test aircraft before a final horizontal tail is chosen (Prouty [47]). This is often the case, as horizontal tails developed in early design iterations often prove to have unfavorable handling qualities once implemented on a real helicopter (Prouty [47]).

group		number of aircraft	average error %
wing		25	3.4
rotor blade	AFDD82	37	7.7
rotor hub	AFDD82	37	10.2
rotor blade	AFDD00	51	7.9
rotor hub	AFDD00	51	9.2
horizontal tail		13	22.4
vertical tail		12	23.3
tail rotor		19	16.7
fuselage	AFDD82	30	8.7
fuselage	AFDD84	35	6.5
alighting gear		28	8.4
engine support		12	11.0
engine cowling		12	17.9
air induction		12	11.0
accessory		16	11.5
fuel tank		15	4.6
gear box + rotor shaft	AFDD83	30	7.7
gear box + rotor shaft	AFDD00	52	8.6
drive shaft		28	16.0
rotor brake		23	25.1
rotary wing flight controls	non-boosted	20	10.4
rotary wing flight controls	boost mechanisms	21	6.5
rotary wing flight controls	boosted	20	9.7

Table 6.2: Percentage error between NDARC estimated component weights and actual component weights of various helicopters (Johnson [30]).

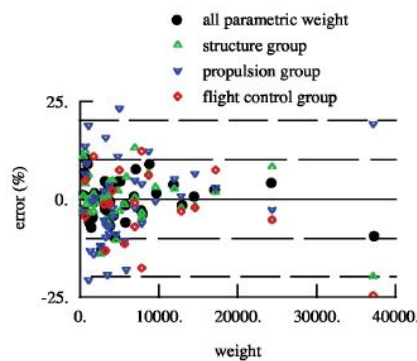


Figure 6.1: Percentage error between NDARC estimated component weights and actual component weights of various helicopters, categorized per functional category (Johnson [30]).

From the aforementioned, it is decided to use NDARC, in combination with Flightlab, to size the main rotor shaft, main rotor radius, and to determine the permissible increase in GW. Flightlab is used for load predictions, while NDARC is used for sizing based on altered rotor radius.

## 6.2. RESULTS

Flightlab is used to provide weight estimations for main rotor radius downsizing. It is also attempted to iteratively tune GW till loads are similar to those of the baseline helicopter. However, this approach proves erroneous further on. Using Flightlab, the main rotor shaft downsizing is performed. Inner and outer shaft radii are iteratively tuned using simple stress analysis with the output loads of Flightlab.

From this, the shaft's mass is determined. For main rotor radius, Flightlab is again used to determine the main rotor radius before similar loads are reached as baseline helicopter. NDARC is subsequently used to indicate the GW reduction, for this change in rotor radius. For this, NDARC is not used for load prediction. For the permitted GW increase, the GW of the helicopter is tuned in Flightlab, till stresses are similar to the baseline helicopter. Results for these three iterative approaches are given in the following sections. While it was attempted to develop a hybrid method to size helicopter GW by using both Flightlab and NDARC, this approach proved unfruitful.

### 6.2.1. MAIN ROTOR SHAFT DOWNSIZING

As stated earlier, the reduction of main rotor shaft bending moment  $M_y$  provides opportunities to downsize the main rotor shaft, when permitting the same main rotor normal stresses as experienced by the baseline helicopter, performing the same doublet manoeuvre at 130kts. Normal stresses occur in the shape of tensile or compressive stresses, as well as bending stresses. Tensile stresses are caused by hub force  $F_z$ ; bending stresses are the result of shaft bending moments  $M_x$  and  $M_y$ . Aside from normal stresses, shear stresses are also of significance. These stresses are the result of main rotor shaft torque  $M_z$  and in-plane forces  $F_x$  and  $F_y$ .

At first, the reduction in shaft radius is determined. Inner and outer shaft radius are chosen for which normal stresses are equal to those of the baseline helicopter. The reduced shaft radius will result in a change in shear stresses, which will be assessed further on. The iterative approach used for rotor shaft downsizing is shown in figure 6.2.

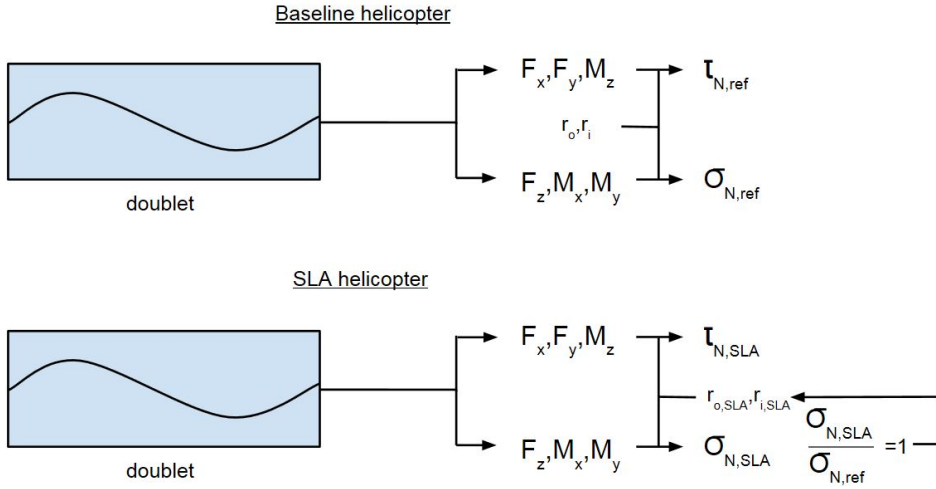


Figure 6.2: Iterative approach used for main rotor shaft downsizing.

Equation 6.2 provides the formula for normal stresses. Subscript 'max' indicates the maximum value of that load experienced during the doublet doublet. These normal stresses are directed perpendicular to the cross-section plane of the main rotor shaft.

$$\sigma_N = \left| \frac{M_{x,max}d}{I_{zz}} \right| + \left| \frac{M_{y,max}d}{I_{zz}} \right| + \left| \frac{F_{z,max}}{A} \right| \quad (6.2)$$

The absolute value is used in the above equation, since there will be two locations along the cylinder's outer diameter where the alignment of stress components caused by  $M_x$ ,  $M_y$ , and  $F_z$  will result in the highest structural stresses. By taking the absolute value, the magnitude of this stress will be known at the aforementioned locations. The main rotor shaft is modeled as a hollow cylinder. Figure 6.3 shows a schematic of the cylinder with all relevant parameters. Note that the cylinder is not drawn to scale. The maximum normal stress will occur somewhere on the outer cylinder surface, at location  $(d_y, d_x)$ , depending on the ratio of  $M_x$  and  $M_y$ .

The parameters of the current UH-60A main rotor shaft are provided in table 6.3. In this sizing optimization, all parameters are kept constant, with the exception of the outer and inner shaft radius, maintaining a constant wall thickness. Radii will be reduced till normal stresses of the SLA helicopter match those of the baseline helicopter.

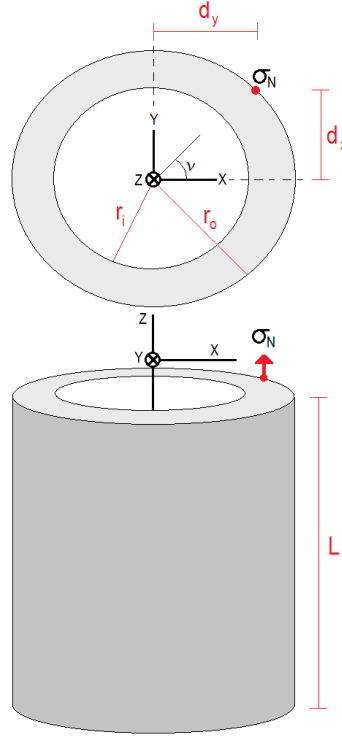


Figure 6.3: A depiction of the cylinder used to approximate the main rotor shaft. Relevant geometric parameters are included. Maximum normal stress  $\sigma_N$  will occur at some  $(d_y, d_x)$  location on the edge.

Table 6.3: Parameters for the UH-60A main rotor shaft.

Parameter	Quantity
$r_i$ [mm]	42.037
$r_o$ [mm]	44.45
$L$ [m]	7.544
Aluminium density $\rho$ [ $\frac{kg}{m^3}$ ]	2800

For a cylinder, the moment of inertia is given by equation 6.3.

$$I_{zz} = \frac{1}{2}m(r_i^2 + r_o^2) \quad (6.3)$$

Shaft mass will depend on the inner and outer cylinder radius, as given in equation 6.4.

$$m = \rho\pi(r_o^2 - r_i^2)l \quad (6.4)$$

Lastly, equation 6.5 defines  $d_x$  and  $d_y$  in terms of angle  $v$  and  $r_o$ .

$$\begin{aligned} d_x &= r_o \sin v \\ d_y &= r_o \cos v \end{aligned} \quad (6.5)$$

From this, the normal stress formula used for analysis is given in equation 6.6.

$$\sigma_N = \left| \frac{M_{x,max}r_o \sin v}{\rho\pi(r_o^4 - r_i^4)} \right| + \left| \frac{M_{y,max}r_o \cos v}{\rho\pi(r_o^4 - r_i^4)} \right| + \left| \frac{F_{z,max}}{\pi(r_o^2 - r_i^2)} \right| \quad (6.6)$$

Concerning shear stresses, these are caused by torsion moment  $M_z$  and in-plane forces  $F_x$  and  $F_y$ .

Shear stresses act in the plane of the cross-section of the rotor shaft. Here, the torsion moment causes a linearly increasing component with the radius, while  $F_x$  and  $F_y$  provide uniform components in the cross-section. The maximum shear stress will occur at the angle where the resultant vector of  $F_x$  and  $F_y$  is largest, and at the outer radius, where the stress caused by  $M_z$  is largest. As such, equation 6.7 provides a formula for the resultant shear stress, as a function of angle  $v$ . The resultant shear stress at each radial location is directed perpendicular to angle  $v$ .

$$\tau = \left| \frac{M_{z,max}r_o}{I} \right| + \left| \frac{F_{x,max}}{A} \right| \cos v + \left| \frac{F_{y,max}}{A} \right| \sin v \quad (6.7)$$

$$\tau = \left| \frac{M_{z,max}r_o}{\frac{1}{2}m(r_o^2 + r_i^2)} \right| + \left| \frac{F_{x,max}}{\pi(r_o^4 - r_i^4)} \right| \cos v + \left| \frac{F_{y,max}}{\pi(r_o^2 - r_i^2)} \right| \sin v \quad (6.8)$$

In similar fashion to the normal stresses, the maximum shear stress is determined for a full revolution of angle  $v$ .

As loads and resultant stresses will differ per cg configuration, maximum stresses will be assessed for the forward, normal, and aft cg locations. One sample calculation will be performed for the forward center of gravity. Calculations for the normal and aft center of gravity occur in similar fashion, and are therefore omitted.

It is chosen to size the main rotor shaft based on loads experienced during the reverse doublet manoeuvre. This manoeuvre is identical to the regular doublet, however, starting with a pushover, followed by a pull-up. The reverse doublet is used since  $M_y$  is negative for the regular doublet, and becomes less negative when reducing rotor shaft dimensions, increasing  $M_y$ . Thus, the magnitude of  $M_y$  will reduce with smaller shaft radii. Therefore, one cannot minimize radius for the regular doublet. With the reverse doublet, shaft bending moment  $M_y$  is positive, and increases in value when shaft radius is reduced. This way, one may iterate to a shaft radius where the normal stress is similar to that of the baseline situation.

For the baseline helicopter, performing the reverse doublet at 130kts with a forward cg, loads are filled into equation 6.6. Here, normal stress is still a function of angle  $v$ . For a full revolution of  $v$ , the maximum normal stress is determined. For this situation, the maximum shear stress is 267.87MPa, occurring at the 6deg and 186deg  $v$  positions. When looking at fig. 6.3, with the point of maximum stress lying in closer proximity to the x-axis than the y-axis, it is evident that  $M_y$  causes a much larger normal stress component than  $M_x$ . These angles are, however, not of further interest in this research; only the magnitude of stresses are of interest. The normal stress for the baseline helicopter's shaft will be the reference for permissible loads of the SLA helicopter. Similarly, peak forces  $F_x$  and  $F_y$  and shaft torsion moment  $M_z$  are substituted into equation 6.8 to find the maximum shaft shear stress experienced by the baseline helicopter. Maximum shear stress has a magnitude of 96.7MPa.

The maximum loads experienced by the SLA helicopter are substituted into equation 6.6 to determine normal stresses. This time, however, the outer shaft radius is iteratively chosen till normal stresses match the baseline's normal stresses. The inner radius is altered accordingly, maintaining constant wall thickness. Results are provided in table 6.4.

The change in outer shaft radius will impact shear stresses. The maximum shear stress is found to be 119.72MPa, representing a 23.8% increase as compared to the baseline helicopter.

In similar fashion, the maximum normal stresses are found for the normal and aft cg configurations, performing the 1.75g doublet at 130kts. Results for all three center of gravity configurations are given in table 6.4. Values for the baseline helicopter are provided as well, being a reference for allowable normal stresses, for which the SLA helicopter's shaft radii were tuned accordingly.

Table 6.4: Main rotor shaft radius for the original baseline helicopter, as well as for the reduced shaft radius SLA UH-60A, when permitting similar normal stresses.

Parameter	C.G. fore			C.G. normal			C.G. aft		
	baseline	SLA	% incr	baseline	SLA	% incr	baseline	SLA	% incr
$r_o$ [mm]	44.45	36.92	-10.69	44.45	41.65	-6.30	44.45	43.22	-2.77
$r_i$ [mm]	42.52	34.99	-17.71	42.52	39.72	-6.58	42.52	41.29	-2.89
$\sigma_N$ [MPa]	267.87	267.22	-0.24	248.03	247.98	-0.02	243.05	243.03	-0.01
$\tau$ [MPa]	96.68	119.72	23.83	86.73	92.84	7.04	90.54	90.23	-0.34
$m_{shaft}$ [kg]	11.11	9.19	-20.77	11.11	10.40	-6.39	11.11	10.80	-2.79

From table 6.4, it may be concluded that the aft cg configuration is the most constricting, allowing least main rotor shaft downsizing. Rotor shaft downsizing allows for a local mass reduction of 0.31kg, or 2.8% of shaft mass weight. In this flight condition, shear stress is reduced by 0.34%.

### 6.2.2. MAIN ROTOR RADIUS DOWNSIZING

Instead of reducing the main rotor shaft, the main rotor may potentially be downsized for the same reasons. At first, rotor radius is iteratively changed till the maximum shaft bending moment  $M_y$  matches that of the baseline helicopter. From this, the minimum rotor radii are found for the three center of gravity conditions. These are listed in table 6.5. The iteration scheme used here is similar to that of fig. 6.4, through iterating for  $M_y$  instead of normal stresses.

Table 6.5: Main rotor radius downsizing based on maximum permissible shaft bending moment  $M_y$  only.

	C.G. fore	C.G. normal	C.G. aft
$R_{MR}$ [m]	7.80	8.02	8.14

With a rotor radius input, NDARC can parametrically size the entire helicopter in terms of component weights without performing a flight analysis. Conversely, if a GW is supplied as well as a required manoeuvre, NDARC will perform rotor sizing so that available power equals required power for the most demanding mission segments. Nonetheless, an 'off-design' analysis is conducted, where component sizing depends solely on input rotor radius, instead of required performance for a given manoeuvre. Other sizing parameters such as engine power, rotor torque, GW and component cg locations are chosen as defined in Flightlab, and are not provided here for sake of brevity. Detailed input for the NDARC model is provided in the appendix. Table 6.6 indicates the changes in rotor mass and helicopter empty weight (WE) following the rotor radius change. The rotor mass is reduced by 14kg, while the helicopter sees a 26kg reduction in weight empty. Of the rotor mass, this is in part related to a change in blade mass, depending on blade length, as well as additional fixtures scaled with rotor radius. The 26kg reduction in empty weight is caused by slight downsizing of various subcomponents, scaled with rotor radius. Appendix D provides the empty weight breakdown for both rotor radii, for more insight.

A look will again be taken at the normal and shear stresses at the rotor hub. The iteration schematic is provided in figure 6.4. Equation 6.6 is again applied for both baseline and SLA helicopters, this time maintaining shaft dimensions. The radius is iteratively reduced for the SLA helicopter, till normal hub stresses match those of the baseline helicopter. This is done for a forward, normal, and aft center of gravity. However, unlike main rotor shaft downsizing, the iterative adjustment of main rotor radius leads not only to stress changes, but also in the alteration of loads in the main rotor. Therefore, this iteration includes successive simulations of the doublet in Flightlab.

Table 6.6: Main rotor radius for the original baseline helicopter, as well as for the downsized SLA UH-60A, when permitting similar  $M_y$  bending moments.

Parameter	Current	Optimized	% decr
$R_{MR}$ [m]	8.23	8.14	1.1
$m_{MR}$ [kg]	506	492	2.8
$WE$ [kg]	4254	4228	0.6

For main rotor downsizing, results will not converge. This is because while main rotor shaft bending moment  $M_y$  will increase with a smaller main rotor radius, the decrease of shaft force  $F_z$  has a greater effect on the normal stresses. This is the case for all three center of gravity conditions considered. As an example, reduced normal stresses are shown in table 6.7 for the forward cg situation when reducing rotor radius. Here, the normal stress  $\sigma_n$  is decomposed into bending stress  $\sigma_b$  caused by  $M_x$  and  $M_y$ , and the tensile stress  $\sigma_t$  caused by  $F_z$ .

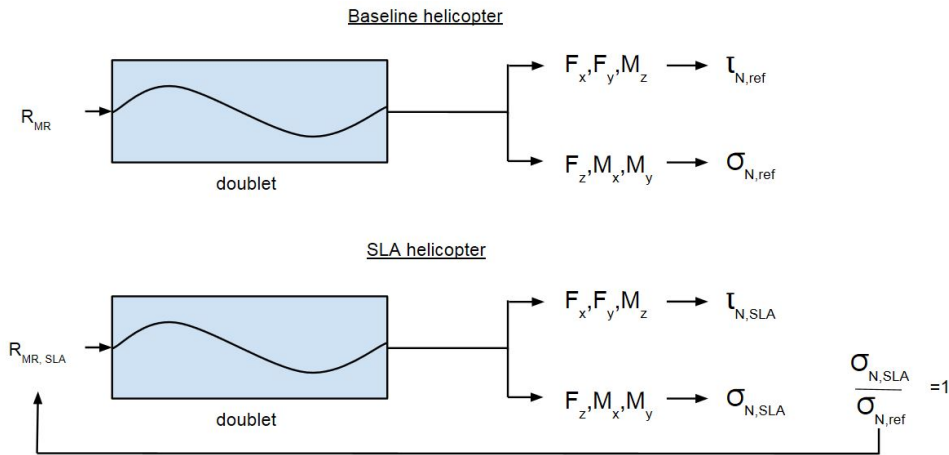


Figure 6.4: Iterative approach used for main rotor radius downsizing.

Table 6.7: The effect of M.R. radius downsizing on normal stresses, for the forward C.G. configuration.

Parameter	C.G. fore, standard rotor	C.G. fore, reduced rotor radius
$R_{MR}$ [m]	8.23	7.89
$M_x$ [kN]	2.47	1.69
$M_y$ [kN]	7.80	15.10
$F_z$ [kN]	106.72	97.42
$\sigma_b$ [MPa]	15.40	28.62
$\sigma_t$ [MPa]	202.74	185.07
$\sigma_n$ [MPa]	218.14	213.69

Thus, when main rotor shaft bending moments  $M_y$  are only of importance, the main rotor radius may be reduced from 8.23m to 8.14m. This is determined on the basis of the reverse doublet. However, most likely, shaft stresses are more important, where the shaft bending moment  $M_y$  is but one constituent. When observing how all loads vary when reducing main rotor radius, normal stress will reduce with decreasing rotor radius. A minimum rotor radius can therefore not be found on the basis of these

stresses. Instead, the minimum main rotor radius should be chosen on the basis of required power instead of normal stresses. It is therefore decided to leave the main rotor radius unaltered.

### 6.2.3. INCREASE IN DESIGN GROSS WEIGHT

In case of no structural alterations to the main rotor, the helicopter may operate with a higher gross weight (GW) before reaching permissible normal stresses. Optimization is done for the SLA helicopter with forward cg configuration. The reason for omitting the normal and aft cg configurations is that the helicopter will fly with such a nose-down attitude in level cruise, that shaft bending moment  $M_y$  is negative. When performing the regular or reverse doublet with a higher GW,  $M_y$  will increase, making it less negative. Therefore, the absolute value of this moment will decrease when performing either doublet. This is shown in figure 6.5 for the normal cg configuration, performing the reverse doublet. If GW is increased to the point where  $M_y$  becomes positive during the manoeuvre, bending stresses will again increase. However, the GW for which the positive  $M_y$  will be equal in magnitude (and opposite in sign) to that of the baseline helicopter, will be at much higher values than for the forward cg configuration. For the forward cg condition,  $M_y$  is positive in cruise flight, and will rise further when performing either doublet. Thus, this is the flight condition allowing the most restricted increase in GW.

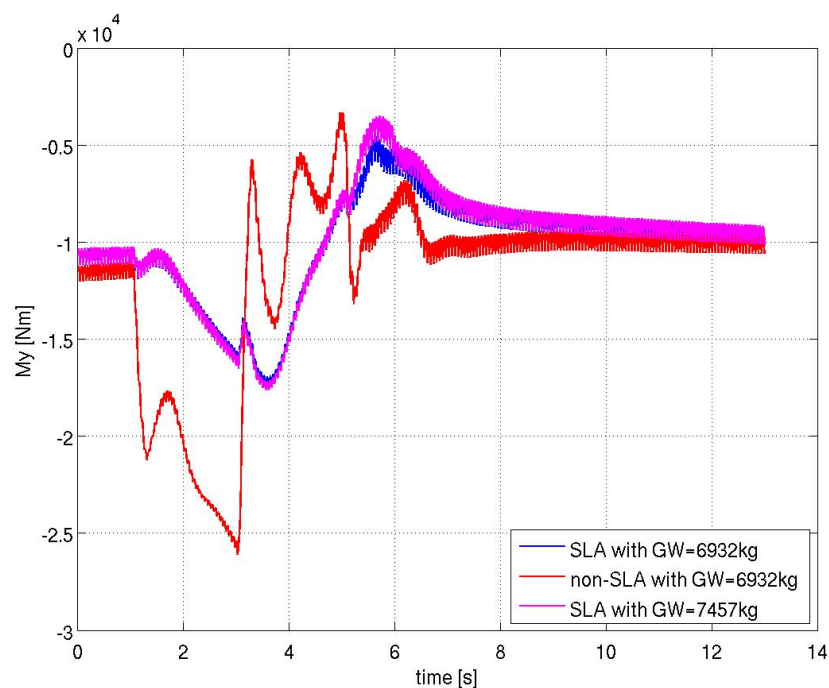


Figure 6.5:  $M_y$  transient for the normal cg configuration performing the reverse doublet. Note the decrease in magnitude of  $M_y$  during the manoeuvre.

The baseline helicopter with forward center of gravity will first perform both doublets to determine maximum permissible normal stresses. Equation 6.6 is used for baseline and SLA helicopters, where main rotor shaft dimensions remain unchanged. The GW is iteratively increased for the SLA UH-60A till loads are reached for which normal stresses are equal to those of the baseline helicopter. The iterative procedure is shown in figure 6.6. It is chosen to fly both regular and reverse doublets to determine which manoeuvre is most restricting on the GW increase.

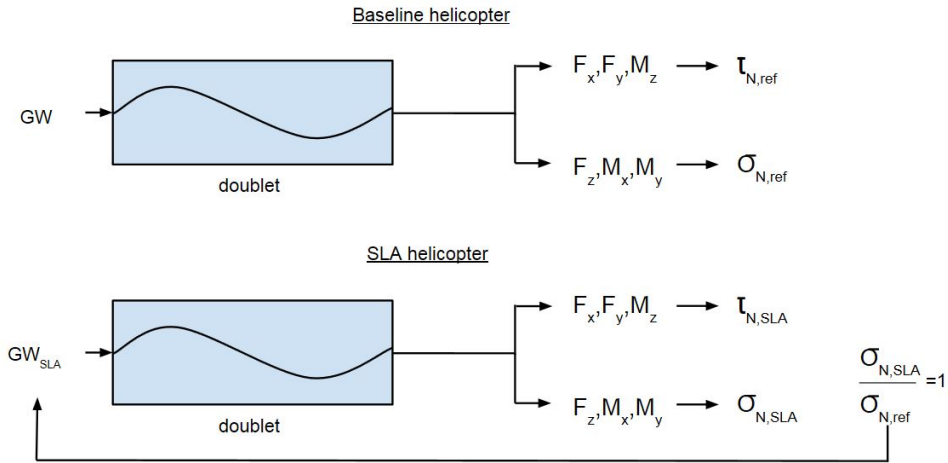


Figure 6.6: Iterative approach used for helicopter GW increase.

Table 6.8: GW for the original baseline and SLA UH-60A, when permitting similar normal stresses during the regular doublet; 130kts airspeed.

Parameter	C.G. fore		
	baseline	SLA	% incr
$\sigma_N$ [MPa]	251.84	251.73	-0.045
$\tau$ [MPa]	105.95	100.94	-4.73
$GW$ [kg]	6932	7881	13.68

Table 6.9: GW for the original baseline and SLA UH-60A, when permitting similar normal stresses during the reverse doublet; 130kts airspeed.

Parameter	C.G. fore		
	baseline	SLA	% incr
$\sigma_N$ [MPa]	250.19	250.18	-0.0026
$\tau$ [MPa]	96.68	101.13	4.60
$GW$ [kg]	6932	8274	19.37

For the regular doublet, table 6.8 indicates the permissible GW increase. Similarly, table 6.9 indicates the permissible GW increase when flying the reverse doublet. From these tables, it is evident that the reverse doublet sets tighter constraints on the allowable GW increase. Therefore, when performing either doublet, when increasing GW till normal stress matches that of the baseline helicopter, GW may increase from 6932kg to 7881kg. The 7881kg helicopter also performs the reverse doublet, for insight in shear stress development. As compared to the baseline helicopter, the shear stress will be reduced by 4.19%.

Lastly, the required power is plotted for various airspeeds for the UH-60A. This is done to determine the effect of the higher GW on the power properties of the helicopter, when operating in cruise flight. Airspeeds range from hover to maximum forward airspeed, with intervals of 20kts. Fig. 6.7 shows the required power versus airspeed for the forward and aft cg configurations.

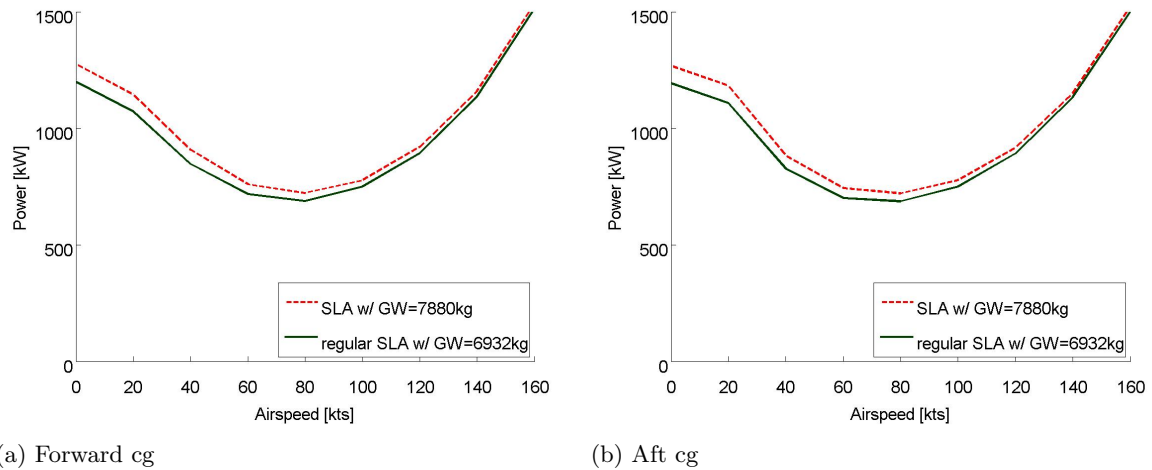


Figure 6.7: Power curves for forward and aft center of gravity positions.

From figure 6.7, it can be seen that the required power will be higher for an increased GW; this being self evident. At lower speeds, the difference in required power is larger than at higher airspeeds. A higher GW will require the helicopter to produce more thrust for vertical lift capability. At low airspeeds, the power required is mainly dependent on the amount of thrust needed to maintain lift. At higher airspeeds, the forward motion causes additional rotor lift. With increased airspeed, the rotor power provides less vertical lifting capability, and is increasingly used to tilt the rotor disc forward to attain higher airspeeds. As such, the difference in required lift for differing GW will become smaller at these airspeeds.

### The use of NDARC for load predictions

While it was initially desired to use NDARC for entire helicopter sizing, NDARC currently cannot perform iterative sizing based on loads. Sizing is solely performed for performance, in terms of power available. Since NDARC does allow for main rotor hub load prediction during a manoeuvre, it was considered to use this tool alongside Flightlab to determine the accuracy of this simple, rapid predictive tool in load predictions. Control deflections are hard-coded. For each segment of the doublet, the maximum longitudinal cyclic and stabilator incidence is taken from Flightlab, and supplied as input to NDARC. This is done for the baseline helicopter, as well as the SLA helicopter. Since changes in GW will affect the amount of longitudinal control actuation, each GW change for the SLA helicopter is supplied to Flightlab to see subsequent control changes. This is then fed to NDARC, determining shaft loads, from which shaft stresses are calculated. The iterative process is shown in figure 6.8.

Through trial and error, it is seen that pure GW or cg adjustments in NDARC have no impact on load prediction, when controls are kept constant; changes in control deflection only alter hub loads. This seems inconsistent, since a change in GW or cg should put the helicopter at another aircraft attitude, changing flapping and therefore loads. For the baseline and unaltered SLA helicopters, NDARC predicts the following stresses, as given in table 6.10. Compared to Flightlab stress predictions, shear stresses are in the same region, while normal stresses are significantly larger. These normal stresses are highly dependent on aircraft attitude. However, since NDARC does not provide any information on aircraft attitude, it is decided not to use these results for further optimization.

Furthermore, inflow and interference models make use of very basic empirical correlations in NDARC. Effects of stall, compressibility, or non-uniform inflow are also not considered. Therefore, these results show that use of NDARC should be limited to parametric sizing based on rotorcraft geometry, but should not be used for load predictions.

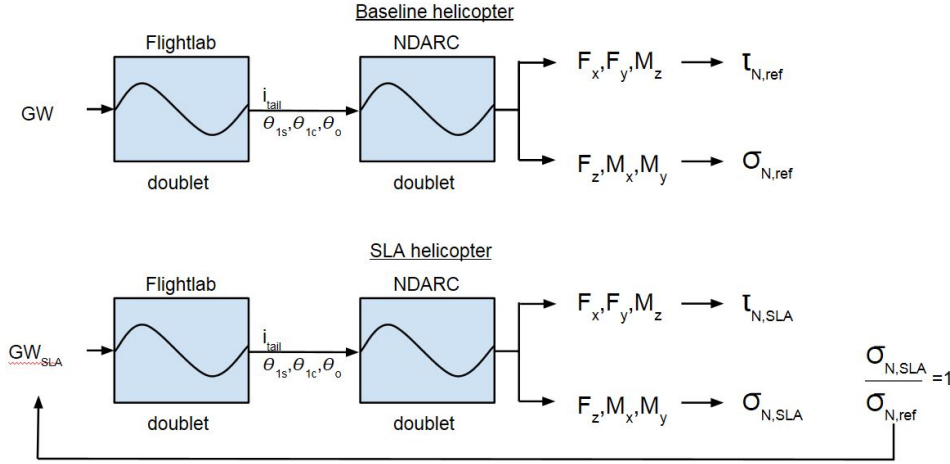


Figure 6.8: Hybrid iterative approach using Flightlab and NDARC, for helicopter GW increase.

Table 6.10: Prediction of main rotor normal and shear stresses for Flightlab and NDARC.

Parameter	Flightlab		NDARC	
	baseline	SLA	baseline	SLA
$GW$ [kg]	6932	6932	6932	6932
$\sigma_N$ [MPa]	218.14	251.73	634.45	669.27
$\tau$ [MPa]	83.8	100.94	89.03	101.47

### 6.3. CONCLUSIONS ON WEIGHT ALTERATIONS

Three approaches were utilized to optimize the SLA-equipped UH-60A in terms of weight alterations. These alterations include the downsizing of main rotor shaft or main rotor radius to reduce WE, or to increase permissible GW. Normal stresses in the baseline helicopter's main rotor shaft were used as a reference, according to which the SLA helicopter was iteratively tuned.

Based on the reverse doublet performed at 130kts for three center of gravity configurations, the main rotor shaft can be downsized, reducing outer radius by 2.7%. This results in a mass reduction of 0.31kg from the original 11.11kg mass. Shear stress levels furthermore decrease by 0.34%.

While main rotor radius downsizing results in a higher shaft bending moment  $M_y$ , the subsequent decrease in force  $F_z$  results in an overall decrease in normal stresses. As such, the main rotor radius should not be downsized concerning loads. Downsizing of the main rotor radius will furthermore affect the power required. Nonetheless, NDARC allows for a preliminary empty weight estimation based on changes in rotor radius. However, due to the aforementioned conclusion, this weight adjustment will not be considered.

Instead of performing geometric alterations, the GW of the SLA UH-60A may be increased before similar normal stresses are experienced as the baseline UH-60A. It is found that the regular 1.75g doublet manoeuvre is most constricting in terms of additional GW. GW may be increased from 6932kg to 7881kg.

Similar GW tuning was attempted by using a hybrid NDARC-Flightlab. However, NDARC shows significant limitations in load predictions. Due to load dependency on helicopter attitude, and the lack information on the latter parameter, load prediction results are discarded. According to NDARC, loads do not alter depending on GW or cg location; varying only with changes in blade actuation. In its current form, NDARC should only be applied for preliminary sizing based on performance or rotor geometry. Sizing should not be performed based on load predictions.

Pertaining to the NDARC preliminary design tool, it is recommended to enhance load predictions, and to expand sizing capability to include structural loads. Helicopter states such as aircraft attitude

should be incorporated in load predictions. NDARC currently solely allows for main rotor and GW sizing based on performance, in terms of available power. As such, the main rotor diameter is sized so that available power is equivalent to the required power for the most demanding flight segment. It is felt that structural loads should be incorporated as well, as this too is of great importance in sizing components. Furthermore, while blade pitch angle may be prescribed, the resulting changes in lift and drag are determined with constant  $c_{l\alpha}$  and  $c_{d\alpha}$ , for any angle. While the attractiveness of a preliminary sizing tool is its simplicity and its ability to rapidly generate results, it is felt that incorporation of stall onset requires minor additional complexity, and allows for more accurate results.

Note that while this SLA system allows for main rotor component downsizing or a GW increase, the inclusion of stabilator actuators may increase the empty weight of the helicopter, when currently featuring a fixed horizontal tail. As a rough indication of an upper bound component mass increase, Colegrove et al. [12] indicates that the stabilator actuators of the F-15 combat aircraft have a mass of 31kg. Since this research is concerned with the UH-60A, the impact of additional actuator weight is not considered further.



# 7

## Conclusions

In this research, a novel SLA scheme has been assessed on its feasibility, as applicable to the Sikorsky UH-60A Blackhawk helicopter. The proposed mixed control SLA system utilizes stabilator actuation for main rotor load alleviation, following pilot inputs in longitudinal axes. Of particular interest are load reductions in terms of main rotor shaft bending moment  $M_y$ . Because the UH-60A sees significant  $M_y$  loads when performing the UTTAS doublet, and because the UH-60A currently features a variable incidence horizontal tailplane, it is chosen to assess the mixed control SLA scheme on this helicopter. The feasibility of real-life application will depend on various factors, including off-design performance, safety after FCS failure, and potential weight alterations. Per sub-section, each of the following three research questions will be addressed:

1. To which extent does the SLA system reduce loads in off-design conditions?
2. Is this novel SLA approach feasible for implementation on the UH-60A Blackhawk concerning safety after system failure?
3. If controller properties are altered to guarantee a safe helicopter, what is its impact on overall aircraft performance in terms of agility?
4. With the SLA system in place, what is the permissible component downsizing or design gross weight increase, if similar structural loads are deemed acceptable?

### 7.1. CONCLUSIONS ON OFF-DESIGN LOAD ALLEVIATION PERFORMANCE

For all variations in center of gravity and airspeed, the mixed control SLA system must still allow for load reduction in terms of shaft bending moment  $M_y$ , when performing a similar maneuver. Four off-design conditions are chosen, with maximum forward (28.5ft) and aft (30.5ft) center of gravity, as permitted for the UH-60A, and with airspeeds of 80kts to 160kts. The former is the lowest airspeed at which the SLA system will be fully functional, while the latter is the maximum airspeed of the UH-60A. The combination of these parameters define the corners of the entire operating realm of the SLA system. Thus, analysis at these conditions will show maximum unfavorable deviations. The third variable with which the SLA system was designed, the helicopter's gross weight, is not altered during the off-design analysis. Since the stabilator is used for pitch attitude control at low airspeeds, it is decided to phase in the mixed control SLA system at airspeeds above 60kts, being fully functional at 80kts flight or higher.

Figures 4.22 and 4.23 demonstrate that the performed manoeuvre is sufficiently similar for SLA and baseline helicopters. This similarity allows conclusions to be drawn in terms of load reduction capability. In these off-design flight conditions, load reduction is assessed in terms of shaft bending moment  $M_y$ . From figure 4.21, load alleviation capability is considered sufficient, reducing shaft bending moment by at least 10% for any off-design condition. Also, due to the similarity of observed aircraft angular rate transients, it can be concluded that an (auto)pilot, represented here by the longitudinal and lateral-directional controllers, can still properly follow desired angular rate transients in off-design conditions.

While variations in control allocation was considered for various airspeed regimes, the SLA scheme's performance in terms of shaft bending load reduction for a given longitudinal maneuver, have resulted in the choice to maintain a single control allocation, designed around the 130kts, normal cg condition.

## 7.2. CONCLUSIONS ON SAFETY AND HANDLING QUALITIES

Actuator limits have been chosen to guarantee safety after maximum stabilator deflection. With actuation deflection and rate limits in place, the SLA system's agility is assessed as compared to the baseline UH-60A. Lastly, validity of results are determined, by assessing differences in response for various inflow and interference conditions.

### 7.2.1. ACTUATOR LIMITS THAT PROVIDE SAFETY

For the mixed control SLA system, the criteria listed in table 7.1 are considered guiding in determining safety after system failure. In the final column, conclusions on each criterion are displayed.

Table 7.1: Safety criteria after SLA failure.

Crit. nr.	Criteria	Outcome
1	Helicopter can be trimmed after SLA failure	Max. stabilator angles: -7deg and 27deg
2	Sufficient longitudinal cyclic margin to reduce airspeed	Max. stabilator angles: -7deg and 10deg
3	Maximum load factor of 1.5g after failure	Slight exceedance of loadfactor by 0.04g
4	No attitude beyond -6deg (down) or 15deg (up) when flying at 60kts	Never exceeds -1.5deg and 6.8deg

Based on the first and second criteria, trimsweeps are conducted with respect to airspeed, determining the most critical airspeeds with lowest longitudinal cyclic margin. The 140kts and 160kts airspeed situations appear to be most critical. To allow for trim in terms of pitch rate, it is determined that the stabilator should not deflect beyond a -7deg or 27deg position. At the upper longitudinal cyclic bound, the helicopter's forward airspeed will be restricted, while the lower bound will result in the helicopter not being able to pitch up and slow down. At positive stabilator incidence angles, the UH-60A shows speed instability, where the amount of longitudinal cyclic in trim is less at a higher airspeed. This is an undesirable quality. Based on the 80kts airspeed condition, being the lowest airspeed at which the SLA system will be fully functional, maximum stabilator angles are chosen; -7deg and 10deg. The mixed control SLA system will gradually phase in, starting at airspeeds of 60kts. As such, maximum stabilator deflection may occur at this airspeed. In case of 10deg stabilator deflection, the helicopter will posses slight speed instability between airspeeds of 60kts and 100kts, in the order of  $0.1 \frac{deg}{kts} \frac{\partial \theta_{1s}}{\partial V}$ . This is considered acceptable, due to the sufficient longitudinal cyclic margin available to reduce airspeed. It is furthermore chosen to allow for 45deg/s stabilator deflection angles, based on required actuation rates for full load reduction at 80kts. This will require minimal hardware modifications for the current UH-60A. With these actuator deflection angle and rate constraints, the final two criteria are assessed. Without corrective action provided by the longitudinal and lateral-directional controllers, faulty stabilator deflections result in serious loadfactor exceedances. However, after such failure, a pilot will respond by providing corrective action. With the two aforementioned controllers in place, maximum loadfactor transients remain below 1.5g for most combinations of tailplane deflection, cg location and airspeed. Only when flying at airspeeds of 160kts with a stabilator deflection rate of 45deg/s, resulting in a final stabilator incidence of 10deg/s, will loadfactor be slightly higher, at 1.54g. Concerning a safe landing at 60kts, when trimmed by pilot action, the mixed control SLA system will never cause attitude excursions beyond 1.5deg nose-down or 6.8deg nose-up attitudes, for any center of gravity. As such, the helicopter can safely perform an emergency landing if necessary; aircraft attitudes do not exceed maximum permissible attitudes for landing.

### 7.2.2. NEWLY PROPOSED AGILITY METRICS

Aside from findings on helicopter dynamic behavior of the SLA system, this research has resulted in the development of two novel handling quality metrics; flightpath attitude quickness and flightpath bandwidth. This is because it is considered that current metrics, provided by ADS-33E and MIL, do

not provide a complete picture concerning handling qualities. Flightpath quickness is a metric derived from attitude quickness, yet now determining rate of change of flightpath trajectory instead of aircraft attitude. By dividing peak flightpath by change in flightpath, there is a qualitative measure for response time. With same units as attitude quickness, a direct comparison of agility, in terms of flightpath and attitude changes, can be made.

Flightpath bandwidth is analogous to pitch rate bandwidth, now assessing the flightpath angle response to various stick input frequencies. By comparing flightpath bandwidth to pitch rate bandwidth, differences in agility, in terms of flightpath and pitch rates, can be compared. While ADS-33E sets load factor requirements for aircraft handling at low airspeed failure conditions, high speed constraints are minimal, requiring the helicopter to remain within its operational flight envelope (OFE). Evidently, remaining within the OFE in these conditions should not be considered sufficient; the pilot must still be able to change the flightpath trajectory. Therefore, in style with current ADS-33E metrics, it is felt that this proposed metric can be of value if included within the ADS-33E norms, allowing for better agility and safety assessment of a failed FCS system.

### 7.2.3. AGILITY WITH IMPOSED ACTUATOR CONSTRAINTS

To determine the helicopter's agility after the actuator constraints are imposed, five agility metrics are assessed. These are: attitude quickness, agility quickness, flightpath agility quickness, flightpath bandwidth and pitch rate bandwidth. The first three metrics measure the helicopter's response following a step input in terms of longitudinal cyclic stick. The last two metrics assesses the flightpath and pitch rate response following longitudinal cyclic stick input provided over a range of frequencies. These multiple metrics are required as none of the individual metrics provides a complete picture concerning agility. Attitude quickness determines the helicopter's ability to change pitch attitude. However, ADS-33E does not set HQ boundaries in terms of attitude quickness for high speed flight. Agility quickness measures the ability to change flightpath trajectory, in terms of attainable load factor. Since this metric considers load factor and flightpath angle, units differ from attitude quickness. Results can therefore not be compared on a one-to-one basis to those of attitude quickness. Flightpath agility quickness is proposed in this research, being similar to agility quickness, now assessing flightpath changes instead of load factor, allowing for better comparison with attitude quickness. However, time dependence of response is considered important, and is not considered by the quickness metrics. As such, flightpath bandwidth is proposed. Here, longitudinal stick input is provided at various frequencies, for which flightpath response is assessed. Pitch rate bandwidth analysis is performed in similar fashion, determining the ability to induce a pitch rate at various stick input frequencies. This allows for comparison of frequency response differences in terms of flightpath and pitch rate. Below, results per metric are presented.

- Attitude quickness: ability to change attitude
  - Design condition: SLA system possesses higher agility than baseline system
  - All failure cases show ability to change pitch attitude, also in off-design conditions
- Agility quickness: ability to change flightpath trajectory (quantified by load factor)
  - Design and off-design conditions: All systems perform similarly
  - For a fixed duration input, SLA system required long response time
- Flightpath agility quickness: ability to change flightpath trajectory (quantified by flightpath)
  - Design condition: SLA system performs similarly to baseline system
  - Off-design conditions: SLA system performs better in high speed flight
  - For a fixed duration input, SLA system required long response time
  - All failure cases show ability to change flightpath, also in off-design conditions
- Flightpath bandwidth response: ability to change flightpath for inputs over different frequencies
  - Design and off-design conditions: SLA system performs very similar as compared to baseline system, especially at low frequencies

- Off-design condition: (160kts flight and aft cg) SLA system performs better than baseline helicopter, avoiding RBS
- Failure cases show larger differences in gain per frequency, yet gains are similar to the baseline system; considered sufficient
- Pitch rate bandwidth response: ability to change pitch rate for inputs over different frequencies
  - Design condition: SLA system sees similar gain magnitudes for all frequencies as baseline system
  - Off-design conditions: Near identical response for SLA and baseline systems
  - Off-design condition: (160kts flight and aft cg) SLA system performs better than baseline helicopter, avoiding RBS
  - Failure cases show gains of similar magnitude as baseline system; considered sufficient

From the above results, agility quickness conclusions are combined with those of flightpath agility quickness, due to their similarity. This research aims at assessing response in longitudinal axis, as this is what determines the pilot's ability to slow down. Therefore, based on two quickness and two bandwidth analyses, conclusions on agility in terms of attitude and flightpath can be drawn.

- The SLA system shows an increased ability to change pitch attitude as compared to the baseline system in all (design and off-design) flight conditions for step input.
- For a similar step input, the SLA system shows an equal or higher ability to change flightpath as compared to the baseline system in all flight conditions. Differences in agility are smaller than for attitude quickness due to initial adverse change in net helicopter lift by the stabilator.
- For input over low frequencies, the SLA system shows an almost identical flightpath bandwidth response compared to the baseline system, for most flight conditions.
- For input over high frequencies, the SLA system in general shows lower response magnitude compared to the baseline system, caused by the short term adverse change in net helicopter lift after stabilator deflection.
- For input over different frequencies, the SLA system shows a similar frequency response in terms of pitch rate bandwidth as the baseline system, also in off-design conditions.
- For flightpath bandwidth and pitch rate bandwidth, all failure cases show gains which are similar in magnitude to the SLA and baseline systems, irrespective of flight condition.
- In terms of flightpath and pitch rate bandwidths, agility of the SLA helicopter is not limited by RBS, at 160kts flight with an aft cg.

Therefore, the SLA system provides equal or superior agility compared to the baseline system, both in terms of pitch attitude changes as well as flightpath changes.

#### 7.2.4. VALIDITY OF INFLOW AND INTERFERENCE MODELING

Conclusions drawn in preceding sections are only as good as the simulation model that they are based on. Below, conclusions pertaining to validity are presented.

One cannot attribute differences between various inflow models solely to the degree of model fidelity, since the longitudinal, lateral-directional and SLA systems were designed in the 3-state inflow environment. Nonetheless, when comparing pitch attitude for the 3-state inflow model with the higher fidelity 6-state and Scully inflow models, peak differences remain within 10% in any off-design condition. The longitudinal controller manages to maintain pitch within a 3% to 6% margin. This demonstrates the SLA system's consistent pitch rate response, irrespective of inflow model. In the worst off-design condition, the difference in inflow models resulted in a 20% underestimation of shaft bending moments  $M_y$  by the 3-state inflow model, caused by the larger difference in pitch attitude. Differences in lateral and directional axes is generally larger than in longitudinal axes, though the degree to which this depends on the model fidelity, instead of controller design, is unknown.

Nonetheless, transient behavior of helicopter states and loads in the Peters-He and Scully inflow models show very similar shapes to the Pitt-Peters model. Having based conclusions on transients in the Pitt-Peters environment, the observed trends remain unchanged. As stated by Prouty [47], simulation models have difficulty in capturing the real-life chaotic flow around the tailplane, as caused by the main rotor downwash. For this reason, the differences in peak values between the various inflow models are deemed acceptable; inaccuracies in tailplane interference of these simulation models as compared to flight tests will most likely be of larger magnitude. For this reason, conclusions in the Pitt-Peters domain are deemed acceptable within the scope of simulation model choice. Evidently, before real-life implementation, wind tunnel and flight tests must be carried out to fine tune the system for actual application.

### 7.3. CONCLUSIONS ON WEIGHT ALTERATIONS

Three approaches were utilized to optimize the SLA-equipped UH-60A in terms of weight alterations. These alterations include the downsizing of main rotor shaft or main rotor radius to reduce WE, or to increase permissible GW. Normal stresses in the baseline helicopter's main rotor shaft were used as a reference, according to which the SLA helicopter was iteratively tuned.

Based on the reverse doublet performed at 130kts for three center of gravity configurations, the main rotor shaft can be downsized, reducing outer radius by 2.7%. This results in a mass reduction of 0.31kg from the original 11.11kg mass. Shear stress levels furthermore decrease by 0.34%.

While main rotor radius downsizing results in a higher shaft bending moment  $M_y$ , the subsequent decrease in force  $F_z$  results in an overall decrease in normal stresses. As such, the main rotor radius should not be downsized concerning loads. Downsizing of the main rotor radius will furthermore affect the power required. Nonetheless, NDARC allows for a preliminary empty weight estimation based on changes in rotor radius. However, due to the aforementioned conclusion, this weight adjustment will not be considered.

Instead of performing geometric alterations, the GW of the SLA UH-60A may be increased before similar normal stresses are experienced as the baseline UH-60A. It is found that the regular 1.75g doublet manoeuvre is most constricting in terms of additional GW. GW may be increased from 6932kg to 7881kg.

Similar GW tuning was attempted by using a hybrid NDARC-Flightlab. However, NDARC shows significant limitations in load predictions. Due to load dependency on helicopter attitude, and the lack information on the latter parameter, load prediction results are discarded. According to NDARC, loads do not alter depending on GW or cg location; varying only with changes in blade actuation. In its current form, NDARC should only be applied for preliminary sizing based on performance or rotor geometry. Sizing should not be performed based on load predictions.

Pertaining to the NDARC preliminary design tool, it is recommended to enhance load predictions, and to expand sizing capability to include structural loads. Helicopter states such as aircraft attitude should be incorporated in load predictions. NDARC currently solely allows for main rotor and GW sizing based on performance, in terms of available power. As such, the main rotor diameter is sized so that available power is equivalent to the required power for the most demanding flight segment. It is felt that structural loads should be incorporated as well, as this too is of great importance in sizing components. Furthermore, while blade pitch angle may be prescribed, the resulting changes in lift and drag are determined with constant  $c_{l\alpha}$  and  $c_{d\alpha}$ , for any angle. While the attractiveness of a preliminary sizing tool is its simplicity and its ability to rapidly generate results, it is felt that incorporation of stall onset requires minor additional complexity, and allows for more accurate results.

Note that while this SLA system allows for main rotor component downsizing or a GW increase, the inclusion of stabilator actuators may increase the empty weight of the helicopter, when currently featuring a fixed horizontal tail. As a rough indication of an upper bound component mass increase, Colegrove et al. [12] indicates that the stabilator actuators of the F-15 combat aircraft have a mass of 31kg. Since this research is concerned with the UH-60A, the impact of additional actuator weight is not considered further.

#### 7.4. CONCLUDING REMARKS

In response to the four research questions, it can be concluded that the proposed SLA system provides load reductions of 10% or higher in the considered off-design conditions, potentially allowing for a GW increase of 13.6%, when using the 1.75g doublet at 130kts airspeed as a reference. Concersely, the main rotor shaft radius may be downsized by 2.7%. With the chosen tailplane actuator limits, the SLA system is considered safe for all failure scenarios, while allowing for similar or improved agility in terms of pitch attitude and flightpath trajectory.

# 8

## Recommendations

While research has demonstrated favorable off-design performance, safety and weight alterations of the SLA equipped UH-60A, further research must be done before real-life implementation of this system can take place.

The SLA scheme has demonstrated sufficient off-design performance, when considering variations in center of gravity and airspeed. However, the controller was devised around a third parameter which was not altered in this research. As such, the helicopter's performance for variations in gross weight should be evaluated as well. While this research was mainly concerned with response in longitudinal axes, safety and agility should also be assessed for motion in lateral and directional axes. Also, this assessment has considered analysis where in ground effects (IGE) could be discarded. However, when operating at high speeds in proximity of terrain, these effects may alter handling and safety performance, and should therefore also be assessed. While this simulation model did not consider atmospheric upsets, the SLA system's gust sensitivity may also be of interest.

The mixed control SLA scheme has been developed for the UH-60A with a Pitt-Peters 3-state inflow model, including rotor and fuselage interference effects at the stabilator. An attempt has been made in determining to which extent the inflow model affects the performance of the SLA-equipped UH-60A. Before implementation on series-produced UH-60A helicopters, wind tunnel tests and real-life test flights should be conducted. This is essential, to determine to which extent the conclusions drawn in this research are valid. In particular, the flow field around the horizontal tailplane has proven challenging within current simulation domains (Padfield [42]). As the stabilator sees main rotor downwash at various airspeeds, this should be assessed in a physical test environment.

If the mixed control SLA scheme proves feasible for application to the UH-60A, the scope of this SLA scheme may extend to other helicopter designs currently featuring a stabilator or a fixed horizontal tailplane. For these various helicopter types, similar assessment of simulation models, as well as flight tests, must be conducted to determine applicability of the SLA scheme. Pertaining to weight alterations, this research focuses on main rotor downsizing, in terms of rotor shaft and main rotor radius. However, for assessment of helicopters not currently featuring a stabilator, the additional weight caused by the moving tailplane, actuators, and control systems, must be accounted for. While main rotor downsizing was unfruitful for the UH-60A, other helicopters may see potential main rotor radius downsizing. This will depend on the ratio of the relative increase in bending stresses, and the magnitude of reduced tensile stresses. Nonetheless, the effect on power required must be considered.

Lastly, pertaining to the NDARC preliminary design tool, it is recommended to expand load prediction capability to include aircraft attitude effects, as well as blade stall predictions. Sizing capability should be expanded to include structural loads. While NDARC currently allows for structural load analysis, main rotor and GW sizing is done based on performance. As such, the main rotor diameter is sized so that available power is equivalent to the required power for the most demanding flight segment. It is felt that structural loads should be incorporated as well, as this too is of great importance in the preliminary sizing. Furthermore, while blade pitch angle may be prescribed, the resulting changes in lift and drag are determined with constant  $c_{l\alpha}$  and  $c_{d\alpha}$ , for any angle, even for angles where blade stall will most definitely occur. It is felt that incorporation of stall onset requires minor additional complexity, and allows for more accurate results.



# Bibliography

- [1] Sikorsky s-67 (uh-60a) black hawk. URL [http://atallguy.com/Simple-Multi-View-Plans/S-images/sikorsky\\_blackhawk\\_3v.jpg](http://atallguy.com/Simple-Multi-View-Plans/S-images/sikorsky_blackhawk_3v.jpg).
- [2] Aeronautical design standard performance specification handling qualities requirements for military rotorcraft, March 2000.
- [3] Transverse flow effect, 2004. URL [http://ierwtraining.com/Transverse\\_Flow\\_Effect.htm](http://ierwtraining.com/Transverse_Flow_Effect.htm).
- [4] Flight control systems-design, installation and test of piloted aircraft, general specifications, April 2008.
- [5] J. Bahgwat and J. Leishman. Generalized viscous vortex model for application to free-vortex wake and aeroacoustic calculations. *University of Maryland*.
- [6] F.J. Bailey. A simplified theoretical method of determining the characteristics of a lifting rotor in forward flight. *NACA Report 716*, pages 209–226, 1941.
- [7] R.L. Bisplinghoff, H. Ashley, and R.L. Halfman. *Aeroelasticity*. Dover Books on Aeronautical Engineering Series. Dover Publications, 1996. ISBN 9780486691893.
- [8] J.L. Boiffier. *The Dynamics of Flight: The Equations*. Wiley, 1998.
- [9] K.A. Bordignon. Constrained control allocation for systems with redundant control effectors. *Virginia Polytechnic Institute and State University*, 1996.
- [10] M. Brian and W. Harris. How helicopters work. URL <http://science.howstuffworks.com/transport/flight/modern/helicopter5.htm>.
- [11] R.T.N. Chen. A survey of nonuniform inflow models for rotorcraft flight dynamics and control applications. *NASA Technical Memorandum 102219*, November 1989.
- [12] P.G. Colegrove, B.L. McFadden, and M.D. Braydich. Nonflammable hydraulic power system for tactical aircraft. 1991.
- [13] D.E. Cooper. Yuh-60a stability and control. *Journal of the American Helicopter Society*, 23(3): 2–9, 1978.
- [14] G.E. Cooper and R.P. Harper. The use of pilot rating in the evaluation of aircraft handling qualities, April 1969.
- [15] A. Datta and I. Chopra. Validation and understanding of uh-60a vibratory loads in steady level flight. *American Helicopter Society*, June 2002.
- [16] *Operator's Manual for UH-60A Helicopter, UH-60L, Helicopter EH-60A Helicopter*. Department of Defence, tm 1-1520-237-10 edition, September 2009.
- [17] H. Glauert. *The elements of Aerofoil and Airscrew Theory*. Cam, second edition edition, 1993.
- [18] K. Gotzfried. Survey of tiger main rotor loads from design to flight test. *Journal of the American Helicopter Society*, 47(4):285–296, 2002. cited By 1.
- [19] M.E. Gunduz, A. Khalid, and D.P. Schrage. Weight estimation using cad in the preliminary rotorcraft design. September 2007.
- [20] M. Hamers and P.M. Basset. Application of the finite state unsteady wake model in helicopter flight dynamic simulation. *26th European Rotorcraft Forum*, 2000.

- [21] R.P Harper and G.E. Cooper. Handling qualities and pilot evaluation. 1984.
- [22] J. Horn, A.J. Calise, and J.V.R Prasad. Flight envelope limit detection and avoidance for rotorcraft. *Journal of the American Helicopter Society*, 47(4):253–262, October 2002.
- [23] J. Horn, D.O. Bridges, D.A. Wachspress, and S.L. Rani. Implementation of a free-vortex wake model in real-time simulation of rotorcraft. *Journal of Aerospace Computing, Information, and Communication*, 3:93–114, 2006.
- [24] J.F. Horn and N. Sahani. Detection and avoidance of main rotor hub moment limits on rotorcraft. *Journal of Aircraft*, 41(2):372–379, March-April 2004.
- [25] J. Howitt. Application of non-linear dynamic inversion to rotorcraft flight control. *American Helicopter Society 61st Annual Forum, Grapevine, Texas*, pages 1160–1169, June 2005.
- [26] J. Howitt, P.R. Brinson, and I.J. Woodrow. Expercontrol evaluation of high bandwidth helicopter flight control system ddesign exploiting rotor state feedback. *American Helicopter Society 53rd Annual Forum, Virginia Beach, Virginia*, pages 1452–1465, April-May 1997.
- [27] J.J. Howlett. Uh-60a black hawk engineering simulation program: Volume i- mathematical model. *NASA Contractor Report*, December 1981.
- [28] Y. Huo. Model of f-16 fighter aircraft - equations of motions.
- [29] C.K. Johnson, D. Mittleider, M.B. Tischler, and K.K. Cheung. Analysis, design & optimization of the helicopter active control technology (hact) flight control system. 58th annual forum of the American Helicopter Society, June 2002.
- [30] W. Johnson. *NDARC-NASA Design and Analysis of Rotorcraft Theoretical Basis and Architecture*. THE USE OF PILOT RATING IN THE EVALUATION OF AIRCRAFT HANDLING QUALITIES, Moffett Field, California, 2010.
- [31] W. Johnson. *NDARC NASA Design and Analysis of Rotorcraft*. National Aeronautics and Space Administration-Input, Moffett Field, California, 1.6 edition, February 2012.
- [32] W. Kaufmann. Uber die ausbreitung kreiszylindrischer wirbel in zahren flussigkeiten. *Ing. Arch.*, 31(1):1, 1962.
- [33] R. Kufeld, D. Balough, J. Cross, K. Studebaker, C. Jennison, and W. Bousman. Flight testing the uh-60a airloads aircraft. pages 557–577.
- [34] R.M. Kufeld and W.G. Bousman. High load conditions measured on a uh-60a in maneuvering flight. pages 202–211, Forth Worth, Texas, May 1995. 51st annual form of the American Helicopter Society.
- [35] J.G. Leishman. *Principles of Helicopter Aerodynamics*. Cambridge Aerospace Series. Cambridge University Press, 2006. ISBN 9780521858601.
- [36] R. Leoni. S-70b, (s-60b (sh-60b seahawk, sh-60f cv, hh-60h rescue hawk, hh-60j jayhawk, vh-60n), June 2012. URL [http://www.sikorskyarchives.com/S-70B%20\(SH-60B%20Seahawk,%20SH-60F%20CV,%20HH-60H%20Rescue%20Hawk,%20HH-60J%20Jayhawk,%20VH-60N\).php](http://www.sikorskyarchives.com/S-70B%20(SH-60B%20Seahawk,%20SH-60F%20CV,%20HH-60H%20Rescue%20Hawk,%20HH-60J%20Jayhawk,%20VH-60N).php).
- [37] H.L. LeRoy. Flight investigation of effects of retreating-blade stall on bending and torsional moments encountered by a helicopter rotor blade. *National Advisory Committee For Aeronautics Technical Note 4254*, May 1958.
- [38] K. Loy. Carefree handling and its applications to military helicopters and missions. volume 1, pages 489–494, 1997. cited By (since 1996)4.
- [39] B. Manimala, M. Naddei, and P. Rollet. Load alleviation in tilt rotor aircraft through active control; modelling and control concepts. *American Helicopter Society 59th Annual Forum, Phoenix, Arizona*, May 2003.

- [40] B. Manimala, G.D. Padfield, and D.J. Walker. Load alleviation for a tilt-rotor aircraft in airplane mode. *Journal of Aircraft*, (1):147–156, January-February 2006.
- [41] D.G. Miller, T.M. Black, and Joglekar M. Tiltrotor control law design for rotor loads alleviation using modern control techniques. *Proceedings for the 1991 American Control Conference; Boston, MA, USA*, June 1991.
- [42] G.D. Padfield. *Helicopter Flight Dynamics*. AIAA education series. Wiley, 2008. ISBN 9780470691168.
- [43] M. Pavel and G.D. Padfield. Progress in the development of complementary handling and loading metrics for ads-33 manoeuvres. *American Heli*, 2003.
- [44] D.A Peters and C.J. He. Correlation of measured induced velocities with a finite-state wake model. *Journal of the American Helicopter*, 36(3), 1991.
- [45] D.M. Pitt and D.A. Peters. Theoretical prediction of dynamic-inflow derivatives. *6th European Rotorcraft Forum*, 1980.
- [46] R. Prouty. *Helicopter Aerodynamics Volume I*. Phillips Business Information, Inc., 2004.
- [47] R.W. Prouty. *Helicopter Aerodynamics*. Rotor & Wing International. PJS Publications, 1985.
- [48] R.W. Prouty. *Helicopter performance, stability, and control*. PWS Engineering, 1986. ISBN 9780534063603.
- [49] W.J.M Rankine. Manual of applied mechanics. 1858.
- [50] M.P. Scully and J.P. Sullivan. Helicopter rotor wake geometry and airloads and development of laser doppler velocimeter for use in helicopter rotor wakes. *Massachusetts Institute of Technology Aerophysics Laboratory Technical Report 183*, August 1972.
- [51] T. Theodorsen. General theory of aerodynamic instability and the mechanism of flutter. *NACA Technical Report No. 496*, Washington, DC, 1935.
- [52] Federal Aviation Administration U.S. Department of Transportation, editor. *Basic Helicopter Handbook*. DIANE Publishing Company.
- [53] Kozel V. Vatistas, G.H. and W.C. Mih. A simpler model for concentrated vortices. *Experiments in Fluids*, 11:73–76, 1991.
- [54] M. Voskuijl. Helicopter main rotor load alleviation using active horizontal stabilizer control.
- [55] M. Voskuijl, D.J. Walker, B.J. Manimala, and A.W. Gubbels. Helicopter heave axis control and flight envelope protection.
- [56] M. Voskuijl, M.D Pavel, and J. Vorst, van der. Active control technology for tiltrotor structural load alleviation. pages 295–309, Marseille, France, September 2004. 30th European Rotorcraft Forum.
- [57] M. Voskuijl, M.D Pavel, D.J. Walker, and B.J. Manimala. Helicopter load alleviation using active control. *The Aeronautical Journal*, October 2008.
- [58] H. Wagner. Uber die entstehung des dynamischen auftriebes von tragflugeln. pages 17–35, February 1925.
- [59] J.R. Wright and J.E. Cooper. *Introduction to Aircraft Aeroelasticity and Loads*. Aerospace Series (PEP). John Wiley & Sons, 2008. ISBN 9780470858400.
- [60] G.M. Yamakawa, D.G. Broadhurst, and Smith J.R. Utility tactical transport aircraft system (uttas) maneuver criteria. Technical report, U.S. Army Aviation Systems Command, 1972.
- [61] H. Yeo and W. Johnson. Prediction of rotor structural loads with comprehensive analysis. *Journal of the American Helicopter Society*, 53(2):193–209, 2008. doi: 10.4050/JAHS.53.193. cited By 31.

- [62] H. Yeo, W.G. Bousman, and W. Johnson. Performance analysis of a utility helicopter with standard and advanced rotors. *Journal of the American Helicopter Society*, 49(3):250–270, 2004. cited By 55.



## Prouty's parametric weight estimation

Here all of Prouty's parametric equations can be found, used to evaluate the weight of a helicopter.

Main rotor blades	$W_{b_M} = 0.026b^{.66}cR^{1.3}(\Omega R)^{.67}$
Main rotor hub and hinge	$W_{h_M} = 0.0037b^{.28}R^{1.5}(\Omega R)^{.43}\left(.67W_{b_M} + \frac{gJ}{R^2}\right)^{.55}$
Stabilizer (horizontal)	$W_H = .72A_H^{1.2}A.R.H^{.32}$
Fin (Vertical stabilizer)	$W_V = 1.05A_V^{.24}A.R.V^{.35}(\text{no. of tail rotor gearboxes})^{.71}$
Tail rotor	$W_T = 1.4R_T^{.090}\left(\frac{\text{Transmission h.p. rating}}{\Omega_M}\right)^{.90}$

Figure A.1: Parametric weight estimation for components, part I (Prouty [48]).

Body (fuselage)	$W_F = 6.9 \left( \frac{\text{G.W.}}{1,000} \right)^{.49} L_F^{.61} (Swet_F)^{.25}$
Landing gear	$W_{L.G.} = 40 \left( \frac{\text{G.W.}}{1,000} \right)^{.67} (\text{No. of wheel legs})^{.54}$ (add 10% for retraction)
Nacelles	$W_N = 0.041(\text{Total dry engine wt})^{.1}(\text{No. of engines})^{.24} + 0.33 (Swet_N)^{.13}$
Engine installation	$W_{eng} = (\text{Installed wt. per eng.})(\text{No. of eng.})$
Propulsion subsystems	$W_{P.S.S.} = 2(W_{eng})^{.59}(\text{No. of eng.})^{.79}$
Fuel system	$W_{F.S.} = .43(\text{cap. in gal.})^{.77}(\text{No. of tanks})^{.59}$
Drive system	$W_{D.S.} = 13.6(\text{Transmission h.p. rating})^{.82} \left( \frac{\text{rpm}_{eng}}{1,000} \right)^{.037}$ $\times \left[ \left( \frac{\text{Tail rotor h.p. rating}}{\text{Transmission h.p. rating}} \right) \left( \frac{\Omega_M}{\Omega_T} \right) \right]^{.068} \frac{(\text{No. of gearboxes})^{.066}}{\Omega_M^{.64}}$
Cockpit controls	$W_{C.C.} = 11.5 \left( \frac{\text{G.W.}}{1,000} \right)^{.40}$ (Triple if no boost is used)
Systems controls (boosted)	$W_{S.C.} = 36b_M c_M^{2.2} \left( \frac{\Omega R_M}{1000} \right)^{3.2}$
Auxiliary power plant	$W_{A.P.P.} = 150$ (1980 state-of-the-art)
Instruments	$W_I = 3.5 \left( \frac{\text{G.W.}}{1,000} \right)^{1.3}$
Hydraulics	$W_{hyd} = 37b_M c_M^{1.3} \left( \frac{\Omega R_M}{1,000} \right)^{2.1}$
Electrical	$W_{EL} = \frac{9.6(\text{Transmission h.p. rating})^{.65}}{\left( \frac{\text{G.W.}}{1,000} \right)^{.40}} - W_{hyd}$

Figure A.2: Parametric weight estimation for components, part II (Prouty [48]).

Furnishings and equipment	$W_{FE} = \begin{cases} 6 \left( \frac{\text{G.W.}}{1,000} \right)^{1.3} & \text{(low)} \\ 13 \left( \frac{\text{G.W.}}{1,000} \right)^{1.3} & \text{(avg)} \\ 23 \left( \frac{\text{G.W.}}{1,000} \right)^{1.3} & \text{(high)} \end{cases}$
Air cond. & anti-ice	$W_{AC\&AI} = 8 \left( \frac{\text{G.W.}}{1,000} \right)$
Manufacturing variation	$W_{M.V.} = 4 \left( \frac{\text{G.W.}}{1,000} \right)$

Figure A.3: Parametric weight estimation for components, part III (Prouty [48]).

# B

## Aerodynamics as modeled in NDARC

Using multi-blade coordinates, components are given their location and spatial orientation. In this section, the modeling approaches used by NDARC are evaluated per component. To gain insight in the fundamental solution procedures and iterative sizing and performance tasks, please consult the appendix. Information on cost calculation can also be found in the appendix.

For the main rotor, the inflow is approximated by a simplified approach for a non-uniform inflow distribution, as given by equation B.1.

Here, the inflow has a component caused by forward or sideways flight, as well as a component caused by hub moments. These hub moments are the result of blade flapping. The relation between flapping and the resulting hub moments is given in eq. B.2.

$$\lambda = \mu_z + \lambda_0(1 + \kappa_x r \cos\psi + \kappa_y r \sin\psi) + \frac{f_m}{\sqrt{\mu^2 + \lambda^2}}(-2C_{My} r \cos\psi + 2C_{Mz} r \sin\psi) \quad (\text{B.1})$$

$$\begin{pmatrix} -C_{My} \\ C_{Mz} \end{pmatrix} = \frac{\sigma a \nu^2 - 1}{2 \gamma} \begin{pmatrix} \beta_c \\ \beta_s \end{pmatrix} \quad (\text{B.2})$$

To find thrust and the forces in x- and y-direction, the lift, drag and radial forces are determined. These are modified to take into account effects such as coning and flapping. The velocity used to find lift and drag, is found using blade element theory, based on inflow and helicopter speed. Using the Newton-Raphson method, the iterative process between force in z-direction, and flapping is solved.

The induced velocity of the main rotor will have an interference effect on the fuselage, the vertical and horizontal tails, as well as other components. The wake of the main rotor is described in a local reference frame, known as the wake reference frame. Here, the downward z-axis of this reference frame is aligned with the axis of symmetry of the wake, starting at the main-rotor. Therefore, compared to the body reference frame, the wake reference frame has rotated around the y-axis, such that the z-axis now makes an angle with the vertical by the same amount as the wake. In this coordinate system, the induced velocity at any given location downstream is given by:

$$v_{ind}^F = K_{int} f_w f_r v_1^F \quad (\text{B.3})$$

Here  $f_w$  is a factor indicating the wake development in axial wake direction, while  $f_r$  indicates the radial dependency from the center of the wake outward. Equations B.4 and B.5 are used to calculate these two factors.

Equation B.4 determines the influence of the radial intensity of the wake on the induced downwash. We see that as seen from above, the circular wake is divided into rings, numbered by  $s$  integers. Within a core region, a critical radius,  $R_c$ , the factor is unity. Further outward, the radial factor decreases. Outside the final ring,  $s + 1$ , the radial influence is zero. This makes sense, as this means that the induced velocity caused by the main rotor will be zero, being located outside of the wake region.

$$f_r = \begin{cases} 1 & r \leq R_c \\ 1 - \frac{r-R_c}{sR_c} & 0 \\ 0 & r \geq (1+s)R_c \end{cases} \quad (\text{B.4})$$

The factor that indicates the influence of the axial development of the wake on the induced velocity is given in equation B.5.  $\zeta$  is the distance along the wake axis. This equation implies that the induced velocity far ahead of the main rotor is zero ( $f=0$ ) and that the induced velocity at some distance below the main rotor will be twice the magnitude of the induced velocity at the main rotor disc ( $f=2$ ). This coincides with the induced velocity predictions found through momentum theory (ref.481986Prouty). Variable  $t$  is added to account for the rate of change for the wake to transition.

$$f_w = 1 + \frac{\frac{\zeta_w}{tR}}{\sqrt{1 + \frac{\zeta_w}{tR}^2}} \quad (\text{B.5})$$

This approach takes into account the impact of the main rotor wake, by describing the wake in radial and axial terms. Through equations B.4 and B.5, the radial and axial wake developments are assumed to be independent of one another.

For the component experiencing the rotor downwash, once induced velocity is determined from eq. B.3, the induced angle of attack is given by eq. B.6.

$$\alpha_{ind,rotor} = \frac{v_{ind}}{V} \quad (\text{B.6})$$

From this, the induced drag of the component is determined. For a wing, such as the horizontal stabilizer, this is calculated using equation B.7. In this equation, the induced drag consists of three components. The first term is the conventional term that determines induced drag based on the lift, as well as lift distribution and geometry. The second and third terms are corrective terms, taking into account the induced flow of other wings or rotors, respectively. The effective angle of attack caused by the rotor wake was given in eq. B.6, while that caused by another wing is given in eq. B.8.

$$C_{Di} = \frac{(C_L - C_{L0})^2}{\pi e AR} + C_L \left[ \sum_{otherwings} K_{int} \alpha_{ind,wing} + \sum_{rotors} C_{int} \alpha_{ind,rotor} \right] \quad (\text{B.7})$$

$$\alpha_{ind,wing} = \left( \frac{C_L}{\pi e AR} \right)_{otherwing} \quad (\text{B.8})$$

This simplified analytical approach is applied to determine influences on lift and drag at each component that experiences interference due to induced flow. When looking at the method of modeling the wake region of the rotor, in eq. B.3 the assumption that axial and radial wake development are independent of each other, might cause some degree of inaccuracy. However, this approach takes into consideration the contraction region in axial direction, and subsequent induced flow intensity changes, flow transition, as well as radial changes, allowing for the modelling of vortex phenomena at the edge of the wake. Evidently, the accuracy of the prediction of the radial impact on induced velocity will depend on the size and number of  $s$  rings (eq. B.4) which divides the wake in different areas as seen from above.

A helicopter operates under greatly varying flow regimes; from vertical flow in hover or vertical flight, to near horizontal flow in high speed flight, to large side flow angles at low speed flight. For this reason, all drag terms per helicopter component features horizontal and vertical drag components. Through trigonometric sine and cosine relationships depending on the angle of flow relative to the component, the magnitude of horizontal and vertical drag components are factored in.

It is evident that NDARC is the most advanced preliminary design tool to date. Numerous complex phenomena, such as interference, or horizontal and vertical lift and drag components, that are not taken into account in the other preliminary design tools discussed here, are taken into consideration in NDARC. However, as is indicated by its developers, NDARC currently still is a low fidelity design tool; the phenomena that the tool takes into account, such as interference, are modeled in a very basic fashion. As such, while modeling non-uniform inflow, this inflow model is very basic. Similarly, while rotor wake is accounted for, the method to account for its presence at other components is rather basic,

and counts on numerous empirical factors.

As has been mentioned for Flightlab, one of the significant downfalls in helicopter design tools, has been the inability to properly model the main rotor wake interference at the horizontal tail. While NDARC does incorporate the influence of the rotor wake on the horizontal tail, it is questionable to what extent the fairly uniform wake prediction properly represents the highly irregular and chaotic flow around the horizontal tail.



# C

## Agility with corrective control

### ATTITUDE QUICKNESS

Though this research concerns the sole mixed control SLA system, handling qualities will differ when an (auto)pilot has command over controls and provides corrective action. To provide insight in possible handling qualities when such corrective response is provided, this section provides handling quality results when the longitudinal and lateral-directional controllers are engaged. Though results are not indicative of the response caused purely by the SLA system, these results therefore do provide insight in a real-life operating environment, with an (auto)pilot at the controls. Handling quality results should be similar, to demonstrate that the (auto)pilot is capable of following similar desired pitch rate transients as compared to the baseline helicopter.

The attitude quickness of the SLA, baseline, and three failure cases is shown in figure C.1, when flying in the SLA's design conditions of 130kts and normal center of gravity. For each control case, the attitude quickness was found by providing a step-input pullup command with equal input intensity, yet varying the duration of input without exceeding a 1.75g loadfactor. It can be seen that the SLA system, with stabilator actuation limits in place, has a similar response in terms of pitch rate and attitude change as compared to the baseline UH-60A. For a fixed longitudinal stick input, the helicopter will first see a rapid change in attitude, gradually flattening out. Thus, the longer the step input, the larger the attitude change, and the lower the peak change in pitchrate with respect to attitude change, ie. following a line from left to right through the plot. As such, when comparing the SLA and baseline systems, for shorter longitudinal cyclic inputs of 0.5 to 1 seconds, the baseline system will see a fractionally higher ability to change attitude quickly, with a slightly higher attitude quickness  $Q_\theta$  for a given change in pitch attitude  $\theta$ . For step inputs of longer duration, the SLA system responds in more agile fashion. Differences are, however, very small. This plot, however, shows that the chosen stabilator actuator rates and deflection limits do not reduce the mixed control SLA's agility; the (auto)pilot can still command pitch rate changes with similar agility as the baseline helicopter.

Concerning the three failure cases, this plot demonstrates that the pilot can still command a pull-up. For step inputs of short duration, all failure cases show a lower pitch rate response than the functioning SLA system. This is because there is less control actuation than the controller initially requests; the pitch response will lag that of the functioning SLA system. For longer duration step inputs of 2 to 3 seconds, the control system, through its pitch rate feedback, will notice the discrepancy between desired and actual pitch rate, and will magnify the output signal of control deflection accordingly. Because of this feedback system, the failed SLA states are increasingly able to provide similar agility as compared to the SLA system for inputs of longer duration. This is evident through the closer proximity of agilities for inputs of 2 and 3 seconds, as opposed to inputs of 0.5 or 1 second duration.

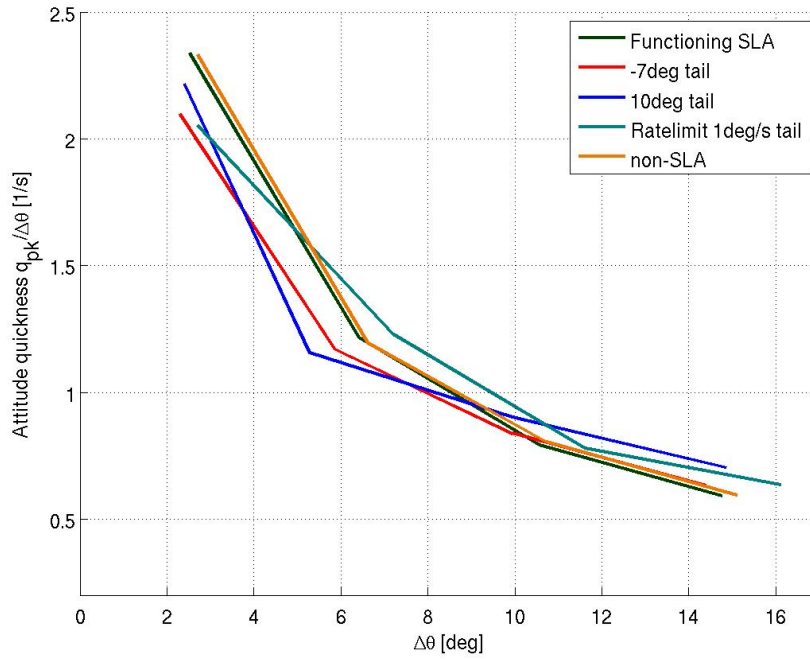
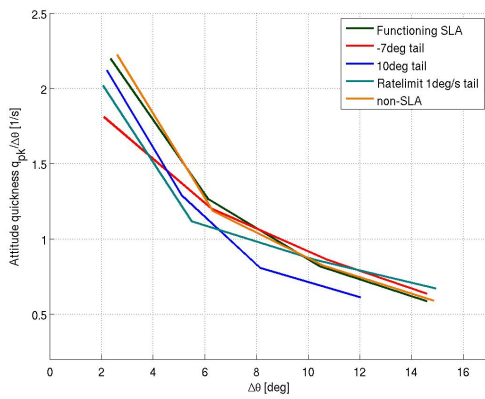
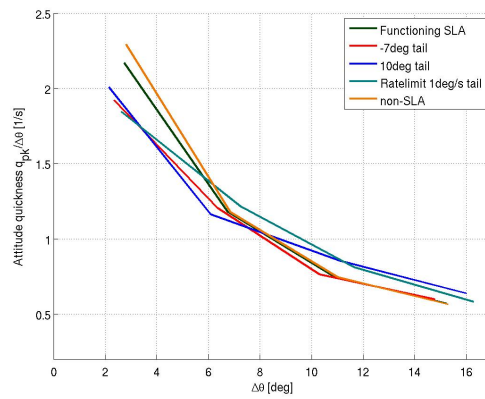


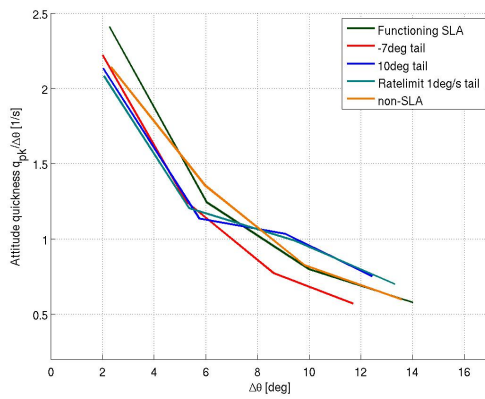
Figure C.1: Attitude quickness when operating under design conditions; 130kts and normal center of gravity.



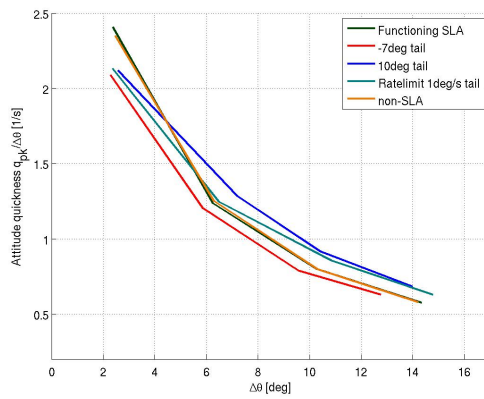
(a) 80kts flight and forward center of gravity



(b) 80kts flight and aft center of gravity



(c) 160kts flight and forward center of gravity



(d) 160kts flight and aft center of gravity

Figure C.2: Attitude quickness for off-design conditions.

Figure C.2 shows the attitude quickness for the four off-design conditions. From these plots, it is evident that the mixed control SLA system has similar agility properties as compared to the baseline UH-60A, when flying with this (auto)pilot system. The two are more similar when flying at 160kts. This is because this is the condition that most closely resembles the 130kts normal center of gravity configuration around which the SLA system was designed. All off-design configurations show that the failed SLA situations show a lower response for a step input of 0.5 or 1 second. Again, with longer step input, the longitudinal controller is more often able to compensate for this difference in desired and actual pitch rate. In the case of an aft center of gravity, or when flying at 160kts, the controller will more often overcompensate. The additional commanded amount of longitudinal to reduce the discrepancy between desired and actual pitch rate is larger than what is needed. This is because the higher airspeed results in a larger pitching moment for a given longitudinal cyclic deflection than the situation around which the controller was designed for.

### AGILITY QUICKNESS

Figure C.3 shows the agility quickness for the SLA and baseline UH-60A when flying at 130kts and with a normal center of gravity; with longitudinal and lateral-directional controller. The three failure cases are furthermore included. When comparing fig. C.2 with fig. C.4, it is evident that the five control situations have a more similar agility, in terms of agility quickness, than in terms of attitude quickness. While SLA and baseline systems had very similar agility as measured by attitude quickness, agility quickness considers the three failed SLA situations to have a more similar agility as well.

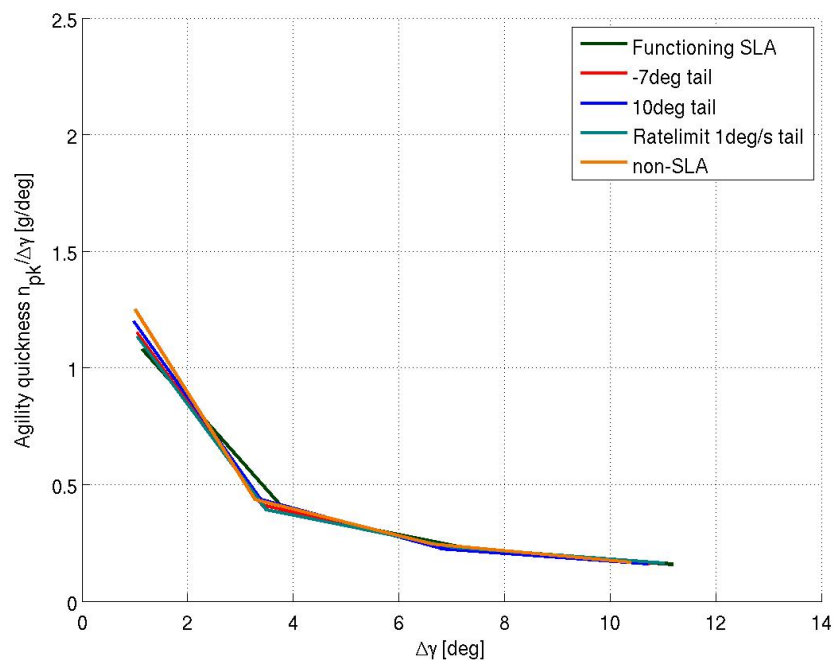
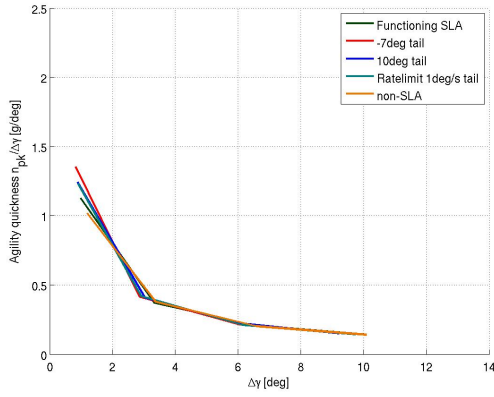
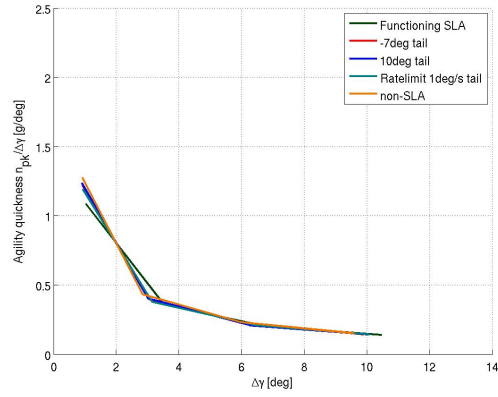


Figure C.3: Agility quickness when operating under design conditions; 130kts and normal center of gravity.

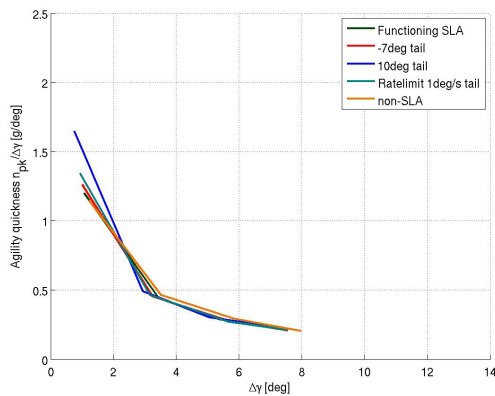
Figure C.4 shows the agility quickness for the off-design conditions, again showing similar agility for the various control situations in terms of flight path trajectory changes.



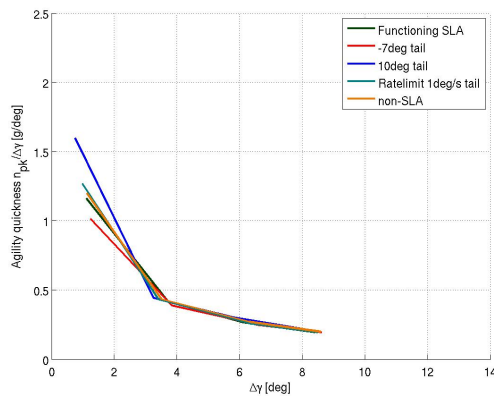
(a) 80kts flight and forward center of gravity



(b) 80kts flight and aft center of gravity



(c) 160kts flight and forward center of gravity



(d) 160kts flight and aft center of gravity

Figure C.4: Agility quickness for off-design conditions.

### FLIGHTPATH AGILITY QUICKNESS

Figure C.5 shows the flightpath agility quickness for the five control situations when flying with normal center of gravity at 130kts, with an (auto)pilot system.

When agility is measured in terms of flightpath changes, the SLA system will indeed possess lower agility than the baseline system, and the failed SLA situations. Reasons are similar to those provided for the non-(auto)pilot situation. During a pull-up command, the SLA system will increase downforce at the stabilator, causing a pitch up attitude. In terms of pitch rate response, the SLA system performs similarly to the baseline system, as can be seen from agility quickness. When the stabilator incidence is fixed, as is the case for the baseline system, the -7deg and 10deg stabilator angle, flightpath agility is highest. However, by increasing downforce at the horizontal stabilizer, net helicopter lift is reduced, and the ability to change flightpath trajectory is reduced.

Rating the various systems in terms of flightpath agility, the functioning SLA system with (auto)pilot functionality engaged performs worst, followed by the rate limited malfunctioning SLA system. Of the various fixed stabilator situations, the baseline system possesses the highest flight path agility. This is attributed to the fact that none of the controller's output signal concerning surface deflection is 'lost', as is the case for the -7deg and 10deg stabilator situations. The rate-limited control failure sees a performance in between the SLA system and the fixed-tail situations.

Therefore, the stabilator allows a higher agility in terms of attitude quickness, reducing lift and generating a pitch-up moment. Contrary, this local reduction in lift results in lower flightpath agility, seeing a smaller gain in altitude and a smaller change in flightpath. The fixed tail situations allow for lower attitude agility, not generating the pitching moment at the stabilator. However, because of this, lift of the helicopter as a whole increases more significantly during the pull-up, and the helicopter sees a larger change in flightpath.

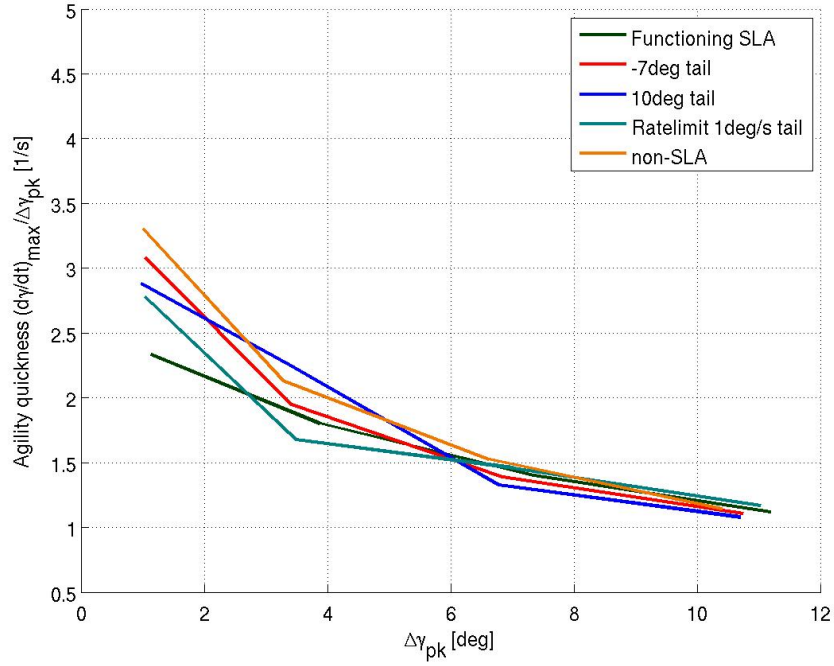
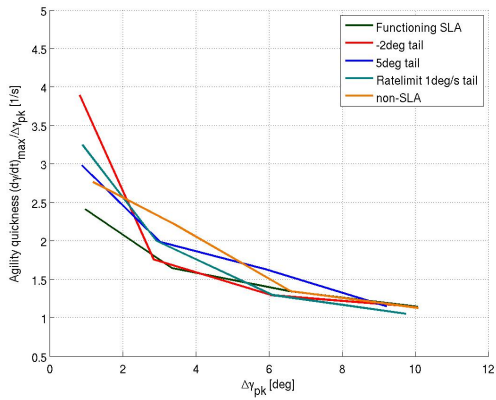
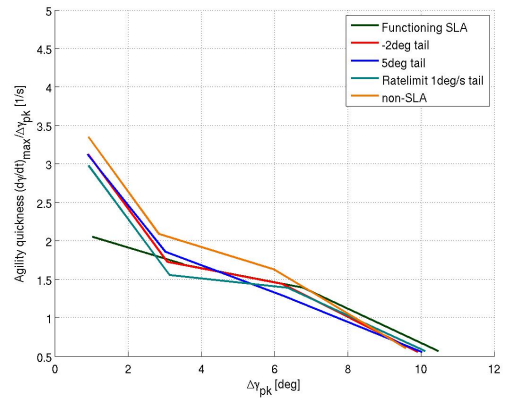


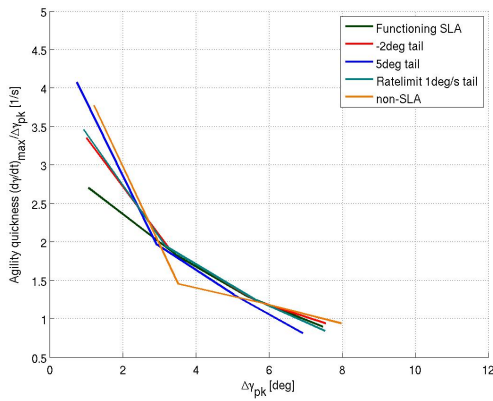
Figure C.5: Flightpath agility quickness when operating under design conditions; 130kts and normal center of gravity.



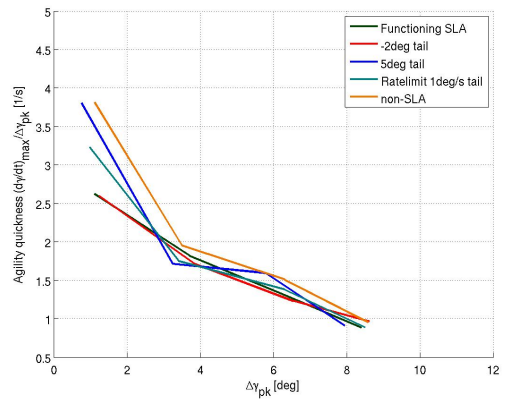
(a) 80kts flight and forward center of gravity



(b) 80kts flight and aft center of gravity



(c) 160kts flight and forward center of gravity

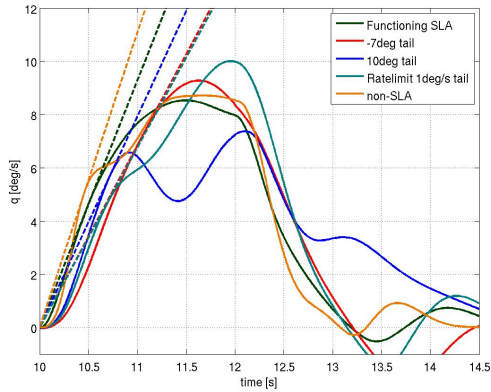


(d) 160kts flight and aft center of gravity

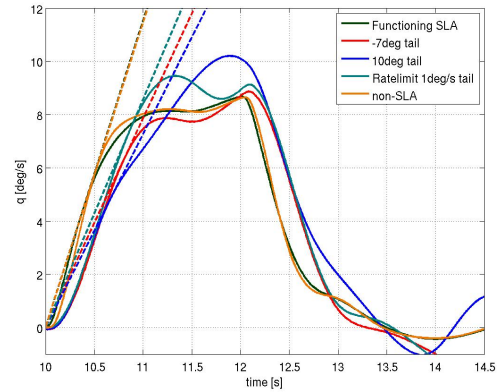
Figure C.6: Flightpath agility quickness for off-design conditions.

From these plots, it is seen that, in general, the SLA system will perform with less agility than the baseline system and the SLA failure modes. The rate limited SLA failure mode sees performance in between the fixed tail and the functioning SLA system situation, due to the aforementioned effect of local lift reduction at the stabilator. With an aft center of gravity, flightpath agility is lower for the functioning SLA system, and for the rate limited SLA system.

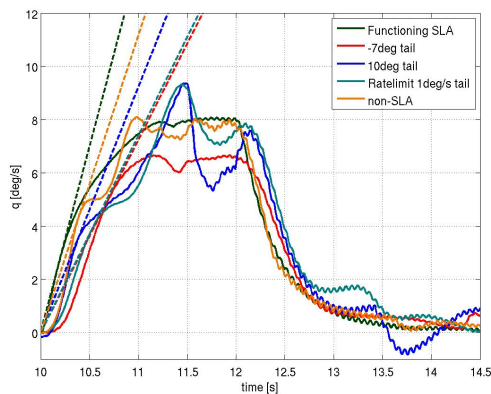
Lastly, fig. C.7 demonstrates the pitch rate transients when performing the pull-up. Tangent lines are included as a qualitative measure to indicate the time required for maximum average change in response after control input.



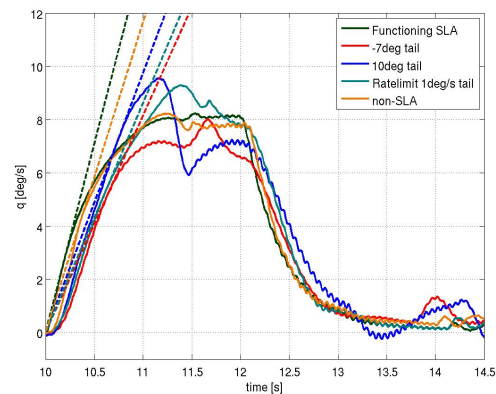
(a) 80kts flight and forward center of gravity



(b) 80kts flight and aft center of gravity



(c) 160kts flight and forward center of gravity



(d) 160kts flight and aft center of gravity

Figure C.7: Transient pitch rate response and peak change in pitch rate after doublet input, for various control situations.

**D**

Empty weight alteration for main  
rotor downsizing

Aircraft Weight (x=fixed)	lb	%DGW	tech factor	Aircraft Weight (x=fixed)	lb	%DGW	tech factor
DESIGN GROSS WEIGHT	15283.0x			DESIGN GROSS WEIGHT	15283.0x		
STRUCT Design GW	15283.0	100.0		STRUCT Design GW	15283.0	100.0	
Weight Max Takeoff	15283.0	100.0		Weight Max Takeoff	15283.0	100.0	
WEIGHT EMPTY	9211.7	60.3		WEIGHT EMPTY	9155.4	59.9	
STRUCTURE	3659.4	23.9		STRUCTURE	3624.7	23.7	
rotor group	1116.4	7.3		rotor group	1084.9	7.1	
blade assembly	586.5	3.8	1.000	blade assembly	571.4	3.7	1.000
hub & hinge	529.9	3.5		hub & hinge	513.5	3.4	
basic	529.9	3.5	1.000	basic	513.5	3.4	1.000
empennage group	274.4	1.8		empennage group	273.3	1.8	
horizontal tail	110.1	0.7		horizontal tail	110.1	0.7	
basic	110.1	0.7	1.000	basic	110.1	0.7	1.000
vertical tail	61.0	0.4		vertical tail	61.0	0.4	
basic	61.0	0.4	1.000	basic	61.0	0.4	1.000
tail rotor	103.2	0.7	1.000	tail rotor	102.2	0.7	1.000
fuselage group	1593.3	10.4		fuselage group	1591.2	10.4	
basic	1503.2	9.8	1.000	basic	1501.2	9.8	1.000
crashworthiness	90.2	0.6	1.000	crashworthiness	90.1	0.6	1.000
alighting gear	509.8	3.3		alighting gear	509.8	3.3	
basic	443.3	2.9	1.000	basic	443.3	2.9	1.000
crashworthiness	66.5	0.4	1.000	crashworthiness	66.5	0.4	1.000
engine sect/nac	135.5	0.9		engine sect/nac	135.5	0.9	
engine support	36.6	0.2	1.000	engine support	36.6	0.2	1.000
engine cowling	98.9	0.6	1.000	engine cowling	98.9	0.6	1.000
air induction	29.9	0.2	1.000	air induction	29.9	0.2	1.000
PROPULSION GROUP	2722.3	17.8		PROPULSION GROUP	2710.0	17.7	
engine system	837.4	5.5		engine system	837.4	5.5	
engine	555.5	3.6	1.000	engine	555.5	3.6	1.000
exhaust system	185.2	1.2	1.000	exhaust system	185.2	1.2	1.000
accessories	96.8	0.6	1.000	accessories	96.8	0.6	1.000
fuel system	305.1	2.0		fuel system	305.1	2.0	
tanks and supp	95.6	0.6	1.000	tanks and supp	95.6	0.6	1.000
plumbing	209.6	1.4	1.000	plumbing	209.6	1.4	1.000
drive system	1579.7	10.3		drive system	1567.5	10.3	
gear boxes	1277.3	8.4	1.000	gear boxes	1268.2	8.3	1.000
trans drive	84.4	0.6	1.000	trans drive	83.3	0.5	1.000
rotor shaft	190.9	1.2	1.000	rotor shaft	189.5	1.2	1.000
rotor brake	27.1	0.2	1.000	rotor brake	26.5	0.2	1.000
SYSTEMS AND EQUIP	2599.8	17.0		SYSTEMS AND EQUIP	2591.8	17.0	
flight controls	536.2	3.5		flight controls	530.9	3.5	
cockpit controls	100.0x	0.7		cockpit controls	100.0x	0.7	
auto flight cont	100.0x	0.7		auto flight cont	100.0x	0.7	
system controls	336.2	2.2		system controls	330.9	2.2	
fixed wing sys	40.6	0.3		fixed wing sys	40.6	0.3	
non-boosted	4.1	0.0	1.000	non-boosted	4.1	0.0	1.000
boost mech	36.6	0.2	1.000	boost mech	36.6	0.2	1.000
rotary wing sys	295.6	1.9		rotary wing sys	290.3	1.9	
non-boosted	75.5	0.5	1.000	non-boosted	74.4	0.5	1.000
boost mech	125.9	0.8	1.000	boost mech	124.0	0.8	1.000
boosted	94.2	0.6	1.000	boosted	91.9	0.6	1.000
auxiliary power	200.0x	1.3		auxiliary power	200.0x	1.3	
instruments group	200.0x	1.3		instruments group	200.0x	1.3	
hydraulic group	87.6	0.6		hydraulic group	86.3	0.6	
fixed wing	3.7	0.0	1.000	fixed wing	3.7	0.0	1.000
rotary wing	83.9	0.5	1.000	rotary wing	82.7	0.5	1.000
electrical group	437.8	2.9		electrical group	437.1	2.9	
aircraft	400.0x	2.6		aircraft	400.0x	2.6	
anti-icing	37.8	0.2	1.000	anti-icing	37.1	0.2	1.000
avionics (MEQ)	400.0x	2.6		avionics (MEQ)	400.0x	2.6	
furnish & equip	600.0x	3.9		furnish & equip	600.0x	3.9	
environ control	100.0x	0.7		environ control	100.0x	0.7	
anti-icing group	38.1	0.2	1.000	anti-icing group	37.4	0.2	1.000
VIBRATION	230.3	1.5		VIBRATION	228.9	1.5	
FIXED USEFUL LOAD	855.0	5.6		FIXED USEFUL LOAD	855.0	5.6	
crew	720.0x	4.7		crew	720.0x	4.7	
fluids	75.0x	0.5		fluids	75.0x	0.5	
other fixed UL	60.0x	0.4		other fixed UL	60.0x	0.4	
OPERATING WEIGHT	10066.7	65.9		OPERATING WEIGHT	10010.4	65.5	
scaled operating wt	7111.7	46.5		scaled operating wt	7055.4	46.2	
fixed operating wt	2955.0	19.3		fixed operating wt	2955.0	19.3	
core vehicle weight	7951.9	52.0		core vehicle weight	7897.9	51.7	
mil features in WE	1259.8	8.2		mil features in WE	1257.5	8.2	
WEIGHT EMPTY	9211.7	60.3		WEIGHT EMPTY	9155.4	59.9	
Fixed UL for DGW	855.0	5.6		Fixed UL for DGW	855.0	5.6	
Fuel for DGW	1600.0	10.5		Fuel for DGW	1600.0	10.5	
Payload for DGW	3616.3	23.7		Payload for DGW	3672.6	24.0	
USEFUL LOAD for DGW	6071.3	39.7		USEFUL LOAD for DGW	6127.6	40.1	
DESIGN GROSS WEIGHT	15283.0x			DESIGN GROSS WEIGHT	15283.0x		

Figure D.1: NDARC empty weight prediction for change in rotor radius; original rotor radius 8.23m (left) and downsized rotor radius 8.14m (right)